Project BIGBEN

Constitutive Equations for Sodium and Calcium Bentonites

Supported by:

Federal Ministry
for Economic Affairs
and Energy

on the basis of a decision
by the German Bundestag

GRS - 615

Gesellschaft für Anlagen-
und Reaktorsicherheit
(GRS) gGmbH

Project BIGBEN

Constitutive Equations for Sodium and Calcium Bentonites

Klaus-Peter Kröhn
Michael Kröhn

October 2020

Remark:

This report refers to the research project 02E11284 which has been funded by the German Federal Ministry of Economic Affairs and Energy (BMWi).

The study was conducted by the Gesellschaft für Anlagen- und Reaktorsicherheit (GRS) gGmbH.

The authors are responsible for the content of the report.

GRS - 615
ISBN 978-3-949088-01-8

Key-Words:

Bentonite, Buffer, Confined Conditions, Free Swelling, Geological Repository, Isotherm, Re-saturation, Retention Curve, Scanlines, Temperature

Acknowledgements

Funding of experimental as well as theoretical work in the framework of project BIGBEN (FKZ 02 E 11284) by the German Federal Ministry for Economic Affairs and Energy (BMWi) is gratefully acknowledged.

Highly valuable was the help of Juan Vertelman (atum3D) and Ben Illesch (KEYANCE Deutschland GmbH) with respect to the measurements concerning the accuracy of 3D-printed materials. They provided generously test prints that expanded the range of materials and of tested printing techniques considerably. Also, the open scientific exchange about 3D-printing for hydraulic tests with Patrick Bruines and Martin Stigsson (both SKB) is much appreciated.

Many thanks are also due to the GRS Geotechnical Laboratory, particularly to Rüdiger Miehe and Karsten Hellwald for their engagement in devising and commencing the tests with the desiccators in the oven. The same applies to the subsequent meticulous supervision of Bernd Zehle who took over from them when they went into retirement. Where the chemistry for maintaining the humidity in the desiccators was concerned, Felicia Garbe has also contributed substantially with her skilful support. Thank you to you all!

Abstract

Compacted air-dry bentonite is foreseen in many repository designs to be utilised as a geotechnical barrier since its hydrophilic and thereby swelling properties let it appear to be ideally suited for this purpose. For predicting the re-saturation dynamics of a bentonite barrier, isotherms or the equivalent retention curves form a vital constitutive equation, relating the relative humidity in the pore atmosphere to the water content of the bentonite.

Several retention properties of MX-80 and Calcigel bentonite were investigated in the framework of project BIGBEN[1]: (1) the hysteresis of adsorption and desorption isotherm, (2) the adsorption and desorption scanlines substituting the isotherms when changing from adsorption to desorption and vice versa under partially saturated conditions, (3) dependence of the isotherms on temperature, (4) changes in the isotherms due microstructural reconfigurations as a consequence of repeated wetting and drying of compacted specimen under spatial confinement.

(1) The measurements concerning isotherms and scanlines resulted in an unusual amount of data points. The data validate the complex shapes of the isotherms determined as known from the literature from earlier measurements with similar data resolution. The majority of the data in the literature does not show this complexity, though, indicating that it was lost due to insufficient data resolution.

(2) Entirely unexpected was the result that the scanlines do apparently not connect adsorption and desorption isotherms. When changing from adsorption to desorption or vice versa, the scanline branches off from the previously followed isotherm and ends at an extreme condition, either completely dry or fully saturated, without touching the opposite isotherm. The isotherms can thus be considered to be particular cases of scanlines.

(3) Quite some effort went into the measurements concerning water loss due to an increase in temperature as a function of the relative humidity. Characteristic curves for MX-80 as well as Calcigel could nevertheless be derived. It appears that these curves depend significantly on the dominant cation in the bentonite.

[1] **B**entonitaufsättigung **I**n **G**eotechnischen **B**arrieren im **E**ndlager-**N**ahfeld (Bentonite re-saturation in the near-field of a repository)

(4) It was tried to investigate the influence of successive wetting-drying cycles on the isotherms by using a device with a controlled climate chamber and automatic weighing. In order not to overstrain the delicate scale, extremely light and tough test cells were required. Construction of conventional metallic cells always threatened to exceed the weight requirements, though. In the end, the cells were therefore built from tough plastics by means of 3D-printing.

While this new technique is quite promising, there appeared some unexpected difficulties. In particular, uptake of water by the plastic material had apparently not been addressed in the literature about hydraulic tests with printed test devices, yet. Pre-tests about weight changes and dimensional accuracy of the cell material were therefore performed. While a test with a printed cell could be conducted eventually, supplemental tests would have been required to distinguish the water uptake of the cell from the actual the sample weight. These could unfortunately not be undertaken anymore due to time limitations.

For the results concerning topics (1) to (3), analytical functions have been formulated and implemented in the re-saturation code VIPER. Subsequent simulations of some generic set-ups using the new features indicate exemplarily their impact on model results. The differences to simpler formulations proved not to be overly dramatic. However, the observed differences in the results appear to increase with model complexity. They may thus become important for models that are more complex in terms of geometry, initial and boundary conditions or considered physics.

Zusammenfassung

Weltweit ist in vielen Konzepten für geologische Endlager für radioaktive Abfälle kompaktierter lufttrockner Bentonit als geotechnische Barriere vorgesehen. Wasserbindung bei gleichzeitiger Quellung lässt dieses Material gut geeignet für diesen Zweck erscheinen. Für die modellhafte Vorhersage des Aufsättigungsvorgangs einer Bentonitbarriere bilden Isothermen bzw. die äquivalenten „retention curves“ eine wesentlich konstitutive Beziehung, indem sie eine Beziehung zwischen der relativen Luftfeuchtigkeit der Porenatmosphäre und dem Wassergehalt des Bentonits herstellen.

Diese konstitutive Beziehung wurde für MX-80 und Calcigel Bentonit mit Blick auf verschiedene Eigenschaften im Projekt „**B**entonitaufsättigung **I**n **G**eotechnischen **B**arrieren im **E**ndlager-**N**ahfeld“ (BIGBEN) untersucht: (1) die Hysterese der Adsorptions- und Desorptionsisotherme, (2) die Form der Adsorptions- und Desorptionsscanlinien, die die Isothermen bei einem Wechsel von Adsorption zu Desorption – oder umgekehrt – ersetzen, (3) die Abhängigkeit der Isothermen von der Temperatur und (4) Änderungen der Adsorptionsisotherme infolge von Mikrostrukturänderungen nach wiederholter Auf- und Entsättigung eines kompaktierten Bentonitkörpers unter eingespannten Bedingungen.

(1) Die im Labor bestimmten Isothermen und Scanlinien beruhen auf einer ungewöhnlich großen Anzahl an Messpunkten. Diese bestätigen die komplexe Form der Isothermen, die in den sehr wenigen früher veröffentlichten Messungen mit vergleichbarer Datendichte gefunden wurden. Die Mehrzahl der veröffentlichten Isothermen zeigt diese Komplexität nicht, was darauf hindeutet, dass sie infolge unzureichenden Datendichte verloren gegangen ist.

(2) Völlig unerwartet war das Ergebnis, dass Scanlinien keine Verbindungslinien zwischen Adsorptions- und Desorptionsisotherme darstellen. Wenn die Hydratation von Adsorption zu Desorption oder umgekehrt wechselt, zweigen die Scanlinien von der zuvor verfolgten Isotherme ab und enden bei den Extrembedingungen vollständiger Trocknung oder Sättigung, ohne die jeweils andere Isotherme vorher zu berühren. Insofern können Isothermen als Spezialfälle von Scanlinien betrachtet werden.

(3) Unter erheblichem Aufwand und unter Verfolgung einiger Irrwege konnte der Verlust von hydratisiertem Zwischenschichtwasser infolge Temperaturerhöhung als Funktion der relativen Luftfeuchtigkeit bestimmt werden. Charakteristische Kurven wurden für

MX--80 und für Calcigel abgeleitet. Offenbar hängt die Form dieser Kurven vom dominierenden Kation in den Zwischenschichten ab.

(4) Es wurde versucht, den Einfluss aufeinanderfolgender Aufsättigungs- und Trocknungsphasen auf die Isothermen von kompaktiertem Bentonit mit Hilfe eines Geräts zu untersuchen, das im Wesentlichen aus einer kleinen kontrollierbaren Klimakammer mit automatischer Wägung besteht. Um die außerordentlich empfindliche Waage nicht zu überlasten, wurden dafür extrem leichte und trotzdem druckfeste Zellen benötigt. Die Konstruktion einer metallischen Zelle führte jedoch auf Probleme mit der Größe und der Gewichtsbeschränkung, so dass schließlich zu Zellen aus festem Kunststoff mit Hilfe eines 3D-Druckers übergangen wurde.

Während diese neue Technik im Grundsatz vielversprechend ist, zeigten sich ein paar unerwartete Schwierigkeiten. Insbesondere die Wasseraufnahme von Kunststoffmaterialien war in der Literatur über hydraulische Tests in gedruckten Versuchsaufbauten bislang nicht erwähnt. Aus diesem Grunde wurden Vortests zur Gewichtszunahme und Maßhaltigkeit von gedruckten Testkörpern durchgeführt. Ein Test mit kompaktiertem Bentonit in einer gedruckten Zelle erfolgte schließlich wie geplant. Der zusätzlich erforderliche zweite Test mit einer leeren Zelle zur Unterscheidung der Wasseraufnahme von Bentonit und Zellenmaterial konnte dagegen aus Zeitgründen nicht mehr durchgeführt werden.

Die Messergebnisse zu den Themen (1) bis (3) wurden in analytische Funktionen überführt, welche wiederum im Code VIPER zur Simulation der Bentonitaufsättigung implementiert wurden. Nachfolgende Rechnungen mit VIPER zu generischen Modellen zeigen exemplarisch den Einfluss der neuen Features auf die Modellergebnisse. Bei den einfachen Modellen war dieser Einfluss nicht sonderlich dramatisch. Mit zunehmender Modellkomplexität nahmen die beobachteten Veränderungen in den Ergebnissen zu. Daher kann nicht ausgeschlossen werden, dass die neuen Features dennoch von großer Bedeutung für Modelle mit komplizierteren Geometrien, Anfangs- und Randbedingungen oder physikalischen Prozessen sind.

Table of contents

1 Introduction

1.1 Background

Multiple barriers are envisaged to prevent radionuclide escape from underground radioactive waste repositories. If the geological barrier is a water bearing host rock like granite, the geotechnical barriers are of particular importance as they have also to protect the waste canisters and the waste matrix against a corrosive attack of the water. Presently, compacted air-dry bentonite is foreseen in a number of repository designs in different countries to be utilised as a geotechnical barrier since its hydrophilic and thereby swelling properties let this material appear to be ideally suited for this purpose. However, the behaviour of bentonite during re-saturation is very complex and may be controlled by hydraulic, mechanical and thermal processes.

The working principle of a bentonite barrier is that water reaching the bentonite starts the process of re-saturation. The clay minerals of the bentonite take up water, swell and reduce the pore space and thereby the permeability. Thus, water entering the bentonite is buffered to a certain extent, and concurrently, further inflow is impeded very effectively. In a fully saturated bentonite, the mobile water moves (a) very slowly due to the low permeability and (b) in little quantities due to the small pore volume.

While isothermal re-saturation can often be described by adsorption of water in the interlamellar space of clay particles, non-isothermal conditions in particular may lead also to local drying which is a desorption process on a microscopic level. These processes are characterized by isotherms (or the equivalent retention curves) that relate the relative humidity in the pore space of the bentonite to the water content. The isotherms form a vital constitutive equation for a mathematical model of bentonite re-saturation.

1.2 Hysteresis of the sorption and desorption

Desorption and particularly adsorption isotherms have been measured quite often in the past 70 years. Already from very early works such as /MOO 52/ it is known that water adsorption in clays follows a different path than the desorption. More recent data confirming this observation can be found for instance in /KAH 86/, /CAS 92/, /DUE 04/, and /SEI 14/.

By and large, two different types of adsorption isotherms have been presented in the literature. The majority of references e.g. /MOO 52 /, / WAD 04/, /DUE 04/, or /PUS 06/ suggest smooth bended curves as shown in Fig. 1.1. However, the notion of such simple curves might be caused by the comparative scarceness of the single data points. Data from other sources such as /KAH 86/, /GAI 05/, and partially also from /SEI 14/, depicted in Fig. 1.2, show a more complex course of the isotherms as they show a higher data density. The results presented in this report fall into the second category.

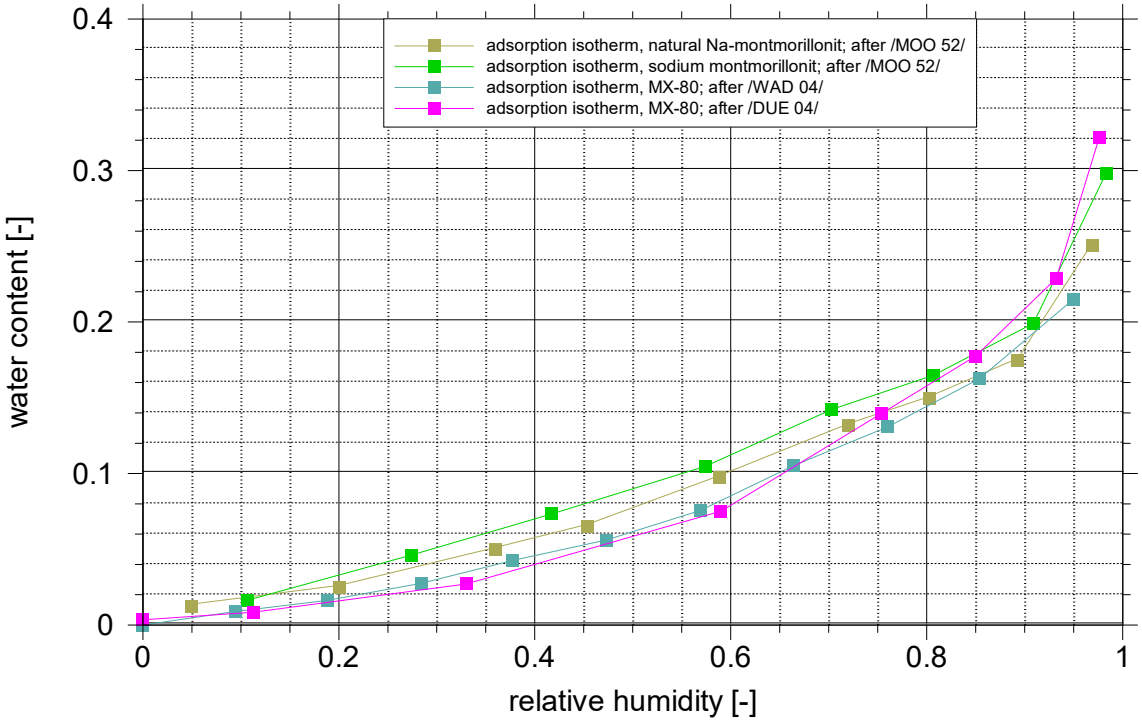

Fig. 1.1 Smooth adsorption isotherms after /MOO 52 /, /WAD 04/, and /DUE 04/

1.3 Scanlines

As mentioned above, non-isothermal bentonite re-saturation implies changing from adsorption to desorption and vice versa. In case of such a change, water saturation follows subsequently a path somewhere between the isotherms since adsorption and desorption isotherms are only connected at the end points either for completely dry or for fully saturated conditions. These paths are called “scanlines” further on. As there are the two isotherms from which scanlines can branch off, there are also two types of scanlines. Those branching of an adsorption isotherm to follow a desorbing path are called “desorption scanlines” in the following, the ones starting at a desorption isotherm to describe

subsequent adsorption are called “adsorption scanlines”. A plot illustrating these definitions is given in Fig. 1.3.

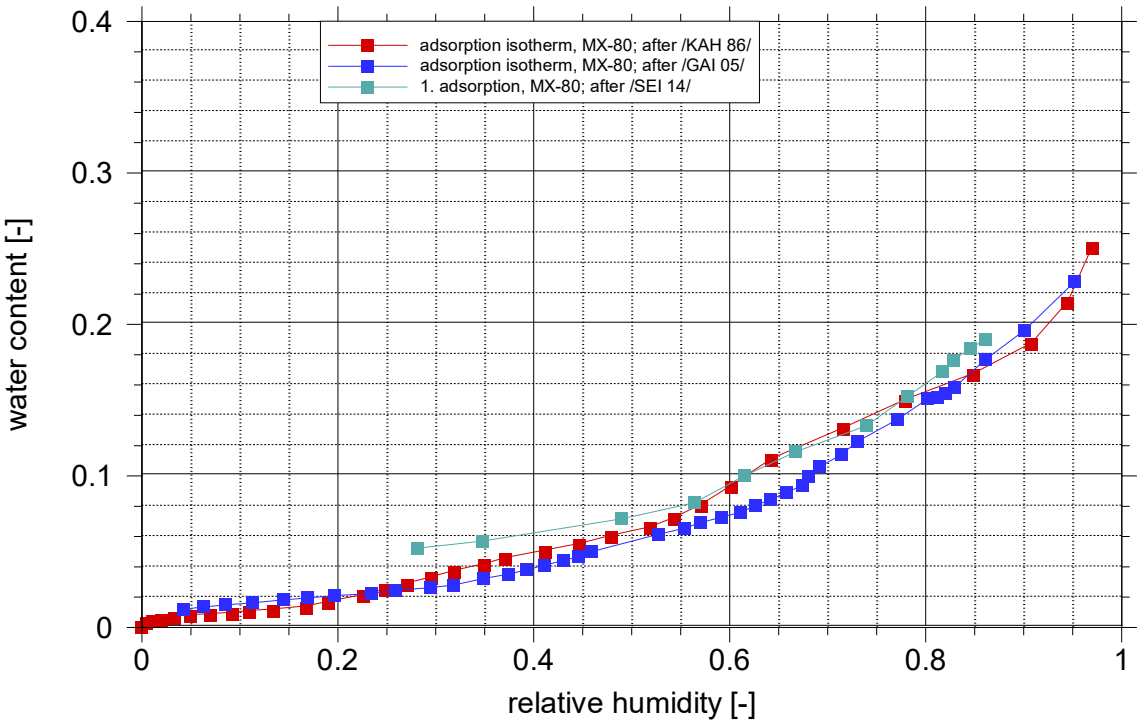

Fig. 1.2 Complex adsorption isotherms after /KAH 86/, /GAI 05/, and /SEI 14/

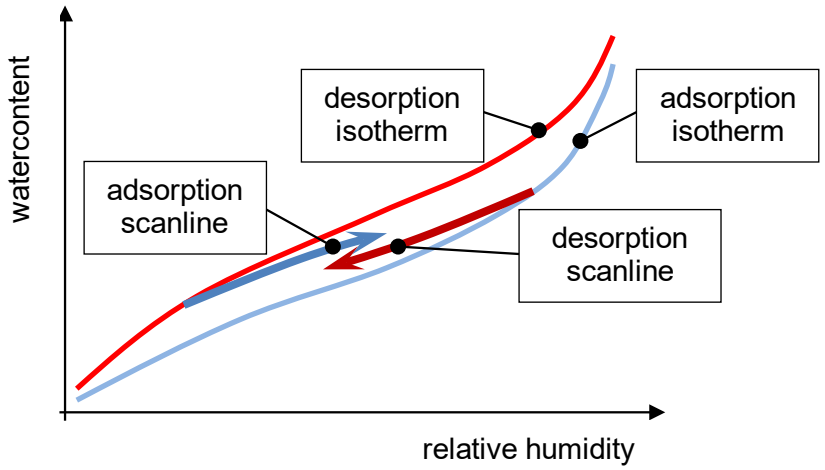

Fig. 1.3 Definition of scanline types

While the existence of scanlines is acknowledged in the literature for quite some time (e.g. /KRI 11/, /SEI 14/) there has not been a systematic investigation before as the

determination of a single isotherm is already quite time consuming (e.g. /DUE 04/). This gap could be closed now with the help of a new testing machine, the Vapor Sorption Analyzer (VSA) /VSA 20/.

1.4 Temperature-dependence of the isotherms

A second major gap in the knowledge about isotherms is the temperature-dependence of isotherms. Since isotherms means literally “at the same temperature“, this ambition appears to be contradictory. However, detailed measurements of the adsorption isotherm of MX-80 bentonite at temperatures between 25 and 99 °C have shown slight reductions of the equilibrium water content with increasing temperature (Fig. 1.4 from /GAI 05/). At that, the degree of reduction depends also on the relative humidity. The maximum deviation in the investigated temperature range amounts to about 2 % in water content at around 70 % relative humidity.

1.5 Conventions

In the framework of this report, the processes of adsorption and desorption are also called “hydration state”. The related changes of relative humidity and water content are referred to as “hydration path”. While particularly relative humidity and water content are given in percent in the text, they are plotted as dimensionless numbers in the graphics.

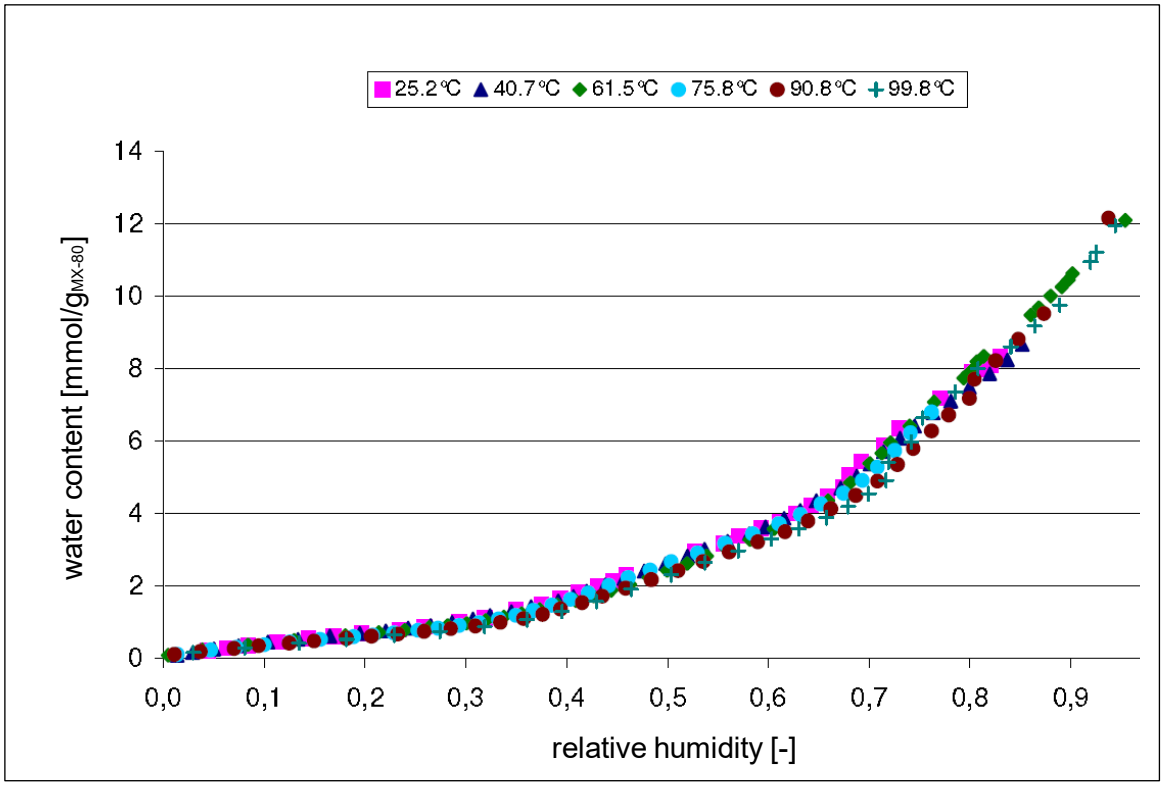

Fig. 1.4 Adsorption isotherm at different temperatures[2]; after /GAI 05/

This deviation seems to be small. But it means that a certain amount of adsorbed water in the interlamellar space – believed to show approximately the density of free liquid water – is set free in the form of water vapour at a density in the range of 0.01 kg/m³. Since this phase change means a volumetric expansion by a factor of about 10000, this effect has considerable impact on non-isothermal model calculations with GRS‘ extended vapour diffusion model (/KRÖ 11/, /KRÖ 19/).

Another interesting feature of the data from /GAI 05/ is that there appears to be no temperature-dependence at the extreme ends of the relative humidity. In case of complete dryness, the assumption of a water content of 0 % at a relative humidity of 0 % is intuitively reasonable and consequently wouldn´t allow for a temperature-dependence at dry conditions. An analogous conclusion for the observation in a fully vapour-saturated atmosphere is difficult to justify. For the purposes in this report, however, it is assumed for the sake of

[2] Note: 1 mmol of water corresponds to a mass of 0.018 g. The value of 1 mmol/g is therefore roughly equivalent to a water content of 2 %.

simplicity that the assumption of no temperature-dependence of the water content in fully vapour-saturated air holds.

Unfortunately, the six isotherms determined by /GAI 05/ can hardly be distinguished in Fig. 1.4. Moreover, they are obviously affected by uncertainties in the measurements. These uncertainties lead to unphysical intersections of isotherms for different temperatures, most plainly recognizable in case of the isotherm for 99.8 °C. However, a certain trend of water loss with increasing temperature as well as an additional dependence of this loss on the relative humidity is rather clearly indicated. Based on these soft data, an ad hoc formulation is implemented in code VIPER to take care of the temperature-induced changes in the isotherm in the model.

Since the published data do not allow for a clearer picture of the temperature- and humidity-dependent changes in the equilibrium water content (that is to say „the isotherm“), replacement of the ad hoc formulation by an analytical function based on further measurements appeared to be highly advisable. These measurements were also enabled by the VSA.

1.6 Microstructural changes by swelling in a confined space

All measurements and considerations so far refer to free swelling bentonite. This is obviously not the case in a real repository. In case of confinement, the retention curves have been shown to require an adjustment that acknowledges the fact that only a limited amount of water can be taken up by a compacted and confined bentonite body (e.g. /DUE 07/). Moreover, tests with confined samples of MX-80 compacted to different dry densities have been shown to undergo structural changes on the microscopic level during a full wetting that appear to change the water uptake characteristics, namely the isotherms/retention curves /SEI 14/.

In order to quantify the influence of structural changes on the adsorption isotherm, supplemental measurements of isotherms for compacted bentonite in the VSA were performed. Small cells had to be constructed for that purpose similar to the microcells described by /SEI 14/. The use in the VSA increased the functional requirements of the envisaged GRS-cells compared to the microcells, though, as they had not only to be small and tough but also very light in order not to overstrain the sensitive scale of the VSA.

1.7 Motivation for investigating different bentonites

Bentonite is a mixture of different minerals (e.g. /PUS 06/). The favourable properties of bentonite for geotechnical barriers are accounted for by montmorillonite which is a type of clay. On the micro-scale, montmorillonite consists of negatively charged crystal alumino-silicate platelets, called lamellae, that have typically a thickness of about 1 nm but a lateral size of about 200 nm (e.g. /DRU 05/). Three to twenty lamellae can be stacked on top of each other to form a clay particle. They are bonded by cations e.g. Na^+, K^+, Ca^{2+} or Mg^{2+} in the interlamellar space, the space between the lamellae. Re-saturation is closely related to hydration of the interlamellar cations. Hydration leads either to swelling in an unconfined configuration or to swelling pressure if volumetric swelling is obstructed.

The processes of hydration, swelling and developing swelling pressure are in principle independent of the charge of the cations. The shape of the adsorption and desorption isotherms, however, is clearly affected by the charge of the cations (e.g. /KAR 86/). Note that the dependence of swelling pressure on the water content is different as well (see also /KAR 86/) which applies also to the stability of the hydrated bentonite barrier against saline groundwater (e.g. /KRN 06/). In order to investigate principal differences between a bentonite with dominant monovalent cations and a bentonite with dominant divalent cations, the tests presented in this report are exemplarily performed with the sodium bentonite MX-80 and the calcium bentonite Calcigel.

2 Measurement techniques

2.1 Set-up with desiccators

The idea behind the test with desiccators was straight forward. Bentonite samples were to be kept under constant relative humidity as well as under constant temperature. They were weighed from time to time until no weight change could be observed. The weight of the samples was a measure to determine the water content for specific humidity and temperature conditions. Each sample thus provided one data point for a specific condition in the relative humidity-water content plane in which an isotherm is defined.

The controlled humidity was achieved by placing the bentonite samples in desiccators over a salt solution. Ten salts were selected to provide ten data points along the isotherm. They are listed in Tab. 2.1 together with the target humidity. For the highest humidity, K_2SO_4 was used instead of pure water to prevent condensation in case of slight temperature changes. Note that the desiccators are numbered in ascending order of the target relative humidity.

Tab. 2.1 Dissolved salts and target humidities

desiccator #	salt	target relative humidity
1	NaOH	6 %
2	LiCl	12 %
3	$MgCl_2$	33 %
4	K_2CO_3	43 %
5	$Mg(NO_3)_2$	54 %
6	KI	70 %
7	NaCl	75 %
8	KCl	85 %
9	$BaCl_2$	90 %
10	K_2SO_4	97 %

To improve the degree of data certainty, four bentonite samples were used per desiccator adding up to a total of 40 samples. The mass of the samples needed to be optimised between accuracy of the weight measurements – calling for a large mass – and the required time for reaching equilibrium – calling for little mass. To support a decision, a pretest with MX-80 bentonite powder was performed as described in Appendix A. As a result,

the sample mass was chosen to be about 100 g and the test began with heaping MX-80 bentonite powder of this mass loosely in Petri dishes. The samples were oven-dried at 105 °C for 24 hours, immediately before commencing the test in order to assure that the first data points lay on the adsorption isotherm. The four water content values per desiccator that were determined at equilibrium, were averaged before being used for setting up an isotherm.

The temperature was adjusted by placing the desiccators in a temperature-controlled oven. For the test, it was set to the following sequence: 30, 60, 90, 60, and 30 °C. The set-up is illustrated in Fig. 2.1.

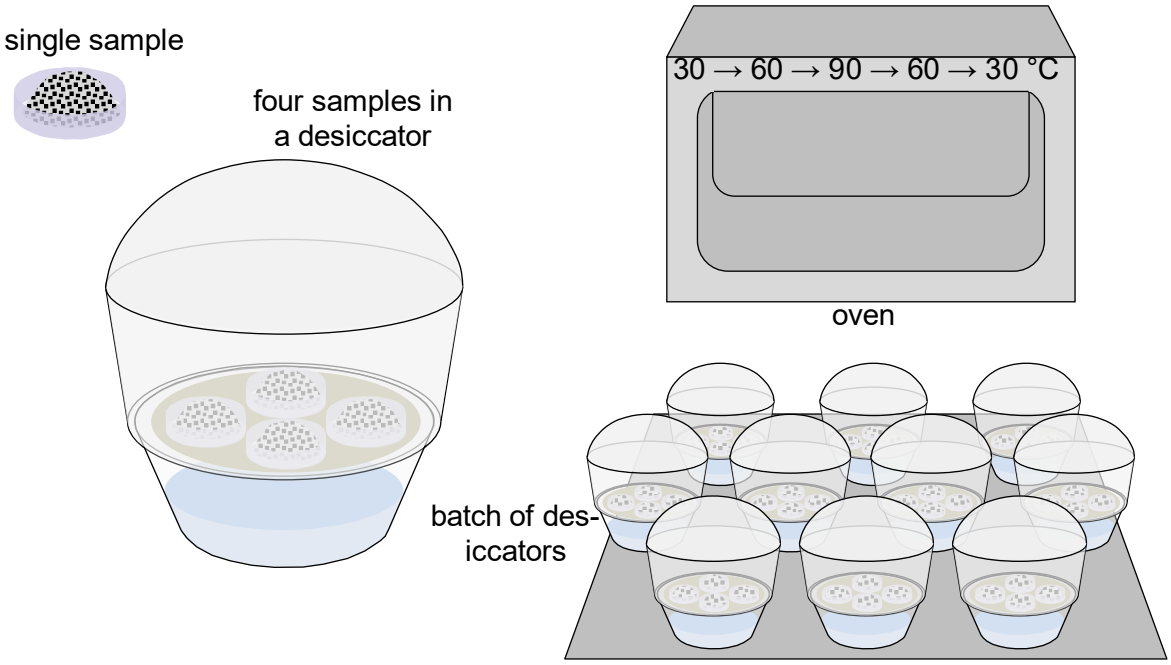

Fig. 2.1 Water content measurements in the desiccators

2.2 Set-up with the Vapour Sorption Analyzer

Initially, it had been planned to repeat the desiccator tests with Calcigel bentonite in order to investigate the influence of the dominant cation in the clay material. However, the tests with MX-80 used up time excessively. It was thus that already at an early stage of the desiccator tests with MX-80 it was decided to look for an alternative measurement technique that provided results faster and with higher precision.

This alternative was found in form of a new testing machine, the Vapour Sorption Analyzer (VSA) /VSA 20/. Basically, the VSA is a climate chamber, photographed and depicted schematically in Fig. 2.2, where the relative humidity can be varied between 3 and 95 % and the temperature between 15 °C and 60 °C[3]. Bentonite samples with a mass of up to 5 g are continuously weighed with a resolution of 100 µg and the weight as well as the related climate conditions are recorded at pre-set fixed intervals.

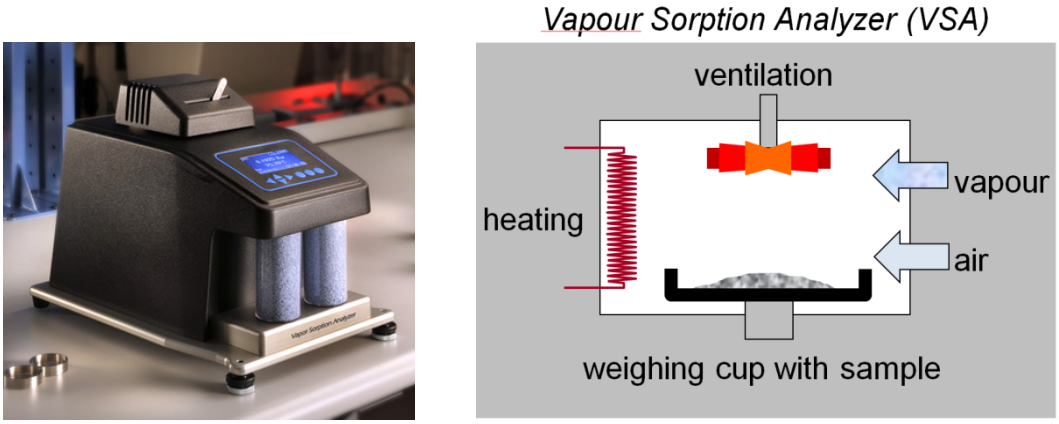

Fig. 2.2 Image and working principle of the VSA

First tests with the VSA performed in parallel to the desiccator tests and again with MX-80 bentonite, showed that the VSA works more efficiently and more precisely than the

[3] Working with temperatures below ambient temperatures should be avoided, though, because the VSA draws air from outside of the machine. Depending on the ambient humidity, this can easily cause condensation in the climate chamber as experienced unexpectedly on a particularly hot summer day.
For reasons that are not entirely clear, the same observation has been made when testing MX-80 bentonite at 55 °C and at a relative humidity above 85 %. It is noteworthy, though, that the test with Calcigel at 55 °C worked without a problem up to 95 % relative humidity.
In general, it appears advisable to be careful with the extreme settings in terms of relative humidity and temperature.

method described in the previous section. The tests with Calcigel in the desiccators were therefore cancelled while the tests with MX-80 in the desiccators required little attention at that stage and were thus continued.

The VSA has two measuring modes called Dynamic Dew Point Isotherm (DDI) and Dynamic Vapour Sorption (DVS) which were checked with respect to applicability. In DDI-mode, the VSA increases and decreases the relative humidity slowly and monitors the related response in sample weight continuously. The result is a continuous curve of weight over relative humidity where the weight can easily be converted into a water content. This method is fast, a complete hysteresis cycle required less than 3 days, and the hysteresis curves measured for MX-80 were quite convincing at a first glance. Later, however, it was discovered that the water uptake of a bentonite sample was not fast enough to reach an equilibrium between the ever-changing relative humidity and the water content in the sample. The isotherms measured with the DDI-method were therefore always somewhat off.

The DDI-method was therefore abandoned in favour of the DVS-method where a series of related relative humidity and temperature values are pre-set manually. Starting the test, each of these conditions is sequentially set by the VSA and maintained until the change rate of the sample weight falls below a certain threshold value. In comparison to the DDI-mode the DVS-method is more time consuming. A complete hysteresis cycle required 12 days and provided in this case only discrete values every 5 % relative humidity. The confidence in the determined data is rather high, though, as the precision of the measurements is appeared to be well controlled.

The high expectations into the new measurement technique were somewhat dampened by a number of difficulties that were encountered while working with the VSA. They were mostly technical in nature and fixed generously by the manufacturer. A lot of time was lost by the repairs, nevertheless. Additionally, a more than usual amount of control measurements appeared to be necessary, firstly, when difficulties were suspected and, secondly, later to assure a successful repair. Furthermore, failures were often not immediately noticed with the consequence that some errors in the measurements might have gone unnoticed or, if noticed, required repetitions. Some measurement campaigns were suspended for a considerable period of time for the same reason and might have been performed under (slightly) different conditions. It has to be mentioned, though, that the

objectives of the project could eventually be accomplished despite all these difficulties. Tab. 2.2 shows the matrix of successfully performed measurements with the VSA.

Tab. 2.2 Measurement matrix

temperature	**subject**		**MX-80**	**Calcigel**
25 °C	hysteresis		x	x
	scanlines	adsorption	x	x
		desorption	x	x
30 °C	hysteresis		-	x
	scanlines	adsorption	-	x
		desorption	-	x
50 °C	hysteresis		x	-
	scanlines	adsorption	x	-
		desorption	x	-
55 °C	hysteresis		-	-
	scanlines	adsorption	x	-
		desorption	x	x
25 – 55 °C	weight change	at r_h=10 %	x	
		at r_h=20 %	x	
		at r_h=25 %	x	x
		at r_h=30 %	x	
		at r_h=40 %	x	x
		at r_h=50 %	x	
		at r_h=55 %	x	x
		at r_h=60 %	x	x
		at r_h=70 %	x	x
		at r_h=80 %	x	x
25 °C	hysteresis under confined conditions		(x)	-
Symbol explanation:	x : performed - :not performed			

3 Hysteresis of the isotherms

3.1 Measurements

3.1.1 MX-80

The results for the adsorption and desorption isotherm for MX-80 at 25 °C are depicted in Fig. 3.1. It is based on five single measurement campaigns aiming exclusively at the hysteresis properties whose results are compiled in Appendix A, section A.1.1.

Seemingly, more data points can be observed in Fig. 3.1 for the adsorption than for the desorption isotherm for technical reasons. The measurements were set to change the relative humidity in the climate chamber of the VSA by a step of 5 %. There should thus have been several data points compiling at multiples of 5 % relative humidity. The initial water content of the bentonite sample and thereby the initial relative humidity in the climate chamber varied from campaign to campaign, though. The first hydration path, in this case the adsorption path, was therefore measured between the multiples of 5 %, falsely creating the impression of a larger number of data points but also giving a better insight into the run of the adsorption isotherm.

The technical limits for measuring the isotherms are 5 % and 95 % relative humidity, respectively. Since the bentonite samples could not be fully dried or fully saturated, this leads to a certain error in the starting points of the isotherms. In case of the adsorption isotherm, however, this concerns a data range that is rarely encountered in the framework of repositories for radioactive waste.

At the other end of the spectrum, an equilibrium humidity of 95 % can easily be reached so that uncertainties in this range would be more serious. However, the same practical applications as mentioned above concern bentonite that is compacted to a certain degree and emplaced in a confined space. In that case, the bentonite cannot take up as much water as under free swelling conditions. The water content at 95 % relative humidity under free swelling conditions marks the maximum uptake by bentonite with a dry density of close to 1500 kg/m³ /KRÖ 11/. For MX-80 bentonite this refers to the minimum degree of compaction that is relevant for use in a nuclear waste repository thus rendering these data uncertainties in the isotherms for free swelling bentonite irrelevant.

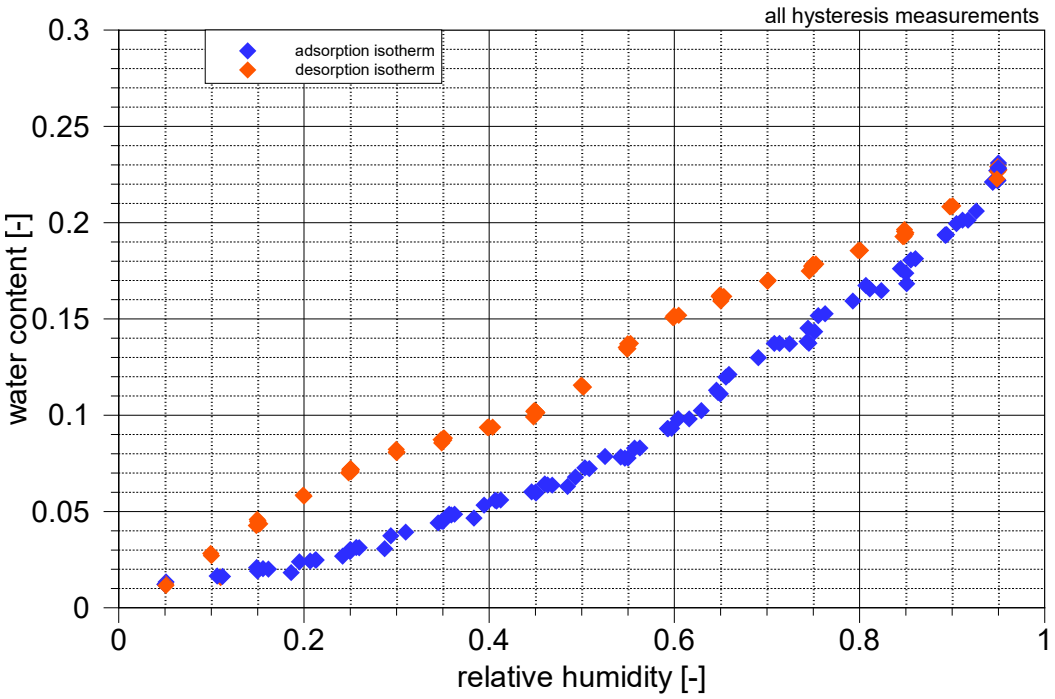

Fig. 3.1 All data on the Hysteresis of the isotherm for MX-80 at 25 °C

The resulting shapes of the isotherms are rather complex containing several inflection points. A change to a strongly exponential increase of the water content beyond 95 % relative humidity as observed in the literature[4] is indicated. The maximum difference of water content between adsorption and desorption isotherm amounts to about 5 % in the range between 55 % and 60 % relative humidity.

The present measurements compare favourably with the highly resolved isotherms determined by /KAH 86/. A comparison with these data as depicted in Fig. 3.2 shows a good match which appeared to justify confidence in the accuracy of further measurements.

[4] cp. /KRÖ 11/.

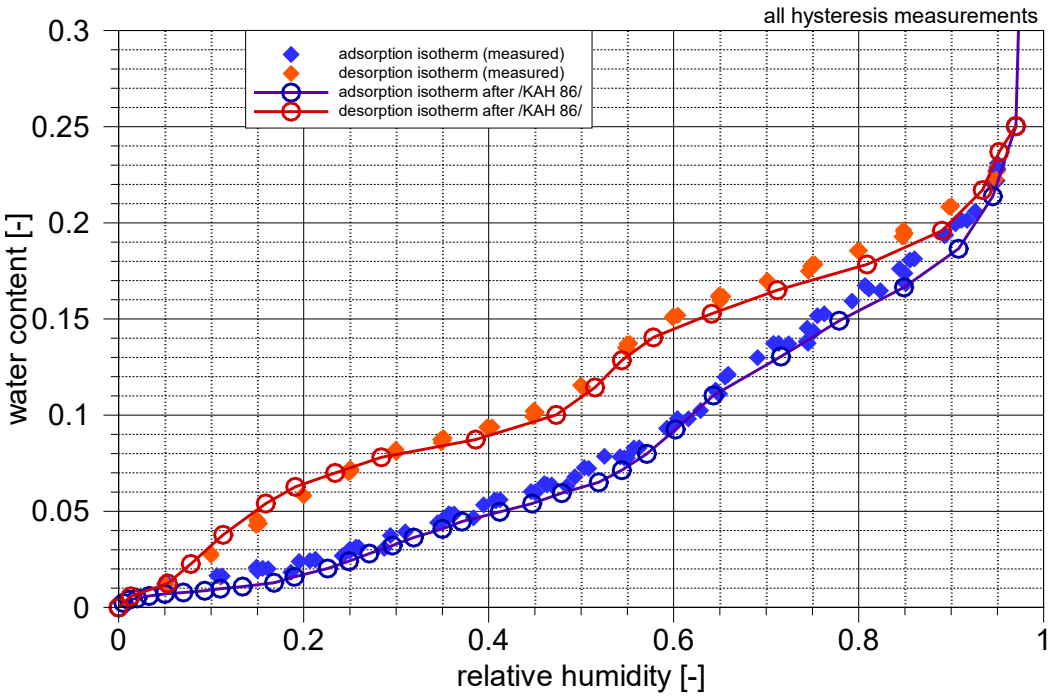

Fig. 3.2 Comparison of the data from /KAH 86/ with the data from the VSA

3.1.2 Calcigel

The results for the adsorption and desorption isotherm for Calcigel at 25 °C are depicted in Fig. 3.3. It is based on two single measurement campaigns aiming exclusively at the hysteresis properties whose results are compiled in Appendix A, section A. 2.1.

In comparison to the data for MX-80 as depicted in Fig. 3.1, the difference between adsorption and desorption isotherm is much less. Compared to the maximum difference in water content for MX-80 of about 5 %, for Calcigel this difference amounts only to about 2 % between 60 % and 70 % relative humidity.

Another striking difference between the isotherms of MX-80 and Calcigel is the shape of the curves. For Calcigel, they appear to be much more smoothly curved than those of MX-80.

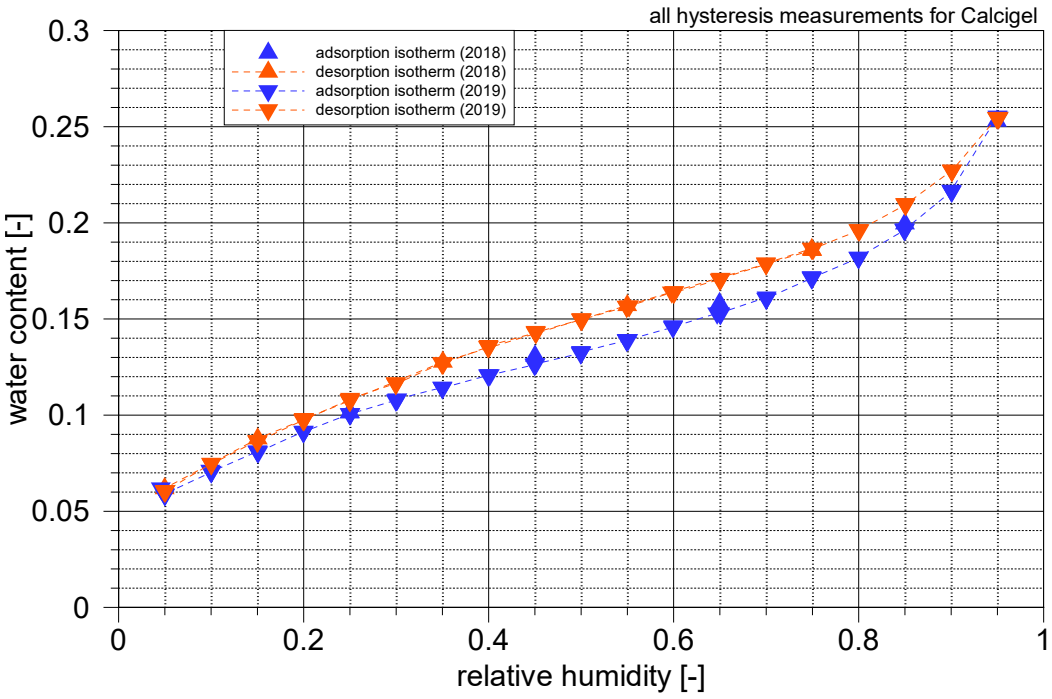

Fig. 3.3 All data on the hysteresis of the isotherm for Calcigel at 25 °C

3.2 Analytical functions

3.2.1 MX-80

An analytical function describing the isotherms of MX-80 has been found with

$$w_{iso} = \left\{\sum_{i=1}^{6}\left(-(a_i + b_i * r_h) * \left\{\frac{1}{1+e^{[-c_i*(r_h-d_i)*e_i]}} + \frac{1}{1+e^{[-f_i*(g_i-r_h)]}}\right\} - 1\right)\right\} + a_7 * r_h^{b_7} \quad (3.1)$$

w_{iso} - water content of the isotherms, $w(r_h)$ [-]

r_h - relative humidity [-]

$a_i, b_i, c_i, d_i, e_i, f_i, g_i$ - coefficients [-]

Formulation (3.1) describes the adsorption as well as the desorption isotherm using the appropriate accompanying sets of coefficients $a_i, b_i, c_i, d_i, e_i, f_i, g_i$. These sets are compiled in Tab. 3.1 and Tab. 3.2, respectively.

A graphical comparison of formulation (3.1) with the measured data as given in Fig. 3.1 is depicted in Fig. 3.4.The resulting match appears to be satisfying.

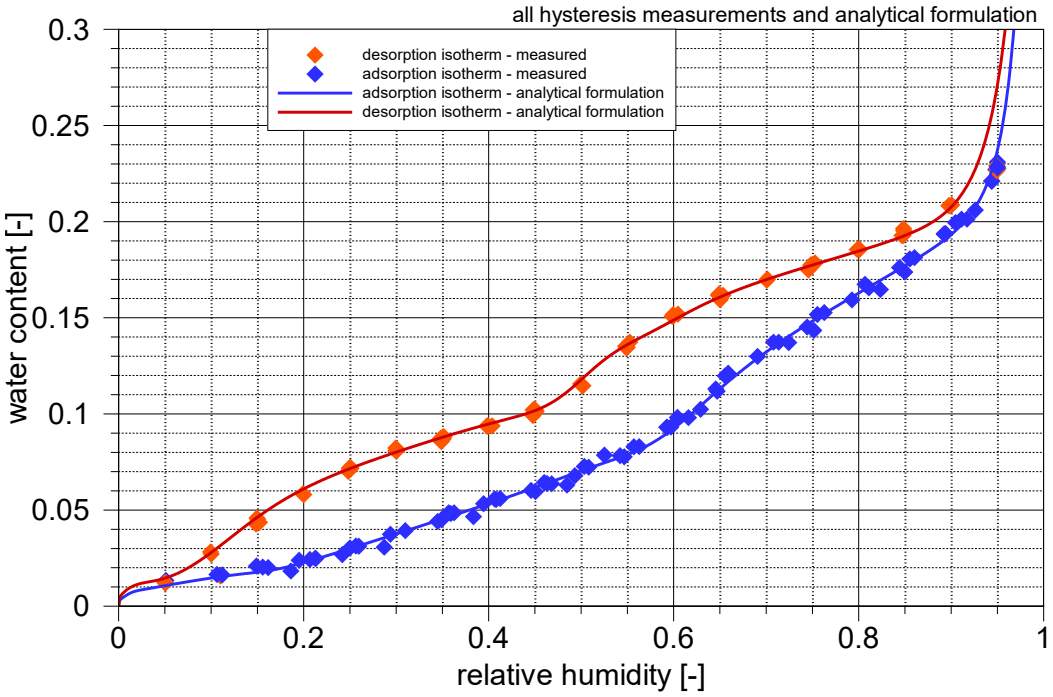

Fig. 3.4 Hysteresis of the isotherms for MX-80 at 25 °C and analytical formulations

Tab. 3.1 Coefficients for the analytical adsorption isotherm for MX-80

	a	b	c	d	e	f	g
1	0	0.25	300	-0.05	1	200	0.012
2	0.003	0.08	200	0.012	1	45	0.175
3	-0.013072	0.154	50	0.175	1	30	0.56
4	-0.060	0.273	25	0.572	1	50	1.1
5	-1.1657	1.46	40	1.000	1	50	1.1
6	-1.	0	1.0	0	0	100	1
7	0.005	0.1	0	0	0	0	0

Tab. 3.2 Coefficients for the analytical desorption isotherm for MX-80

	a	b	c	d	e	f	g
1	0	0.39	300	-0.05	1	75	0.012
2	0.03	0.15	25	0.10	1	30	0.55
3	-0.220	0.486	40	0.485	1	30	0.581
4	0.0667	0.140	28	0.58	1	80	1.1
5	-0.813	1.14	35	0.99	1	50	1.5
6	-1.0	0	1	0	0	85	1.002
7	0.006	0.05	0	0	0	0	0

In the context of the classic THM-codes for simulation of bentonite re-saturation, the adsorption isotherm is used in the equivalent form of a retention curve. It is usually expressed in terms of suction s vs. degree of saturation S which relates the retention curve to a specific bentonite dry density ρ_d.

Relative humidity can be converted into suction using the Kelvin equation (e.g. /KRÖ 11/)

$$s = \frac{RT\rho_w}{M_w}\ln(r_h) \qquad (3.2)$$

s - suction [Pa]
T - temperature [K]
R - universal gas constant; R=8.31 [J/(mol K)]
ρ_w - density of liquid water; ρ_w = 1000 [kg/m³]
M_w - molecular mass of water; M_w = 0.018 [kg/mol]
r_h - relative humidity [-]

and conversion between water content and degree of saturation is given by

$$S = \frac{w}{w_{tot}} \qquad (3.3)$$

S - degree of saturation [-]
w - water content [-]
w_{tot} - maximum water content [-]

The maximum water content in eq. (3.3) can be calculated from the bentonite dry density ρ_d and the grain density ρ_s assuming that the pore space is completely water-filled (e.g. /KRÖ 04/):

$$w_{tot} = \rho_w \left(\frac{1}{\rho_d} - \frac{1}{\rho_s} \right) \qquad (3.4)$$

ρ_d - bentonite dry density [kg/m³]

ρ_s - particle density [kg/m³]

In Fig. 3.5, the analytical solution for the isotherms is shown together with the equivalent retention curves. The arrows indicate the direction in which the water content changes. In order to ascertain a more general impression of the impact of hysteresis on the retention curves, the resulting suction values are plotted over the water content instead over the degree of saturation. Note that a suction of 500 MPa relates roughly to a relative humidity of 2.7 %.

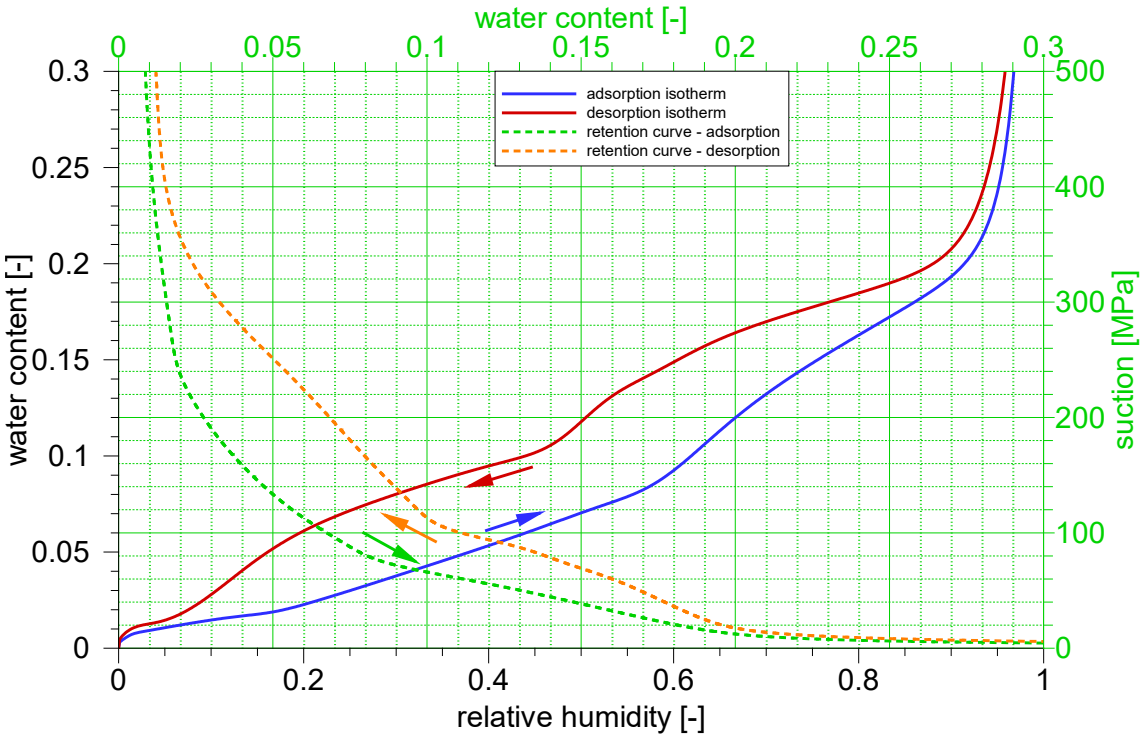

Fig. 3.5 Hysteresis of isotherms for MX-80 at 25 °C and equivalent retention curves

The difference stemming from the mode of hydration – adsorption or desorption – is substantial. Exemplarily, the situation at 10 % water content is highlighted. At 10 % water

content, the relative humidity on the adsorption isotherm amounts to 62 % while it reads 44 % on the desorption isotherm. Analogously, the two retention curves in Fig. 3.5 indicate at 10 % water content a suction of 66 MPa on the adsorption path in comparison to 113 MPa on the desorption path. Since a change in the mode of hydration can easily occur under non-isothermal conditions, these differences should have a considerable impact on re-saturation-simulations.

3.2.2 Calcigel

An analytical function describing the adsorption isotherm of Calcigel $w_{ads}(r_h)$ has been derived as follows:

$$w_{iso\ ads} = \left(\frac{0.9}{(r_h + 0.15)^8} * 4 \cdot 10^{-7} + 0.005\right) * r_h + 0.175 * {r_h}^{0.42} + 2000 * \left(\frac{r_h}{4}\right)^{7.2} + 4 \cdot 10^{-10}\left(\frac{1}{1.07 - r_h}\right)^8 \quad (3.5)$$

The formulation for the desorption isotherm is (again) in principle the same but goes with different coefficients:

$$w_{iso\ des} = \left(\frac{1.2}{(r_h + 0.15)^8} * 4 \cdot 10^{-7} + 0.005\right) * r_h + 0.2 * {r_h}^{0.45} + 2140 * \left(\frac{r_h}{4}\right)^{7.5} + 1.65 \cdot 10^{-9}\left(\frac{1}{1.07 - r_h}\right)^{7.47} \quad (3.6)$$

A graphical comparison of formulations (3.5) and (3.6) with the measured data as given in Fig.3.3 is depicted in Fig.3.6. The resulting match appears to be satisfying.

The difference between adsorption and desorption isotherms/retention curves is not as big as for MX-80. Following the example for MX-80, the situation at 10 % water content is looked at again. At 10 % water content, the relative humidity on the adsorption isotherm amounts to 21 % while it reads 26 % on the desorption isotherm. Analogously, the two retention curves in Fig.3.5 indicate a suction of 188 MPa on the adsorption path in comparison to 216 MPa on the desorption path at 10 % water content. Even if smaller compared to MX-80, these differences should still have a noticeable impact on simulations of bentonite re-saturation.

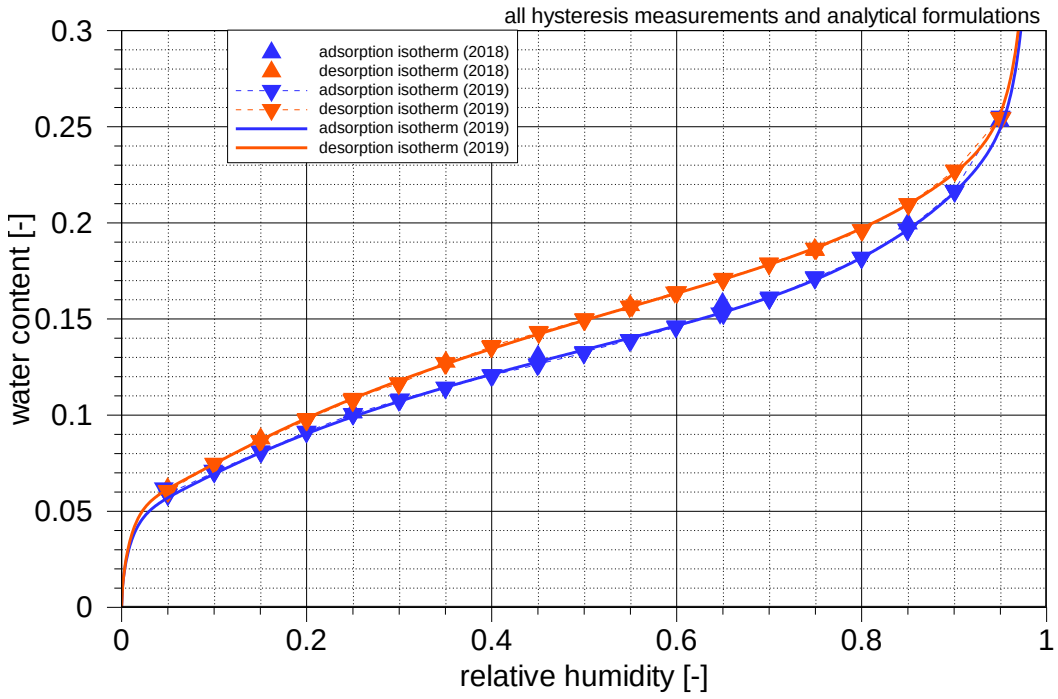

Fig.3.6 Hysteresis of the isotherms for Calcigel at 25 °C and analytical formulations

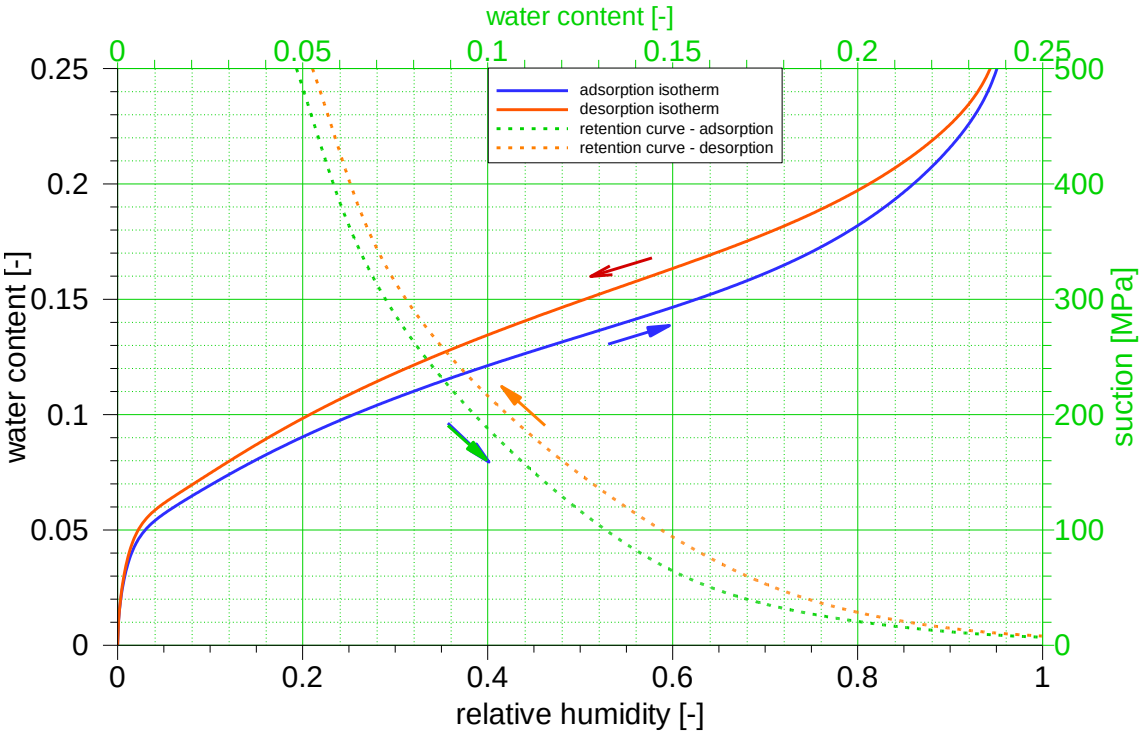

Fig.3.7 Hysteresis of isotherms for Calcigel at 25 °C and equivalent retention curves

4 Scanlines

4.1 Assumptions and conventions

The mode of hydration in the bentonite can be either adsorption or desorption. If starting adsorption at completely dry conditions, the equilibrium state of relative humidity and water content follows the adsorption isotherm. Starting desorption from full saturation means the equilibrium state follows the desorption isotherm.

Changing the mode of hydration at partly saturated condition after initially following one of the isotherms means that equilibrium states are subsequently described by a scanline. The scanline branches off from the isotherm where the change of the hydration mode occurred. This state is uniquely characterized by the related relative humidity r_{h0} defining the starting point of a specific scanline. The endpoint, by contrast, is unknown[5]. Switching from one hydration mode to the other can of course also happen at any point within the hysteresis loop which is defined by the bounding isotherms. The switch is triggered by a change in the sign of the temporal derivative of the water content.

Two types of scanlines have to be differentiated according to the switch of hydration mode. The first one refers to scanlines branching off the adsorption isotherm and thus describing a desorption process. They are called “desorption scanlines” further on. Scanlines branching off the desorption isotherm, describing an adsorption process will be called “adsorption scanlines”.

For the following considerations it is assumed that scanlines of one type – adsorption or desorption scanlines – are unique and that scanlines of one type do not intersect each other.

[5] In the beginning, it was intuitively expected that the scanlines might have a complex shape but would rather directly connect both isotherms.

4.2 Measurements

4.2.1 MX-80

4.2.1.1 Additional data on the isotherms

Measurements aiming at the scanlines were performed in adsorption-desorption cycles. The resulting data added therefore also to the data from the hysteresis-only measurements. The results for the adsorption and desorption isotherm for MX-80 at 25 °C including new data from the adsorption scanline measurements are depicted in Fig.4.1. It is based on five single measurement campaigns aiming exclusively at the hysteresis properties (see Appendix A, section A.1.1) and the three measurement results from Appendix A, section A.1.2.

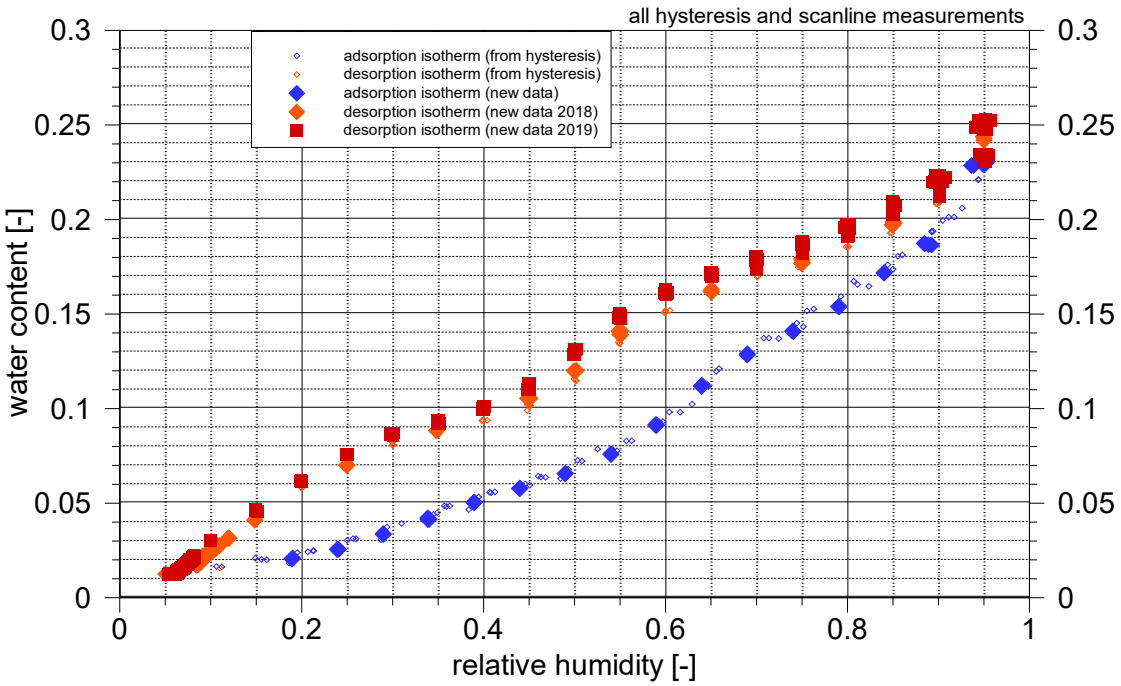

Fig. 4.1 Hysteresis of the isotherm for MX-80 at 25 °C incl. additional data from scanline measurements

The additional data for the adsorption isotherm fit in nicely with the older data. Basically, the same applies to the measurements on the desorption isotherm in 2018. However, the data from 2019 deviates from the earlier ones. The water content measured in 2019 appears to be higher by up to 1 % in the range between 50 % and 60 %.Because of the

good match between the hydration-only data and the data from the 2018-campaign concerning the scanlines, the deviating newer data will be ignored in the following.

4.2.1.2 Adsorption scanlines

One consequence of ignoring the newer data on the desorption isotherm (see previous subsection) is that the scanlines measured in different measurement campaigns are not entirely comparable. This is illustrated in Fig.4.2 where, exemplarily, the adsorption scanlines r_{h0} = 30 % and r_{h0} = 50 % from the two campaigns are compared. Since the data for the desorption isotherm deviates strongest in the range between 50 % and 60 %, the resulting scanlines for r_{h0} = 30 % are much less affected than the scanlines for r_{h0} = 50 %.

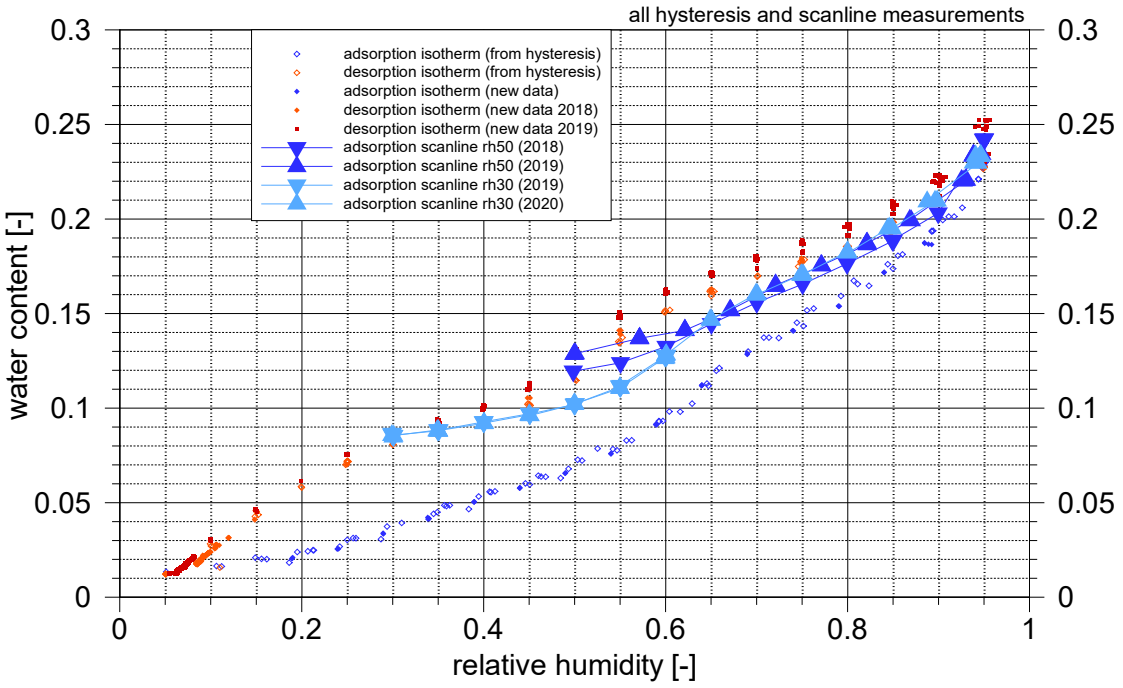

Fig. 4.2 Accuracy check for adsorption scanlines for MX-80 at 25 °C starting at 50 and 30 % relative humidity

A much better understanding of the characteristics of the adsorption scanlines thus follows from looking at the results of the two measurement campaigns separately as done so with Fig.4.3 and Fig.4.4.

At a first glance it appears as if the scanlines from 2018 merge later, at above 85 to 90 % relative humidity than the scanlines from 2019. It has to be taken into account, though, that both measurement campaigns suggest a quite similar initial gradient of the adsorption scanlines irrespectively of the starting point. This must result in a quite complex pattern of adsorption scanlines for different r_{h0}-value as indicated in Fig.4.4 where the scanlines from 2019 are neighbouring more closely that in 2018 (Fig.4.3).

What has to be considered additionally, is that the data uncertainties as observed for the desorption isotherms may also become relevant for scanline measurements. This applies particularly where scanlines are running closely together as in some parts in Fig.4.4. The data from the 2019-campaign thus suggests that the individual data point may be less relevant than the general trends.

As discussed earlier, the maximum achievable relative humidity amounts to 95 % for technical reasons. Other than in the campaign from 2018, the derived water content from the 2019-campaign diverges considerably at 95 %. The measurements of 2018 thus inspire more confidence than those of 2019.

Note that the linear connection of data points rather indicates a trend than a realistic feature. This becomes evident at very high relative humidities where isotherms and scanlines become strongly curved as being underpinned by data points for the adsorption isotherm between 90 and 95 % relative humidity.

Finally, from the data uncertainties concerning the desorption isotherm follows also that the measured data for the scanlines may eventually not hit the adopted analytical function for the hysteresis curves precisely. The general approach followed here with respect to finding analytical formulations for the scanlines is therefore, when in doubt, to put emphasis rather on the general characteristics than on perfect matching of the data points.

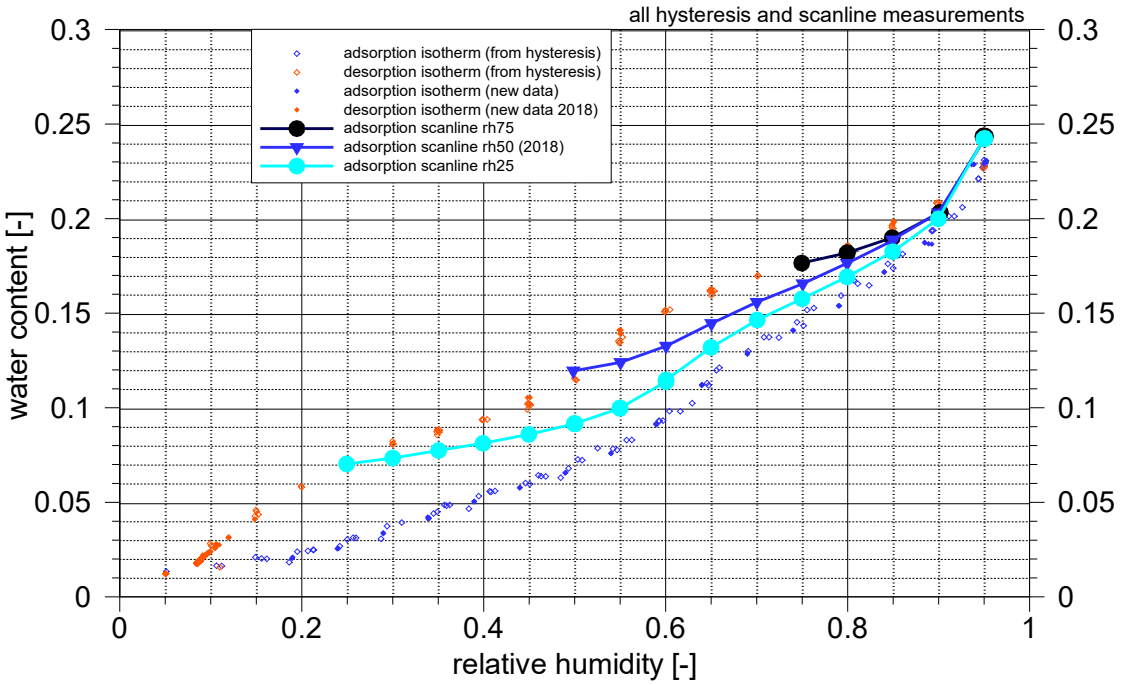

Fig. 4.3 Adsorption scanlines for MX-80 at 25 °C starting at 75, 50, and 30 % relative humidity from the 2018 measurement campaigns

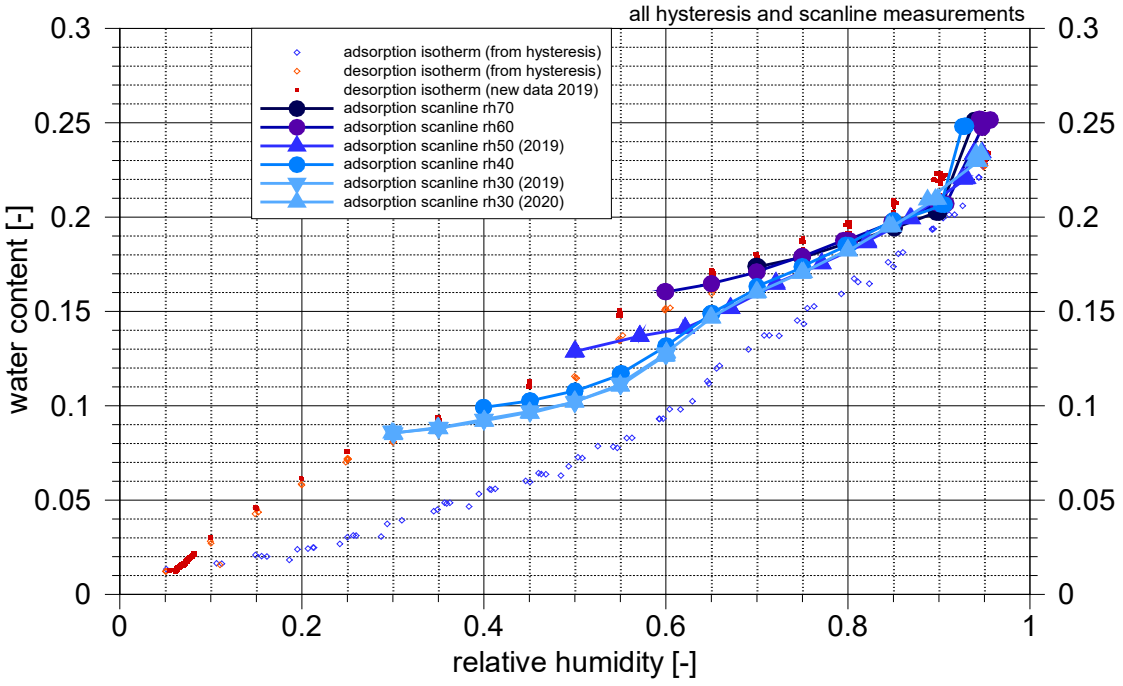

Fig. 4.4 Adsorption scanlines for MX-80 at 25 °C starting at 75, 50, and 30 % relative humidity from the 2019 measurement campaigns

4.2.1.3 Desorption scanlines

The results for the desorption scanlines including the old data for the adsorption and desorption isotherm for MX-80 at 25 °C are depicted in Fig. 4.5. It is based on five single measurement campaigns aiming exclusively at the hysteresis properties (see Appendix A, section A. 1.1) and the three measurement results from Appendix A, section A.1.3. The new data for the adsorption isotherm fit the older data quite well. The desorption scanlines look very convincing.

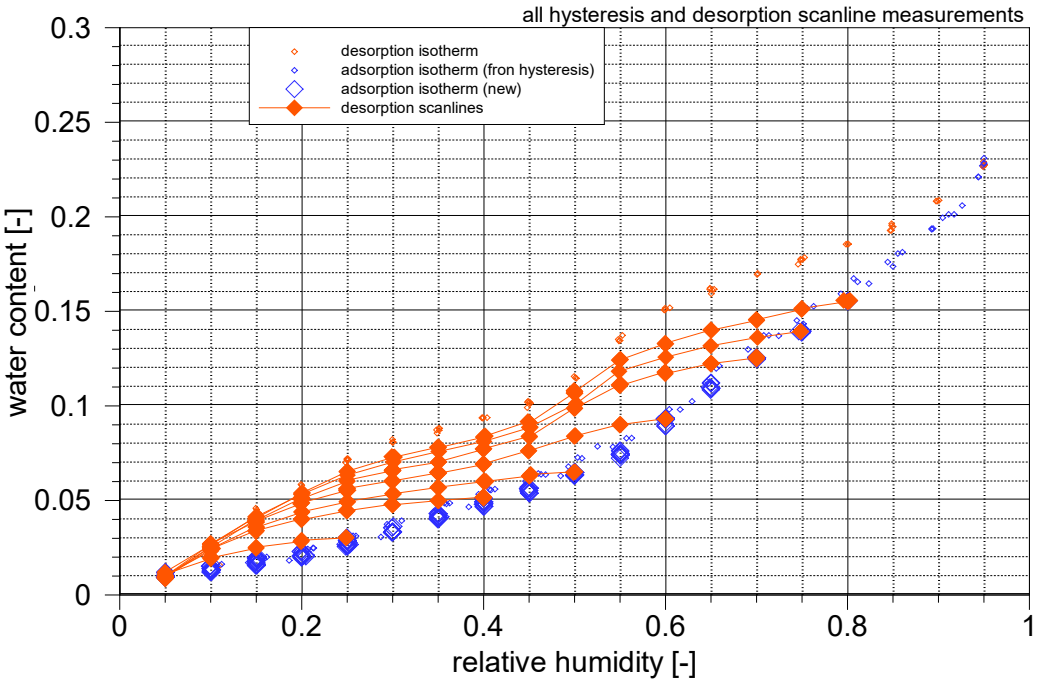

Fig. 4.5 All data on the Hysteresis of the isotherm for MX-80 at 25 °C

4.2.2 Calcigel

4.2.2.1 Additional data on the isotherms

The results for the adsorption and desorption isotherm for MX-80 at 25 °C including new data from the desorption scanline measurements are depicted in Fig.4.6. It is based on five single measurement campaigns aiming exclusively at the hysteresis properties (see Appendix A, section A.1.1) and the three measurement results from Appendix A, section A. 2.2.

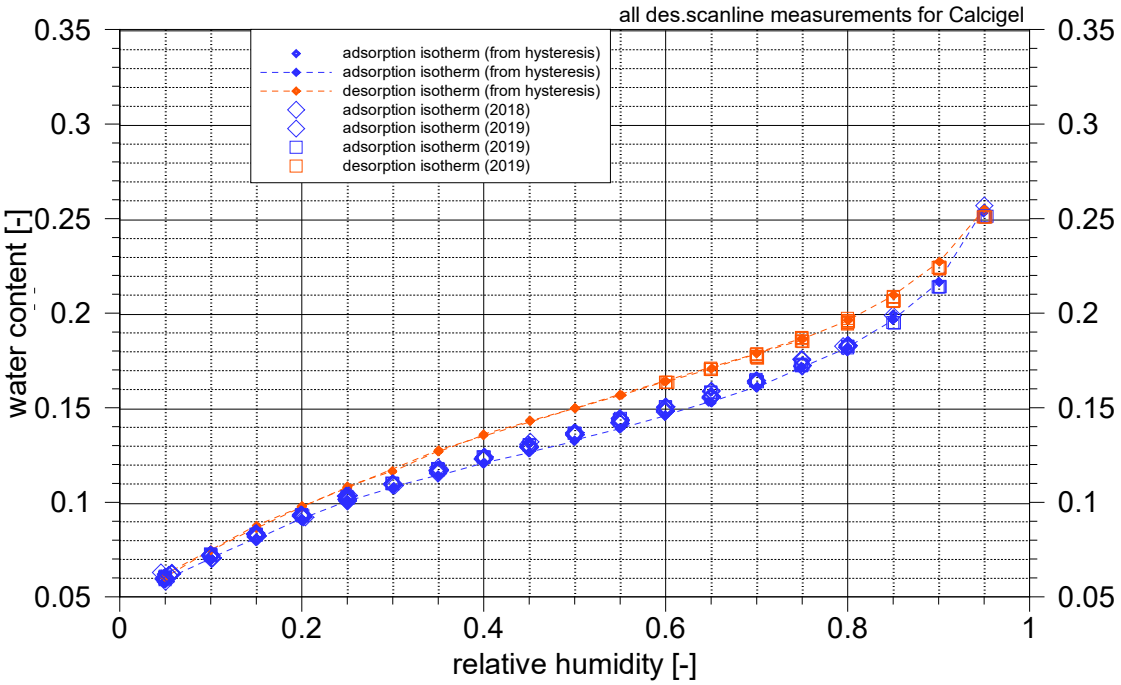

Fig. 4.6 Hysteresis of the isotherm for Calcigel at 25 °C incl. additional data

Right opposite to the results for MX-80 (see Fig. 4.1) the new results for the desorption isotherm for Calcigel fit nicely in the results from the previous isotherm measurements while the new water content data for the adsorption isotherm lie in the middle range of relative humidities up to about 0.5 % higher than the earlier data. Again, there is no apparent reason for this outcome.

4.2.2.2 Adsorption scanlines

The narrow bandwidth of the hysteresis loop for Calcigel makes it difficult to differentiate between the individual adsorption scanlines. Therefore, the results from the 2018 and the 2019 measurement campaigns are plotted separately in Fig. 4.7 and Fig. 4.8. To facilitate this even further, the new data for the adsorption isotherm are not shown in these graphs.

The general impression is similar to the observations made for the adsorption scanlines for MX-80 where the scanlines appear to be more closely bundled above a relative humidity of about 70 to 75 %. Also, the measurements of 2018 appear to be more trustworthy than those of 2019.

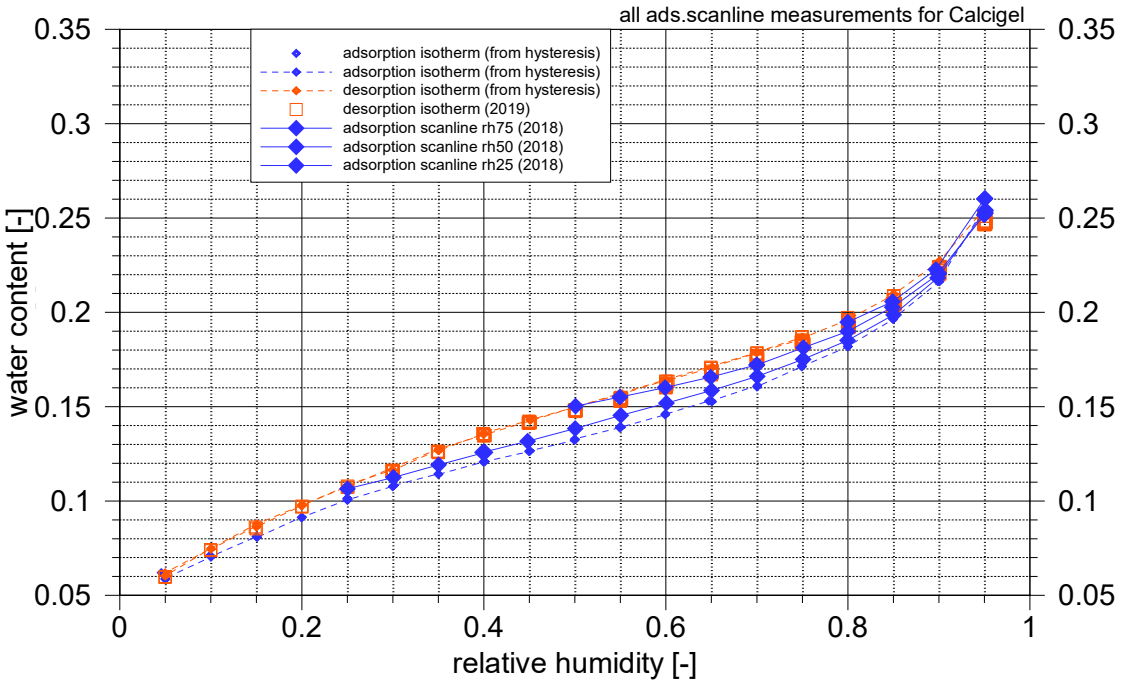

Fig. 4.7 Adsorption scanlines for Calcigel at 25 °C starting at 75, 50, and 30 % relative humidity from the 2018 measurement campaigns

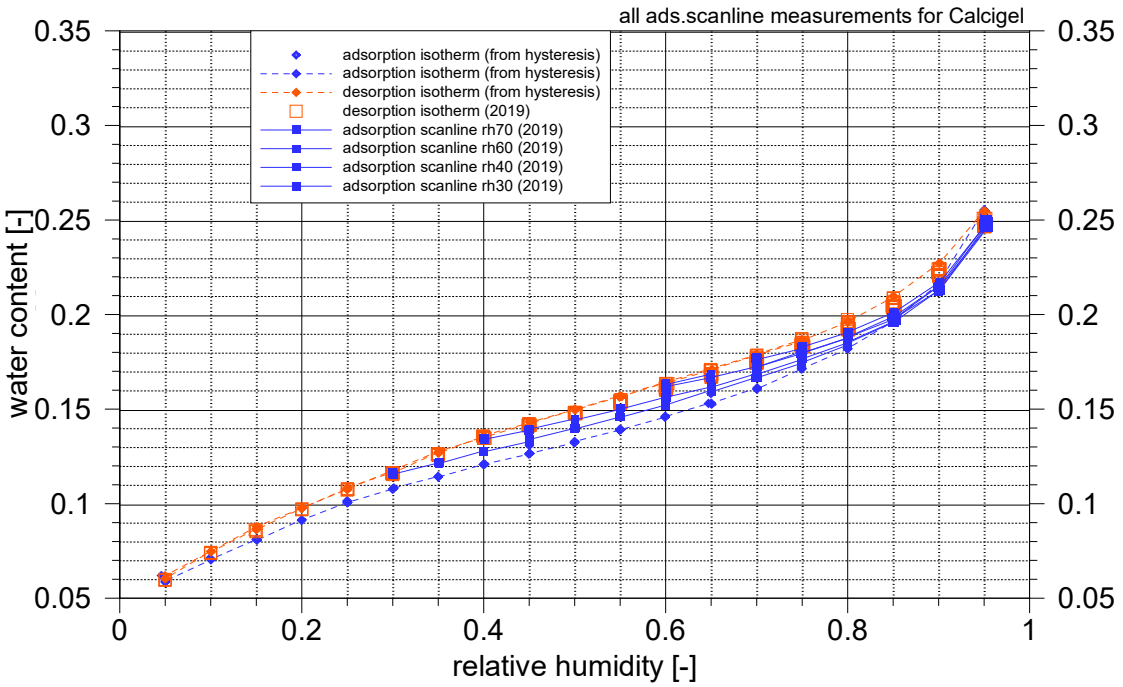

Fig. 4.8 Adsorption scanlines for Calcigel at 25 °C starting at 70, 60, 40, and 30 % relative humidity from the 2019 measurement campaigns

4.2.2.3 Desorption scanlines

With the same arguments as discussed in section 4.1.2.2 for the adsorption scanlines of MX-80 bentonite, the results for Calcigel are shown in Fig. 4.9 and Fig. 4.10 separately for the measurement campaigns of 2018 and 2019. However, a number of desorption scanlines have been measured 2019 calling for a close-up of Fig. 4.10 as depicted in Fig. 4.11.

Two characteristics can be observed from the desorption scanlines: there is a certain bundling of curves below 50 to 60 % relative humidity and there is a close approximation of scanlines towards the desorption isotherm between 25 % and 40 % relative humidity. This approximation is more pronounced than in the desorption scanlines of MX-80.

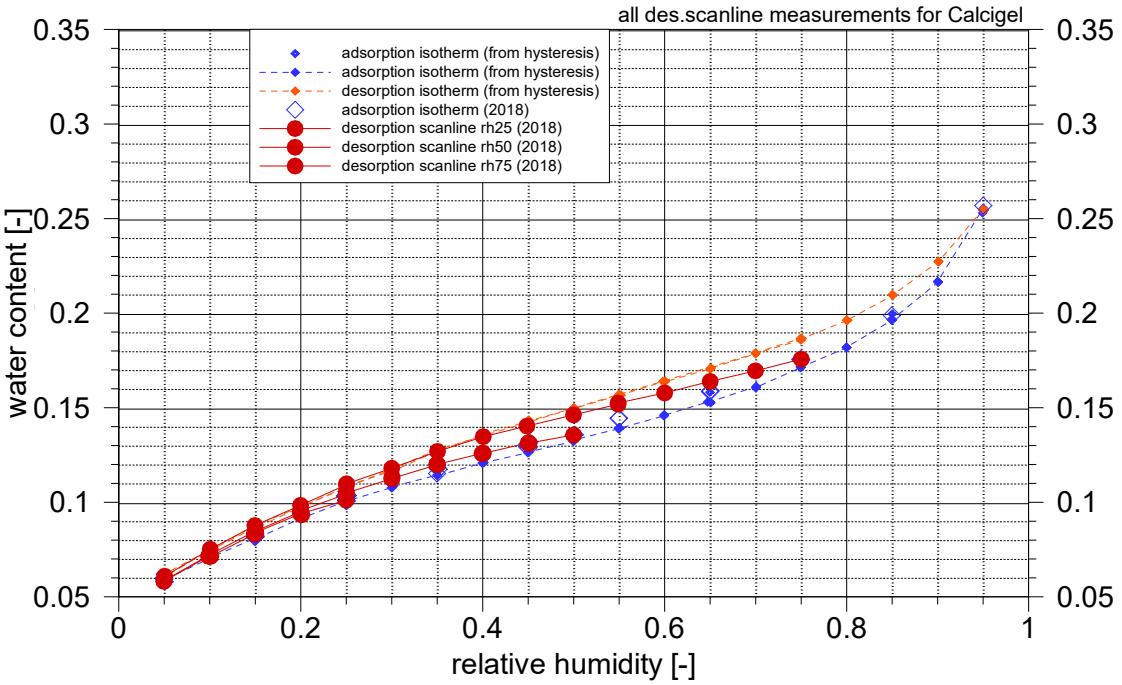

Fig. 4.9 Desorption scanlines for Calcigel at 25 °C starting at 75, 50, and 30 % relative humidity from the 2018 measurement campaign

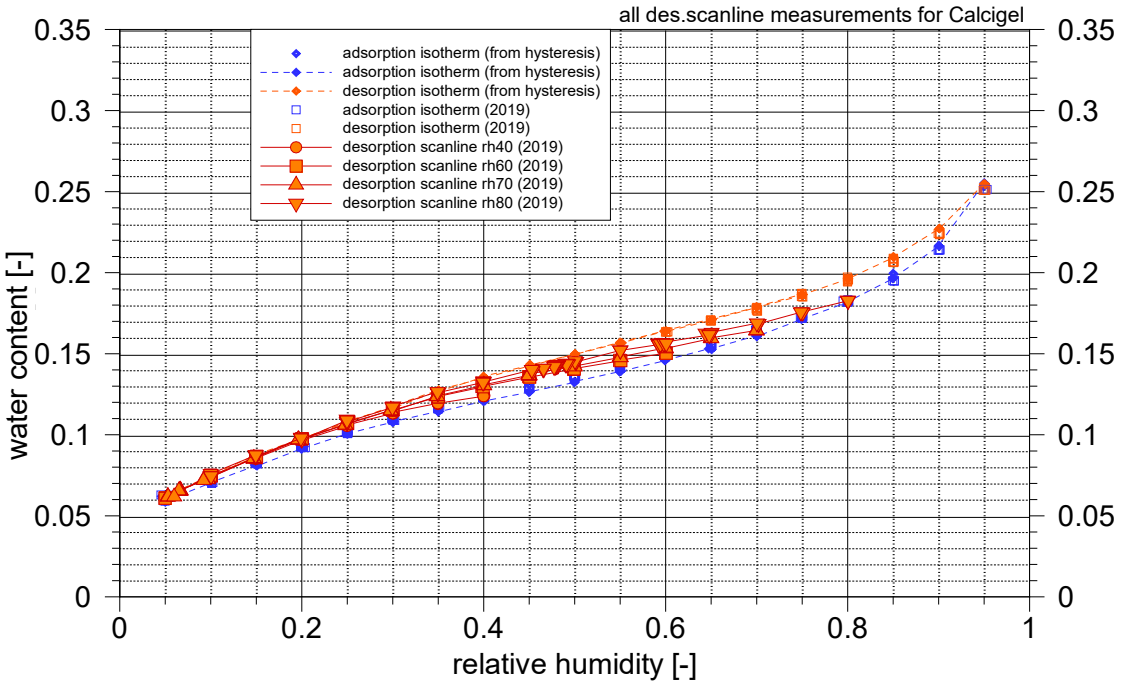

Fig. 4.10 Desorption scanlines for Calcigel at 25 °C starting at 75, 50, and 30 % relative humidity from the 2019 measurement campaign

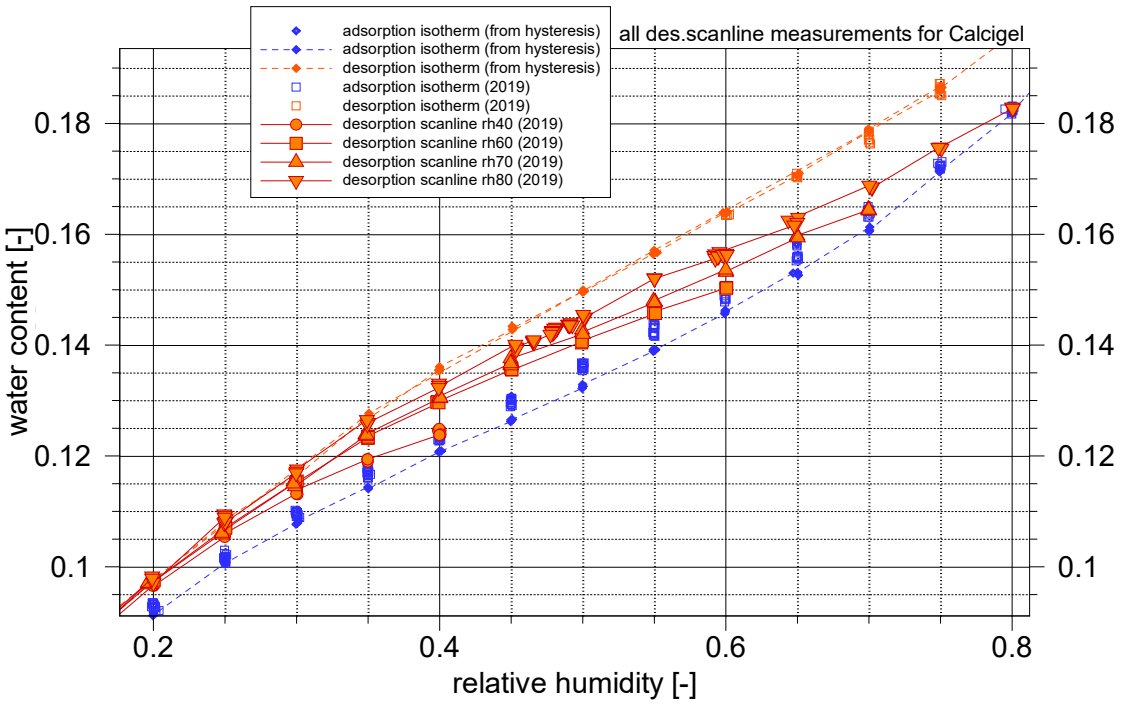

Fig. 4.11 Desorption scanlines for Calcigel at 25 °C starting at 75, 50, and 30 % relative humidity from the 2019 measurement campaign; close-up

4.3 Analytical functions

4.3.1 Principle considerations

The bounding isotherms are simply functions describing the dependence of the water content on the relative humidity. Scanlines, by contrast, form two families of functions – adsorption and desorption scanlines – that require each an additional free parameter with a one-to-one relation to a specific scanline. This parameter is ad hoc defined here as the relative humidity at the point where a desorption scanline branches off the adsorption isotherm or the adsorption scanline branches off the desorption isotherm, respectively. Such a point can be clearly identified and described by the related relative humidity r_{h0}. Subsequently, this point is called the "starting point of a scanline".

The range of possible starting points is obviously the same as the range of the relative humidities. The extreme values at both ends of the spectrum, however, have a special meaning. The starting point $r_{h0} = 0$ for an adsorption scanline actually describes the adsorption isotherm while $r_{h0} = 1$ simply represents the endpoint of the adsorption isotherm. Analogously, the desorption scanline with the starting point $r_{h0} = 0$ is the endpoint of the desorption isotherm.

A bit more complex is the matter of the starting point $r_{h0} = 1$ of a desorption scanline. Theoretically, this scanline would describe the desorption isotherm. However, at full vapour saturation ($r_h = 1$) the isotherms show the characteristics of a singularity. In fact, for free swelling bentonite there appears to be no clear equilibrium water content at 100 % relative humidity. The measurements from the literature usually do not exceed a humidity value of 97 to 98 % but indicate a water content at free swelling conditions that could lie in the range of 100 % or even higher. Any definition of a desorption scanline with the starting point $r_{h0} = 1$ would therefore be somewhat arbitrary. However, desorption scanlines with starting points above $r_{h0} = 0.95$ are not considered relevant in this work, anyway, as discussed earlier in section 3.1.1.

The isotherms can nevertheless be interpreted as particular cases of the scanlines. For usage in a simulation code it appears therefore to be advantageously if the mathematical formulations for the scanlines include the isotherms as a special case.

4.3.2 MX-80

In general, the isotherms for MX-80 bentonite are quite complex. This applies even more so to the family of adsorption scanlines which is reflected in the mathematical formulation (4.1). Formulation (4.1) consists of a comparatively simple basic equation, listed on top, with a large amount of auxiliary equations.

$$w_{scan\,ads} = {\xi_m}^3 * w_1 + \left(1 - {\xi_m}^3\right) * w_2$$

$$\xi_m = (1 - g) * \frac{r_{h\,05} - r_h}{r_{h\,05} - r_{h0}}$$

$$g = \frac{sign(r_h - r_{h\,05}) + 1}{2}$$

$$r_{h\,05} = \left(r_{h0} + \left\{[1 - 0.5^{(2 * r_{h0})}] * (1 - r_{h0}) - 4 * r_{h0} * (1 - r_{h0})^{30}\right\}\right)^2$$

$$w_1 = w_{iso\,des\,0} + (0.04 + 0.08 * r_{h0}) * \Delta r_h + 0.2 \cdot 10^{(4 * r_{h0} - 1)} * {\Delta r_h}^{(4 * r_{h0} + 1)}$$

$$\Delta r_h = r_h - r_{h0}$$

$$w_{iso\,des\,0} = w_{iso\,des}(r_{h0})$$

$$w_2 = w_{iso\,des} - (w_{iso\,des} - w_{iso\,ads}) * f$$

$$w_{iso\,ads} = w_{iso\,ads}(r_h)$$

$$w_{iso\,des} = w_{iso\,des}(r_h)$$

$$f = 1 - a - \xi_p * \left(1 - \xi_p\right) * 0.5 * a^{0.1}$$

$$a = (1 - \xi_a)^m$$

$$m = \frac{0.5}{r_{h0}}$$

(4.1)

$$\xi_p = h * \frac{(r_h - \sqrt{r_{h\,05}})}{(1 - \sqrt{r_{h\,05}})}$$

$$h = \frac{sign(r_h - \sqrt{r_{h\,05}}) + 1}{2}$$

$$\xi_a = \frac{(r_h - r_{h0})}{(1 - r_{h0})} * (1 + 15 * r_h * (1 - r_h)^{15})$$

Formulation (4.1) has been adapted according to the data points that were available from the measurements. Fig. 4.12 shows the bounding isotherms with dashed lines and a selection of adsorption scanlines with starting points at an interval of 5 % relative humidity indicating the general layout of the family of adsorption scanlines. Note that the scanline for $r_{h0} = 0$ is identical with the adsorption isotherm.

Exemplarily, data points from the measurements are included and the referring scanlines are highlighted with thick black lines. The match is not perfect but satisfying, particularly considering that the measured data points are affected by a little uncertainty. This becomes evident in a close-up at high relative humidities as depicted in Fig. 4.13. The deviations, however, amount to less than 1 % water content.

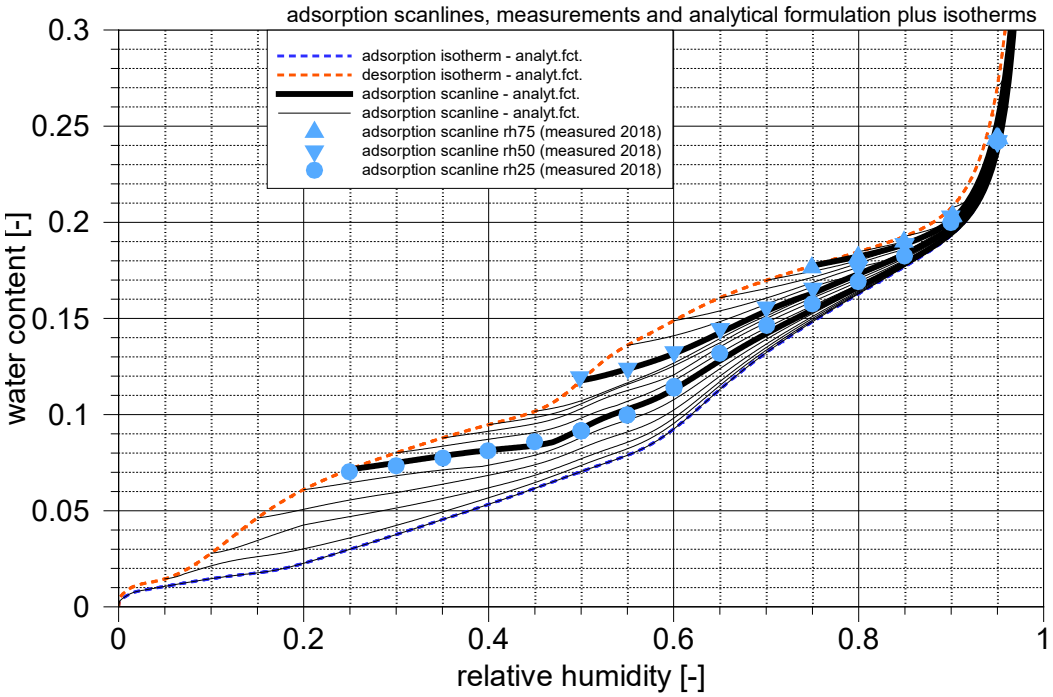

Fig. 4.12 Analytical isotherms and adsorption scanlines for MX-80 at 25 °C

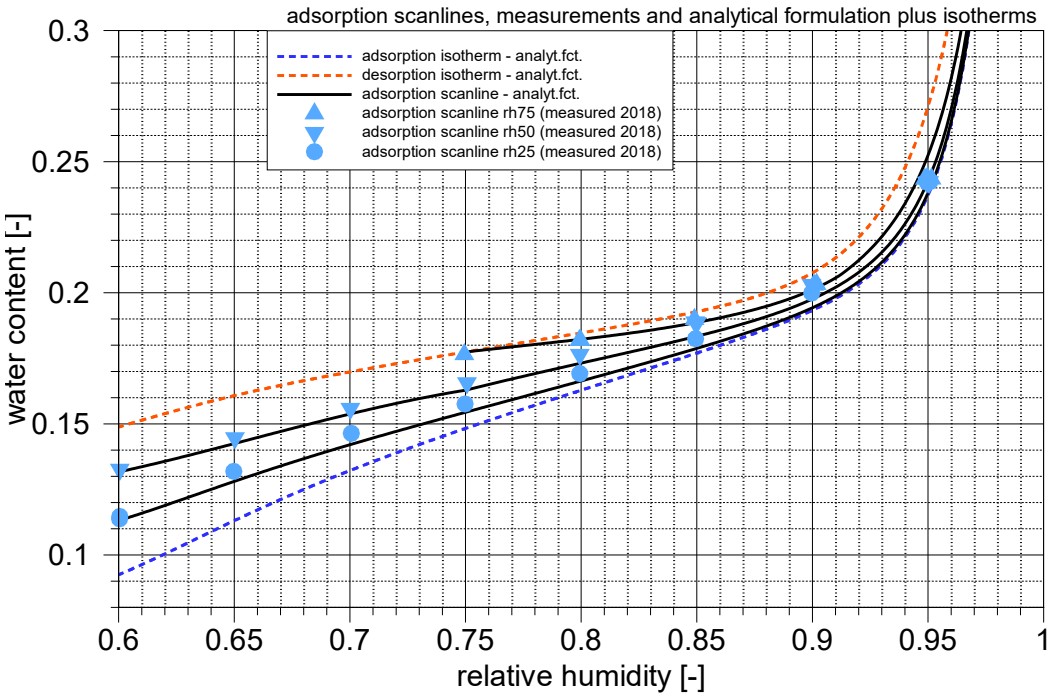

Fig. 4.13 Analytical isotherms and adsorption scanlines for MX-80; close-up

Even more difficult was, surprisingly, deriving formulation (4.2) for the desorption scanlines. Regularities in the shape of different scanlines were hard to identify. The match between measurements and formulation (4.2) that was eventually achieved, is indicated by Fig. 4.14. The plot shows selected measured data as well as desorption scanlines starting every 5 % up to 95 %, depicted in thin lines to give a general impression of the family of desorption scanlines. For comparison with the measurements, the scanlines for 25, 40, 60 and 75 % are exemplarily plotted in thick lines. Analytical formulation and measurements appear to agree reasonably well.

$w_{scan\ des}$

$$= \begin{cases} \overline{w_{scan\ des}} & for\ r_{h0} \le 0.8 \\ \left[\left(1-\hat{\xi}\right) * \overline{w_{scan\ des}} + \hat{\xi} * w_{iso\ des}\right] * f_3 + w_{iso\ ads} * (1-f_3) & for\ r_{h0} > 0.8 \end{cases}$$

$$w_{iso\ ads} = w_{iso\ ads}(r_h)$$

$$w_{iso\ des} = w_{iso\ des}(r_h)$$

$$\hat{\xi} = \frac{r_{h0}-0.8}{0.2}$$

$$f_3 = \left\{\left[\frac{1}{1+e^{\left(-200*(r_h+0.05)\right)}} + \frac{1}{1+e^{\left(-50*(r_{h0}-r_h)\right)}}\right] - 1.5\right\} * 2$$

$$\overline{w_{scan\ des}} = w_{iso\ des} - (w_{iso\ des} - w_{iso\ ads}) * \xi^{(2*r_{h0})} + f_1 + f_2$$

$$\xi = \begin{cases} \frac{r_h}{r_{h0}} & for\ r_h \le r_{h0} \\ 1 & for\ r_h > r_{h0} \end{cases}$$

$$f_1 = \begin{cases} 0.02 * {\xi_{rh0}}^2 * (1-\xi_{rh0}) & for\ r_h > 0.35\ and\ r_{h0} > 0.55 \\ 0 & otherwise \end{cases}$$

$$\xi_{rh0} = \frac{r_h-0.35}{r_{h0}-0.55}$$

$$f_2 = \begin{cases} \overline{\xi_{rh0}}^f * \left(1-\overline{\xi_{rh0}}\right)^2 * g & for\ r_h > 0.40\ and\ r_{h0} > 0.60 \\ 0 & otherwise \end{cases}$$

$$\overline{\xi_{rh0}} = \frac{r_h-0.4}{r_{h0}-0.6}$$

$$f = \begin{cases} 50 * (r_{h0}-0.85)^2 + 1.5 & for\ r_{h0} \le 0.85 \\ 1.5 & for\ r_{h0} > 0.85 \end{cases}$$

$$g = \begin{cases} 0.3 & for\ 0.60 < r_{h0} < 0.75 \\ (-2) * r_{h0} + 1.8 & for\ 0.75 < r_{h0} < 0.825 \\ 0.15 & for\ \ r_{h0} > 0.825 \end{cases}$$

(4.2)

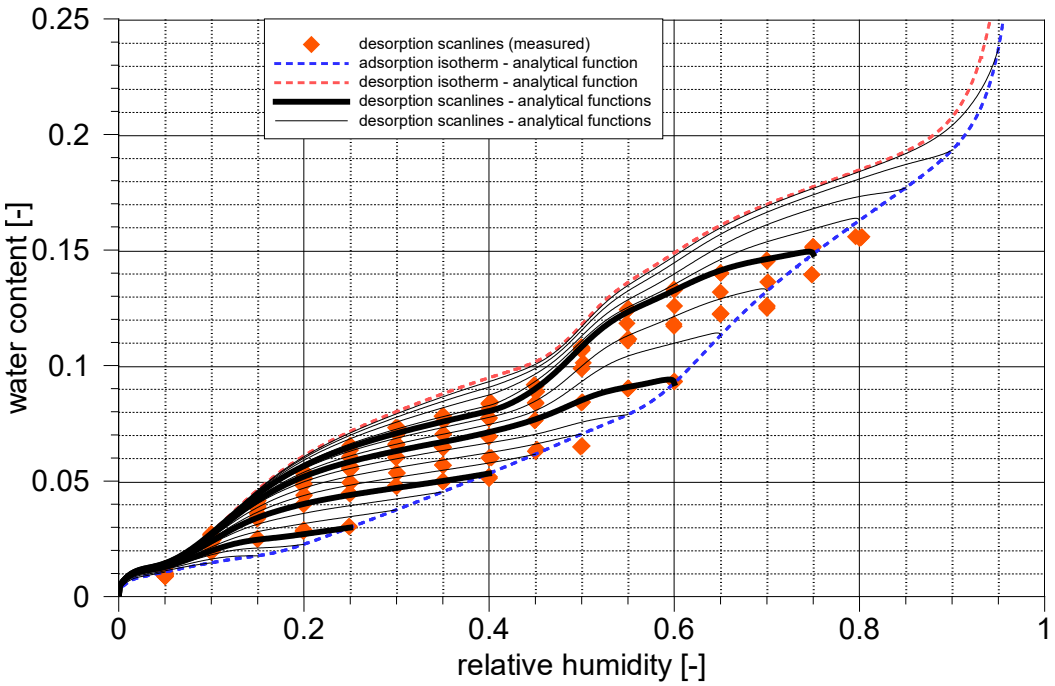

Fig.4.14 Analytical isotherms and desorption scanlines for MX-80 at 25 °C

In some cases, there is a certain mismatch between the measured starting points of the scanlines and the analytical adsorption isotherm. As discussed in subsection 4.2.1.2, this is due to uncertainties in the measurements of the isotherms as well as the scanlines.

In subsections 3.2.1 and 3.2.2 it has been shown that the shapes of isotherms and retention curves do not relate to each other in an intuitive way. To facilitate a relation of the derived scanlines to the retention curves, a comparison analogously to Fig. 3.5 is given in Fig. 4.15 and Fig. 4.16 for the adsorption and the desorption scanlines, respectively.

Note: the retention curve for adsorption is most often approximated by a capillary pressure curve after van Genuchten /VGN 80/ and the shape of the scanlines does not differ qualitatively from this isotherm as shown by Fig. 4.15. Isothermal re-saturation principally leads to an increase of water content. In practical applications, though, the initial state of saturation of the bentonite may lie somewhere between the bounding isotherms due to an uncontrolled history of drying and wetting. As a result, the water uptake follows an adsorption scanline that may mathematically also be described by the approach after /VGN 80/ but with different parameters. This observation might explain the scatter of van Genuchten-parameters that have been found from calibrating re-saturation experiments in the past /KRÖ 16/.

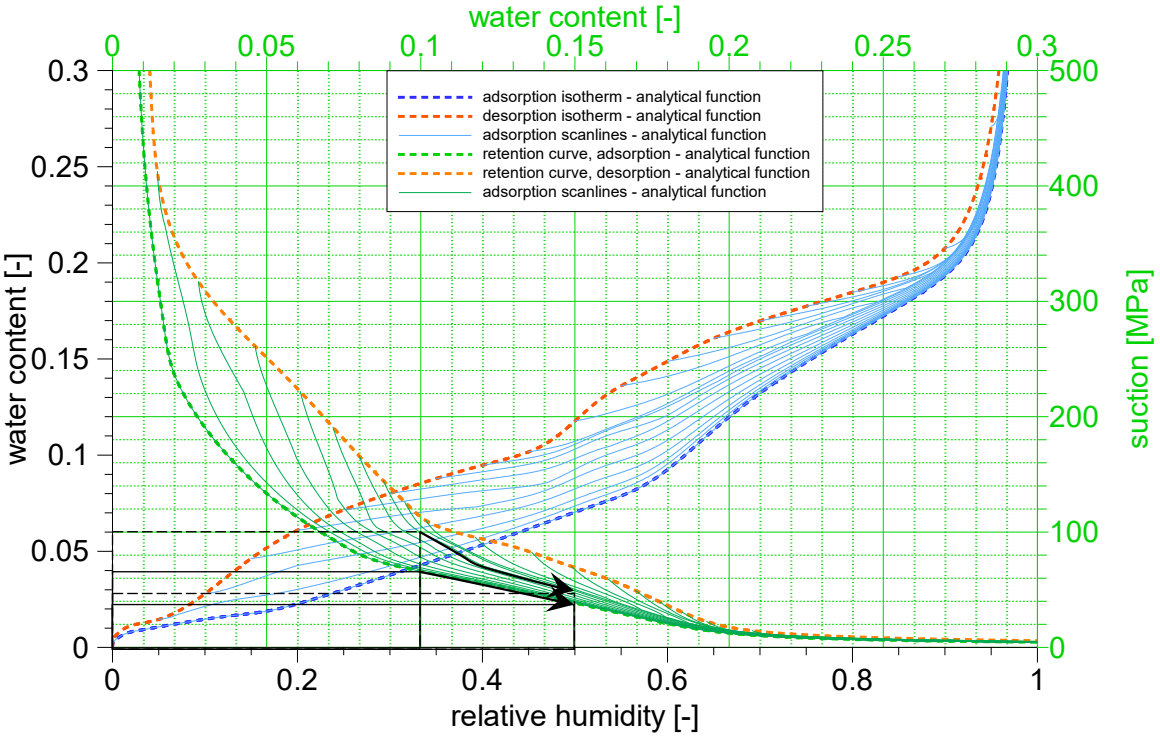

Fig. 4.15 Adsorption scanlines for MX-80 at 25 °C and equivalent retention curves

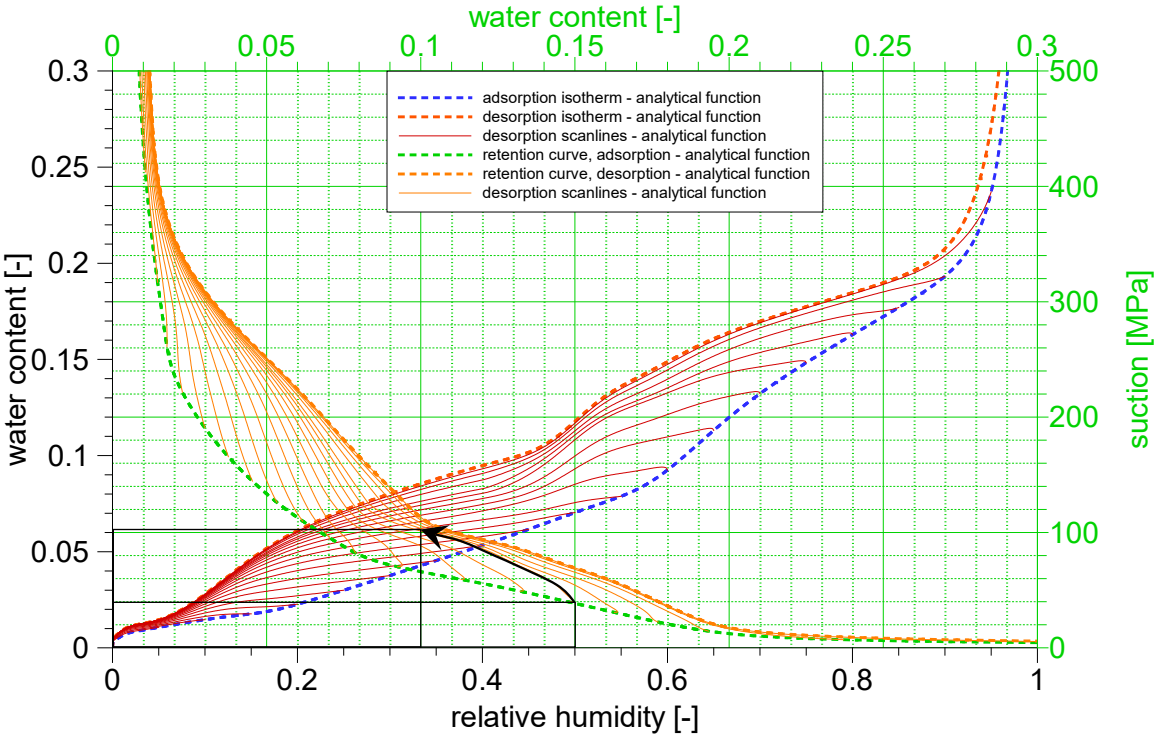

Fig. 4.16 Desorption scanlines for MX-80 at 25 °C and equivalent retention curves

4.3.3 Calcigel

The comparatively simple shape of the isotherms for Calcigel also helps to find less demanding formulations for the scanlines. The referring equations (4.3) and (4.4) for the adsorption scanlines and the desorption scanlines, respectively, were found rather quick and yet produce a sufficient match between measurements and mathematical formulation. Examples are given with Fig. 4.17 for the adsorption scanlines and with Fig. 4.18 for the desorption scanlines.

$$
\begin{aligned}
&w_{scanads} = w_{isodes} - (w_{isodes} - w_{isoads}) * \xi - f * g \\
&\quad w_{isoads} = w_{isoads}(\mathrm{r_h}) \\
&\quad w_{isodes} = w_{isodes}(\mathrm{r_h}) \\
&\quad \xi = \tfrac{(r_h - r_{h0})}{(1 - r_{h0})} \\
&\quad f = \xi^{0.8} * (1 - \xi)^{1.5} \\
&\quad g = \begin{cases} 0.12 * [(0.5 - r_{h0}) - (0.5 - r_{h0})^2] & for\ r_{h0} < 0.5 \\ 0 & for\ r_{h0} \geq 0.5 \end{cases}
\end{aligned}
\qquad (4.3)
$$

$$
\begin{aligned}
&w_{scandes} = w_{isodes} - (w_{isodes} - w_{isoads}) * \xi^3 \\
&\quad w_{isoads} = w_{isoads}(r_h) \\
&\quad w_{isodes} = w_{isodes}(r_h) \\
&\quad \xi = \tfrac{(r_h - r_{h0})}{(1 - r_{h0})}
\end{aligned}
\qquad (4.4)
$$

As the isotherms and scanlines for Calcigel let already expect, the retention curves are similar unspectacular. They are plotted in Fig. 4.19 and Fig. 4.20. Noteworthy is here the smoothness with which the scanlines approach the opposite isotherm.

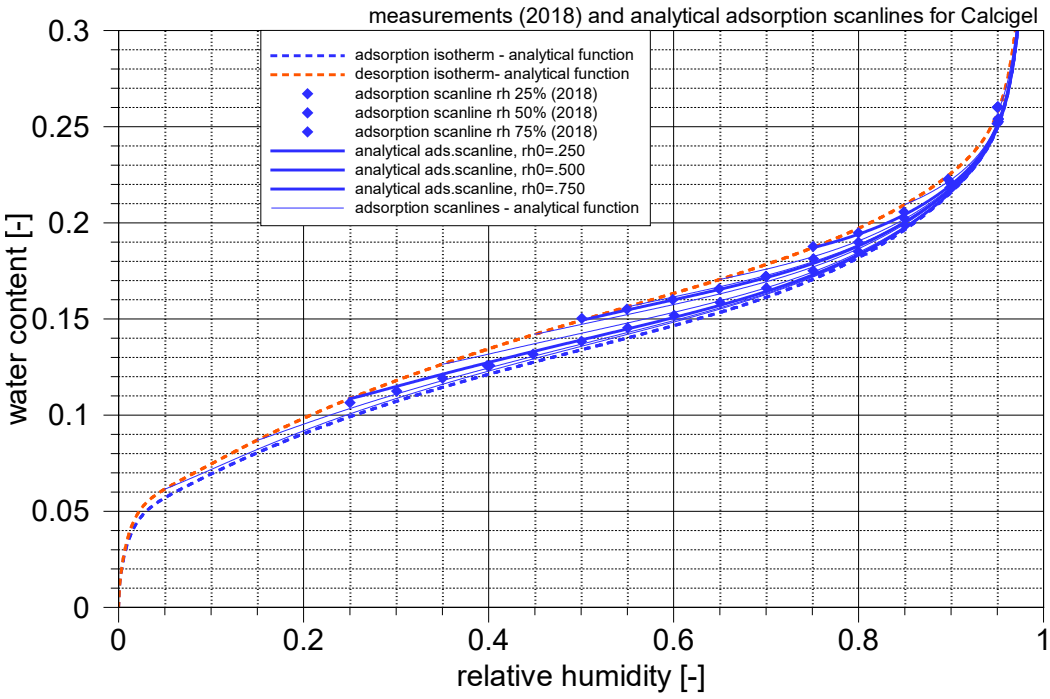

Fig. 4.17 Analytical isotherms and adsorption scanlines for Calcigel at 25 °C

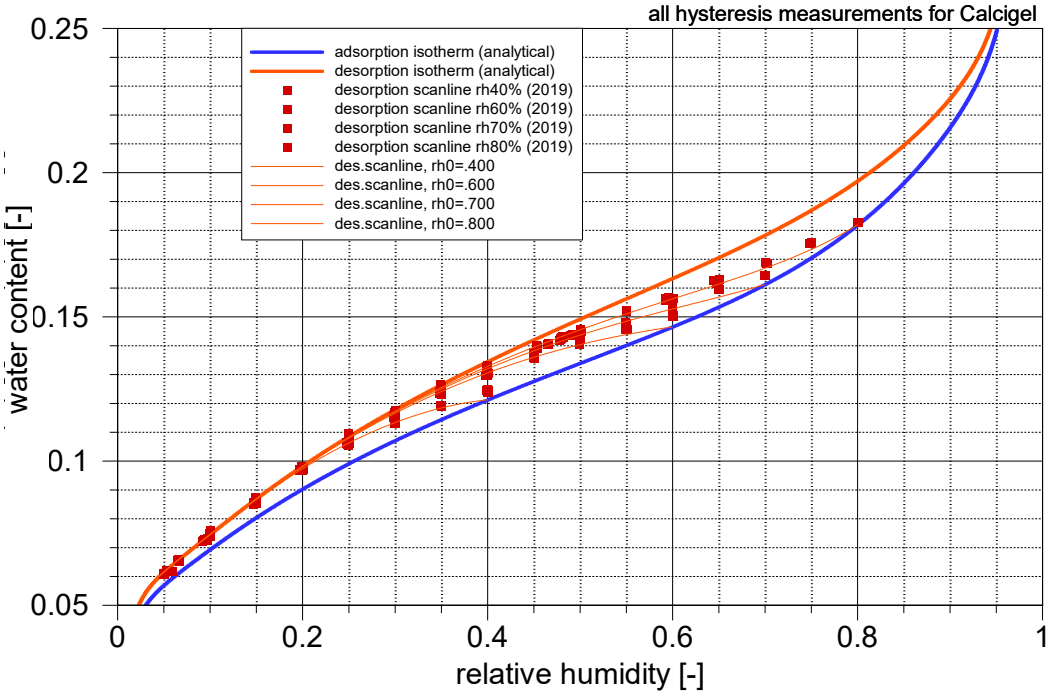

Fig. 4.18 Analytical isotherms and desorption scanlines for Calcigel at 25 °C

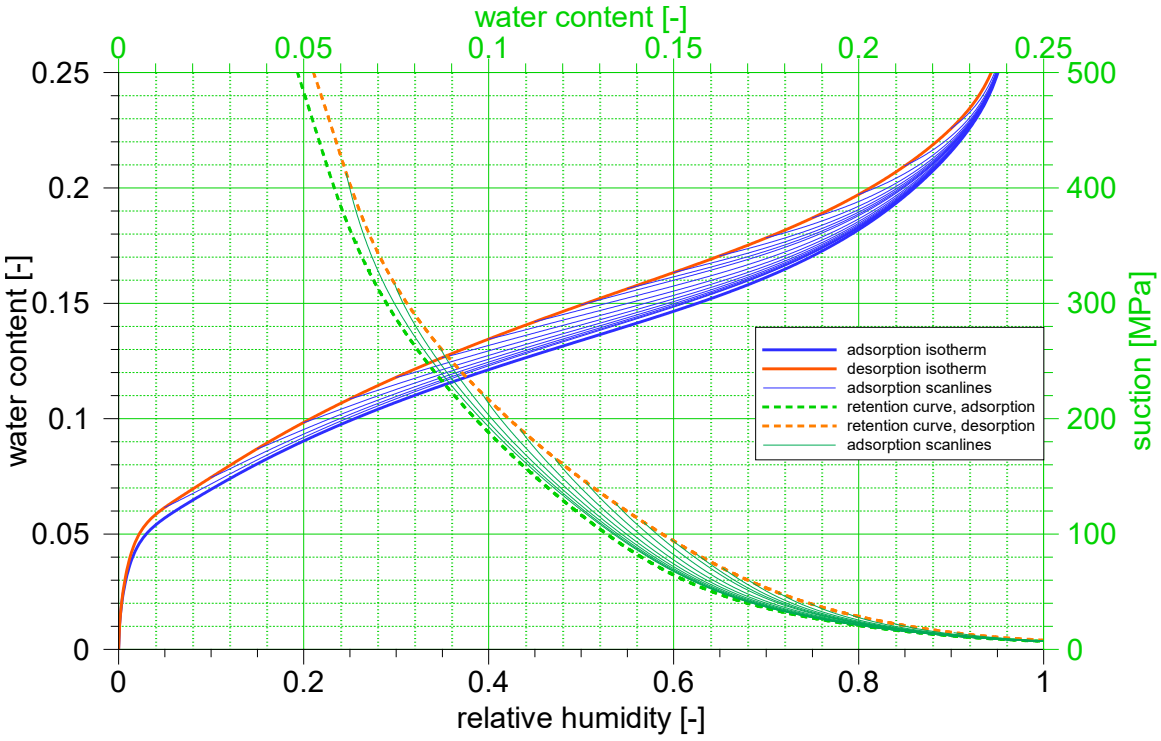

Fig. 4.19 Adsorption scanlines for MX-80 at 25 °C and equivalent retention curves

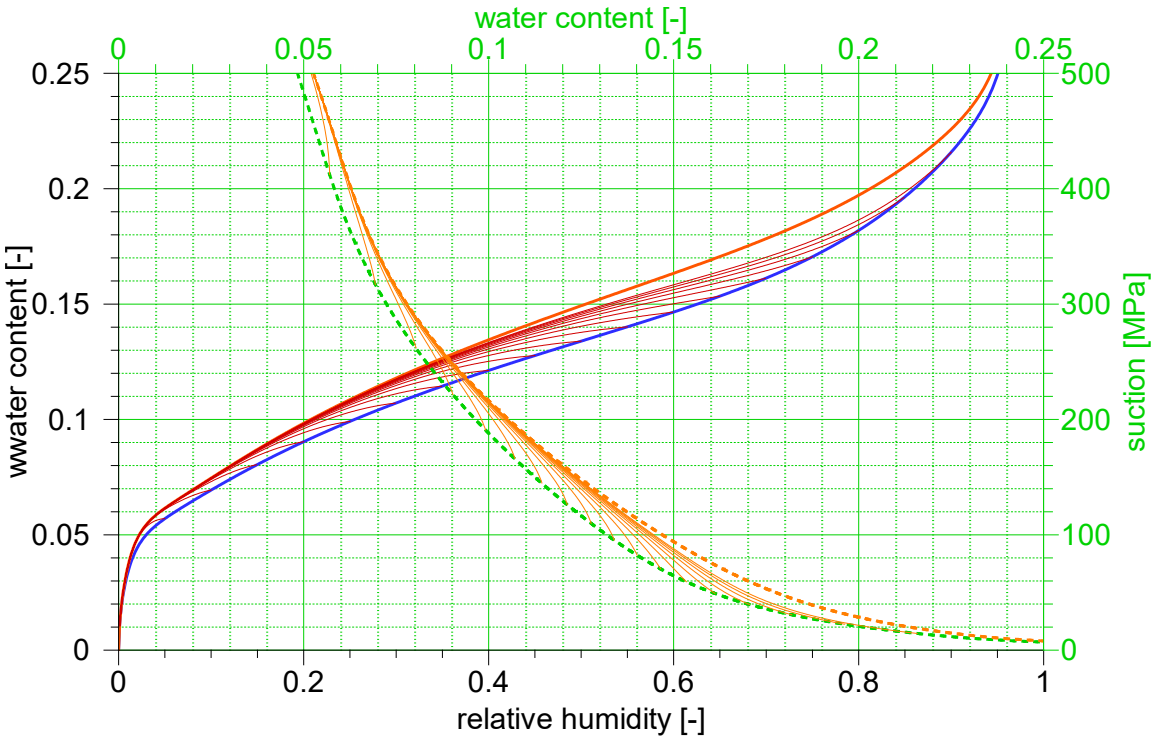

Fig. 4.20 Adsorption scanlines for MX-80 at 25 °C and equivalent retention curves

5 Dependence on temperature

5.1 Measurements up to 90 °C in an oven

5.1.1 Temperature evolution

The temperature evolution in desiccators 1 to 10 is depicted in Fig. 5.1. The adjusted temperature steps are clearly recognizable, and the temperature curves are matching each other reasonably well.

Around day 232 there had been a power loss in the laboratory that caused the valves to cut off the oven from power. This condition went unnoticed for 5 weeks (until day 266) since data from the desiccators were taken only every one to two months. During that time, the temperature in the oven dropped to ambient temperature which amounted to little less than 23 °C. Fortunately, this happened while the temperature was set to 30 °C, thus influencing the results only marginally.

Because of different problems during the first equilibration at 30 °C (see section 5.1.3), desiccators 3, 5, and 10 were taken out of the oven before heating up to 60 °C. The referring temperature data are thus showing room temperature during this heating phase. The remaining sensors except that for desiccator 8 show a very slight trend of decreasing temperature (see Fig. 5.2).

Some difficulties arose with temperature sensors in cells 6, 9 and 10. In desiccators 9 and 10 there are events where the sensors didn’t record data. In desiccator 6 the temperature sensor became displaced on day 666 and subsequently showed an increase of temperature that exceeded the maximal reading value of 125 °C. This erroneous reading lasted until the next weighing campaign on day 755 when the sensor position was eventually corrected.

The subsequent temperature steps 60 °C and 30 °C were satisfyingly stable. The overall impression from the sensor data is that the temperature could be kept constant to a sufficient degree.

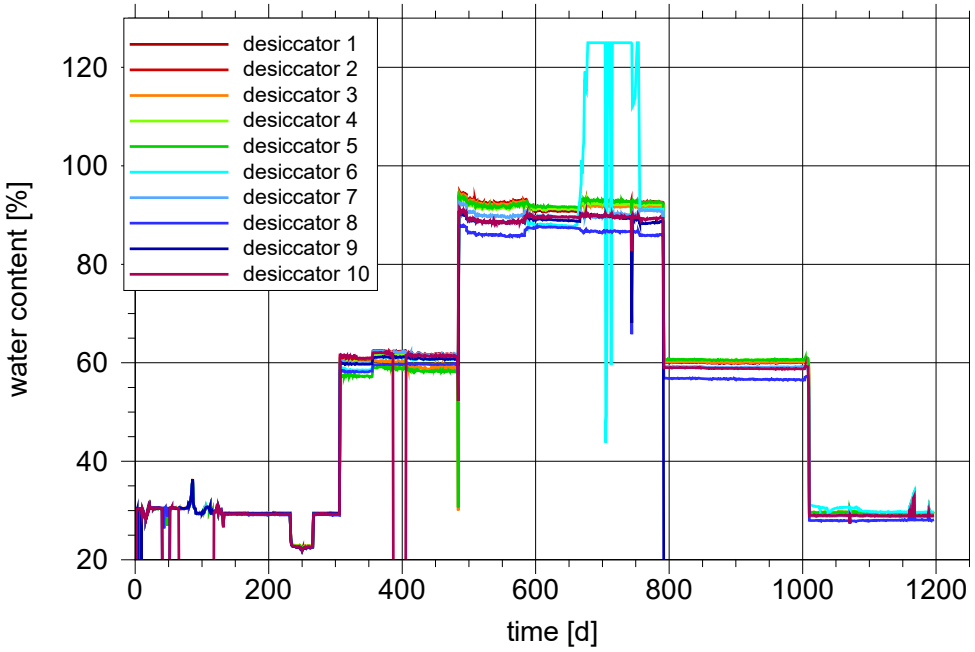

Fig. 5.1 Temperature evolution in the desiccators[6]

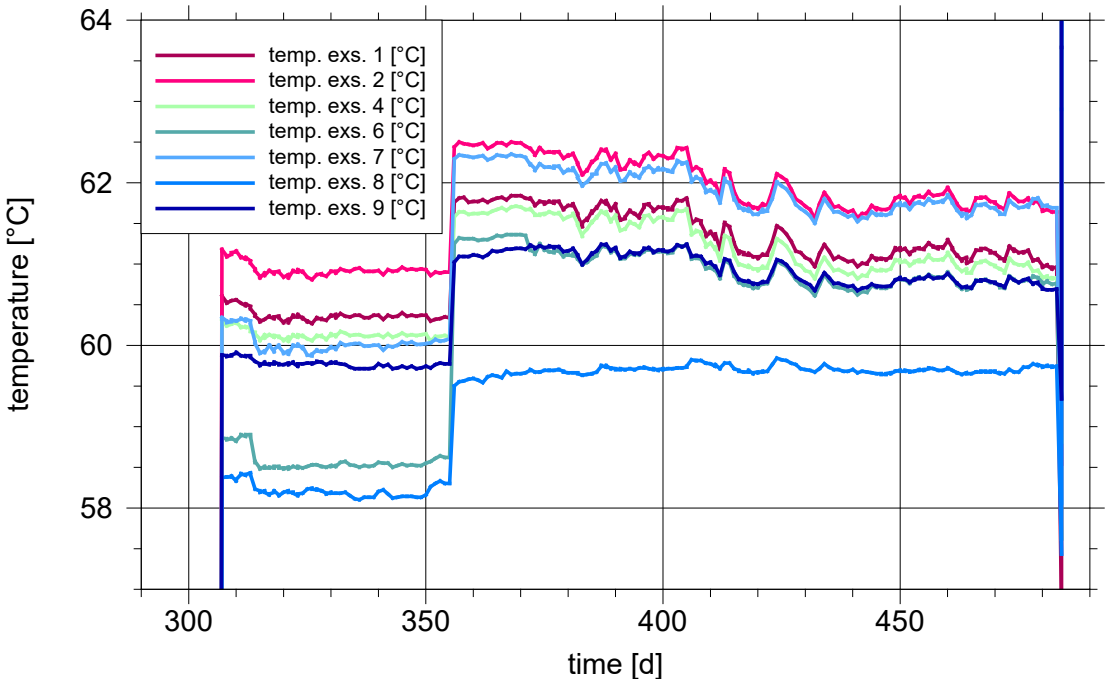

Fig. 5.2 Temperature evolution in the desiccators at 60 °C (heating phase)

[6] Due to a different data acquisition system that was used for the measurements presented in this subsection, water content and relative humidity are given here in [%] instead in the dimensionless form [-] as elsewhere in this report.

5.1.2 Stability of the desiccator atmospheres and timeline

During the test it proved to be a problem that the target relative humidities as listed in Tab. 2.1 refer to room temperature. The relative humidity over the surface of a salt solution can be highly dependent on temperature, though. A change of the equilibrium humidity as such would not seriously affect the goals of the test since the isotherms are eventually constructed from discrete data points anyway. Increase following decrease and vice versa, however, would change the hydration mode from desorption to adsorption and vice versa, thereby switching to scanlines. This sort of changes thus introduces errors in the interpretation of the equilibrium data.

In some cases, also the salt solubility increased with temperature which has led to an under-saturated solution in some cases. Where this went undetected, unstable humidity conditions followed with the same consequences as to changing relative humidity.

The timeline of the test with a view to weight measurements, temperature changes and the problems pointed out in this subsection is summarised in Tab. 5.1.

5.1.3 Relative humidity and water content

Isotherms reflect the relation between relative humidity and water content at equilibrium. At the end of each heating phase one data point should ideally be obtained from each desiccator. Note that ideally there are 10 data points per temperature step.

The relevance of these data points depends on the evolution of relative humidity and water content. In the following these conditions are discussed separately for each individual desiccator to acknowledge and evaluate the measured data. This includes

– the discussion of all humidity measurements during periods of constant temperature
– the synthesis of all data
– filtering of humidity data down to one or few data points per day; therefore, visualization by symbols without a connecting line

Tab. 5.1 Timeline of the test

Date	Runtime [days]	Prevailing temperature	Remarks
18.03.2015	0	24 °C	Putting desiccators into oven Start of data acquisition
20.03.2015	2		Temperature change
28.03.2015	10	30° C	Emplacement of the samples in desiccators Weight measurement
22.07.2015	126	30° C	Weight measurement
10.08.2015	145	30° C	Weight measurement
02.09.2015	168	30° C	Weight measurement
08.10.2015	204	30 °C	Weight measurement
05.11.2015	232	23 °C	Power failure
09.12.2015	266	23 °C	Power re-established
14.12.2015	271	30 °C	Weight measurement
06.01.2016	294	30 °C	Weight measurement
19.01.2016	307		Temperature change Remove desiccators 3,5,10 from oven New samples for desiccators 3 and 5
07.03.2016	355	60 °C	Weight measurement
07.07.2016	477	60 °C	Weight measurement
14.07.2016	484	60 °C	Putting desiccators 3, 5 and 10 into oven
16.07.2016	485		Temperature change
21.10.2016	583	90 °C	Replenishing water/salt where necessary
03.11.2016	596	90 °C	Replenishing water/salt where necessary
12.01.2017	666	90 °C	Weight measurement
10.04.2017	754	90 °C	Weight measurement Replenishing water/salt where necessary
17.05.2017	792	90 °C	Weight measurement Replenishing water where necessary Removal of desiccator 9
17.05.2017	792		Temperature change
15.12.2017	1003	60 °C	Weight measurement
18.12.2017	1006	60 °C	Replenishing water where necessary
22.12.2017	1010		Temperature change
21.02.2018	1071	30 °C	Weight measurement
03.05.2018	1142	30 °C	Weight measurement
25.06.2018	1195	30 °C	End of automatic data acquisition (T, r_h)
11.07.2018	1211	30 °C	Weight measurement
11.07.2018	1211	30 °C	Test terminated

5.1.3.1 Test preparations – days 0 to 10

On day 0, the desiccators were emplaced in the oven at ambient temperature which amounted to 24 °C. The position of the desiccators in the oven was noted. The temperature and humidity sensors in each desiccator were installed. On day 2 the oven was set

to a temperature of 30 °C and switched on. On day 10 the four samples were placed in the desiccators and the position of the four samples in each desiccator was noted as well. This ensured that the position of the desiccators in the oven as well as the position of the samples in the desiccators did not change while removed from the oven for a weight measurement.

5.1.3.2 Heating up to 30 °C – days 10 to 307

Relative humidity

As expected from the pre-tests the relative humidity in the desiccators increased very slowly, particularly at higher humidities. Constant conditions were reached between 10 and 110 days for all samples below 50 % relative humidity depending on the target humidity as shown in Fig. 5.3. All others took still up water to the extent that the atmospheres in the desiccators were affected.

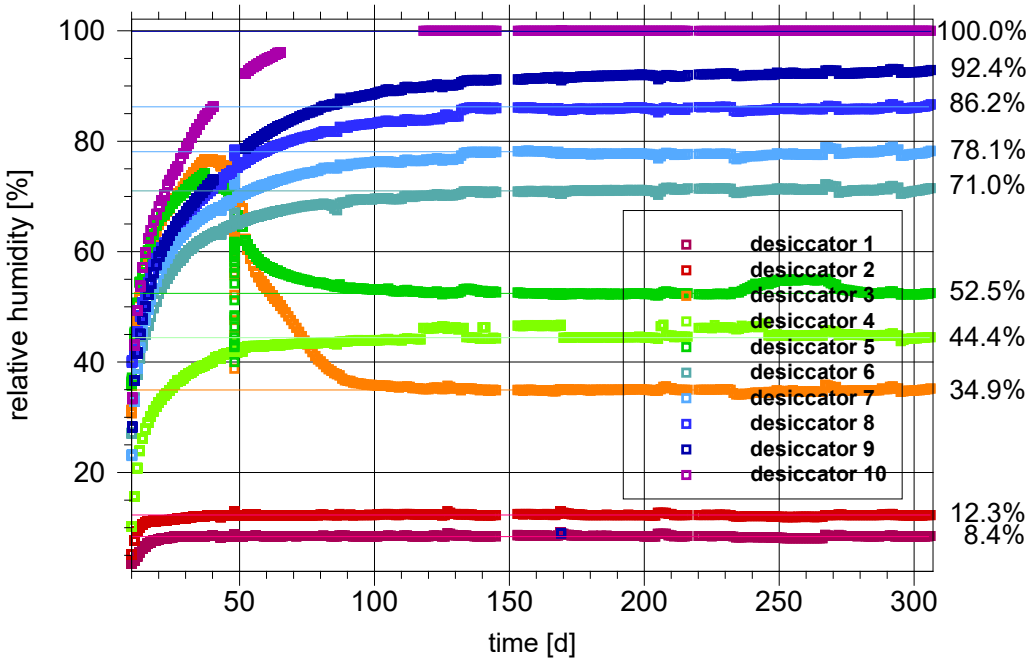

Fig. 5.3 Humidity evolution at 30 °C (days 10 to 307)

While preparing the desiccators with salt solutions an error had happened in desiccators 3 and 5. Here, salts had been used that produced far too high humidity values for about 40 days. This error was corrected immediately after discovery. Later, however, it was

suspected that the quite low water content related to the intended solutions might already have been exceeded. This would have meant that the samples would have been under desorption conditions at equilibrium. The results from these desiccators were therefore ignored for this heating step.

After about 200 days the humidity in all desiccators had more or less levelled off at about the target value. The temperature drop from 30 °C down to ambient temperature (23 °C) between days 232 and 264 had minimal effect on the prevailing humidity in the desiccators. While in most cases the humidity went down by about 0.5 % it went up by 2.5 % in case of desiccator 5 showing a solution-specific reaction.

The end value of the relative humidity measured in the desiccators was visually determined in the graph in Fig. 5.3. The target values along with the deviations for this temperature step are compiled in Tab. 5.2. All target values were met within a margin of about 3% relative humidity.

Tab. 5.2 Relative humidities in the desiccators after temperature step 1 at 30 °C

desiccator	**1**	**2**	**3**	**4**	**5**	**6**	**7**	**8**	**9**	**10**
target humidity [%]	6,0	12,0	33,0	43,0	54,0	70,0	75,0	85,0	90,0	97,0
measured humidity [%]	8,4	12,3	34,9	44,4	52,5	71,0	78,1	86,2	92,4	100,0
difference [%]	2,4	0,3	1,9	1,4	-1,5	1,0	3,1	1,2	2,4	3,0

Water content

The water content in the bentonite was fairly constant for the samples in

– desiccators 1 and 2 right from the first test on day 126 on,
– desiccator 4 after 160 days,
– desiccator 6 after 190 days, and
– desiccators 7 to 9 after 250 days (cp. Fig. 5.4).

From these data it was deduced that the samples in desiccators 3 and 5 would have reached equilibrium after about 170 days, if everything had gone according to plan. It was therefore decided to repeat the test at these two humidity levels at room temperature, thereby skipping the phase at 60 °C, and changing afterwards from room temperature directly to 90 °C.

As the bentonite in desiccator 10 had apparently not reached equilibrium at the end of temperature step 30 °C, this desiccator was treated in the same way as desiccators 3 and 5, effectively extending the 30 °C temperature step.

Accordingly, desiccators 3, 5 and 10 were removed from the oven right before increasing the temperature to 60 °C However, even after 480 days the bentonite samples in desiccator 10 still took up water (cp. Fig. 5.4).

To be noted are two final observations concerning the measurements:

– Generally, constant water content conditions were reached much later than constant humidity.
– Two measurements of water content for desiccator 5 on consecutive days resulted in a difference of about 1 % in water content.

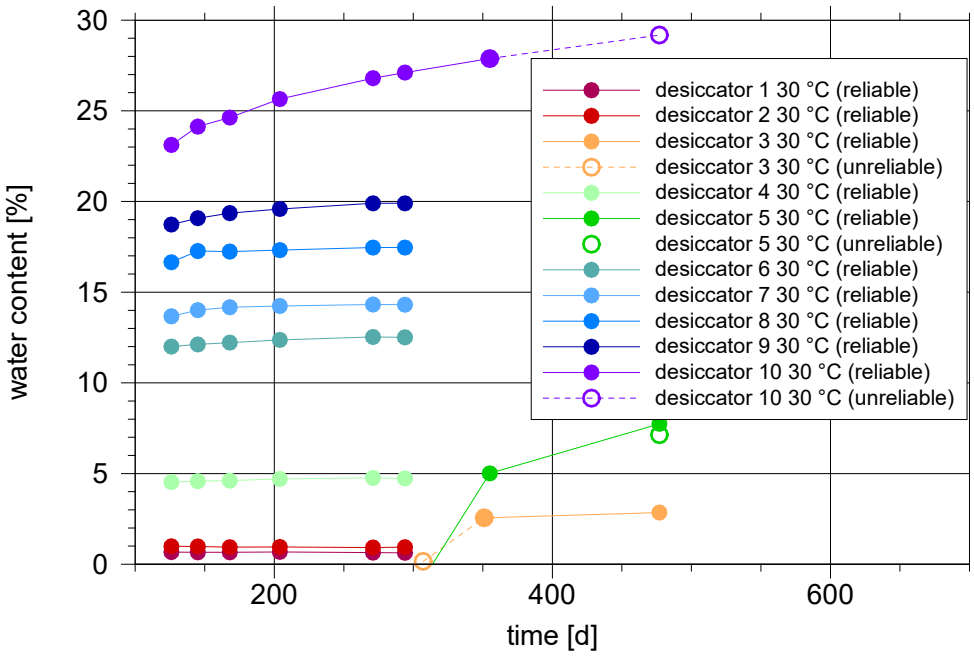

Fig. 5.4 Water content evolution during the heating phase at 30 °C

Water content at the end of the 30 °C phase was seen/assumed to be constant for all sample ensembles except for desiccator 10. The water content value for desiccator 10 is therefore somewhat unreliable. For lack of better understanding the two diverging data for the samples in desiccator 5 were averaged. The data are compiled in Tab. 5.3, the unreliable value being indicated by brackets.

Tab. 5.3 Water content data for heating at 30 °C

desiccator	1	2	3	4	5	6	7	8	9	10
target humidity [%]	6	12	33	43	54	70	75	85	90	97
water content [%]	0,63	0,94	2,9	4,7	7,7	12,5	14,3	17,5	19,9	(29,2)

5.1.3.3 Heating up to 60 °C – days 307 to 484

Relative humidity

Many curves in Fig. 5.5 show a slight trend to lower humidity that might be related to the slight decrease of temperature during this phase (cp. Fig. 5.2 in section 5.1.1). This could in turn have influenced the equilibrium humidity. The little kinks in the curves at day 355 and day 477 were caused by measurement campaigns (see Tab. 5.1).

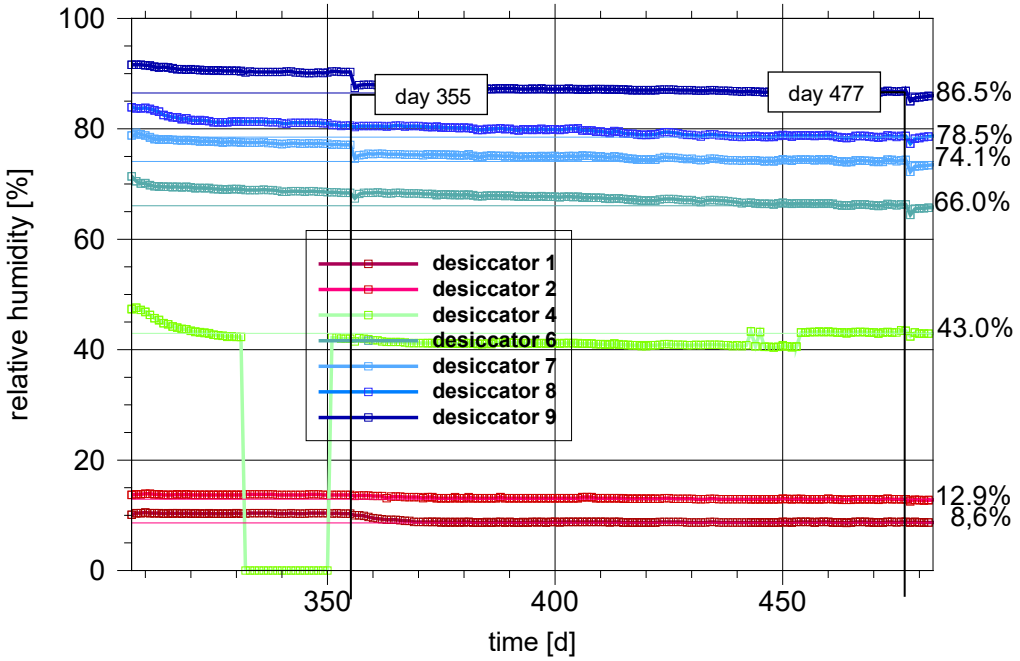

Fig. 5.5 Humidity evolution (days 307 to 484) during the heating phase at 60 °C

There are no data from desiccators 3, 5 and 10. As it turned out, it was technically much safer and easier to remove the sensors from these desiccators when taking them out of the oven than to remove the sensor cables from the insulated inlet into the oven.

The relative humidities in the desiccators at the end of the second temperature step (60 °C) are not as fitting with the target values as in the first step. The data from Tab. 5.4

show higher deviations up to 6.5 % humidity. This has not been considered to be alarming, though.

Tab. 5.4 Relative humidities in the desiccators after temperature step 2 at 60 °C

desiccator	1	2	3	4	5	6	7	8	9	10
target humidity [%]	6,0	12,0	33,0	43,0	54,0	70,0	75,0	85,0	90,0	97,0
measured humidity [%]	8,6	12,9	-	43,0	-	66,0	74,1	78,5	86,6	-
difference [%]	2,6	0,9	-	0,0	-	-4,0	-0,9	-6,5	-3,4	-

Water content

Seven desiccators were exposed to 60 °C over a period of 179 days. Judging from the previous heating phase this time span was assumed to be sufficient to reach a new equilibrium which is underpinned by the referring water content data depicted in Fig. 5.6. The data from this heating stage is summarized in Tab. 5.5.

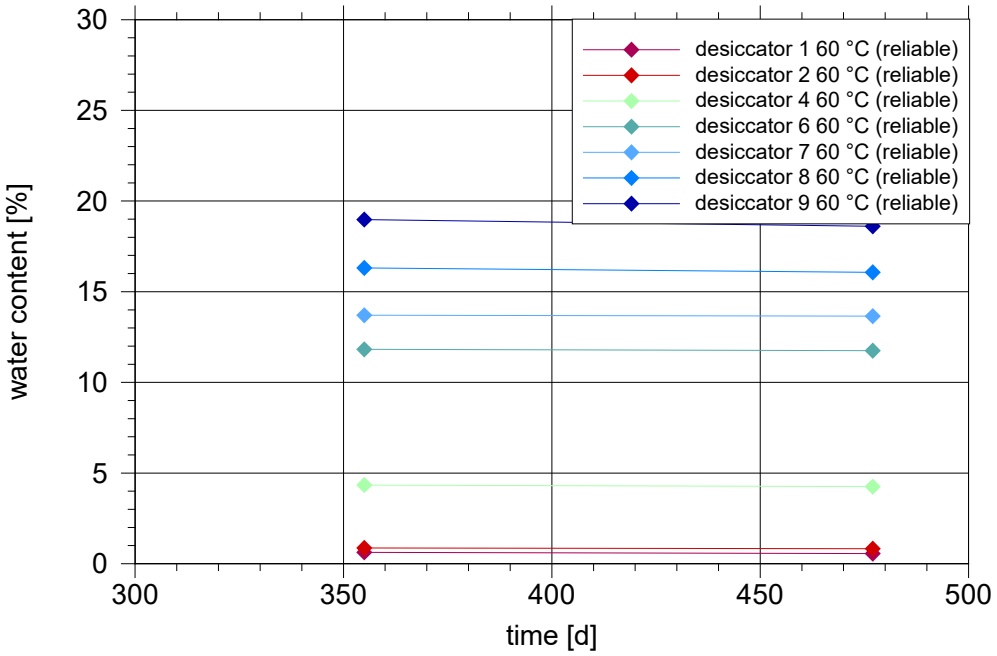

Fig. 5.6 Water content evolution during the heating phase at 60 °C

Tab. 5.5 Water content data for heating at 60 °C

desiccator	1	2	3	4	5	6	7	8	9	10
target humidity [%]	6	12	33	43	54	70	75	85	90	97
water content [%]	0,56	0,83	-	4,3	-	11,8	13,7	16,1	18,6	-

5.1.3.4 Heating up to 90 °C – days 485 to 791

Relative humidity

In comparison to the other heating periods, the evolution of relative humidity looks quite disturbed in most cases (see Fig. 5.7) for various reasons. There were technical problems with some sensors as well as with the tightness of some of the desiccators. Moreover, weighing at 90 °C was kind of problematic and seems to have seriously disturbed the samples in some instances. Then, there was the matter of the solution properties which are in some cases highly dependent on temperature, particularly the solubility of the salts. And the test was quite sensitive to single events, to weight measurements as well as to replenishing of water and/or salt (on days 596, 666 and 754, cp. Tab. 5.1).

Before this background, the measurements of relative humidity are therefore discussed for each desiccator separately. The discussions are more often than not restricted to a description since the reason for the observed patterns remained often in the dark. For better recognition, the ten curves are grouped in 4 separate plots in Fig. 5.8.

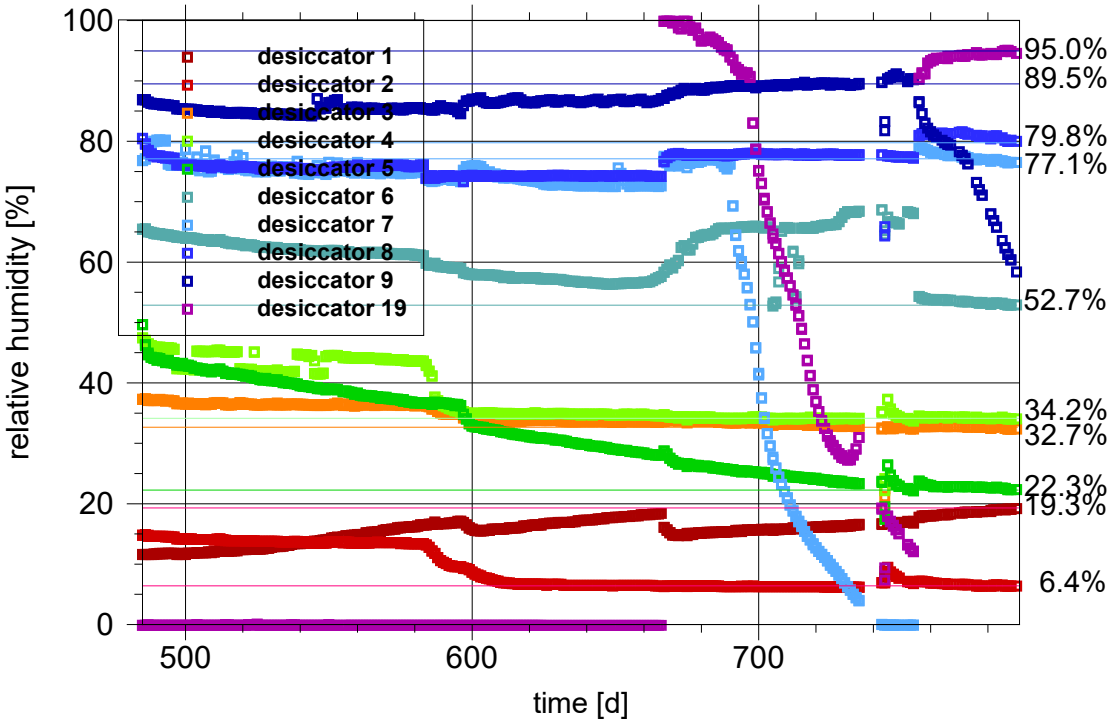

Fig. 5.7 Humidity evolution (days 485 to 791) during the heating phase at 90 °C

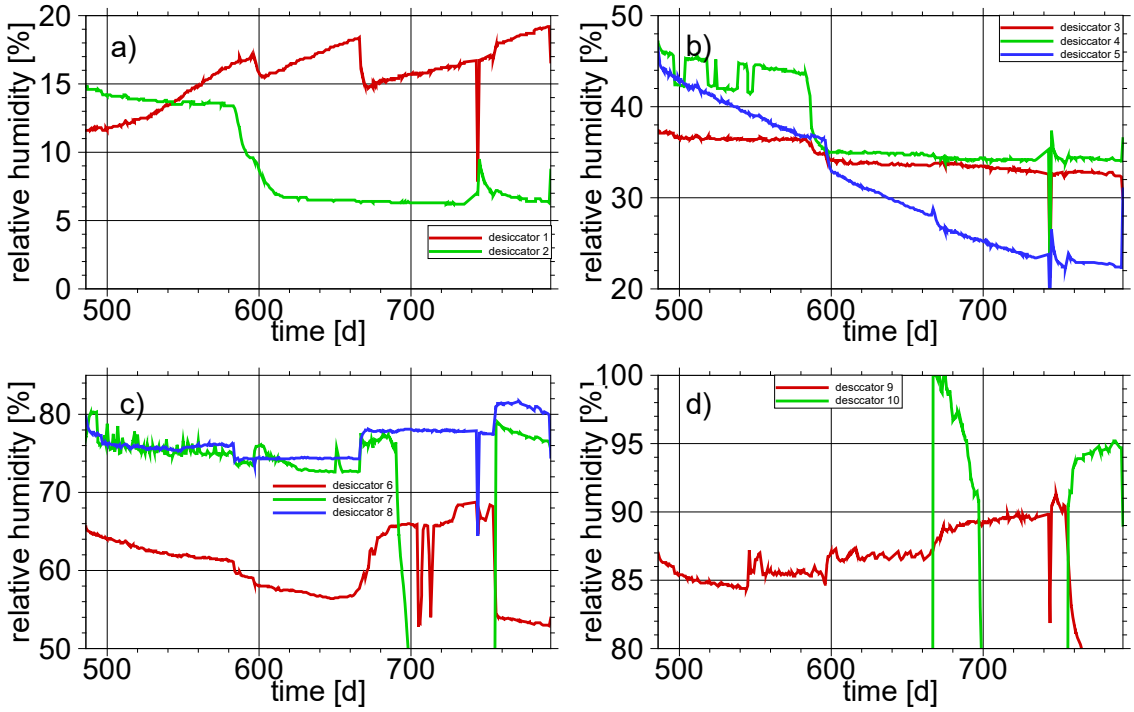

Fig. 5.8 Humidity evolution during the heating phase at 90 °C; close-ups

– Humidity in desiccator 1 (see Fig. 5.8 a)) was increasing continuously over the whole period but changed quickly by a few percent after water/salt replenishment or weight measurements (days 596, 666 and 754).
– By contrast, humidity in desiccator 2 seemed to be converging towards a certain value when it was disturbed by water/salt replenishment on day 583. A new equilibrium was approached to afterwards being just shortly disturbed again by the weight measurements on day 754 (Fig. 5.8 a)).
– Humidity in desiccator 3 was also disturbed by the replenishment on day 583 but with less impact (Fig. 5.8 b)). Otherwise only a very slight decreasing trend can be observed.
– Humidity in desiccator 4 is slightly decreasing until day 583 but this is overlain by rather abrupt decreases all of which appear to be of about the same magnitude. After replenishment the humidity is more or less constant (Fig. 5.8 b)).
– The humidity in desiccator 5 shows a distinct downwards trend to the extent that the disturbing events on days 596, 666 and 754 have comparatively little impact. During the remaining time after day 754, however, the curve is more or less horizontal (Fig. 5.8 b)).

– The pattern of the humidity curve for desiccator 6 has a pattern quite similar to that of desiccator 5 until day 666 and from day 754 on again. In between, however, there is basically a short strong increase to a much higher humidity overlain by some seemingly erratic collapse like events (Fig. 5.8 c)).
– In desiccator 7 the humidity seems to have consolidated at day 666 when it suddenly increases a few percent. Beginning with day 691, though, desiccator 7 lost water as the humidity data indicates. The reason could not be found. Water was replenished on day 754 upon which humidity reached a new peak and decreased again apparently converging to the value before the water loss (Fig. 5.8 c)).
– The humidity in desiccator 8 follows the pattern displayed for desiccator 7 without water loss (Fig. 5.8 c)).
– Also, the humidity in desiccator 9 decreases asymptotically but only until day 544 (Fig. 5.8 d)). An unknown event caused a spontaneous increase but with no subsequent changes until day 596 at which another jump upwards occurred followed again by a constant humidity. This condition was disturbed, then, by the measurement on day 666 giving rise to the humidity, this time slowly and asymptotically. With the corrections at desiccators 6 and 7 on day 754 the humidity in desiccator 9 started to decrease. At that time, the $BaCl_2$ was creeping up the walls of the desiccator on the verge of reaching the humidity sensor. Since it was learned in the meantime that this material produces highly toxic gases, the desiccator was withdrawn from the test on day 791.
– Placing back desiccators 3, 5 and 10 into the oven on day 484 – just before commencing the heating phase at 90 °C – probably damaged the relative humidity sensor of desiccator 10. This sensor was replaced during the weight measurements on day 666. In this process desiccator 10 became leaky resulting in a continuous decrease of humidity. In the end the desiccator had run dry and water was refilled on day 754.The target humidity of 100 % was not fully recovered at the end of this heating phase but missed by about 5 % (Fig. 5.8 d)).

Water content

Based on the analysis of the humidity evolution in each desiccator, a choice about the reliability of the derived water content values is made. Clearly, a good approximation of constant humidity conditions at the end of the heating phase was accomplished for desiccators 2, 3, 4, 7 and 8. Less nice but still acceptable are the results from desiccator 1 at

the end of this particular phase (day 791) and from the last weighing for desiccator 9 on day 666. Data from desiccators 5, 6 and 10, however, cannot be reliable as the relative humidity curve had a distinct gradient at the end of this temperature step indicating no equilibrium between relative humidity and water content. These data are put in brackets in the compiled data given in Tab. 5.7.

Tab. 5.6 Relative humidities in the desiccators after temperature step 3 at 90 °C

desiccator	1	2	3	4	5	6	7	8	9	10
target humidity [%]	6,0	12,0	33,0	43,0	54,0	70,0	75,0	85,0	90,0	97,0
measured humidity [%]	19,3	6,4	32,7	34,2	22,3	52,7	77,1	79,8	89,5	95,0
difference [%]	13,3	-5,6	-0,3	-8,8	-31,7	-17,3	2,1	-5,2	-0,5	-2,0

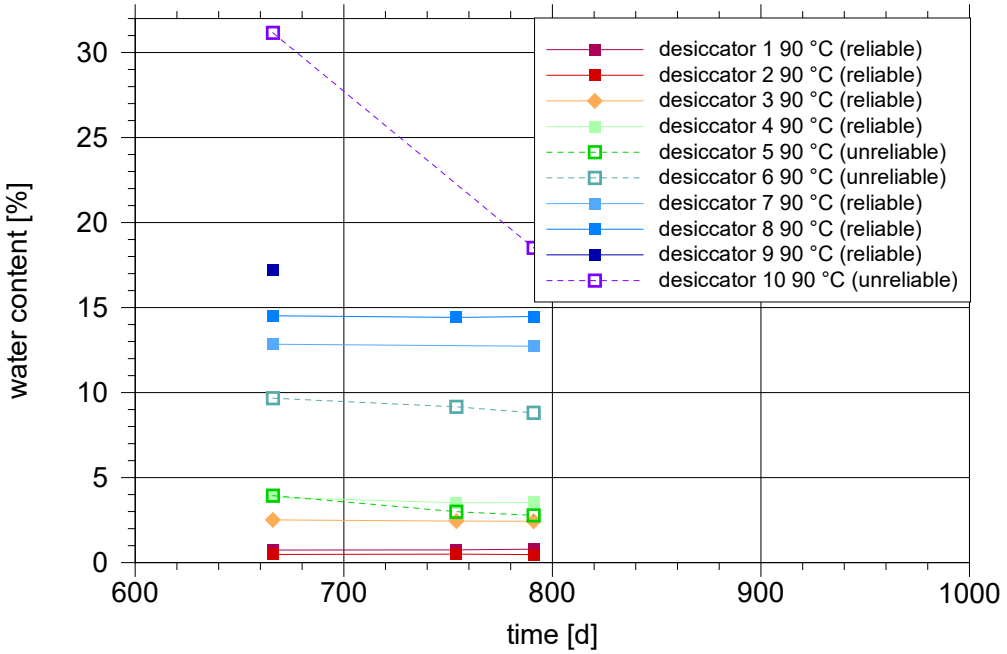

Fig. 5.0 Water content evolution during the heating phase at 90 °C

Tab. 5.7 Water content data for heating at 90 °C

desiccator	1	2	3	4	5	6	7	8	9	10
target humidity [%]	6	12	33	43	54	70	75	85	90	97
water content [%]	0,79	0,47	2,4	3,5	(3,5)	(8,8)	12,7	14,5	17,2	(18,5)

5.1.3.5 Cooling down to 60 °C – days 792 to 1010

Relative humidity

Contrary to the previous heating phase, the first cooling step down to 60 °C looks quite as desired, being marked by a more or less constant humidity during this stage (cp. Fig. 5.9). The only exception can be found with desiccator 10 where apparently some leakage occurred again. It showed effect after day 957.

Tab. 5.8 Relative humidities in the desiccators after temperature step 4 at 60 °C

desiccator	1	2	3	4	5	6	7	8	9	10
target humidity [%]	6,0	12,0	33,0	43,0	54,0	70,0	75,0	85,0	90,0	97,0
measured humidity [%]	15,7	8,7	29,6	40,5	37,4	58,9	75,8	81,3	-	89,0
difference [%]	9,7	-3,3	-3,4	-2,5	-16,6	-11,1	0,8	-3,7	-	-8,0

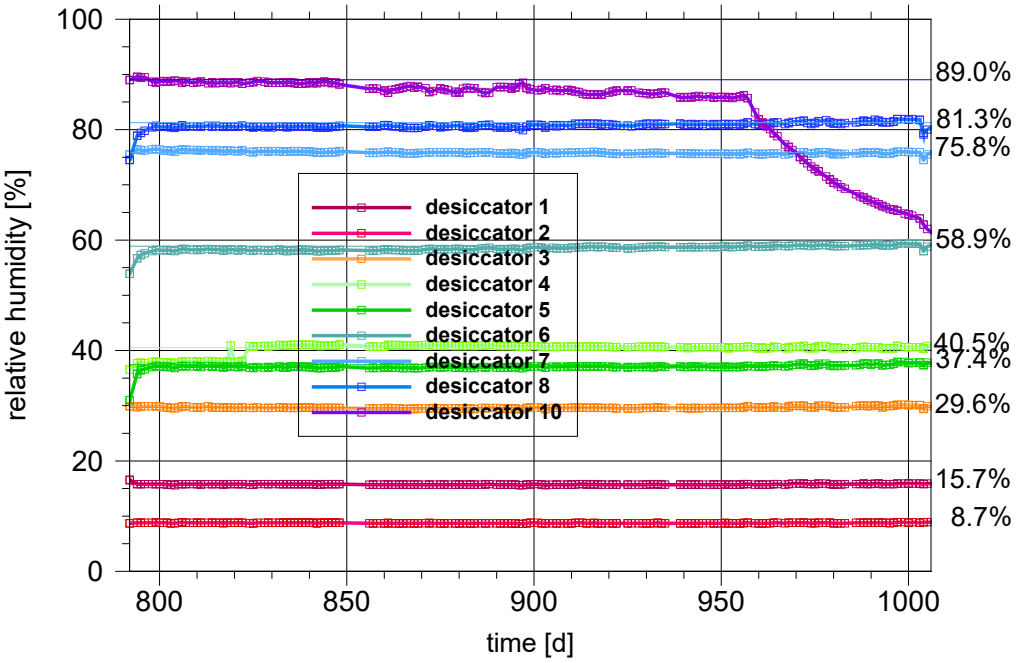

Fig. 5.9 Humidity evolution (day 792 to 1010) during the cooling phase at 60 °C

Water content

The water content value in desiccator 10 determined at the end of this temperature step was compromised by leakage and thus marked as unreliable in Tab. 5.9. All other data are considered to be reliable.

Tab. 5.9 Water content data for cooling at 60 °C

desiccator	**1**	**2**	**3**	**4**	**5**	**6**	**7**	**8**	**9**[7]	**10**
target humidity [%]	6	12	33	43	54	70	75	85	90	97
water content [%]	0,86	0,66	2,6	4,1	4,1	10,6	13,8	15,9	-	(15,4)

5.1.3.6 Cooling down to 30 °C – days 1010 to 1211

Relative humidity

Switching the temperature down to 30 °C on day 1010 had a surprisingly strong effect on the relative humidity. All humidity values increased even if to a different extent except in desiccator 2 where the humidity decreased slightly.

Also, the weight measurement on day 1071 had disturbed the humidity conditions in some cases considerably. Luckily, all but one desiccator returned to the humidity level before the disturbance. Only in desiccator 5, the humidity increased persistently by almost 20 % but at least this increase proved to be stable.

Replenishing water in desiccator 10 during the previous temperature step had apparently the desired effect as the relative humidity increased subsequently up close to the target value.

After about day 1080, all humidity measurements were remarkably stable. The end values are compiled in Tab. 5.10.

[7] Desiccator 9 had been removed during the temperature 90 °C.

Tab. 5.10 Relative humidities in the desiccators after temperature step 5 at 30 °C

desiccator	1	2	3	4	5	6	7	8	9	10
target humidity [%]	6,0	12,0	33,0	43,0	54,0	70,0	75,0	85,0	90,0	97,0
measured humidity [%]	13,2	10,5	31,9	44,8	68,0	64,3	77,0	84,6	-	98,9
difference [%]	7,2	-1,5	-1,1	1,8	14,0	-5,7	2,0	-0,4	-	1,9

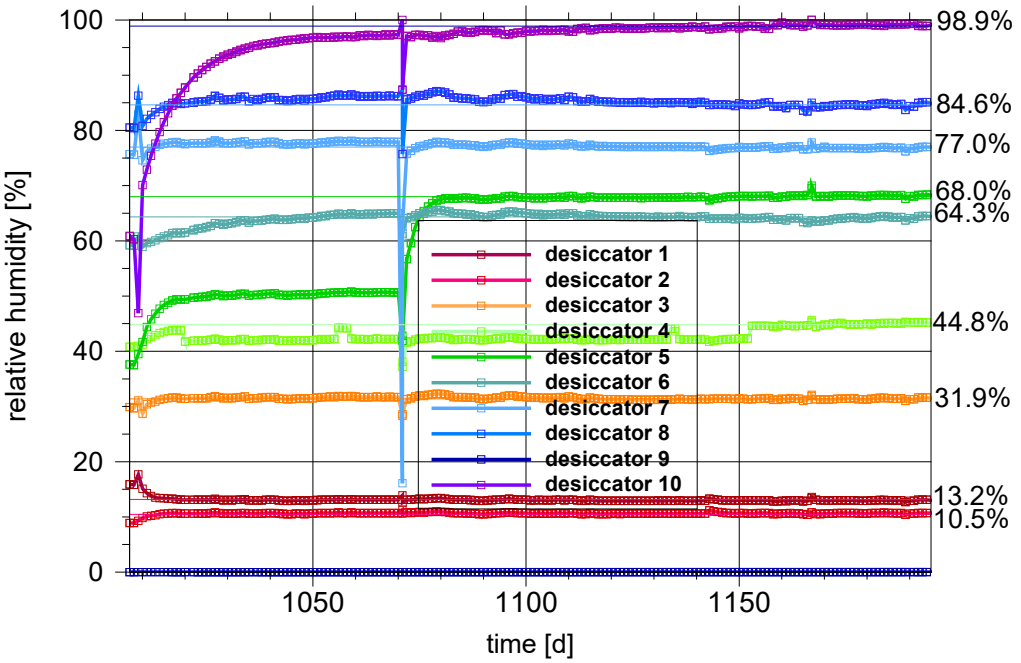

Fig. 5.10 Humidity evolution (days 1010 to 1195) during the cooling phase at 30 °C

Water content

As the humidity values were stable for two thirds of this temperature stage, all water content values listed in Tab. 5.11 are considered to be reliable.

Tab. 5.11 Water content data for cooling at 30 °C

desiccator	1	2	3	4	5	6	7	8	9[8]	10
target humidity [%]	6	12	33	43	54	70	75	85	90	97
water content [%]	0.91	0,84	2.9	4.6	13.0	12.8	14.5	17.1	-	23.8

[8] Desiccator 9 had been removed during the temperature 90 °C.

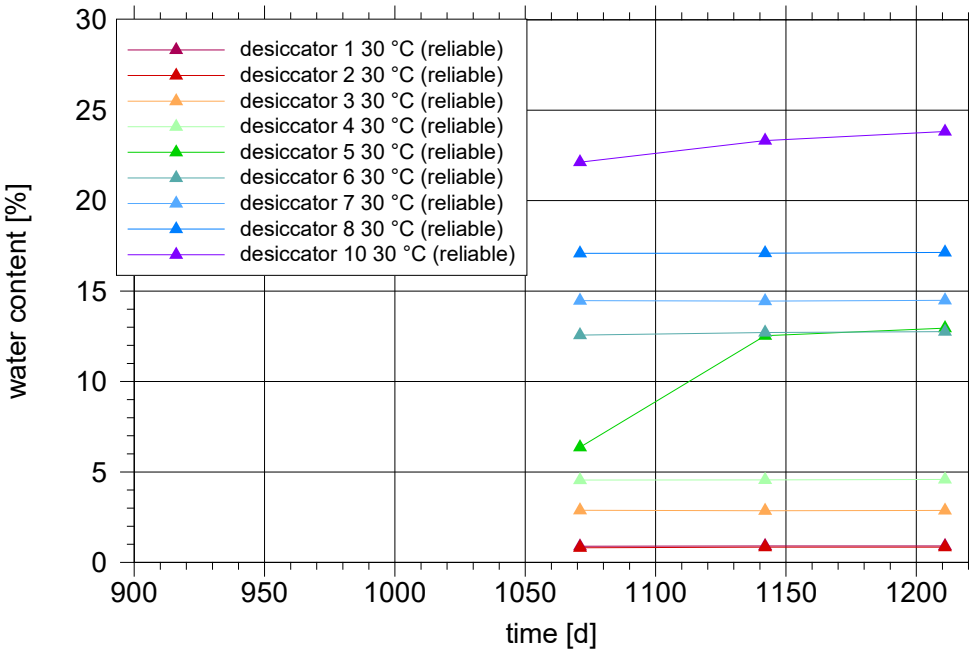

Fig. 5.11 Water content evolution during the cooling phase at 30 °C

5.1.4 Conclusions concerning the isotherms

All water content data determined for the end of each of the five temperature steps are collected from Tab. 5.3, Tab. 5.5, Tab. 5.7, Tab. 5.9, and Tab. 5.11 are compiled in Tab. 5.12. Instead of the target humidity the actually measured humidity is listed here as the humidity was quite off the target value in some cases. A compilation of all water content data is contained in Tab. 5.13.

The data in Tab. 5.12 are visualised in Fig. 5.12. For the sake of clarity, the data points are not connected by lines. While the data in general confirm the adsorption isotherm from /KAH 86/ quite nicely as shown in Fig. 5.13, the goal of this test with a view to determining the temperature dependence of the isotherm has been missed. There is no clear distinction between the data points for 30 and 60 °C. The same applies to the data from 90 °C in the lower range of relative humidity. In the upper range, the water content appears to be somewhat lower than that from 30 and 60 °C, maybe by 1 to 2 %. Unfortunately, there are no data from 90 °C in the middle range, meaning that this observation is only weakly reliable. It has thus to be concluded that the data uncertainty related to the chosen test methodology was inherently too high to reach the intended goal of the test.

Tab. 5.12 Relative humidities in the desiccators after temperature step 5 at 30 °C

temperature	desiccator	1	2	3	4	5	6	7	8	9	10
step 1: 30°C	measured humidity [%]	8,4	12,3	34,9	44,4	52,5	71,0	78,1	86,2	92,4	100,0
	water content [%]	0,63	0,94	2,9	4,7	7,7	12,5	14,3	17,5	19,9	(29,2)
step 2: 60°C	measured humidity [%]	8,6	12,9	-	43,0	-	66,0	74,1	78,5	86,6	-
	water content [%]	0,56	0,83	-	4,3	-	11,8	13,7	16,1	18,6	-
step 3: 90°C	measured humidity [%]	19,3	6,4	32,7	34,2	22,3	52,7	77,1	79,8	89,5	95,0
	water content [%]	0,79	0,47	2,4	3,5	(3,5)	(8,8)	12,7	14,5	17,2	(18,5)
step 4: 60°C	measured humidity [%]	15,7	8,7	29,6	40,5	37,4	58,9	75,8	81,3	-	89,0
	water content [%]	0,86	0,66	2,6	4,1	4,1	10,6	13,8	15,9	-	(15,4)
step 5: 30°C	measured humidity [%]	13.2	10.5	31.9	44.8	68.0	64.3	77.0	84.6	-	98.9
	water content [%]	0.91	0,84	2.9	4.6	13.0	12.8	14.5	17.1	-	23.8

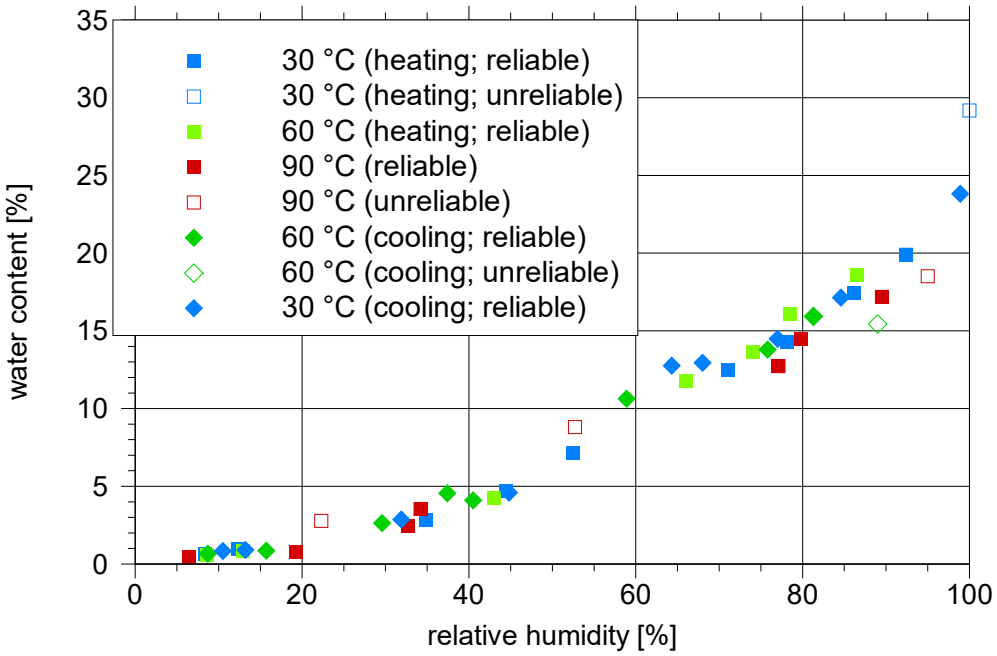

Fig. 5.12 All isotherm-relevant data

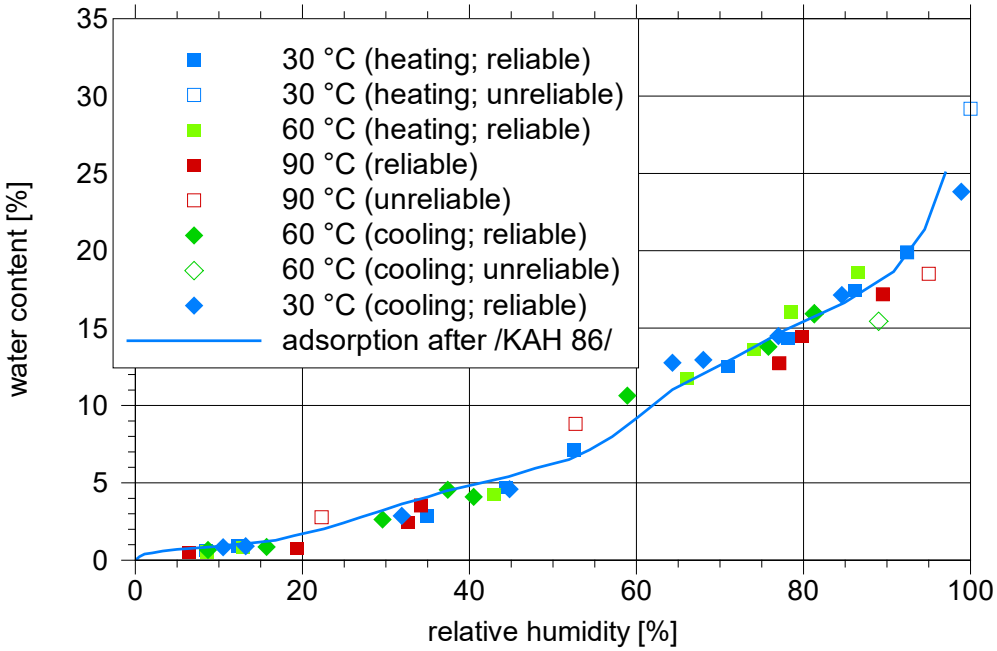

Fig. 5.13 Comparison to data from /KAH 86/

Tab. 5.13 All water content data

day	des.1	des.2	des.3a	des.3b	des.4	des.5a	des.5b	des.6	des.7	des.8	des.9	des.10
10	0.00	0.00	0.00		0.00	0.00		0.00	0.00	0.00	0.00	0.00
126	0.67	0.99	7.28		4.53	9.41		12.00	13.67	16.65	18.73	23.12
145	0.66	0.98	7.27		4.58	9.38		12.12	14.01	17.27	19.08	24.13
168	0.66	0.94	7.25		4.61	9.36		12.22	14.17	17.24	19.36	24.63
204	0.68	0.95	7.21		4.70	9.32		12.37	14.24	17.32	19.59	25.65
271	0.64	0.92	7.18		4.76	9.34		12.53	14.32	17.46	19.90	26.80
294	0.63	0.94	7.14		4.73	9.19		12.51	14.31	17.46	19.90	27.11
307				0.16			-0.83					
351				2.56								
355	0.63	0.87			4.34		5.01	11.82	13.70	16.31	18.98	27.88
477	0.56	0.83		2.85	4.25		7.14	11.75	13.65	16.07	18.61	29.18
478							8.34					
596				2.74								
597				3.59								
666	0.74	0.48		2.51	3.84		3.94	9.67	12.84	14.52	17.19	31.16
754	0.75	0.50		2.44	3.52		2.99	9.16		14.42		
791	0.79	0.47		2.43	3.54		2.78	8.81	12.73	14.47		18.51
1003	0.86	0.66		2.63	4.09		4.55	10.64	13.79	15.93		15.44
1071	0.89	0.81		2.88	4.55		6.37	12.57	14.47	17.09		22.13
1142	0.91	0.84		2.86	4.56		12.53	12.71	14.45	17.10		23.32
1211	0.91	0.84		2.87	4.59		12.95	12.76	14.49	17.14		23.82

temperature
30 °C / 23 °C
60 °C
90 °C

values for isotherms

reliable

unreliable

Note that
(1) the bentonite samples were emplaced in the desiccators on day 10
(2) each value represents the average of all four samples in a desiccator in [%]
(3) new samples were emplaced in desiccators 3 and 5 on day 294
(4) desiccators 3, 5 and 10 were removed from the oven for the period between days 307 and 484 and kept at 23 °C
(5) readings for desiccator 3b on days 596 and 597 were just from one sample each

5.2 Measurements up to 55 °C with the VSA

5.2.1 Finding a successful strategy

When it became clear that the measurements in desiccators would take far too much time, an alternative was sought and found in the Vapour Sorption Analyzer (VSA) /VAP 20/, described in detail in section 2.2. This device proved to be able to measure a complete hysteresis cycle in a matter of weeks instead of months or years. A certain limitation was, though, that the VSA could handle only temperatures up to 60 °C.

With respect to investigating the impact of temperature on the isotherms, the first idea was then to measure complete isotherms and scanlines at different temperatures. While the required testing times were accelerated considerable, it meant that the related measurement campaigns would still take some time. Due to several technical difficulties, the tests had to be interrupted time and again. It was therefore not possible to perform these tests in one go. As a consequence, not all tests were done with the same sample. The results that were acquired for MX-80 over time are graphically compiled in Fig. 5.14.

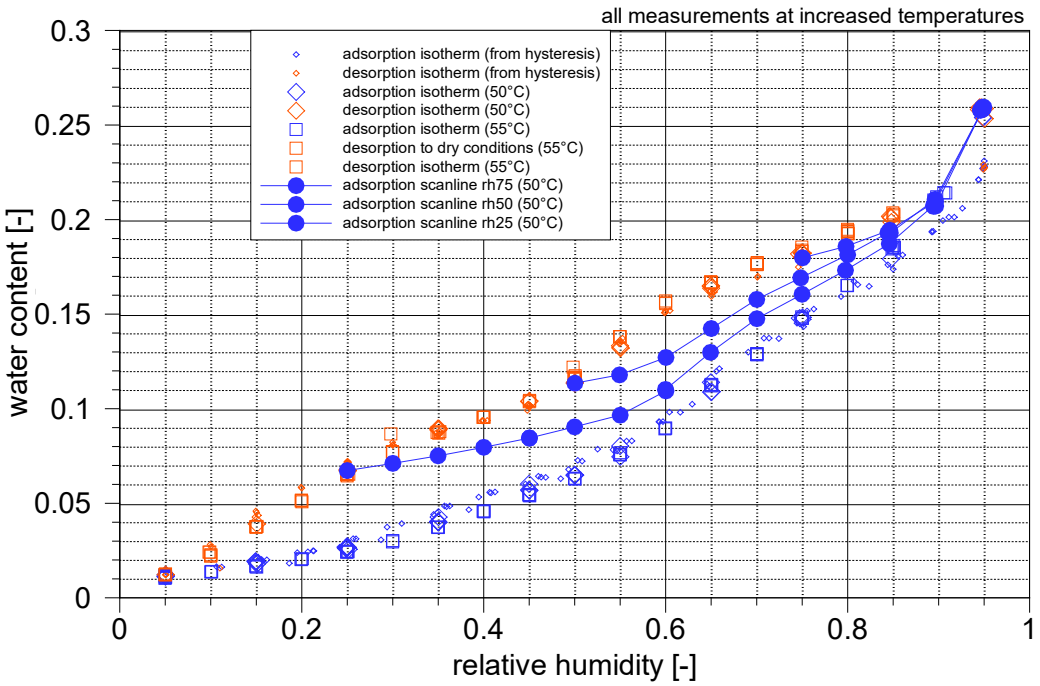

Fig. 5.14 All data on hysteresis and scanlines for MX-80 at elevated temperatures

For the adsorption isotherm there were two measurement campaigns at elevated temperatures, one at 50 °C and one at 55 °C. The temperature-induced changes of the water content were rather little so that the data uncertainties that come with the VSA appeared to be larger than the sought-after differences in the isotherms. The result is a general inconsistency between the adsorption isotherms measured at 25 °C, 50 °C, and 55 °C. The same conclusion applies to the desorption isotherm. As for the scanlines for MX-80, differences between measurements at the same temperature were already found to be quite large at 25 °C, as discussed in sections 4.2.1.1 and 4.2.1.2. Similar results were also found for Calcigel as depicted in Fig. 5.15 for the adsorption and desorption isotherm, measured at 25, 30, and 55 °C.

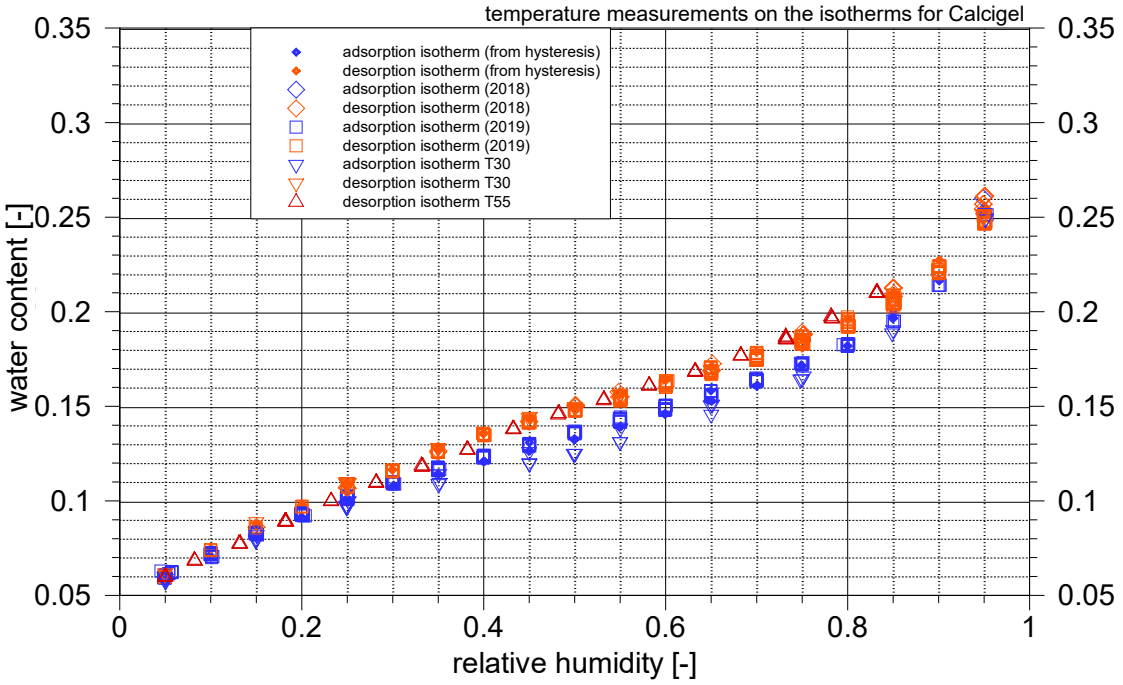

Fig. 5.15 All data on hysteresis and scanlines for Calcigel at elevated temperatures

An alternative strategy was tried and found to be more successful. Instead of running the whole hysteresis cycle up and down at one temperature, the change of water content was measured for specific relative humidities at three different temperatures, namely 25, 40 and 55 °C. Having become aware of the high accuracy requirements, a more stringent accuracy criterium for the equilibrium between relative humidity and weight of the sample was applied. The accuracy criterium is implemented in such a way that the rate at which the sample weight changes, is monitored and compared to a threshold value. The threshold value can be adjusted to a fixed value as well as the number of change rates that fall

consecutively below the threshold. Here, eight instead of four measurements had to fall below the previously used threshold value.

Note that time was running short in the project when these tests have been performed. In the urge to hurry up, the dry density of the samples – required for deriving the correct water content – were not determined. Instead, the water content was calibrated using the already known analytical solutions for the isotherms acknowledging that the samples were either wetted or dried in order to reach the target relative humidity.

5.2.2 Adopted procedure

The conditions of a typical test sequence are plotted in Fig.5.16. The plots for all measurements are compiled in Appendix B, sections B.1.4.2 and B.2.4.2.

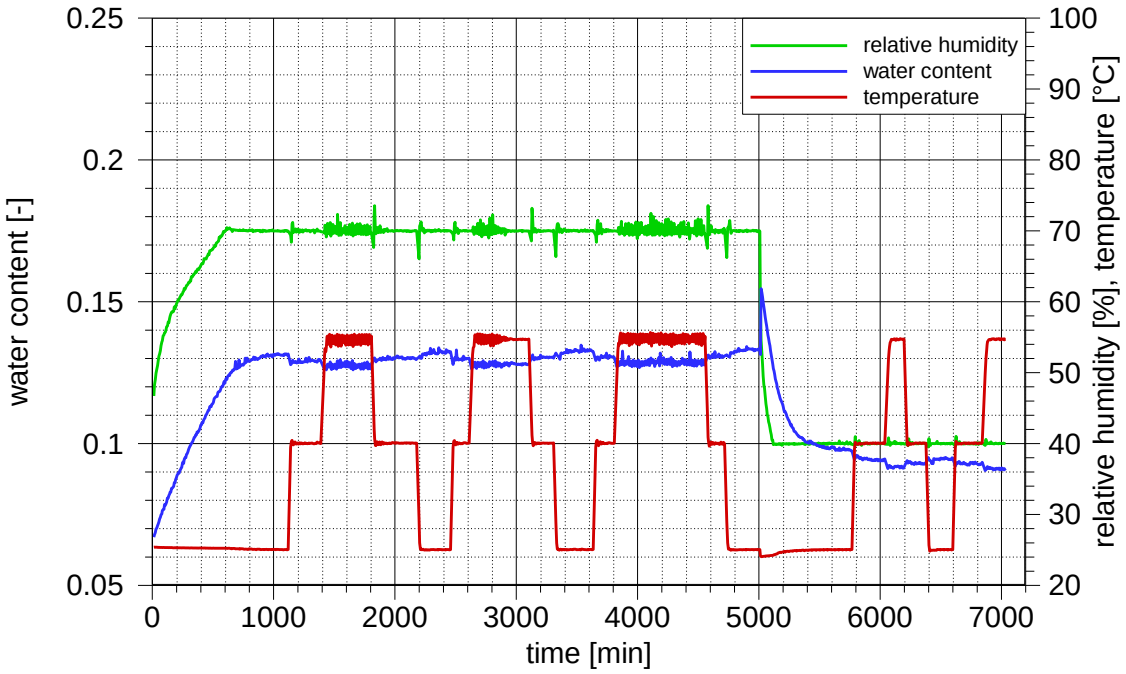

Fig. 5.16 Example of test conditions for MX-80 at 70 and 40 % relative humidity

The graph in Fig.5.16 shows relative humidity, temperature and the resulting water content over time. Initially, the sample had been in equilibrium with ambient conditions meaning a temperature of 25 °C, a relative humidity of about 46 % and a water content of about 6.8 %. The humidity in the VSA was elevated to 70 % and the sample weight was monitored until equilibrium was reached. Then, the temperature was increased, and a new equilibrium was approached. All in all, three cycles of temperature increase and

decrease were executed at 70 % relative humidity and one and a half cycle at 40 %. According to Fig. 5.16, the water content appeared to be corresponding nicely to the changes in temperature.

For closer inspection of the data, all data pairs of relative humidity and water content were extracted from the log file where the mass change rate fell below the threshold value as mentioned above. These data pairs exhibit a certain scatter. When averaged, however, the data give a clear trend. Exemplarily, the data for MX-80 at 70 % relative humidity are depicted in Fig. 5.17. The small filled symbols represent a single measurement, the large open symbols the average of the data points for each equilibrium stage during the test. The shape of the symbols allows for discriminating between first heating (circle), heating (diamond), and cooling (square), respectively. The colours are related to the three temperature levels 25 °C (blue), 40 °C (green), and 55 °C (red).

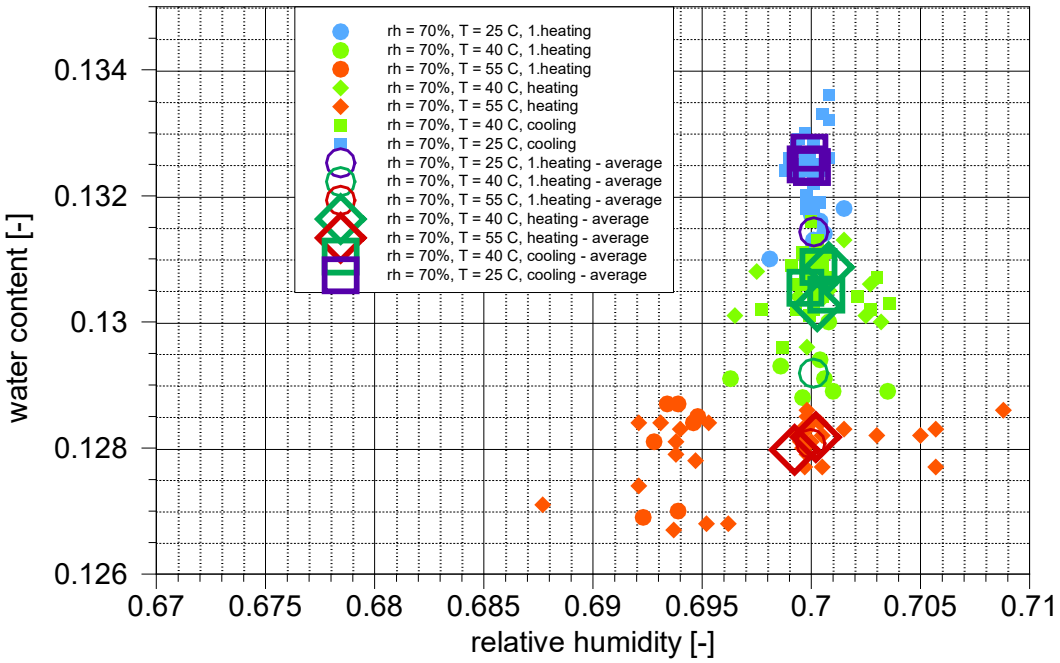

Fig. 5.17 Temperature-dependent water content at 70 % relative humidity

Each test was evaluated in this way in order to get a feeling of the reproducibility of the averages which appears to be good. It shows that there is no significant difference between data from cooling and data from heating. A hysteresis with respect to temperature can thus not be substantiated in the investigated temperature range.

One peculiarity of the data as in Fig. 5.17 has been detected by this procedure, though. The averages for the first heating phase seem to be slightly different by a few tenths of

a percent in water content from the subsequent averages. This is a feature that can be observed for all other relative humidities and both types of bentonite (see Appendix B, sections B. 1.4.2 and B. 2.4.2), except for 55 °C in Fig. 5.17. There is no good explanation, neither for this phenomenon nor for the exception depicted in Fig. 5.17.

5.2.3 Test results

5.2.3.1 MX-80

For the final evaluation, all equilibrium data for the same temperature level were averaged irrespective of determination from a heating or a cooling phase. However, those from the first heating phase were not taken into account.

As adjusting target conditions in the samples for a specific test required either wetting or drying, the water content was assumed to relate either to the adsorption or to the desorption isotherm accordingly. Equilibrium at 25 °C and the target humidity provided the reference values of the water content. This value was then used as a reference for calculating the loss of water content Δw due to heating. The results for MX-80 bentonite are depicted in Fig. 5.18 as a function of relative humidity and of the two elevated temperature levels.

The data for relative humidities 10, 20, 30, and 50 % do not seem to fit the general trend, though. They stem from the two measurement campaigns performed towards the end of the project when, due to the lockdown, work in the laboratory was rather not up to the usual standards. Each campaign provides either consistently high or consistently low water losses which suggest that the data does not reflect measurement uncertainties but rather unfavourable machine conditions. Additionally, the data protocols revealed afterwards, that these measurements were by mistake performed with samples of very high sample mass that was even slightly in excess of the permitted maximum load. The resulting data points are thus marked as unreliable in Fig. 5.18.

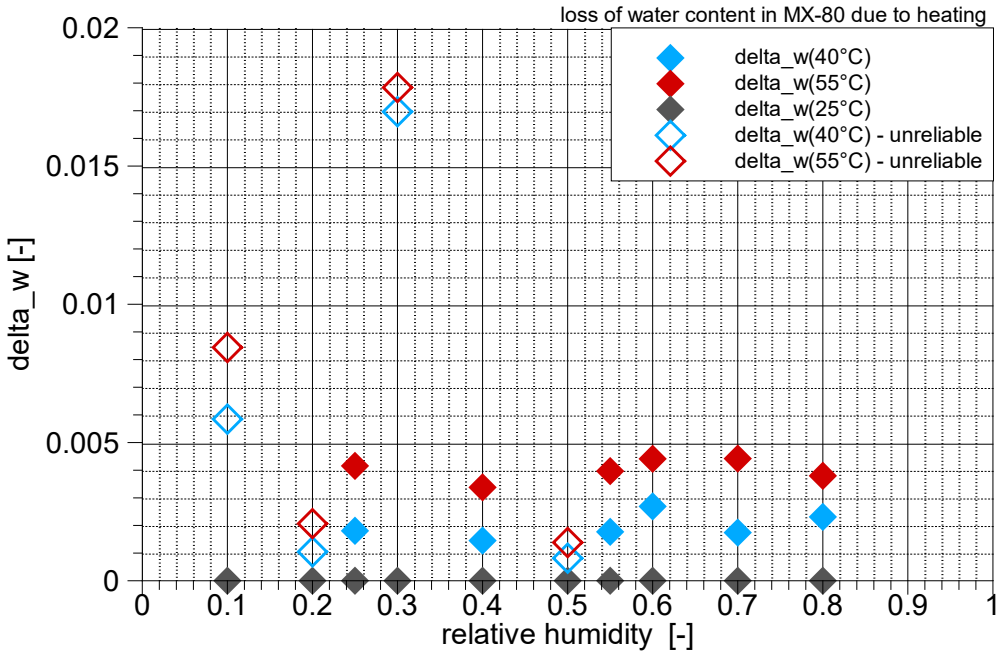

Fig. 5.18 Temperature-dependent loss of water content for MX-80

The data for the water loss due to a temperature increase of 30 °C are represented by filled red diamonds in Fig. 5.18. They appear to be consistent with the data from /GAI 05/ as they show a maximum between 60 and 70 % and indicate a trend towards zero mass loss for a completely dry and a fully vapour-saturated atmosphere (see section 1.4). Only the data for 25 °C seem to be somewhat off.

The next thing to check was therefore the quantitative consistency between the water loss data from in the measurements of /GAI 05/ and those from the present measurements. The maximum water loss at 99.8 °C compared to 25.2 °C provided by /GAI 05/ has been taken to amount to 2 % water content (see section 1.4). Assuming a linear relationship between temperature increase and water loss[9]these data relate to a decrease of 0.0268 $\%_{\text{water content}}$/°C. This constant will be called “thermal water loss” further on. Using the VSA that cannot completely cover this temperature range, a loss of about 0.45 % water content were measured applying a temperature difference of 30 °C, resulting in a thermal water loss of 0.015 $\%_{\text{water content}}$/°C.

[9] as done ad hoc for code VIPER /KRÖ 11/

That divergence might be reconciled, though, at least to a certain extent, considering that the scatter in the data from /GAI 05/ might have led to an overestimation of the maximum bandwidth of adsorption isotherms in Fig. 1.4. This would have reduced the resulting thermal water loss. On the other hand, it cannot be completely excluded that the samples in the VSA had not fully reached equilibrium at the end of each test phase despite the stepped-up termination criterion. Both arguments point towards the conclusion that the true thermal water loss at about 70 % relative humidity should lie somewhere between 0.015 and 0.0268 $\%_{water\ content}$/°C. Note, while this difference appears to be rather little, it has to be kept in mind that it still means a difference of about 40 % in the adsorbed water that is set free as vapour in case of heating.

Another possibility to explain the discrepancy would be a non-linear relation of water loss and temperature increase. With only two elevated temperature levels at comparatively little temperature differences (15 °C) this can only tentatively be decided on the basis of the present data. Nevertheless, the differences in water content that are assumed to be reliable, are compiled in Tab. 5.14for this purpose. They show some scatter, but the average appears to be meaningful, indicating the same mean water loss at both temperature increases. This appears to confirm the ad-hoc approach in code VIPER that relates the water loss linearly with the temperature increase. However, it does not help to explain the divergent water loss data from the two measurements.

Tab. 5.14 Water loss of MX-80 due to heating

r_h [%]	Δw(T=40°C)-Δw(T=25°C) [%]	Δw(T=55°C)-Δw(T=40°C) [%]
25	0.181	0.235
40	0.145	0.192
55	0.177	0.220
60	0.269	0.172
70	0.174	0.267
80	0.231	0.149
Average	**0.196**	**0.206**

Finally, it would have been helpful to compare the montmorillonite contents of the MX-80 samples in question. Unfortunately, no reference to the montmorillonite content could be found in /GAI 05/. It has to be admitted, though, that such a reference might have been overlooked as this thesis is written in French.

5.2.3.2 Calcigel

The same procedure as described in the previous section led to analogous data for Calcigel. Fig. 5.20 shows the loss in water content due to temperature increase in steps of 15 °C. The data points for Calcigel appear to follow a somewhat different trend than those for MX-80 as they indicate a more or less constant water loss with heating over a large range of relative humidities. However, the assumption of no temperature-dependence of the water content for completely dry and fully vapour-saturated air (see section 1.4) is assumed to apply to Calcigel as well but requires a comparatively sharp decrease in the temperature-induced water losses towards the end of the humidity spectrum.

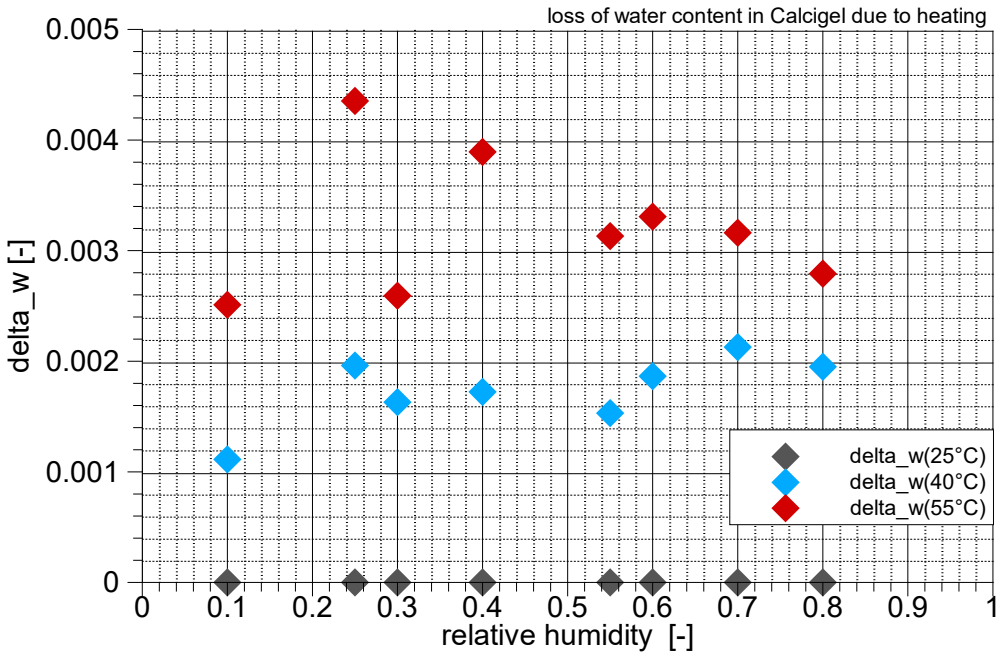

Fig. 5.19 Temperature-dependent loss of water content for Calcigel

5.3 Analytical functions

5.3.1 MX-80

A formulation based on two quadratic parabolas of the general form

$$\Delta w = A \cdot r_h^{\,2} + B \cdot r_h + C \qquad (5.1)$$

has been chosen to describe the water loss due to maximum temperature increase ΔT_{max} as a function of relative humidity. This approach is characterized by the water loss of Δw = 0 % for the relative humidities r_h = 0 % and r_h = 100 %. Further conditions are given by the position $r_{h\,max}$ of the peak value Δw_{max}, the peak value Δw_{max} itself and a horizontal tangent at Δw_{max}. The geometrical concept behind this approach is illustrated by Fig. 5.20.The position $r_{h\,max}$ is assumed to be independent of the temperature.

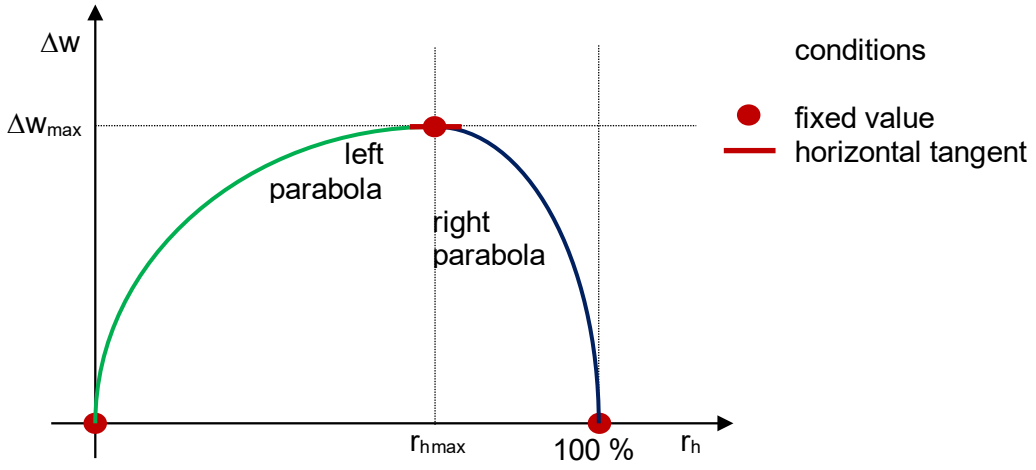

Fig. 5.20 Analytical approach for the loss of water at maximum temperature increase

The water loss is assumed to be linearly related to the increase of the temperature ΔTabove a reference temperature T_{ref} at which the water loss Δw equals zero for all relative humidities. This approach is illustrated in Fig. 5.21 loosely referring to the measurements described in the previous subsections.The complete approach thus reads

$$\Delta w(T) = \left(A \cdot r_h^{\,2} + B \cdot r_h + C\right) \cdot \frac{T - T_{ref}}{T_{\max} - T_{ref}} \qquad (5.2)$$

Applying this approach to the measured data means adopting the reference temperature T_{ref} = 25 °C and the maximum temperature increase ΔT_{max} = 30 °C. The maximum water loss Δw_{max} is set to 0.45 % water content which is in accordance with the thermal water loss of 0.015 $\%_{\text{water content}}$/°C determined from the measurements (cp. section 5.2.3.1). The resulting coefficients for the approach (5.2)are compiled in Tab. 5.15. Note that approach (5.2) allows for the temperature to exceed T_{ref} in a real application.

Tab. 5.15 Coefficients for the approach (5.2) for MX-80

range	A	B	C	T_{ref}[°C]	T_{max}[°C]
r_h<0.7	-0.00918367	0.0128571	0	25	55
r_h>0.7	-0.05	0.07	-0.02		

The fit of the analytical formulation to the data is illustrated in Fig. 5.22. It appears to fit the data for 55 °C very well and the data for 40 °C at least reasonably well.

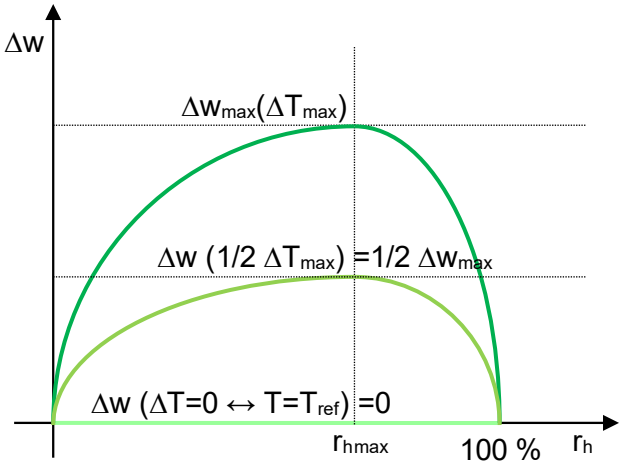

Fig. 5.21 Linear relationship between loss of water and temperature increase

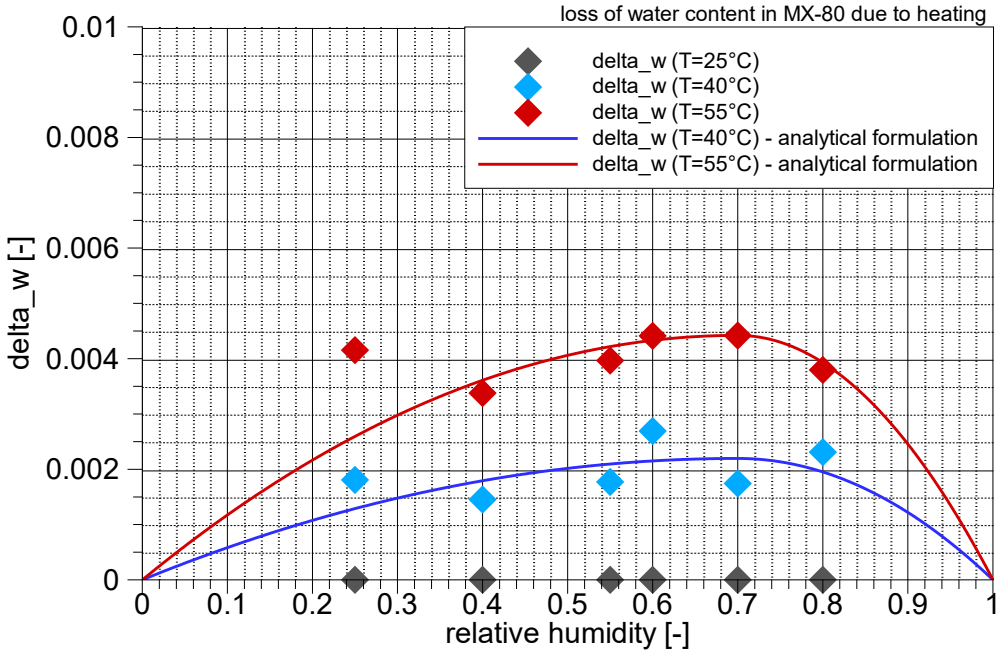

Fig. 5.22 Fit of an analytical formulation to the loss of water content of MX-80

5.3.2 Calcigel

The different trends of the curves for Calcigel in comparison to those for MX-80 were confirmed by tentatively trying to fit the bi-quadratic approach for MX-80 to the data for Calcigel. Neither arranging the peak at 30 % relative humidity nor at 60 % resulted in a fully satisfying fit (see Fig. 5.23).

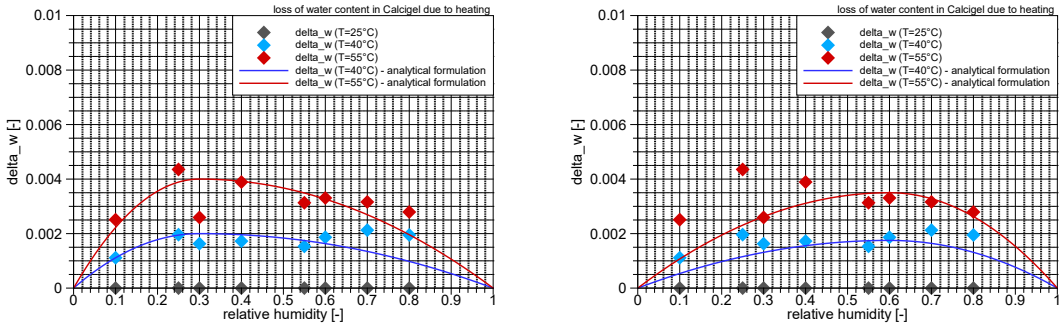

Fig. 5.23 Fits of the analytical formulation for MX-80 to data for Calcigel; left: peak at 30 % relative humidity, right: peak at 60 % relative humidity

Instead, the two quadratic parts in the approach for MX-80 were separated by a straight horizontal line marking a maximum loss in water content of 0.35 %. By that, the peak value of the water loss is reached already at 20 % relative humidity and maintained up to 70 % humidity before going down towards 0 % water content at 100 % humidity again as shown in Fig. 5.24. While the analytical function looks a bit strange, it appears to fit the data best. The resulting coefficients for the approach (5.2) are compiled in Tab. 5.16.

Tab. 5.16 Coefficients for the approach (5.2) for Calcigel

range	A	B	C	T_{ref}[°C]	T_{max}[°C]
r_h<0.2	-0.0875	0.035	0	25	55
0.2< r_h<0.7	0	0	0.0035		
r_h>0.7	-0.0388889	0.05444444	-0.015555556		

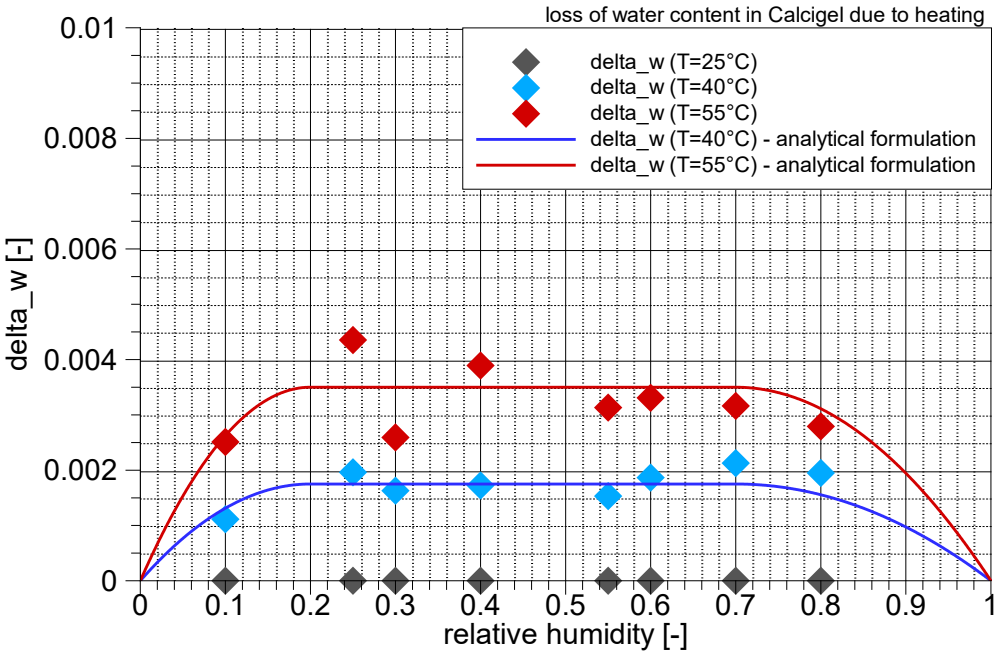

Fig. 5.24 Fit of an analytical formulation to the loss of water content of Calcigel

6 Confined conditions

6.1 Motivation and test plan

All measurements and considerations so far refer to free swelling bentonite. This is obviously not the case in a real repository. In case of confinement, the retention curves have been shown to require an adjustment that acknowledges the fact that only a limited amount of water can be taken up by a compacted and confined bentonite body (e.g. /DUE 07/). Moreover, tests with confined samples of MX-80 compacted to different dry densities have been shown to undergo structural changes on the microscopic level during a full wetting that appear to change the water uptake characteristics, namely the isotherms/retention curves /SEI 14/. Goal of the tests with confined bentonite samples was therefore to find a critical dry density above which the effect of microstructural changes might become relevant for the behavior of a bentonite buffer in a repository.

While the measurements with MX-80 bentonite of /SEI 14/ had been performed up to a dry density of 1800 kg/m³, new requirements for the buffer with respect to the bentonite dry density were formulated by SKB for the KBS-3 concept in 2017. According to new considerations concerning the permissible swelling pressure, the dry density of the buffer was restricted to a range between 1486 and 1591 kg/m³ /LUT 17/.

The most significant test for the purpose at hand was thus considered to be based on MX-80 with a dry density of 1600 kg/m³. In order to find out about possible changes in the isotherm, MX-80 powder was to be compacted in a cell and to be put into the VSA at ambient conditions. The sample was then to be wetted, dried and wetted again utilizing basically[10] the full range of possible humidity states provided by the VSA. A comparison of the weight data that can be translated into water content was envisaged to show possible changes in the isotherm.

6.2 Solutions for the test cells

In order to quantify the influence of structural changes on the adsorption isotherm, supplemental measurements of isotherms for compacted bentonite in the VSA were aimed

[10] Experience from working with the VSA let it appear advisable to leave a safety margin to the nominal maximum and minimum relative humidity, though.

at. Small cells had to be constructed for that purpose similar to the microcells described by /SEI 14/. The use in the VSA increased the functional requirements of the envisaged GRS-cells compared to the microcells, though, as they had not only to be small and tough but also very light in order not to overstrain the sensitive scale of the VSA.

Furthermore, it had to be checked whether a cell in the chamber of the VSA would interfere with the climate control mechanism because the cell design exceeded the height of the standard pans for the VSA. For this purpose, a plastic dummy was produced and installed in the VSA. The VSA showed no deviations from normal climate control while housing the dummy indicating that no interference was to be expected from installing a test cell. Construction constraints for the new GRS-cells were thus a height of less than 8 mm, a diameter of less than 26 mm, mechanical strength against 4 MPa swelling pressure, and a weight of less than 23 g including the sample.

At first it was tentatively tried to come up with a solution using titanium for the cell material. The design for a titanium-based cell construction is shown in Fig. 6.1. It consisted of a flat cap that was to be tightly connected to the cell by a screw in the cell axis. Top and bottom were envisaged to contain an array of boreholes to allow for humid air to connect to the bentonite sample. While all technical construction requirements were met by this cell, the expected weight of the cell proved to be a major problem as it came always uncomfortably close to the acceptable maximum. Furthermore, it was also not entirely clear if the construction details particularly the required threads could be worked out with satisfying precision.

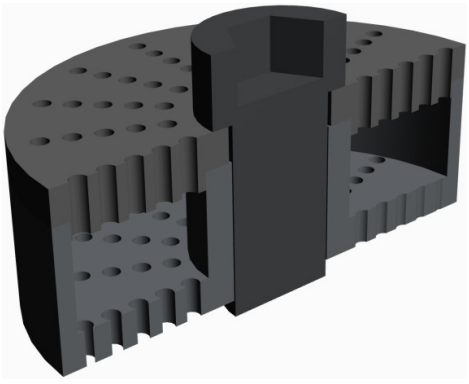

Fig. 6.1 Cell design based on titanium

Since a cell made of titanium would leave little leeway for possibly necessary adaptions of the construction, timewise as well as economically, the idea of using titanium was

dropped. Instead, a cell was designed following the construction principle of the titanium cell that could be 3D-printed with a tough plastic as shown in Fig. 6.2.

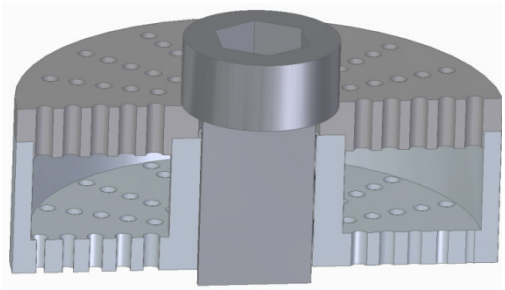

Fig. 6.2 First cell design based on 3D-printing

6.3 Difficulties with printed test cells

While producing a test cell by means of a 3D-printer had obvious advantages over a conventionally manufactured cell, several unexpected difficulties arose with this method. The first problem encountered, concerned the printed threads as external threads on the screw and core threads in the cell need to fit with a certain precision. An ad hoc construction based on a spiral with a triangular cross-section proved to be inappropriate. Trying to drive the screw into the bottom part of the cell always resulted in breaking one of the parts even after extensive cleaning and polishing of the threads. The underlying reasons were suspected to be insufficient printing accuracy and probably also a comparatively high surface friction.

The cell design was therefore changed to get along without threads as depicted in Fig. 6.3. Top and bottom part were now identical and were connected by a simple ring. Three outer segments enwrapping the three cell components were clamping everything together.

Also not anticipated was the fact that mechanical properties of printed materials depend on the curing time, the time required to harden the printed plastics permanently. Tests were therefore performed with the new cells that were filled with compacted bentonite and put into a desiccator to optimize the curing time.

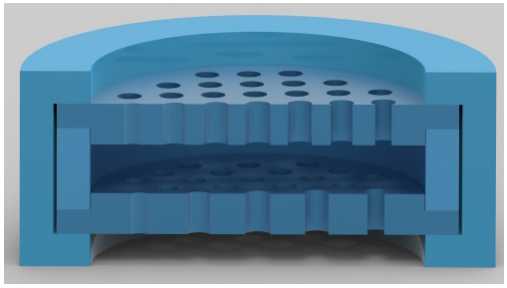

Fig. 6.3 Cell design based on 3D-printing without threads

For a few years now, hydraulic tests with printed test set-ups are reported (e.g. /SUZ 17/). Side-tracked by the totally missing hints in the literature about water uptake by plastic materials, this problem came only delayed into awareness. Plastics generally adsorb water indeed in a way that is remotely similar to water uptake of bentonite in that it leads a) to swelling, b) to weight change, and c) does so with diffusion-like dynamics (e.g. /PSM 19/, /KRV 20/).

Since this effect depends on the type of plastic, reliable figures for weight change and expansion are hard to come by. In order to check the relevance for the resin used in the present test, a simple pre-test was performed in the VSA with a printed empty cell. The cell with a weight of about 6.13 g was installed at ambient conditions. Then, the relative humidity in the climate chamber was stepwise increased and subsequently decreased again while monitoring the sample weight. The result is depicted in Fig. 6.4. Note that immersion in water of 23 °C and storage at a relative humidity of 100 % results has basically the same effect on plastics /STO 98/. The results are therefore also relevant for uptake of liquid water.

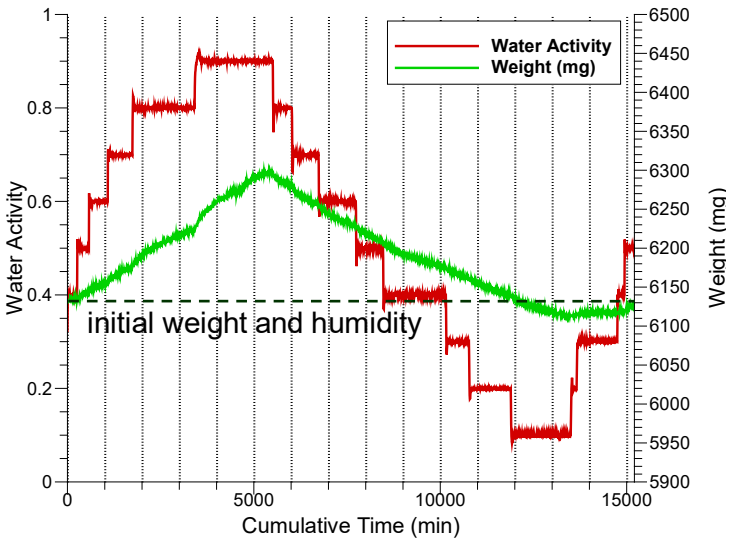

Fig. 6.4 Weight and water activity at varying relative humidity; from /KRÖ 20/

Several characteristic features for resins under influence of water can be observed in Fig. 6.4. Quite clearly, the sample weight follows the ambient humidity. Water uptake is not “instantaneous“ but requires some time. If the weight converges in each humidity step towards a specific level or if it generally converges towards a maximum, is not entirely clear. From the fact that the weight falls below the initial value after decreasing the humidity below the starting conditions it can be speculated, though, that the amount of adsorbed water in the sample depends on the humidity of the surrounding atmosphere.

The printed sample of 6.13 g changed weight by about 0.2 g or 3 % in 4 days (5740 minutes). In comparison, the increase in weight of a MX-80 sample of 2.7 g amounts to about 0.5 g or 19 % in roughly 6 days. The effect of water uptake by the printed material thus needs to be considered.

This has two adverse consequences for the intended test. Firstly, the measured weight does not reflect the water content, and, secondly, expansion of the cell might interfere with the interior of the VSA. Further pre-tests concerning weight changes and dimensional accuracy have thus been performed /KRÖ 20/.

6.4 Further pre-tests on plastic printer materials

When realising the problems with water uptake, it had also not been clear, whether the water would fully penetrate the printed plastics or if it would be stuck in a sort of a skin zone. This has obviously influence on the amount of water that can be taken up by the plastics.

In order to find out about possible limitations of the penetration depth, three transparent printed cubes with a side length of 1 cm were put into a potassium permanganate solution. After 53 days they were removed from the solution and one cube was sawed in half. The two halfs together with two additional complete test cubes are depicted in Fig. 6.5. The solution had coloured the sawn-up cube entirely. The cut surface did not show any shading thereby suggesting that water uptake had been complete and had reached steady-state.

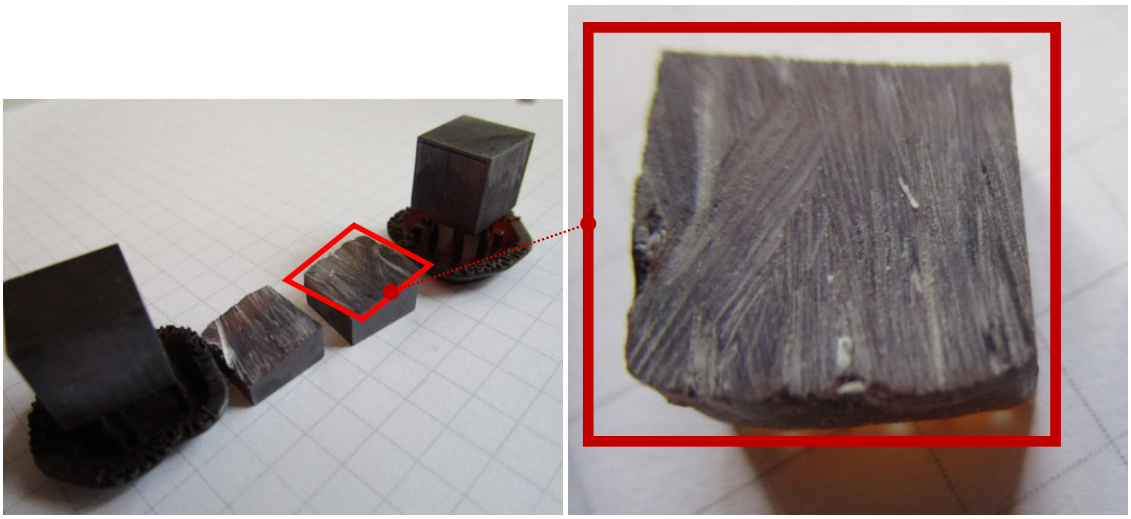

Fig. 6.5 Uptake of potassium permanganate by transparent printed cubes; from /KRÖ 20/

In parallel, tests were performed concerning the water uptake dynamics. Weight change and expansion were checked with test cubes that had a side length of 1 cm. Quite a range of responses to contact with water was expected for different printing materials and printing methods. A collection of cubes was therefore compiled which were produced by 4 different printing principles using 7 printing materials including 3 post processing variants on one material. The whole array of test cubes is shown in Fig. 6.6, specifications are given in Tab. 6.1.

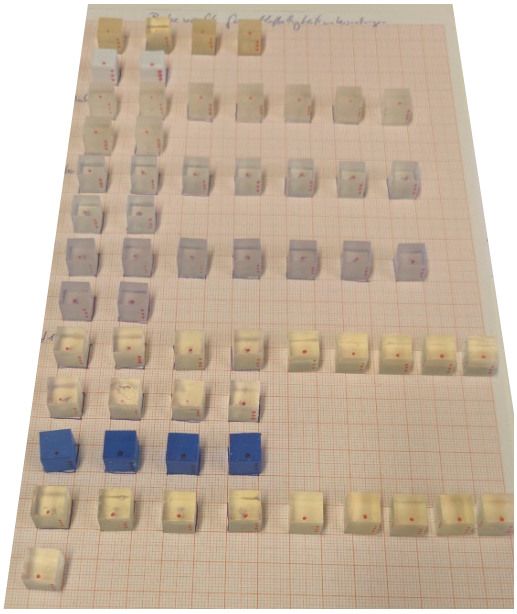

Fig. 6.6 Array of printed test cubes for weight and size changes; from /KRÖ 20/

Tab. 6.1 Specifications of the test cubes

printing method	producer	Material	variations	quantity
SLA[11]	Formlabs	Clear resin	no curing	4
SLA	Formlabs	Clear resin	cured for 15 minutes	4
SLA	Formlabs	Clear resin	cured for 30 minutes	4
SLA	Formlabs	Tough resin		4
DLP[12]	atum3D	Loctite ultra clear		3
DLP	atum3D	3DM tough		3
DLP	atum3D	Mitsubishi Diabeam		3
MJM[13]	Keyance	AR-M2		3
FDM[14]	(unknown)	PLA[15]		2

For the wetting, each batch of 2, 3 or 4 cubes was put into a bottle with tab water. To ensure wetting from all six sides, the bottles were installed in a rotating shaker (see Fig. 6.7) where they stayed all the time except for measurements on the cubes. The weight was determined with a scale of a nominal accuracy of 10 mg. For length measurements, a digital calliper with a nominal accuracy of 10 µm was used. In order to

[11]SLA: Stereolithographic Apparatus
[12]DLP: Digital Light Processing
[13]MJM: Multi-Jet Modelling
[14]FDM: Fused Deposition Modeling
[15]PLA: Polylactic acid

capture printing inaccuracies as well as anisotropic swelling, the cube extension was measured at three locations in each spatial direction according to the scheme sketched in Fig. 6.8. To ensure repeatability of the measurements, three sides of the cubes were marked unambiguously with coloured Sharpies to identify the cube in a batch, the spatial directions of the cube sides and the horizons for the length measurements.

Fig. 6.7 Rotating shaker with a bottle for each batch of cubes

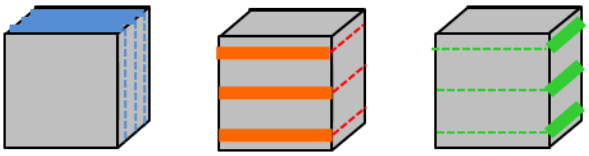

Fig. 6.8 Position of length measurements at the test cubes

The schedule for the measurements had foreseen to cover the wetting as well as a subsequent drying phase with appropriate time steps. However, the corona pandemic compromised that plan. Detailed data thus exist only for the first few days. However, it led also to an unplanned late measurement after120 days of wetting.

The results in terms of weight evolution are exemplarily depicted for the uncured “clear resin” in Fig. 6.9. While the curves for the individual four cubes show some differences in their shape, the mean of all four curves appears to be rather meaningful.

The mean values for each ofthe test batches are shown in Fig. 6.10. Note that the scale in the y-direction is different from Fig. 6.9. As expected, no material is entirely watertight. Water uptake between 0.4 % and 14.1 % by weight were observed within the first 3 days. Later, the cube made of Mitsubishi Diabeam material showed strangely a decrease that could not be interpreted in the framework of this project. However, its comparatively large water uptake had made it unfavourable for the purpose at hand anyway.

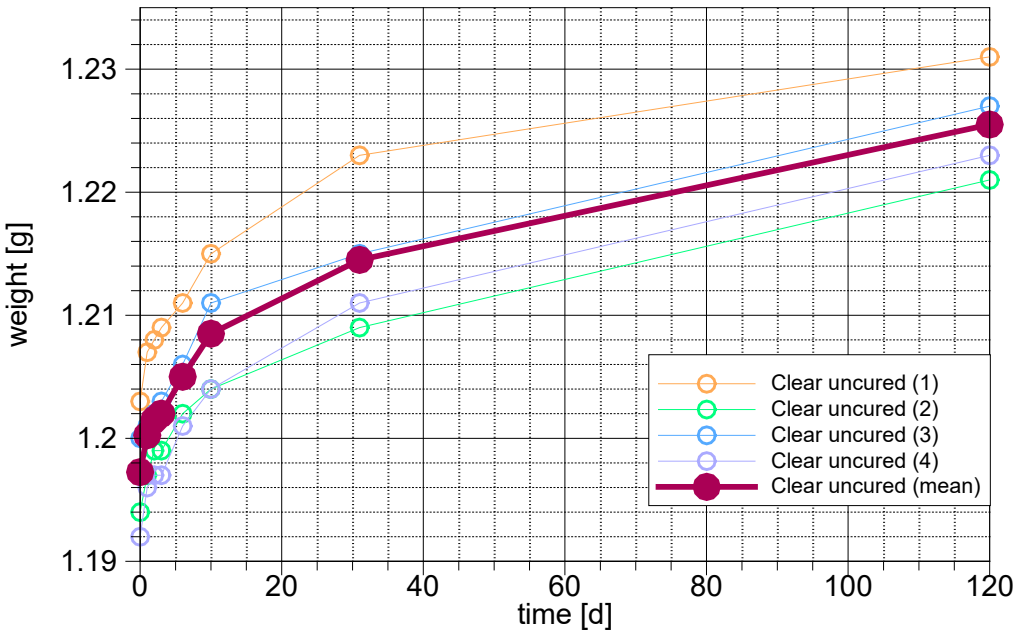

Fig. 6.9 Weight evolution of test cubes made of uncured “clear resin”

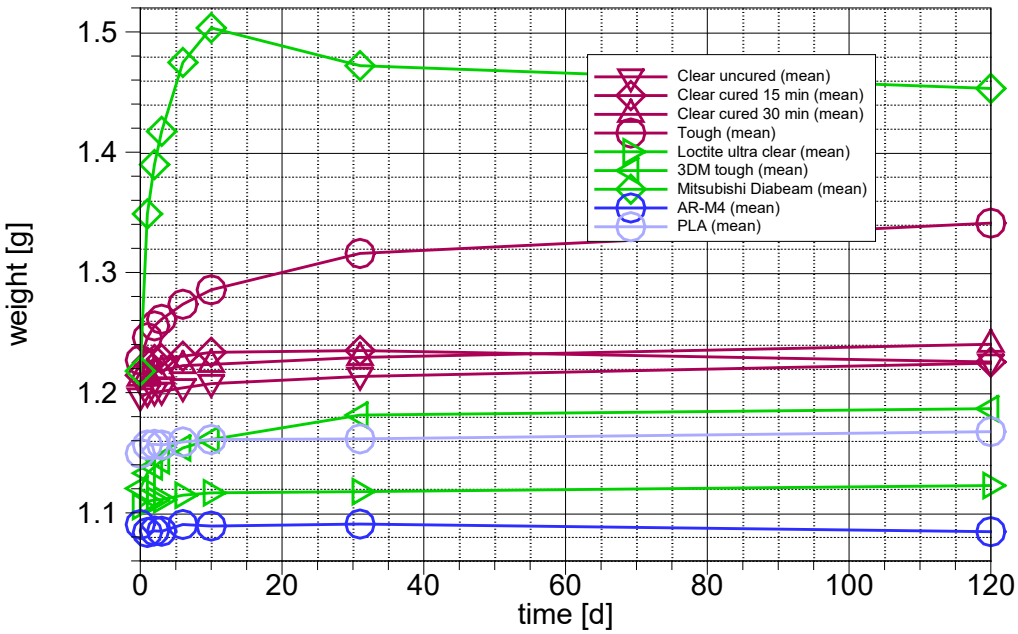

Fig. 6.10 Mean weight evolution for all batches of test cubes

In general, the characteristics of a diffusive process of water uptake that were indicated in the literature for plastics in general (see above), were confirmed by the tests to apply also to printed materials, as shown by reference to the weight gain rates in Fig. 6.11. A

cut-out section of Fig. 6.11 in a log-log plot is depicted in Fig. 6.12. In this figure, a more or less linearly decreasing trend of the gain rates can be identified that reveals a hyperbolic decrease of the water uptake rate.

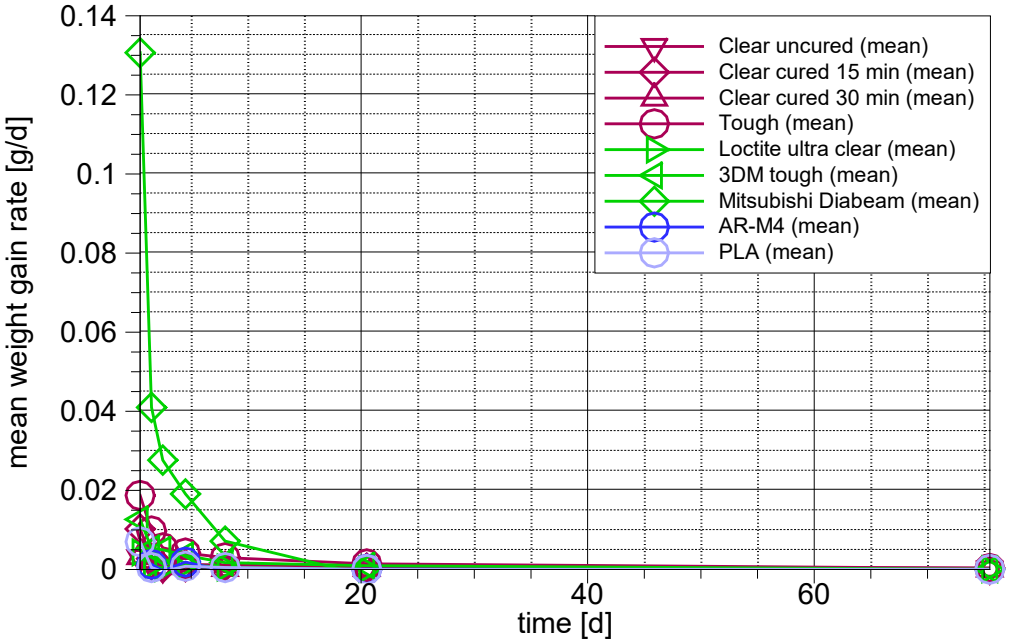

Fig. 6.11 Evolution of mean weight gain rates of all batches of test cubes

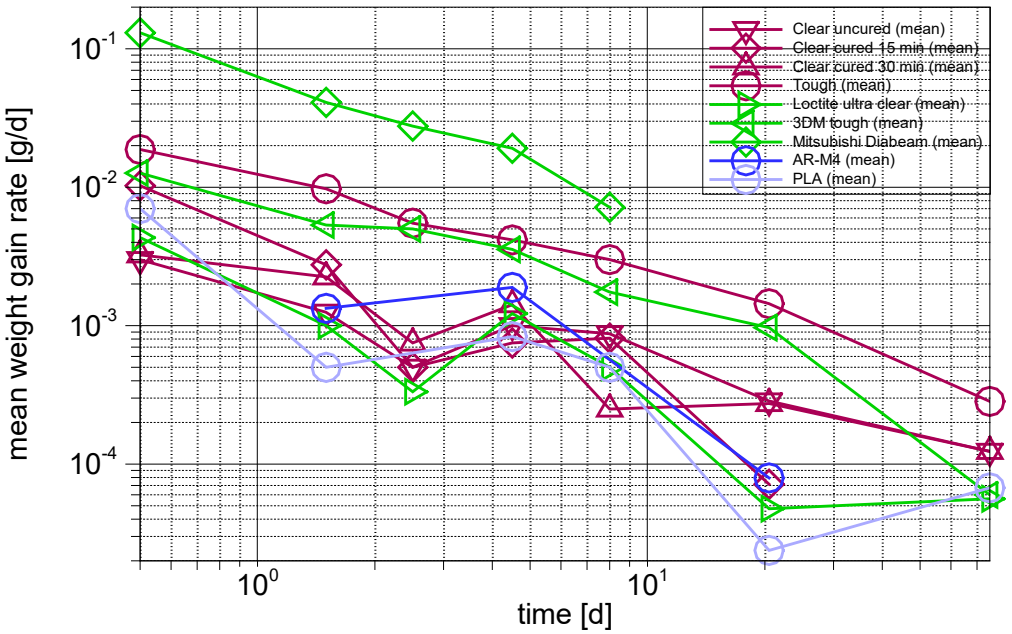

Fig. 6.12 Cut-out region from Fig. 6.11 in a log-log scale

The results from the length measurements were unfortunately not as informative as the weight gain data. Length readings with the calliper were obviously interfered with by printing artefacts such as the remains of support material, leading to rather high uncertainties of the measurements as shown in a close-up in Fig. 6.13. Linear expansion lay between 0.06 % and 5.20 % in the first three days.

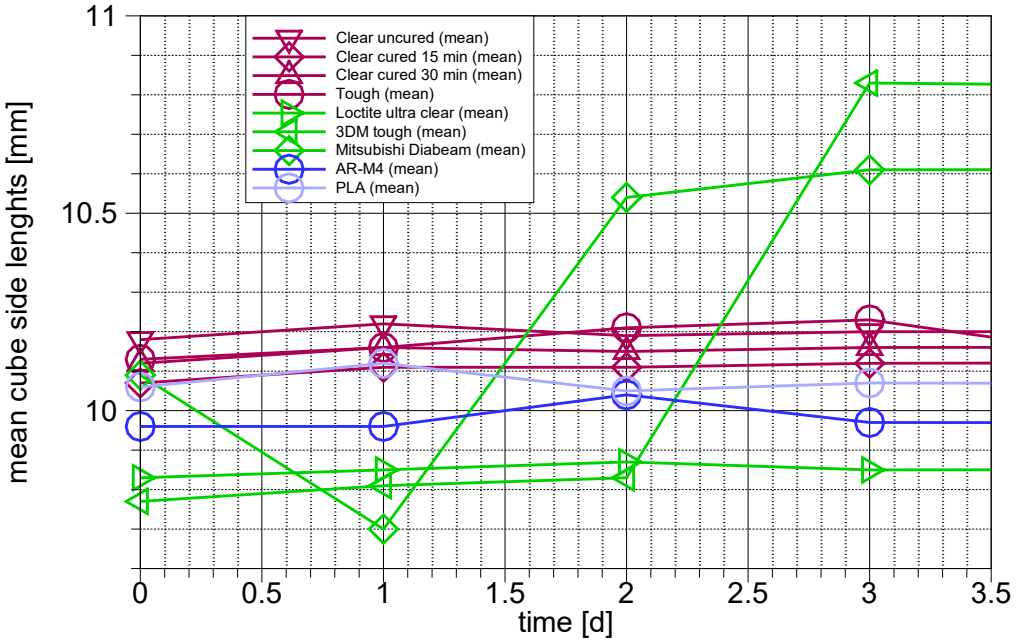

Fig. 6.13 Mean cube side lengths; close-up

Finally, a comparison of these length data from the test cubes with other and larger printing objects showed also that absolute printing errors appear to be independent of the sample size.

6.5 Test plan and results

For finding out of possible changes in the adsorption isotherm due to confinement, the VSA was set to determine the equilibrium between relative humidity and water content for specified relative humidities. It was foreseen to measure these equilibrium points in steps of 10 % relative humidity. The humidity was programmed to decrease from ambient conditions down to 5 % relative humidity, to be followed by an increase to 95 %, a new decrease down to 5 % and a new increase up to 95 %. The resulting data were planned to allow for a comparison of the two adsorption paths.

From the pre-tests it had already become clear that one test alone would not suffice as the measured weight would account for water uptake by the bentonite sample as well as the uptake by the test cell itself. Based on the tests in section 6.3 concerning water uptake of the printer resin, the ratio of water in the sample and the water in the cell in the test can be estimated.

Starting point for this estimation must be the materials at ambient conditions because the “dry” weight of the cell is not known. According to Fig. 6.4, the cell had taken up 0.17 g water in relation to the initial state. In order to reach a dry density of 1600 kg/m³, 1.34 g of bentonite at about 12 % initial water content had to be compacted and installed in the cell. Maximum water content of MX-80 bentonite at a dry density of 1600 kg/m³ is about 27 %. From these figures a maximum water uptake by the bentonite sample of 0.18 g related to the initial conditions can be derived. It can thus be expected that the printed cell had taken up about as much water as the bentonite sample.

The first test with a compacted bentonite sample in a printed test cell could not be finished in the given time frame, though. Since the cell takes up about as much water as the bentonite, the total uptake time is controlled by the material with the lower uptake rate. As it turned out, the printed material obviously takes up water at a much lower rate than the bentonite. This led to excessively long time periods for reaching equilibrium at each target humidity. The measurement for one humidity level lasted up to 80 hours. After about 7 weeks running time, the data storage of the VSA encountered overflow conditions prompting the VSA to stop the whole test just when reaching the most interesting second adsorption phase of the test at a relative humidity of 80 %. So, the most important final 3 data points were missing.

The evolution of the total weight of test cell and bentonite is depicted in Fig. 6.14. While an isotherm could not be established from the data, a few observations are nevertheless noteworthy:

- The shape of the weight curves deviates strongly from the typical shape of the isotherms for MX-80 bentonite confirming the considerable impact of water uptake by the printed test cell.
- Up to 70 % relative humidity, there appears to be no qualitative difference between the first and the second adsorption run.
- Quite some deviations of the full (second) desorption run from the initial desorption are apparent, probably indicating the pathway of a scanline.

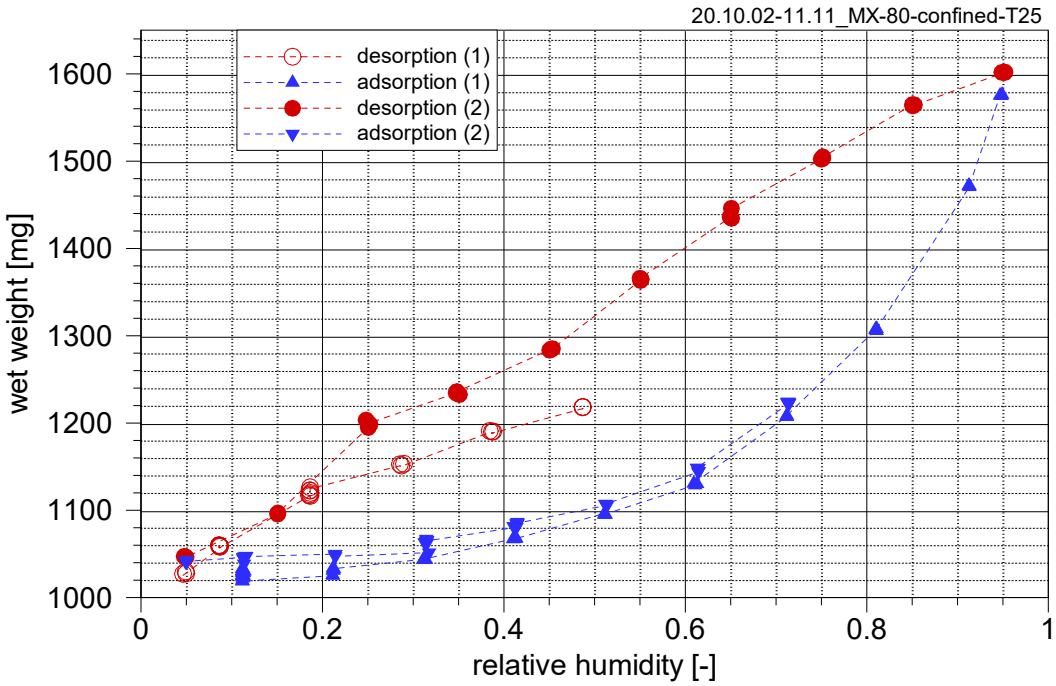

Fig. 6.14 Evolution of the total weight of test cell plus bentonite over relative humidity

To subtract out the effect of the test cell, a second test would have been necessary with an empty cell copying the wetting and drying path in terms of relative humidity as well as time for each humidity level. However, completion of the first test and performing of the second test are presently pending because it was realized too late, that water uptake by the resin and/or the compacted bentonite sample takes so much more time than the measurement of free swelling bentonite alone. As the foreseen tests with the VSA are fully prepared, they should not draw much on resources in terms of costs and workload. It is therefore planned to complete this experiment outside the present project.

7 Implementation of the new features in code VIPER

7.1 New features

Making use of the measurement campaigns described in the previous sections, basically two new features had to be implemented in code VIPER: The adsorption and desorption scanlines for MX-80 and Calcigel including the isotherms as well as the water loss due to heating. The former required an extensive reorganization in the code and also the latter had to be treated differently from the heuristic approach that has been used previously /KRÖ 11/. Some aspects of this work are described in the following.

7.2 Isotherms and scanlines

7.2.1 Labelling individual scanlines

The first challenging task resulted from the fact that by contrast to earlier versions of code VIPER, the constitutive relation between water content w and relative humidity r_h was not a unique one-to-one relation anymore but consisted of two isotherms and a theoretically infinite number scanlines. It did help a little, though, that the adsorption and desorption isotherms could be treated as special cases of the scanlines.

According to the measurements, an individual scanline can be characterized by its starting point (in the relative humidity-water content plane) which is located at the branch-off from the referring isotherm. This starting point can be defined by its relative humidity $r_{h\,0.}$ There are two types of scanlines, though, adsorption scanlines branching off the desorption isotherm and desorption scanlines branching off the adsorption isotherm, meaning that there would always be two scanlines referenced by the same relative humidity at the starting point. As an ad hoc convention, the relative humidity at the starting point of a desorption scanline is taken here to be a negative number by adding a minus-sign. The different analytical formulations prepared in the previous sections for free swelling conditions can thus be subsumed as

$$w_{free} = f\left(\mathrm{r_{h\,free}}, r_{h\,0\ free}\right) \qquad (7.1)$$

7.2.2 Considering confined conditions

The analytical formulations for isotherms and scanlines are based on measurements of free swelling bentonite samples. The purpose of code VIPER is the simulation of water uptake by a geotechnical barrier consisting of compacted and confined bentonite, though. In the past, when the constitutive equation in the model consisted of a unique relation, an isotherm for free swelling could be adapted to confined conditions applying the correcting approach of /DUE 07/. This approach modifies a retention curve in such a way that the maximum water content is reached for a suction of zero. Translated into the framework of isotherms, this correction basically stretches the isotherm for free swelling bentonite in the positive direction of the relative humidity axis by adding a correcting humidity Δr_h (cp. /KRÖ 11/) to obtain the isotherm for confined conditions

$$r_{h\,conf} = r_{h\,free} + \Delta r_h \qquad (7.2)$$

The correcting humidity Δr_h depends on the relative humidity $r_{h\,free}$, the related water content w_{free}, the initial water content w_0, the final water content w_e, and the saturation vapour density $\rho_{v\,sat}$ /KRÖ 11/:

$$\Delta r_h = \Delta r_h\left(r_{h\,free}, w_{free}, w_0, w_e, \rho_{v\,sat}\right) \qquad (7.3)$$

Only the part of the stretched isotherm that is less than or equal to a relative humidity of 1 is used. Advancing the methodology from one isotherm to families of scanlines, it is assumed here without further confirmation that the approach holds for the scanlines as well. The formalism analogous to (7.1) for confined conditions thus reads

$$w_{conf} = f'\left(r_{h\,conf}, r_{h\,0\,conf}\right) \qquad (7.4)$$

The relation f' is not known, though. However,

$$w_{conf} = w_{free} \qquad (7.5)$$

so that

$$w_{conf} = w_{free} = f\left(r_{h\,conf} - \Delta r_h, r_{h\,0\,conf} - \Delta r_h\right) \qquad (7.6)$$

holds. Unfortunately, the correction Δr_h requires as input the unknown water content w_{free} as well as the initial water content w_0 (see eq. (7.3)). This means that (7.6) is non-linear in w_{free} and also in w_0 since it depends in turn on the scanline $r_{h\,0\,free}$. This renders

a purely analytical treatment of the isotherm/scanlines impossile. Two possible ways of approximation exist, though. Rather close to the purely analytical treatment would be solving (7.6) iteratively with respect to two variables. This appears to be unpractical, though. As a last resort, the second alternative is therefore chosen here. At the beginning of a simulation run, two two-dimensional tables are put up instead, one for the adsorption scanlines and on for the desorption scanlines. These tables contain discrete water content values that are calculated as a function of the relative humidity and the starting point of a certain number of scanlines in a confined system. Whenever the water content needs to be calculated from a scanline, it is done so by looking up the appropriate location in the table and interpolating between the four adjacent table entries.

At a first glance, this alternative appears to be fine. However, when it comes to details quite a variety of difficulties appear. A major problem proved to be the fact that in the vicinity of isotherms there might be no four neighbours to a specific point within the hysteresis loop. This is illustrated with the principle sketch in Fig. 7.1. The sketch shows the situation close to the adsorption isotherm. The grid build-up by the tabular data points is represented by circles that are filled if lying inside the hysteresis loop and open if being located outside. The filled circles thus represent the locations with pre-calculated water content values. If the hydration state of a bentonite is characterizes by a data point falling into one of the coloured areas in Fig. 7.1, there are less than four grid points available for interpolation. For the calculations, the case of less than four neighbours must be therefore be identified and special interpolation schemes must be applied.

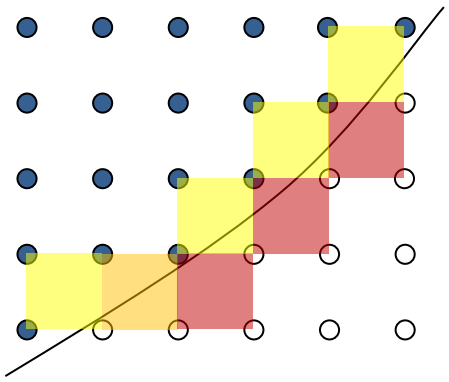

Fig. 7.1 Sketch of tabular data close to the adsorption isotherm;
points inside the hysteresis loop: filled symbols, outside: open;
ranges in coloured squares have less than 4 neighbouring data points:
3 neighbours (yellow), 2 neighbours (orange), one neighbour (red)

Under these circumstances, it is quite apparent, that the accuracy of the interpolated data can only be limited. This is a second major problem that can have serious consequences in case of switching from adsorbing to desorbing conditions (or vice versa). The point representing the actual hydration state of the bentonite can be unphysically shifted by switching thus introducing stability problems with the numerical solution scheme. This phenomenon is particularly serious in case of oscillations in the solution because it can result in alternate switching in a row of consecutive time steps. In a model with just one isotherm it results in temporary little movements along the isotherm and dampens itself out while each switch between scanlines increases the resulting errors.

These difficulties became only apparent while working with the tabular scheme. Not all problems could be satisfyingly solved yet. It is thus that some models presented in the following section required some specific modifications to ensure a completion of calculations.

7.3 Water loss due to heating

Water loss due to heating was initially realised as a lowering function g that was multiplied to the water content w_{iso} from the adsorption isotherm at reference temperature /KRÖ 08/:

$$w(r_h, T) = g(r_h, T) \cdot w_{iso}(r_h, T_{ref}) \qquad (7.7)$$

This had been tentative work based on /GAI 05/. With the newly determined functions (see section 5.3) this approach has to be modified to an additive correction that affects of course the scanlines as well. Assuming that differences arising from switching to scanlines can be neglected, the new approach adopted for code VIPER reads now

$$w(r_h, r_{h\,0}, T) = w_{iso}(r_h, r_{h\,0}, T_{ref}) - \Delta w(r_h, T) \qquad (7.8)$$

8 Influence on numerical models

8.1 Common basis of the numerical models

The numerical models described in this report aim at evaluating clearly the influence of different features in the constitutive relation between relative humidity and water content on the dynamics of bentonite re-saturation[16]. The impact on simulations is illustrated in this report by simple generic and easily comparable one-dimensional numerical models. The modelling refers basically to the isotherms and scanlines as well as to the dependency of water loss due to heating. The following considerations concern, by and large, the alternative concept for bentonite re-saturation as realized in code VIPER. By changing isotherms and scanlines appropriately, MX-80 as well as Calcigel are considered. For the complete set of characterising data refer to Appendix C.

Exemplarily and certainly without claims to conclusiveness, a comparison is set up on the basis of the simple water uptake test described in /KRÖ 04/. It concerns an essentially one-dimensional re-saturation process in a cylindrical confined sample of 10 cm length that is wetted from one side. For the plots of the model results, the open boundary is located on the left-hand side. On the right-hand side, the model is closed to flow. At the open boundary, the bentonite is either connected to free water at atmospheric pressure in case of water inflow or simply open to the atmosphere in case of drying.

The bentonite is compacted to a dry density of 1500 kg/m³ and the temperature is set to 20 °C for the isothermal cases. Initially, water content, relative humidity, dry density, and temperature of the bentonite are constant except at the open boundary where these quantities are set according to the boundary conditions of choice. Since there is very little overlap of the hysteresis loops for MX-80 and Calcigel (cp. Fig. 8.1), it is basically not possible to define common initial conditions for both materials, though.

Adsorption and desorption isotherms as well as the adsorption scanlines that have been measured under free swelling conditions are corrected to the confined conditions assumed here using the approach of /DUE 07/.The modelling results are given as distributions of the vapour partial density, the relative humidity and the water content at t = 0, 1,

[16] They can also be seen as the backbone of a case library that can be used in the future for checking the consistency with older versions in case of further work on code VIPER.

10, and 100 days. These three quantities have been chosen because the vapour density represents the primary variable in the numerical model, the relative humidity is the only measurable transient quantity in water uptake tests and the water content is the actual quantity of interest. The vapour partial density is linearly related to the relative humidity by the vapour saturation density and results in isothermal cases thus qualitatively in the same plot as the relative humidity. It is therefore shown only for wetting model in the next subsection and for the non-isothermal case.

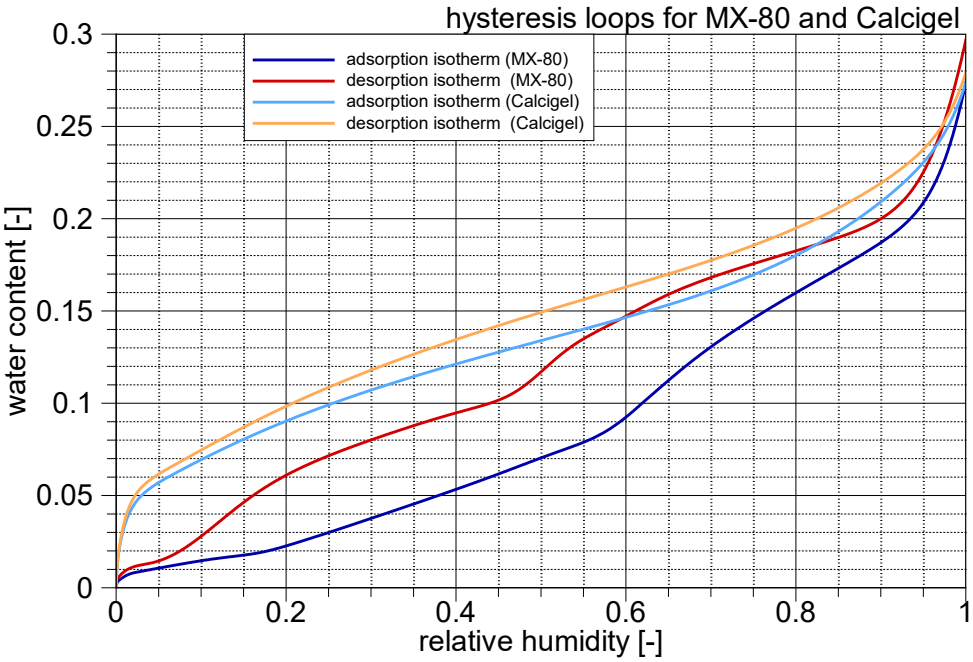

Fig. 8.1 Hysteresis loops for MX-80 and Calcigel

8.2 Isothermal wetting

The most basic re-saturation problem that is relevant for a geologic repository for nuclear waste is that of the isothermal and one-dimensional water uptake where the bentonite is homogeneously compacted, confined and connected to free water at one side. The water migrates from the inflow boundary into the sample and increases the water content continuously on its way which means that the bentonite experiences exclusively adsorption.

The steady-state solution for this set-up is obviously that of a fully saturated bentonite. However, re-saturation is mathematically described as a converging process that is never reaching steady-state. And during the theoretically everlasting transient phase, the shape of the water content distribution varies with the underlying constitutive relation for water content and relative humidity.

The simplest approach to the constitutive relation between water content and relative humidity is that of a linear isotherm where the maximum value at a relative humidity of 100 % is given by the maximum water content. Such an isotherm ignores any material specific features except the final water content which depends on the grain density. For comparison, water uptake has been modelled for this linear isotherm as well as those for MX-80 and Calcigel. The measured hysteresis loops for MX-80 and Calcigel are plotted in Fig. 8.2 together with the initial state for the different models. Note that the initial states for MX-80 and Calcigel are chosen to lie closely to the adsorption isotherm.

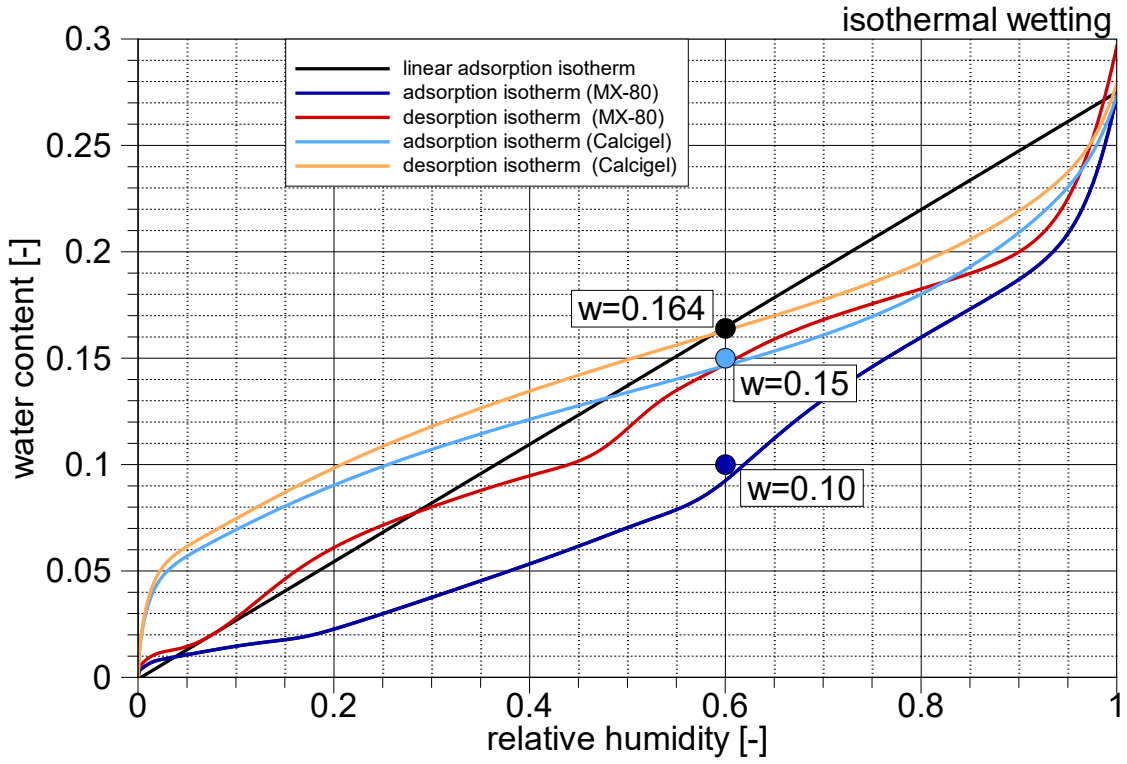

Fig. 8.2 Adsorption isotherms for MX-80 and Calcigel: linear and measured

Modelling results at 0, 1, 10, and 100 days simulation time are given in terms of the primary variable, the vapour partial density (Fig. 8.4), the relative humidity (Fig. 8.5) and the water content (Fig. 8.7). For the three models discussed here, the best basis for a comparison is given by the partial vapour density or the relative humidity (which are linearly related under isothermal conditions) as the same initial values were chosen for these quantities. Since the initial and the final values for these quantities are the same for all three models, the biggest differences can be observed somewhere in between.

The relevant sections of the three isotherms used here show quite different shapes (see Fig. 8.3) that appear to be reflected in the calculated curves. The linear isotherm is

obviously just a straight line while the adsorption isotherm for MX-80 appears to be basically a polygonal chain with two segments where the first section has approximately the same slope as the linear isotherm. By contrast, the isotherm for Calcigel is smoothly curved, converging towards the isotherm for MX-80 when approaching full saturation. Accordingly, the curves for vapour partial density calculated for MX-80 are closely related to those for Calcigel in the upper range of partial densities while they relate to the results from the linear isotherm in the lower range. The same applies analogously to the relative humidity curves. Slope change in the used isotherms seems also to cause inflection points in the resulting curves.

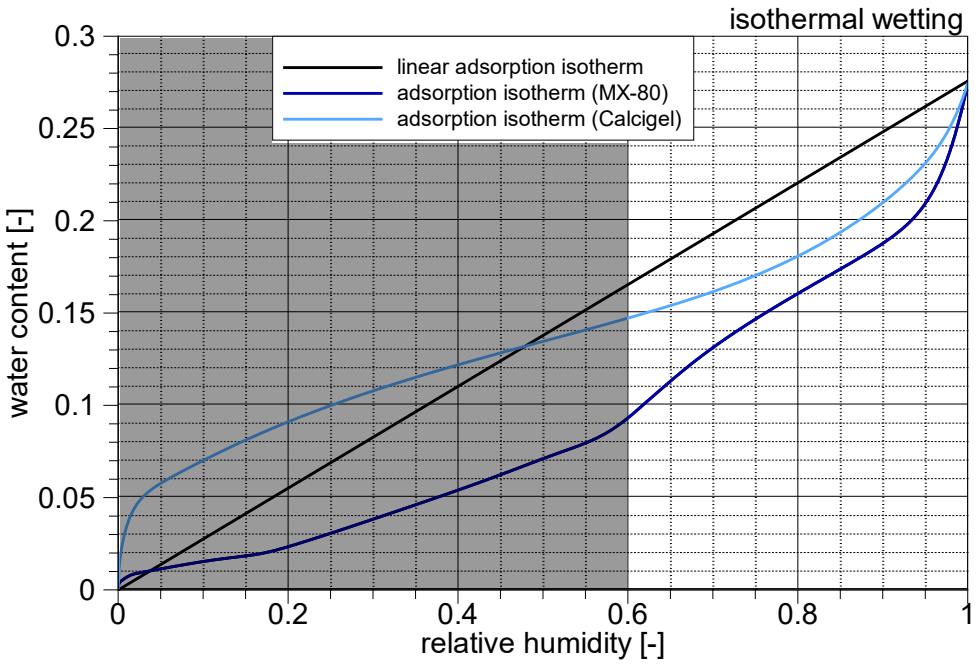

Fig. 8.3 Relevant sections of the adsorption isotherms for the models in section 8.2

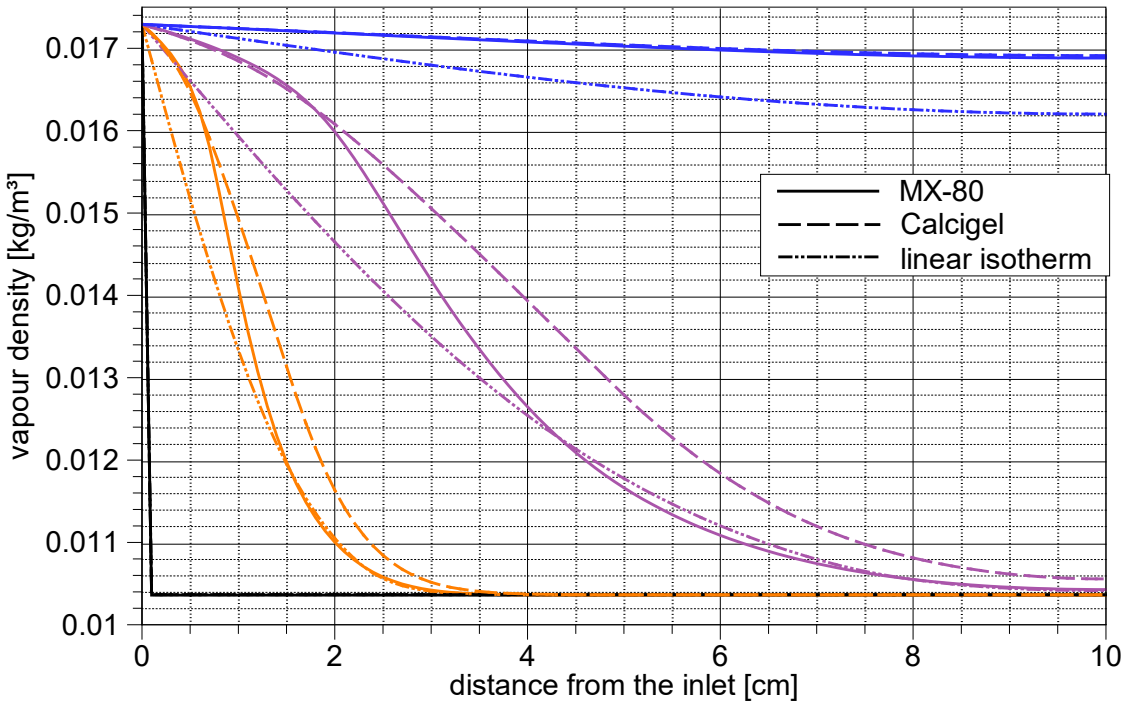

Fig. 8.4 Simulated vapour density distributions based on four adsorption isotherms; results at 0 (black), 1 (orange), 10 (violet) and 100 (blue) days

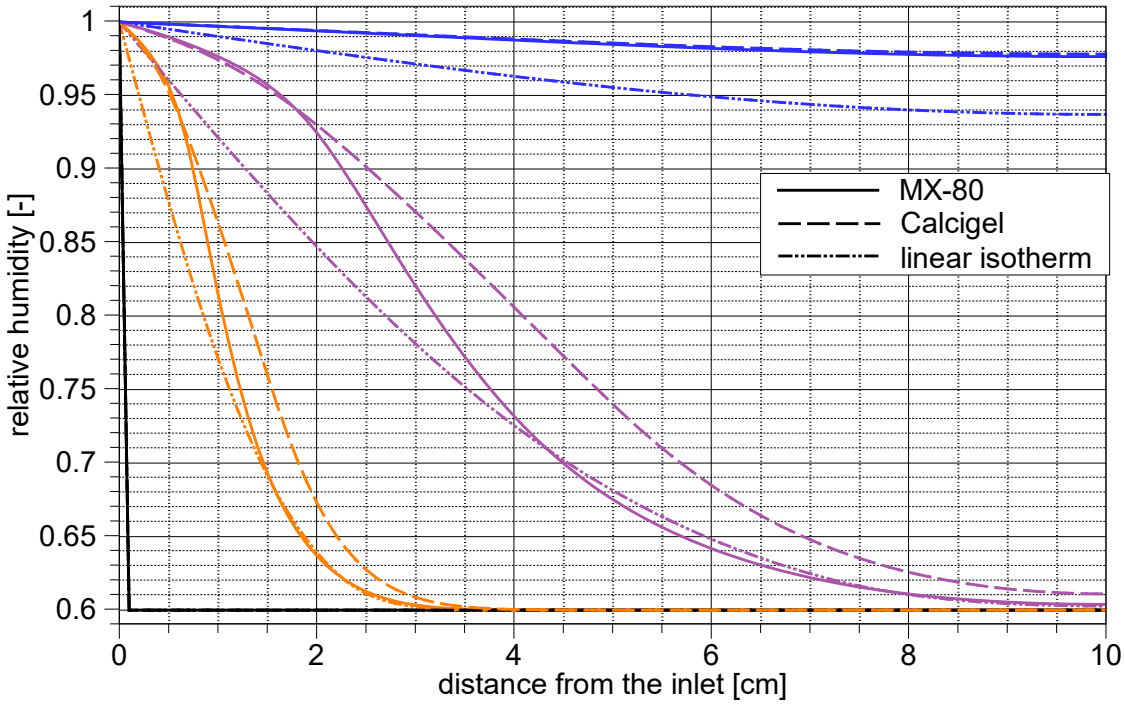

Fig. 8.5 Relative humidity distributions based on four adsorption isotherms; results at 0 (black), 1 (orange), 10 (violet) and 100 (blue) days

By contrast to the previous discussion, the means of comparing the water content curves for the three models are narrowed down to qualitative considerations because of the different initial conditions. The initially low water content in the model for MX-80 means that more water has to enter the model in order to fully saturate the bentonite than in case of the model for Calcigel. The model with the linear isotherm requires even less water uptake. Accordingly, the latter model fills up with water fastest. However, the depth to which the water has penetrated at specific times in the three models appears to be more or less the same, suggesting that water uptake might have not been very different if the initial conditions concerning the water content had been the same.

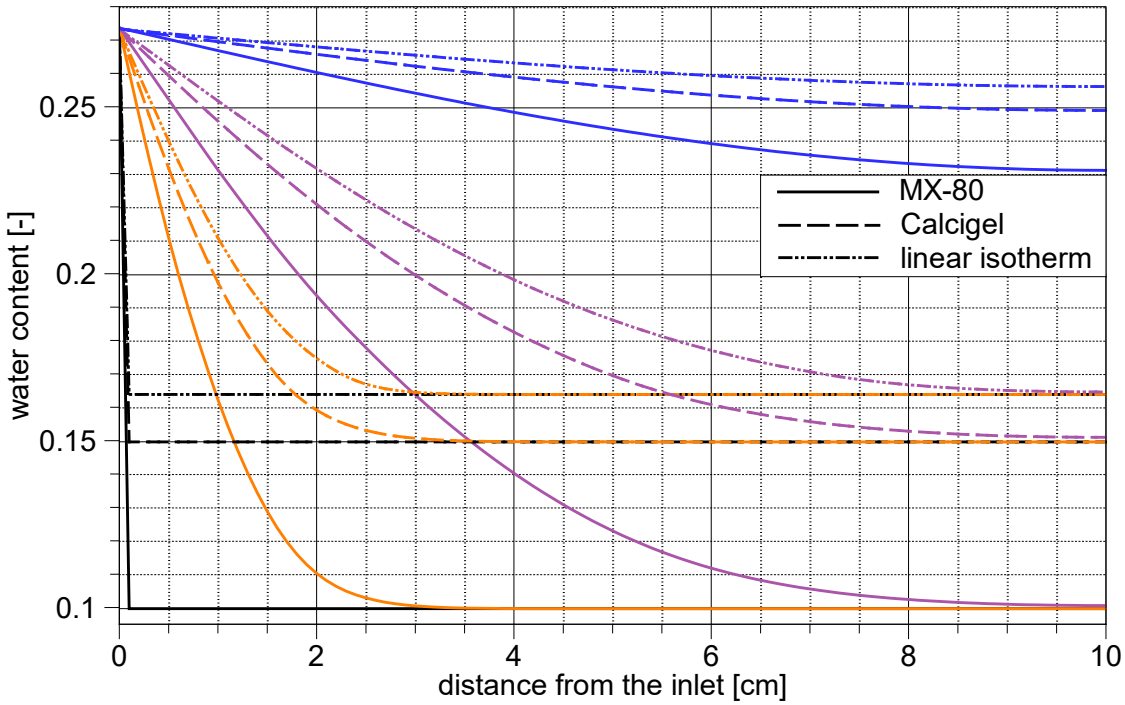

Fig. 8.6 Simulated water content distributions based on four adsorption isotherms; results at 0 (black), 1 (orange), 10 (violet) and 100 (blue) days

8.3 Isothermal drying

As a warm-up exercise for non-isothermal drying in the vicinity of heat-producing waste canisters, the isothermal drying of a bentonite towards an open boundary is investigated here. The bentonite in the models is initially rather saturated and starts out at a relative humidity of 80 %. It is connected to the atmosphere instead to a water source where a relative humidity of 40 % is assumed. As in the previous models, the mathematically convergent process prevents the model from actually reaching steady-state. The initial conditions for the models are depicted as in the previous subsection in relation to the

different desorption isotherms (Fig. 8.7) and the modelling results are given at 0, 1, 10, and 100 days by reference to the relative humidity (Fig. 8.8) and the water content (Fig. 8.9).

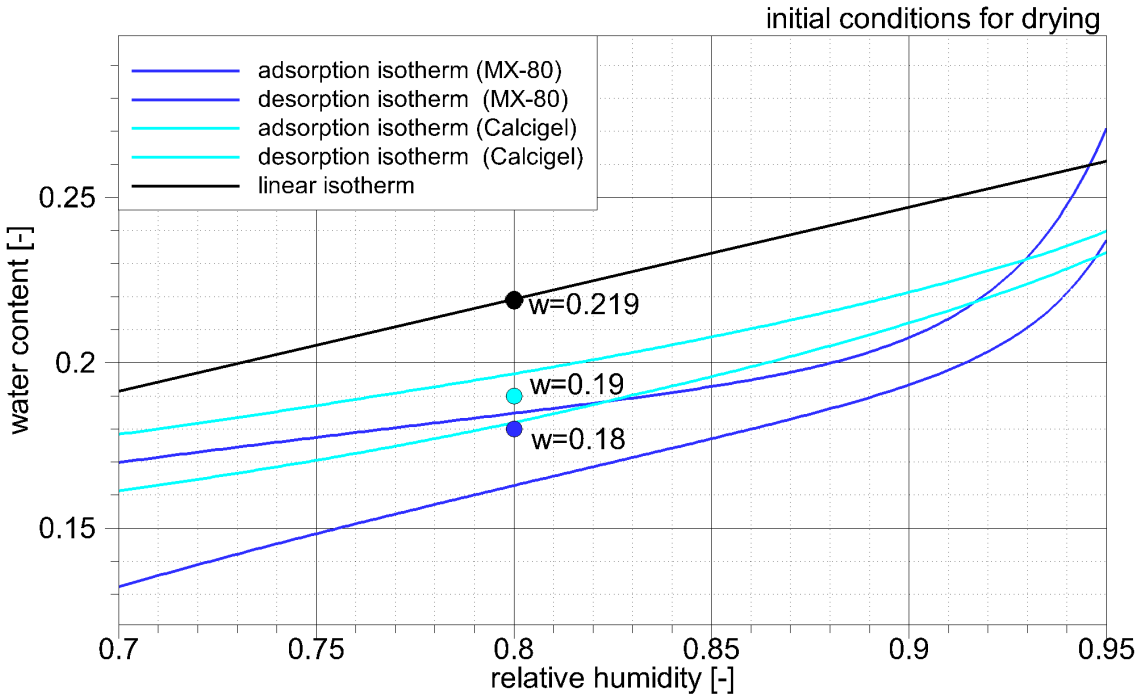

Fig. 8.7 Desorption isotherms for MX-80 and Calcigel: linear and measured

Curves for relative humidity lie much closer together in the drying case than in the wetting case which can probably be ascribed to the fact that the initial values are less widely spread. Also, the difference between initial and boundary values is less pronounced. Again, the complexity of the isotherms/scanlines for MX-80 is reflected in the resulting curves.

The resulting water content curves appear to be rather confused because not only the initial water content values differ according to the different isotherms but also the values at the boundary. However, the dynamics of the water uptake appear to be quite similar. The curves for one day show basically the same penetration depth into the bentonite and at 10 days they just have met the opposite (closed) boundary. As in the wetting case, the results might have been quite similar, had the initial and the boundary water content been the same.

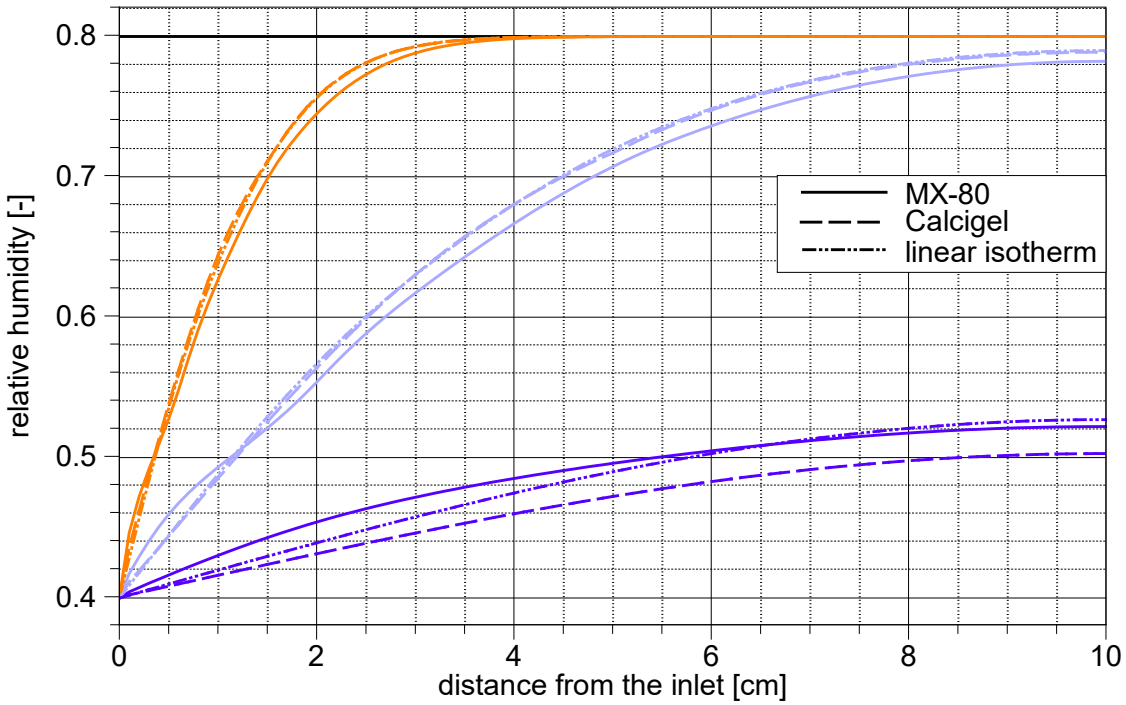

Fig. 8.8 Relative humidity distributions based on four desorption isotherms; results at 0 (black), 1 (orange), 10 (violet) and 100 (blue) days

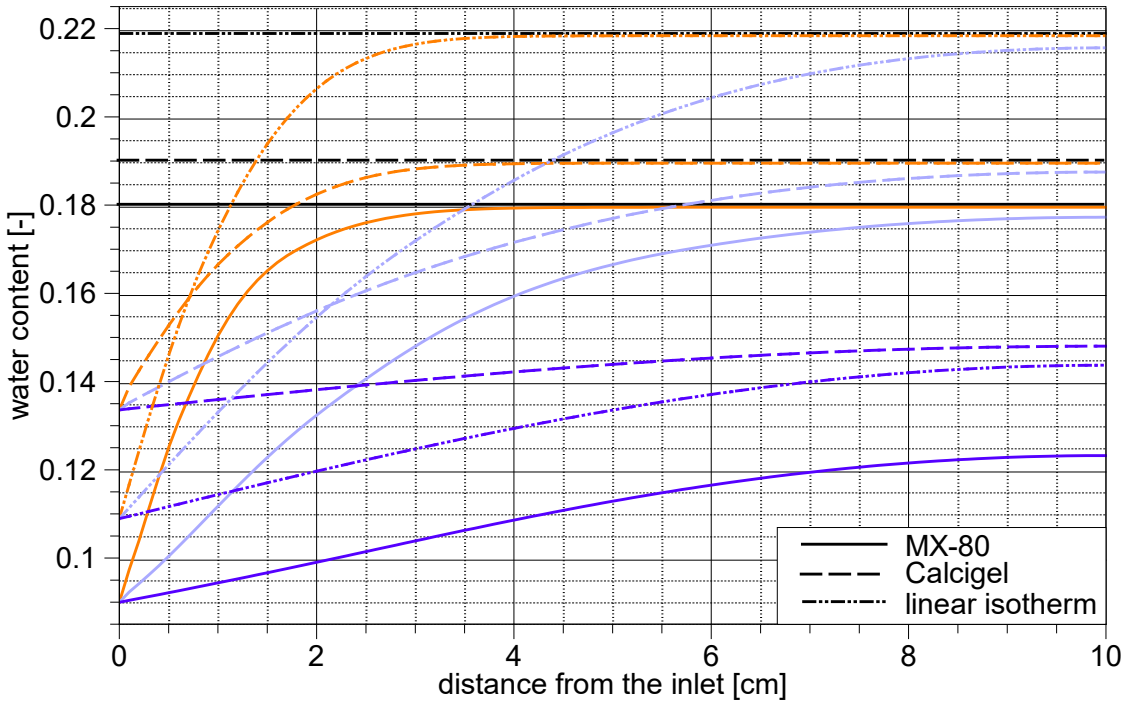

Fig. 8.9 Simulated water content distributions based on four desorption isotherms; results at 0 (black), 1 (orange), 10 (violet) and 100 (blue) days Comparison

8.4 “Arbitrary” initial conditions

Modelling real cases with code VIPER (or its predecessors) had caused some concern in the past since the usage of an isotherm implies that there is a fixed one-to-one relation between relative humidity and water content. In actual tests, though, the data pair of measured relative humidity and water content usually does not fit a previously used isotherm. This may be due to the varying of the natural mineralogical composition of the sample as well as to its individual wetting and drying history. Introducing scanlines opens up the opportunity of using any data pair within the hysteresis loop and the related scanline instead of being stuck to a stringent use of an isotherm. Of interest is then, of course, the impact of the range of possible initial conditions on the simulation results.

This case is differently set up than the isothermal wetting and drying cases as the initial water content is fixed and the relative humidity varies. Therefore, the plots for the vapour partial density and the relative humidity are more difficult to interpret than the one for the water content.

8.4.1 MX-80

Varying initial conditions are introduced by varying the initial relative humidity at a fixed water content of 10 %. Humidity is set to 60 % which is close to adsorption isotherm and to 45 % as being close to the desorption isotherm. For the purpose of comparison, also a linear isotherm is used that connects the point of origin with the maximum water content by a straight line. In this case, the initial relative humidity amounts to about 37 % at 10 % water content. Isotherms and scanlines as well as the initial conditions are indicated in Fig. 8.10. The two relevant scanlines are plotted as solid lines, all other scanlines are given as dashed lines for orientation.

The modelling results are given as distributions of the relative humidity (Fig. 8.11) and the water content (Fig. 8.12) at t = 0, 1, 10, and 100 days.

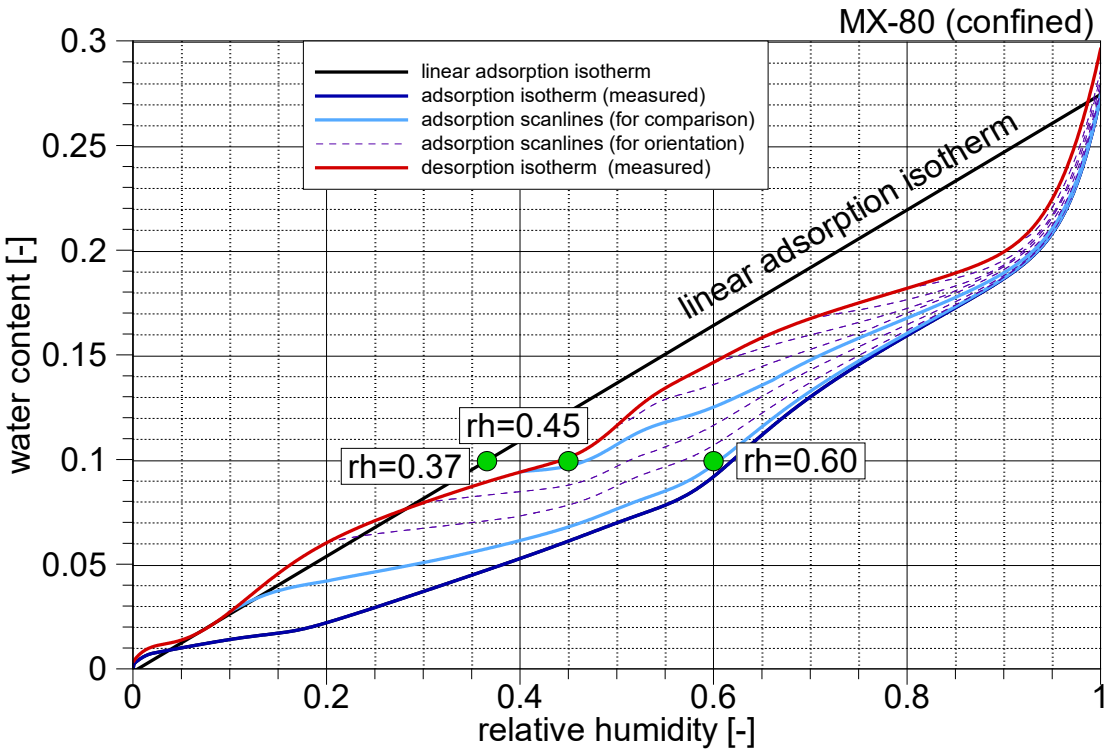

Fig. 8.10 Scanlines and isotherms for MX-80 at 25 °C; basis for comparison

As expected from the set-up, the interpretation of the relative humidity curves are difficult because of the different initial values of the three models. However, with a view to the penetration depth, the notion of comparable results in case of identical initial values applies also for this case.

By contrast, the calculated water content distributions (Fig. 8.12) show very little variation between the three cases. The maximum difference amounts to little more than 1 % water content. With a view to water uptake dynamics and migration, the models considered here appear to be quite insensitive to the initial relative humidity, seemingly confirming the notion of similar results for identical initial values.

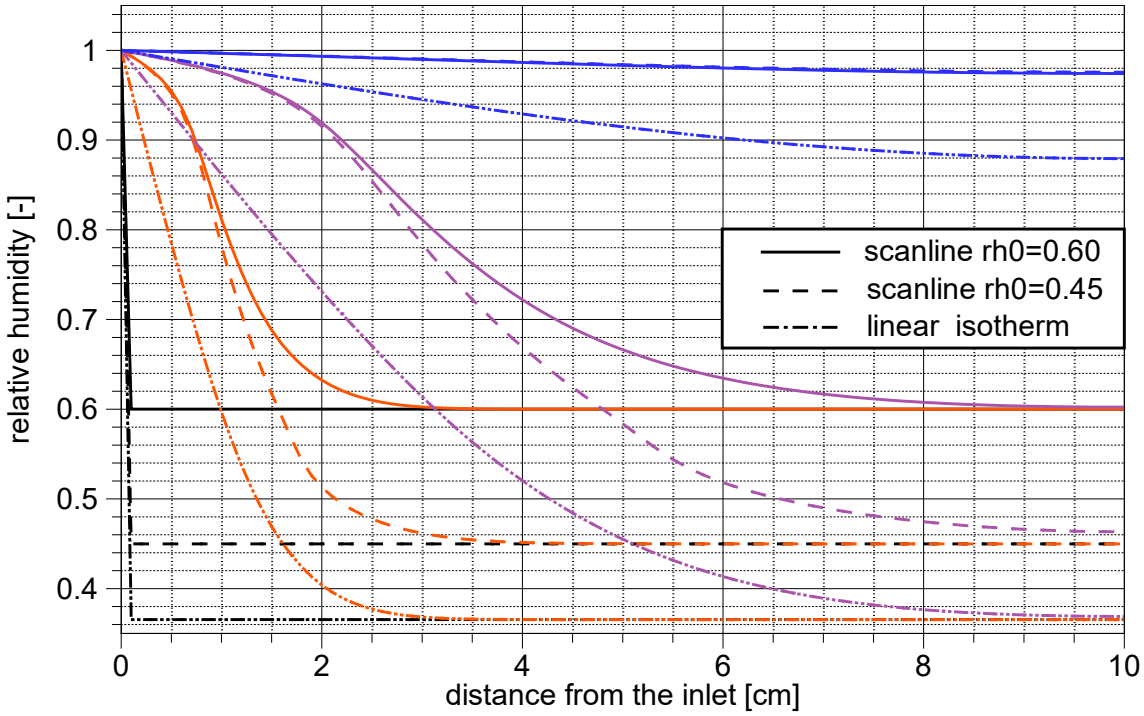

Fig. 8.11 Simulated relative humidity distributions based on three scanlines/isotherms;
results at 0 (black), 1 (orange), 10 (violet) and 100 (blue) days

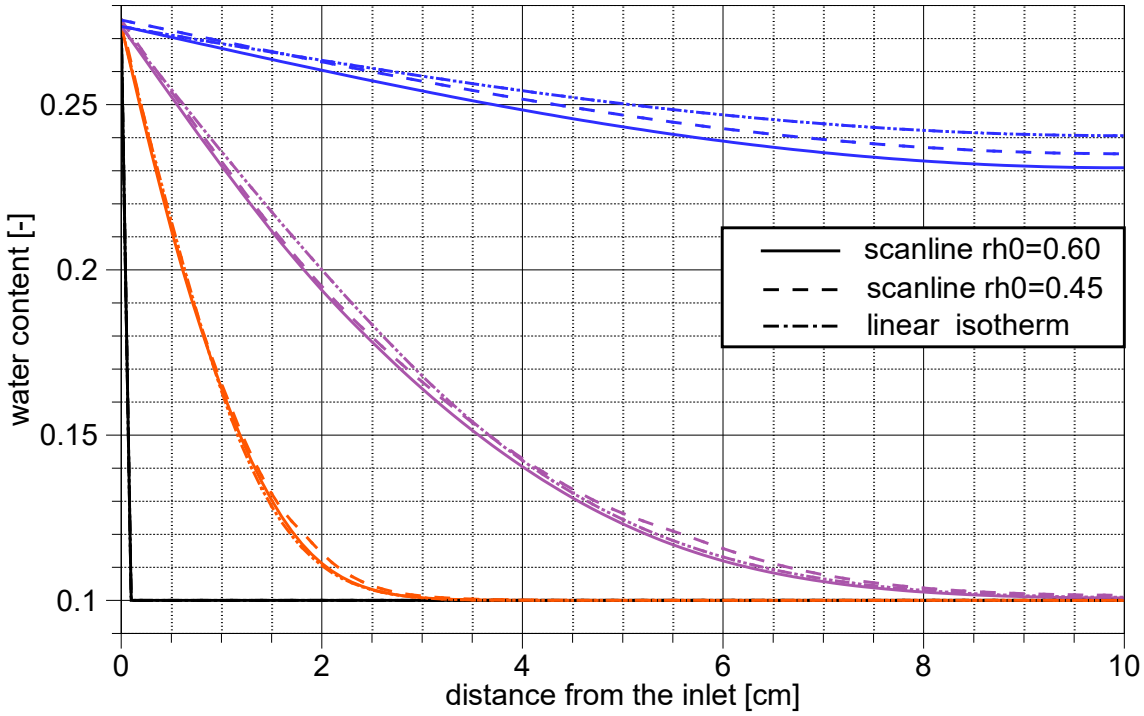

Fig. 8.12 Simulated water content distributions based on three scanlines/isotherms;
results at 0 (black), 1 (orange), 10 (violet) and 100 (blue) days

8.4.2 Calcigel

A analogous model set-up as for MX-80 was used also for Calcigel. The comparison comprises three models varying in the initial relative humidity (51 %, 55 % and 60 %, respectively). In order to maximize the range of initial relative humidity values, the initial water content was increased to 15 %, though. The results are depicted analogously to those for MX-80 showing the initial conditions for the three models in relation to isotherms and scanlines (Fig. 8.13) as well as the development of the relative humidity (Fig. 8.14) and the water content (Fig. 8.15).

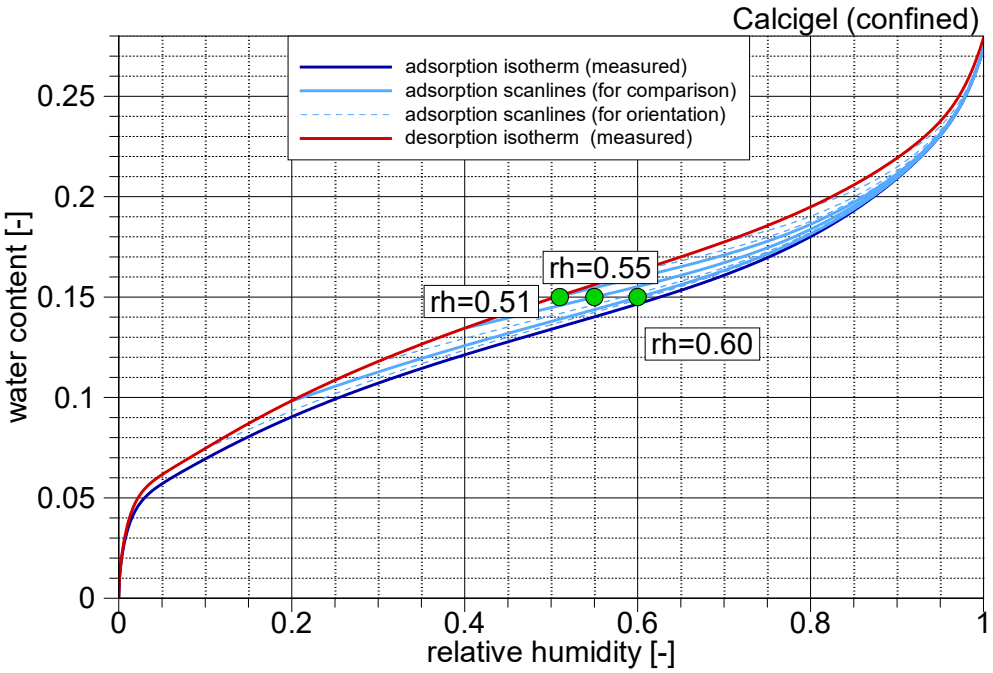

Fig. 8.13 Scanlines and isotherms for Calcigel at 25 °C; basis for comparison

The results for Calcigel are qualitatively quite similar to those for MX-80. They are affected, however, by the different shape of the hysteresis loop of adsorption and desorption isotherm. Since the loop is narrower than that of MX-80, the possible range of initial relative humidity values is smaller. By and large, the bandwidth of results created by the variation of initial conditions is thus noticeably smaller for Calcigel than for MX-80. The differences in the water content distributions are hardly noticeable.

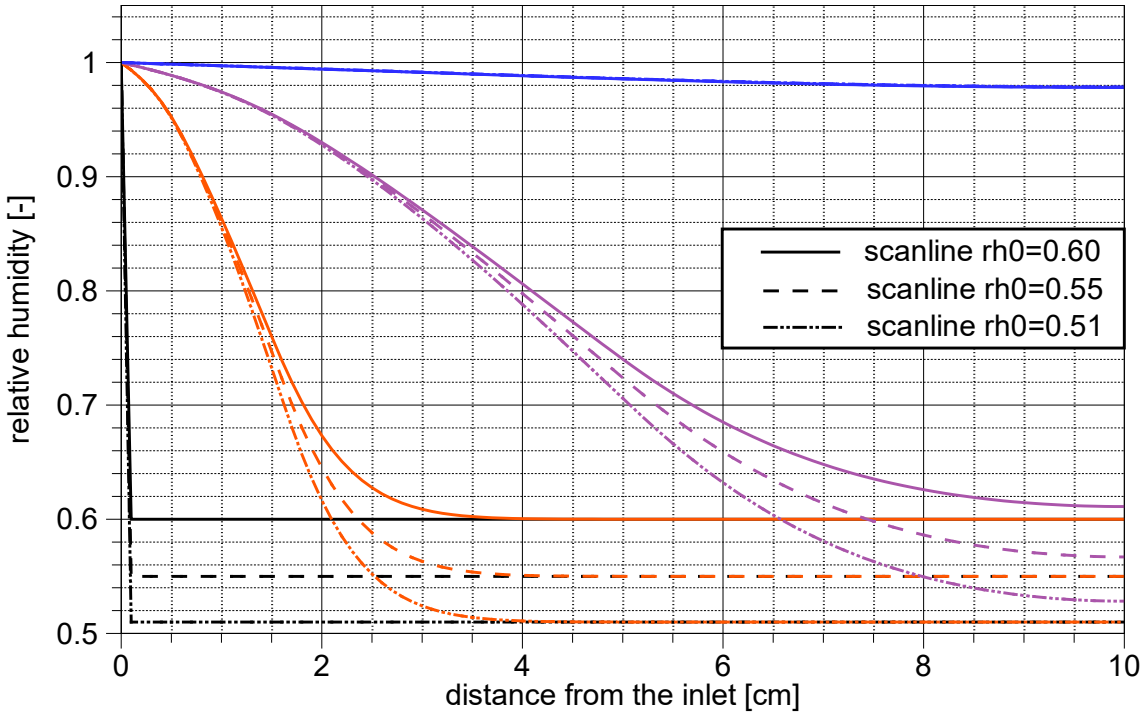

Fig. 8.14 Simulated relative humidity distributions based on three scanlines/isotherms;
results at 0 (black), 1 (orange), 10 (violet) and 100 (blue) days

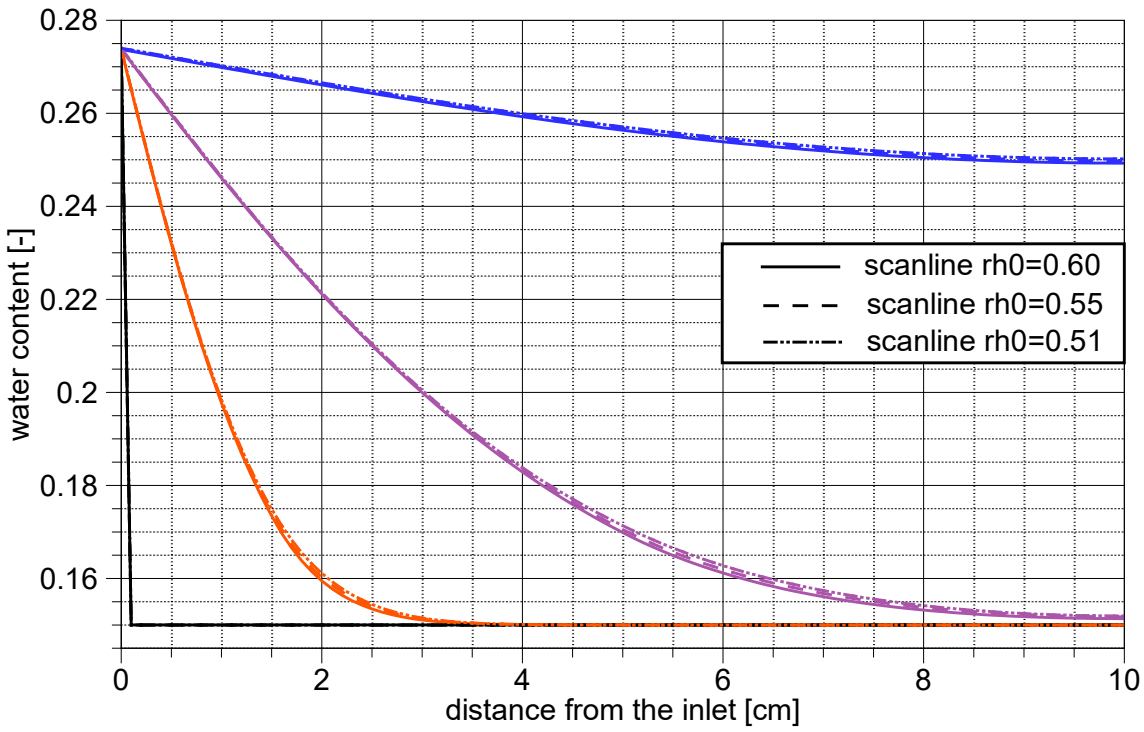

Fig. 8.15 Simulated water content distributions based on three scanlines/isotherms;
results at 0 (black), 1 (orange), 10 (violet) and 100 (blue) days

8.5 Changing boundary conditions between wetting and drying

In the previous models, different but single isotherms and scanlines have been used. The next set of models is addressing switching between them. Under isothermal conditions this can happen when a wetting bentonite is disconnected from the water supply and exposed to ambient conditions. In that case, wetting conditions are swapped for drying conditions. Concerning hydration this means switching from an adsorption path to a desorption path along the related scanlines.

According to this idea, the simulations comprise two phases, first a wetting phase as in the wetting case described in subsection 8.2 but with a boundary humidity of 85 %, and second, half-way into the simulation, a linear decrease of the relative humidity over one day simulation time down to 10 % for the remaining simulation. The initial relative humidity was chosen to be the 60 % in all three models. This has been done first with a model using a linear isotherm that does not include switching scanlines thereby forms a reference for models without capabilities switching scanlines. The plots with the relative humidity (Fig. 8.16) and the water content curves (Fig. 8.17) show results not only for days 0, 1, 10, and 100 as in the previous subsections but also a few curves during day 50 when the boundary conditions are changing.

The results show clearly the wetting pattern (blue curves) and the drying pattern (orange and red curves) as well as the transition in between (violet-like curves). Note that the changes at the boundary have not affected the sample further than 4 cm into the bentonite. Beyond the 4 cm, the moisture gradient was still pointing down in the inflow direction, thereby causing water migration that was still directed deeper into the bentonite. This has led to a re-distribution of water, increasing the water content at the end of the sample up to a point where it was at day 60, 9 days after the transition to a dry boundary, higher than at day 51.

Later, models for MX-80 and Calcigel were run to provide a basis for assessing the effect of varying scanlines on the results. As in the previous models, the initial conditions had to be different due to the different ranges covered by the hysteresis loops (where applicable). In the following two figures, the results for relative humidity (Fig. 8.18) and water content (Fig. 8.19) from the model with a linear isotherm and the models with isotherms/scanlines for MX-80 and Calcigel are compared for days 0, 1, 10, 50, 60, and 100.

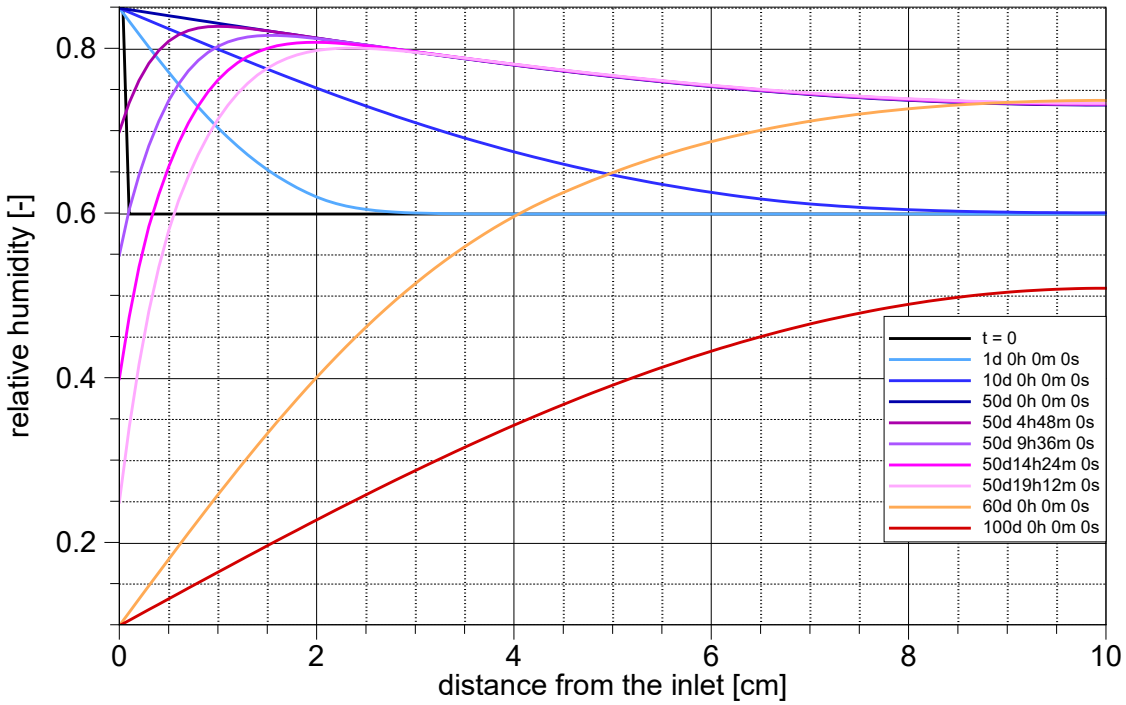

Fig. 8.16 Relative humidity during switching from wetting to drying (linear isotherm)

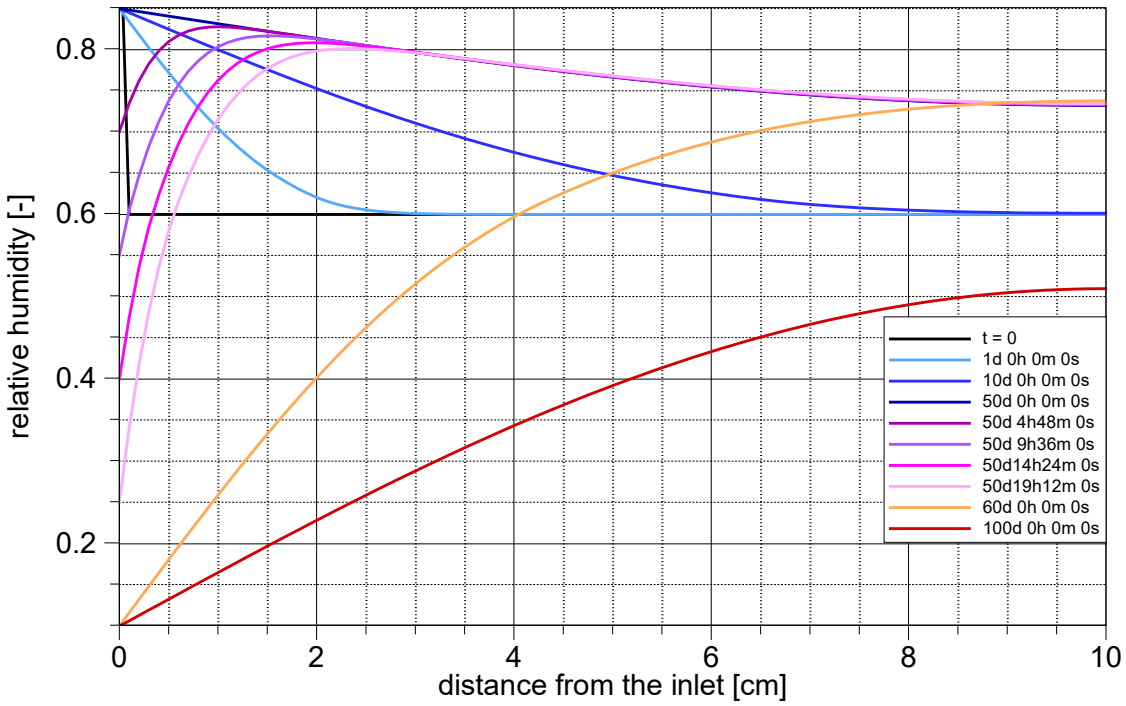

Fig. 8.17 Water content during switching from wetting to drying (linear isotherm)

In terms of the relative humidity, the initial conditions (60 %), the boundary conditions during the wetting phase (85 %) and those during the drying phase (10 %) are easily recognisable in Fig. 8.18. The different (hypothetical) materials result in certain differences in the relative humidity that reaches a maximum of about 10 % relative humidity towards the end of the calculations. The differences are larger in the calculated water contents, though, where a maximum difference of about 5 to 6 % water content is reached.

The results for the wetting phase are rather unremarkable as all curves are comparatively smooth and closely related. Things look different, though, when it comes to the subsequent drying phase. This is due to having a non-uniform distribution of primary and secondary variables at the beginning of the drying phase but even more so due to switching scanlines accordingly.

The switching does furthermore not occur for all nodes at once but successively as the drying front proceeds into the bentonite. This is indicated in Fig. 8.20 which shows the distribution of scanline starting points (relative humidities) for the same points in simulation time as in Fig. 8.16. The early curves for less than 50 days are horizontal lines since the whole domain runs on the initial adsorption scanline with the starting point at about 43 % relative humidity. All these curves are covered by the 50-days curve which is in turn covered by curves for later times. From the sequence in which the plot is drawn, the progress of the drying front can be derived by the stepwise change from adsorption scanline (starting point is a positive number) to the desorption scanline (starting point is a negative number). Thereby, the starting points of the desorption scanlines range between 78 and 88 % indicating different degrees of saturation when the switching of the scanlines occurred.

The effect on the modeling results from switching scanlines is obviously related to the differences in the spatial layout of the scanlines involved. No effect can therefore be seen when using a linear isotherm. Also, comparatively little is noticeable in the results for Calcigel since the scanlines lie quite closely together (cp. section 4.2.2). By contrast more complex are the scanlines for MX-80 as they are more widely spread and additionally rather bended (cp. section 4.2.1). For MX-80 this results in somewhat hump-like shaped relative humidity curves that are not comparable to the results of the other two models. In principle, the same can be said about the results for the water content.

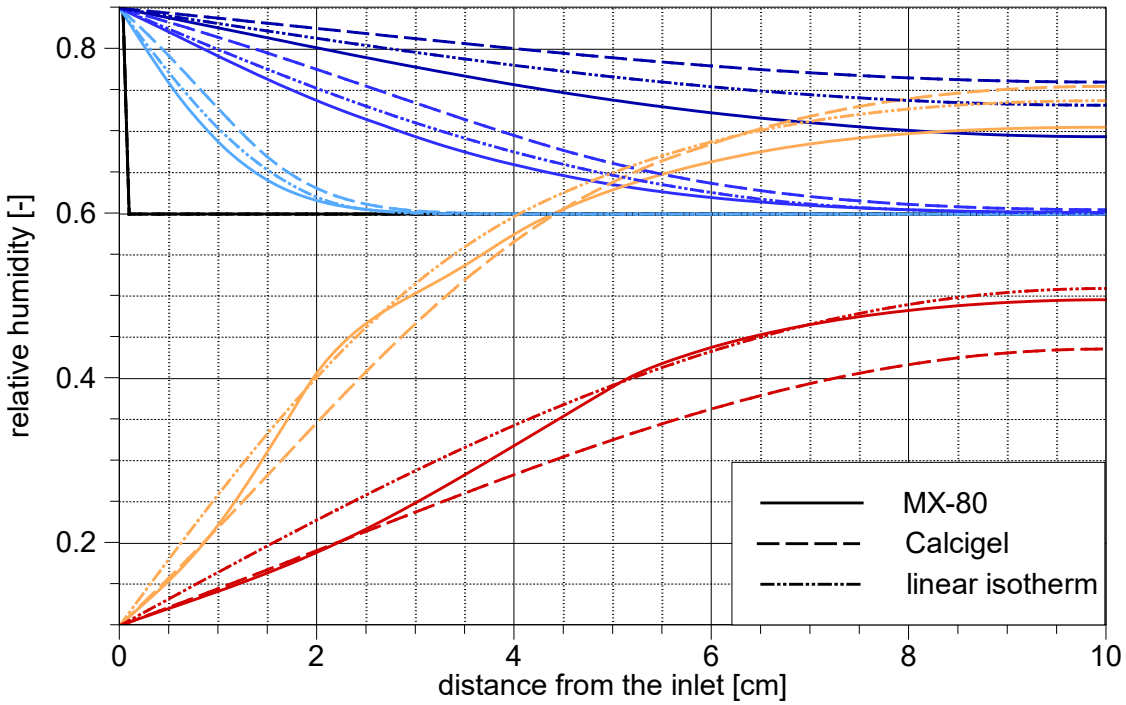

Fig. 8.18 Relative humidity during switching from wetting to drying (linear isotherm); colour coding as in Fig.8.16/Fig.8.17

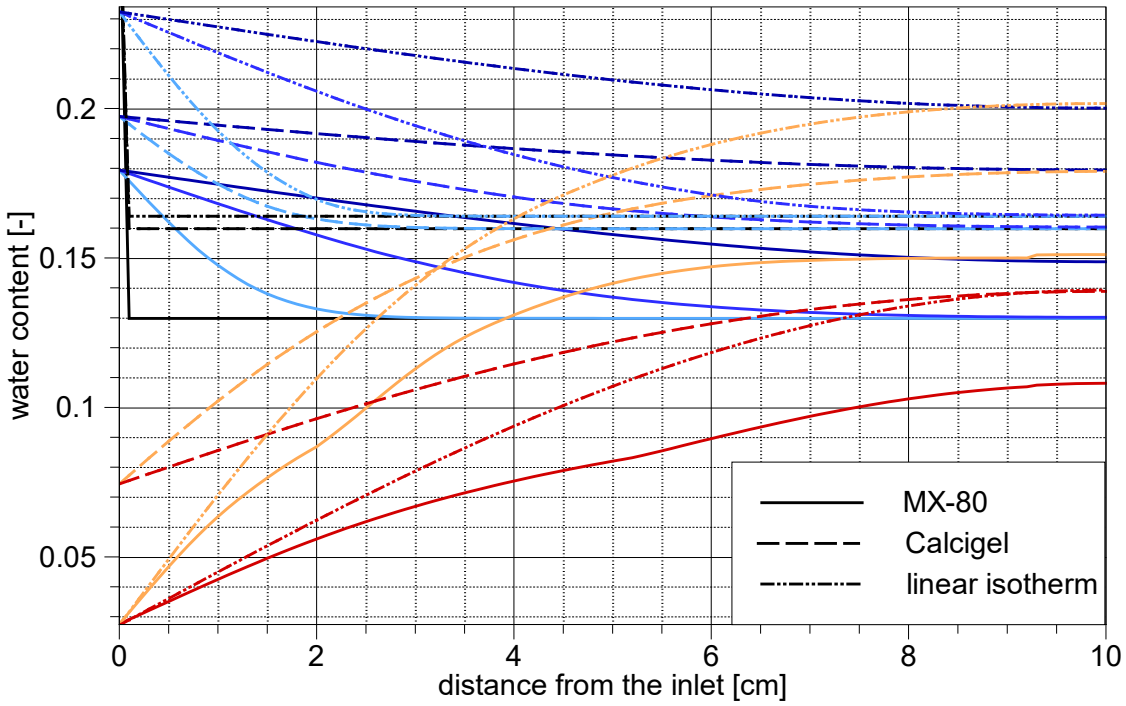

Fig. 8.19 Water content during switching from wetting to drying (linear isotherm); colour coding as in Fig.8.16/Fig.8.17

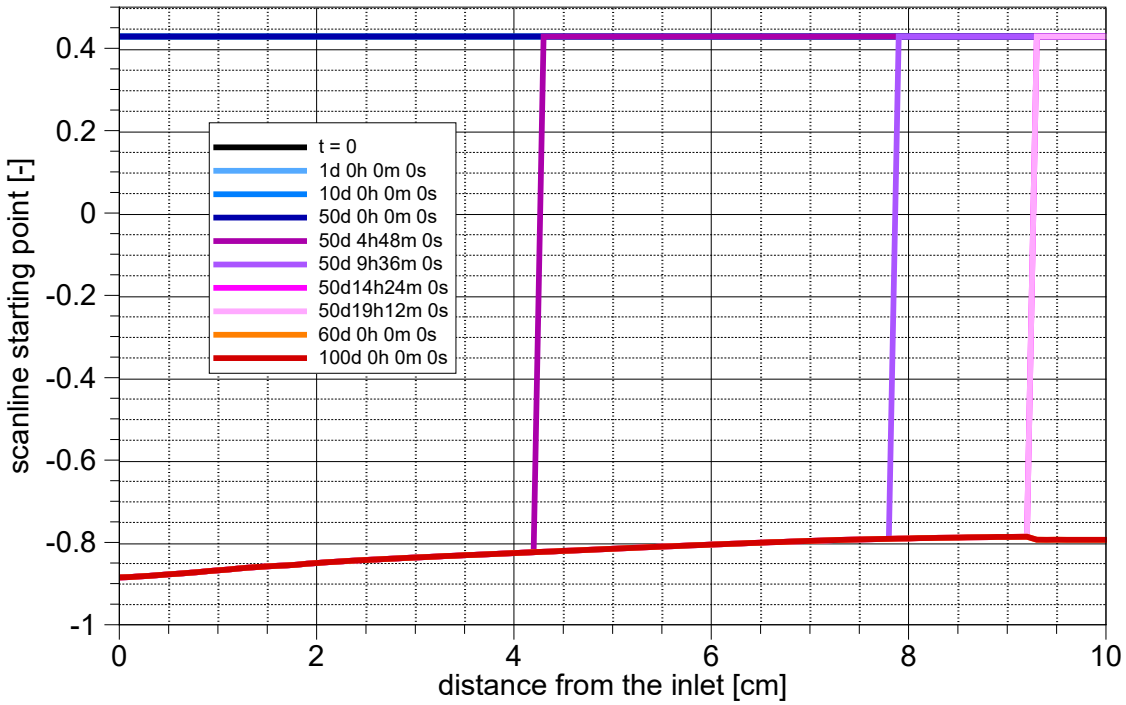

Fig. 8.20 Relative humidity of the scanline starting points during switching from wetting to drying (linear isotherm); colour coding as in Fig. 8.16/Fig. 8.17

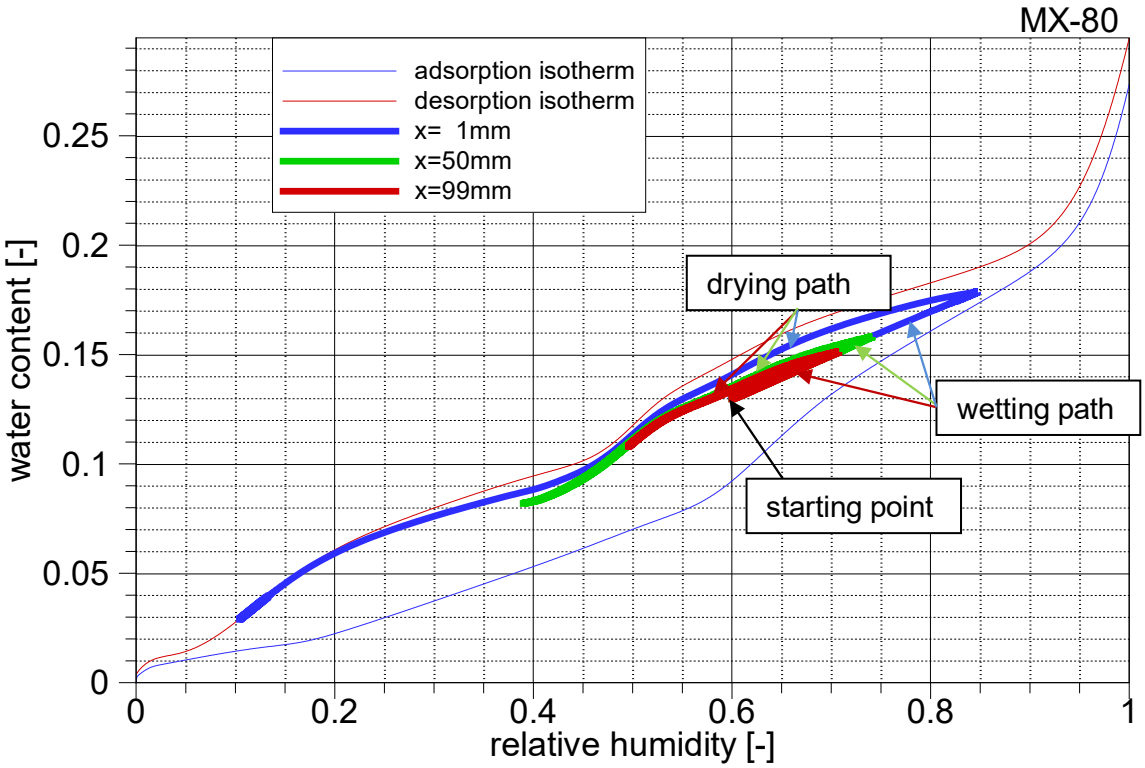

Fig. 8.21 Hydration paths for selected points of the MX-80 model

Note that the boundary values for the water content seem to be erroneously the same for MX-80 model and the model with the linear isotherm during the drying phase. Close inspection shows that they are not identical, though. The reason for this strange looking result can be derived from the hydration paths for three points in the MX-80 model that are shown in Fig. 8.21. The points are located at a distance of 1 (blue), 50 (green) and 99 (red) mm from the inflow boundary. The effect of wetting is obviously strongest close to the inflow boundary which lets the relative humidity increase here most while the effect is weakest at the opposite boundary. Correspondingly, the blue curve reaches furthest to the right in Fig. 8.21 and the red one least when the drying begins.

Drying means decreasing of the relative humidity and thus moving of the hydration state towards the left hand side of Fig. 8.21, the range of lower relative humidities. The end state for the point close to the inflow boundary lies close to the desorption isotherm of MX-80. In Fig. 8.10, for instance, the sets of isotherms of the different models are shown including the desorption isotherm for MX-80. Looking at 10 % relative humidity reveals that at that particular point, the desorption isotherm for MX-80 and the linear isotherm occupy by chance almost the same spot. It is thus that also the boundary values for the two models are almost the same.

8.6 Moisture re-distribution due to heating

8.6.1 Common model features

The model set-up common for all the models that are discussed in this subsection is described in the following. Again, a one-dimensional domain is investigated where one side is open to a water reservoir and the other is closed for flow. The same materials as for the previous test cases are used: MX-80, Calcigel and an artificial material with a linear isotherm. The main difference here is an increase of temperature during the model runs. After the first day (model time) during which the models follow a hydration path like in the wetting case (section 8.2), the models become heated. The temperature increases linearly over the whole model domain and linearly with time during the second day until reaching a maximum temperature of 50 °C at the closed end as depicted in Fig. 8.22. The maximum temperature had been chosen to comply with the measurements (see section 5.2). The temperature-dependent secondary variables such as the saturation vapour pressure, the diffusion coefficients and the loss of hydrated water to the pore atmosphere (see section 5.3) are automatically changed in the model accordingly.

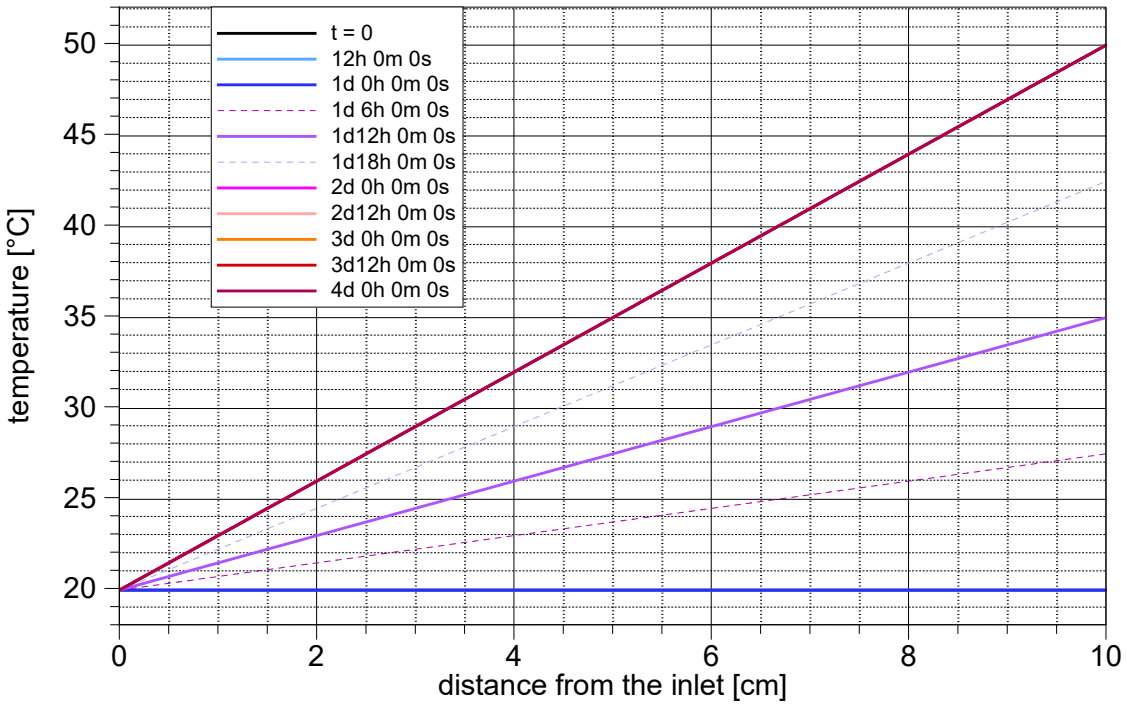

Fig. 8.22 Temperature evolution[17]

Heating leads to a loss of interlamellar water that transfers from the interlamellar space to the pore atmosphere while changing from the hydrated state to gaseous vapour. This process increases locally the vapour density, building up a gradient in vapour density that in turn drives binary vapour diffusion from the heated end of the domain towards the cool end. During the 4 days of simulated model time, two water transport processes can thus be observed: water migration due to conventional inflow towards the heated end of the model and vapour migration towards the cool end due to vapour diffusion.

8.6.2 Discussion of the model for MX-80

While the vapour partial density is the primary variable in code VIPER, the results in terms of the relative humidity – a secondary variable – are easier to understand. They are shown in Fig. 8.23. The distributions are plotted for every 12 hours in thick solid lines and intermediate curves during the heating period are inserted in thin dashed lines. The two water migration processes described in the previous subsection can clearly be recognised in the results: (1) water intruding from the open (left-hand) side of the model

[17] Note that isolines for constant temperatures (t<1d and 2d<t<4d) cover each other

thereby wetting the bentonite and (2) drying at the heated end showing at first an increase of the humidity with heating but subsequently a decrease even below the initial value.

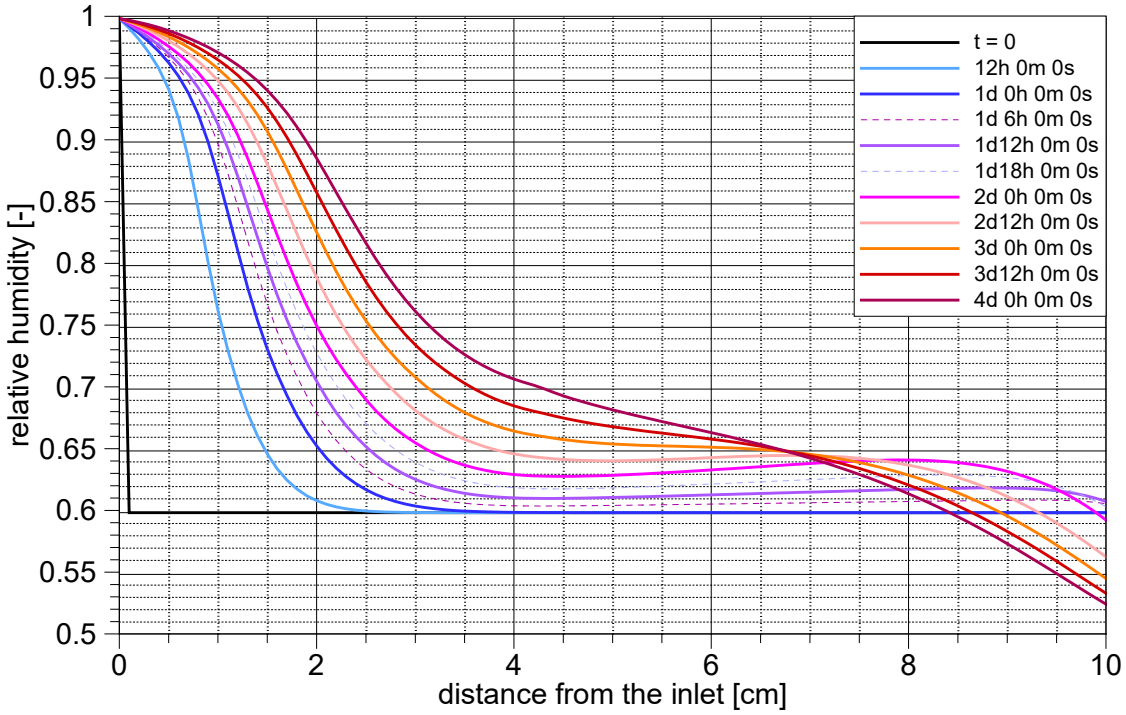

Fig. 8.23 Evolution of the relative humidity in the MX-80 model

The associated plot for the vapour partial density in Fig. 8.24 is much more difficult to interpret since it is strongly influenced by the evolution of the saturation vapour density that increases exponentially with temperature. An impression of that increase is given in Fig. 8.24 by the two curves for the initial vapour saturation density and the one at full heating after 2 days. The definition of the relative humidity as the ratio of vapour density and saturation density explains the difficulties of understanding the curves for the vapour density.

Much more clearly again is the evolution of the water content (see Fig. 8.25) that is as easily interpreted as the relative humidity curves. The glitch at 43 % relative humidity requires some further inspection of the model, though.

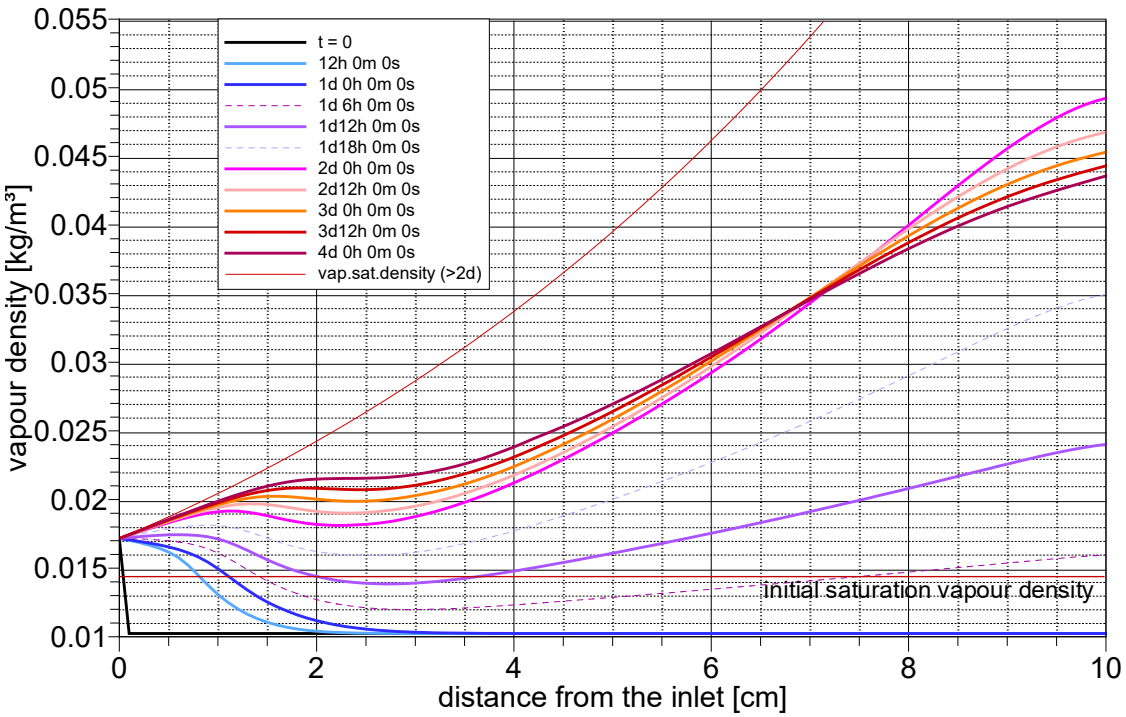

Fig. 8.24 Evolution of the vapour partial density in the MX-80 model

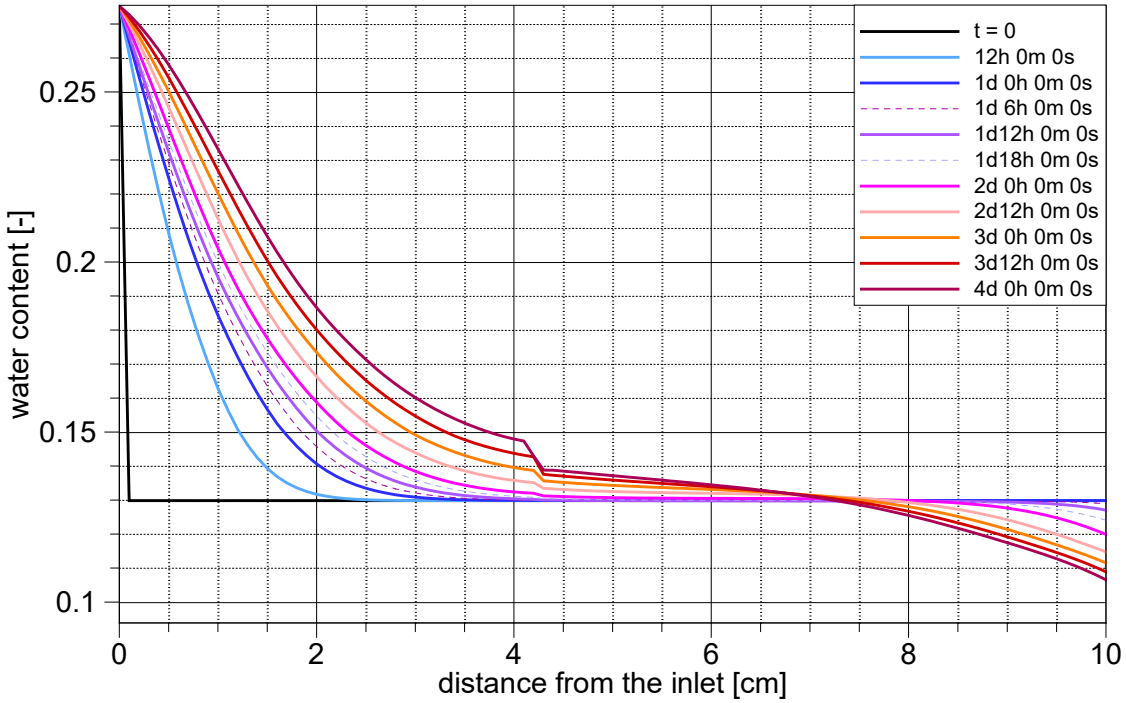

Fig. 8.25 Evolution of the water content in the MX-80 model

Another way of visualizing the hydration dynamics has been introduced in the framework of the models with changing boundary conditions where the evolution of relative humidity

and water content for a specific point in the model is plotted as data pairs in the relative humidity-water content plane (cp. Fig. 8.21). This is the same plotting plane as that for the isotherms/scanlines. As in the case with changing boundaries, the adsorption and desorption isotherms are included in Fig. 8.26 as a reference. It has to be kept in mind, though, that isotherms and scanlines are subject to the heat induced water loss and change accordingly.

The hydration path for the first node next to the inflow boundary at a distance of 1 mm is depicted in Fig. 8.26 (point 1, blue path). This point is affected by the temperature increase to less than one degree Celsius and can thus be considered to be under almost if not quite isothermal conditions. Starting point lies as for all other points at r_h = 60 % and w = 13 %. For MX-80 this relates approximately to the scanline starting at $r_{h\,0}$ = 43.5 %. Wetting at this point follows nicely the isothermal adsorption scanline.

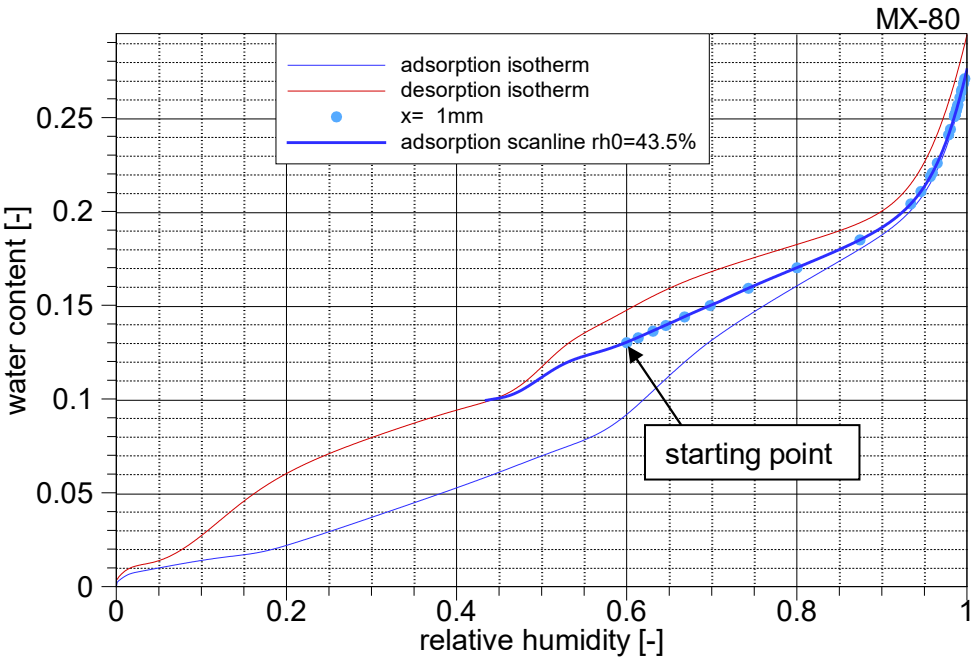

Fig.8.26 Hydration path at 1 mm distance from the inlet in the MX-80 model

The hydration paths for locations that are truly affected by the induced heat look much more complex as shown in Fig. 8.27. Two more locations are discussed in the following, the points at 50 mm distance from the inlet (point 2, green path) and at 99 mm distance (point 3, red path).

At the beginning of heating after one day, both points have not been reached yet by water from the inlet. In other words, the state of hydration remains at point 2 and point 3 at initial conditions until heating.

Afterwards, point 2 experiences exclusively adsorption. Under isothermal conditions, the related hydration path would have been the same as the blue one for point 1, only somewhat delayed. However, isotherms and scanlines are gradually shifted downwards during heating due to the temperature-related loss of hydrated water in the interlamellar space. During heating, the hydration path of point 2 thus deviates increasingly from the blue scanline that represents isothermal conditions. With the stable temperature conditions that begin with day 3, the scanline does not change anymore, and the hydration path follows the modified scanline.

Scanline and thus hydration path of point 2 nevertheless still show an increasing distance from the blue scanline of point 1 even after the beginning of day 3. They do so with a slightly different trend, though, indicating a different reason for the deviation after day 2. This is accounted for by the assumption that the maximum temperature induced water loss occurs at 70 % relative humidity in the model (cp. section 5.3.1) which is not reached by point 2 at termination of the model after 4 days.

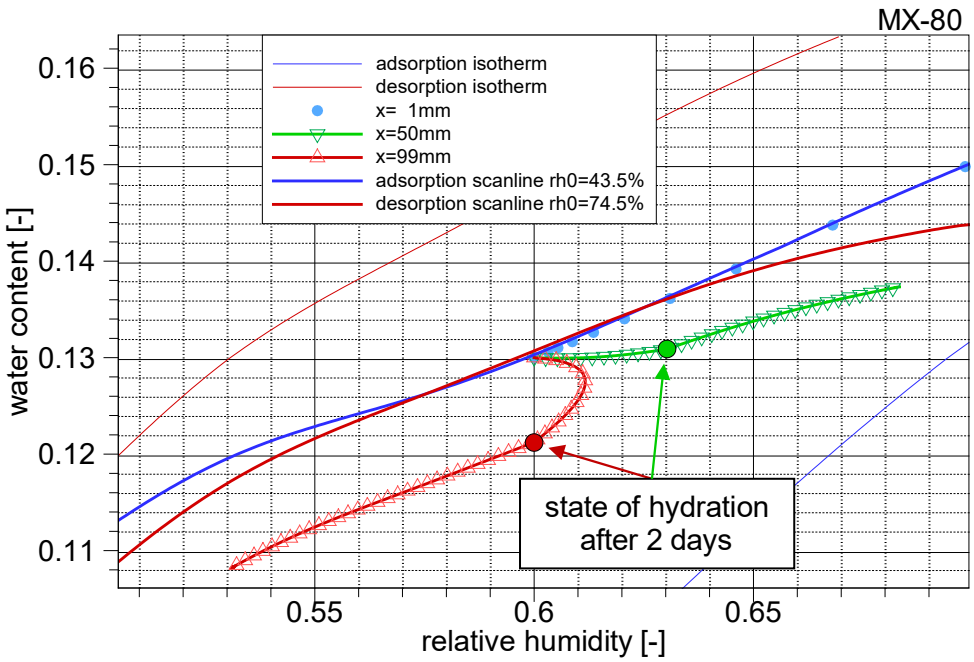

Fig. 8.27 Hydration paths at selected points in the MX-80 model; close-up

Even more interesting is the hydration path at point 3. Right after the onset of heating, the hydration state switches to desorption because the bentonite is losing interlamellar water. In that, point 3 does not experience any noteworthy adsorption. At first, the increase of vapour in the pore space at the cost of interlamellar water is strong enough to increase relative humidity despite an also increasing saturation vapour density. Only at a later stage of heating, the exponential increase of the saturation vapour density with temperature exceeds the only linear increasing accretion of vapour in the pore space. These dynamics lead to the horseshoe shaped hydration path during heating.

Afterwards, the path follows the temperature-corrected desorption isoline that appears to converge to the scanline at initial temperature, also depicted in Fig. 8.27. As in case of point 2, this is consistent with the water loss defined in section 5.3.1 that is decreasing with the relative humidity.

8.6.3 Model comparison

Other than in the previous cases, the complexity of the non-isothermal models prevents from comparing the results from the three models in one graph. Instead, three graphs for each quantity of interest are presented here, showing the evolution of the relative humidity in Fig. 8.28, the vapour partial density in Fig. 8.29 and the water content in Fig. 8.30. Differences therefore appear to be less pronounced as in a direct comparison.

The curves for MX-80 are generally a bit more bended than the others, leading to steeper gradients in relative humidity and water content. The extent of the dried zone at the heated end of the model is comparable for MX-80 and Calcigel. The decrease of water content below the initial value can be observed above about 70 % relative humidity in both models while the model with the linear isotherm shows this effect only above 80 % humidity. However, the total loss of water at the heated end is minimal for the Calcigel model while the other two show a similar degree of drying.

At the end of the simulation, the relative humidity is in the Calcigel model more equally distributed than in the MX-80 model and even more so than in the model with the linear isotherm.

All in all, the model results show moderate differences between each other but there is no clear trend towards particular properties in the results for one of the models.

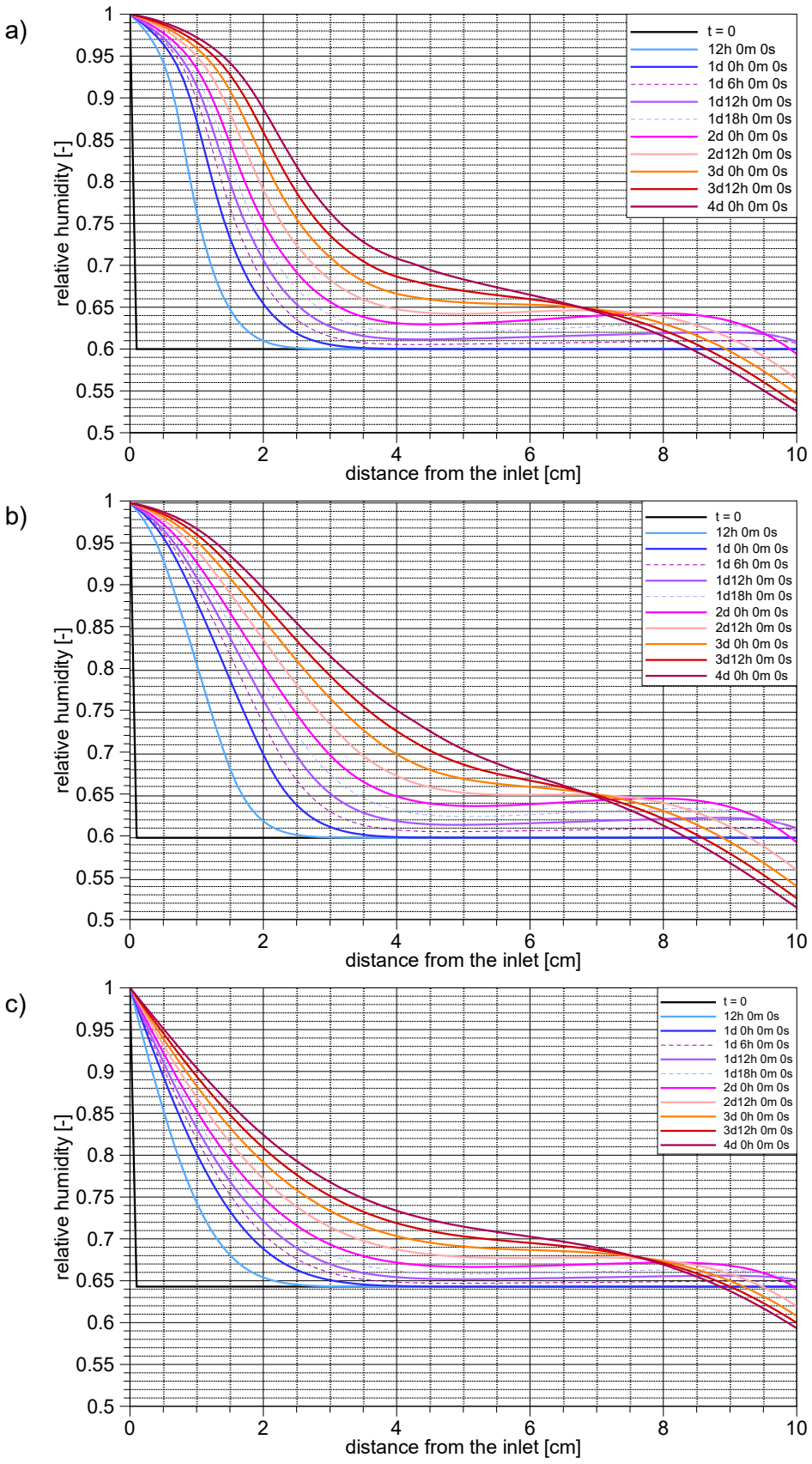

Fig. 8.28 Evolution of the relative humidity in the three models;
a) MX-80, b) Calcigel, c) linear isotherm

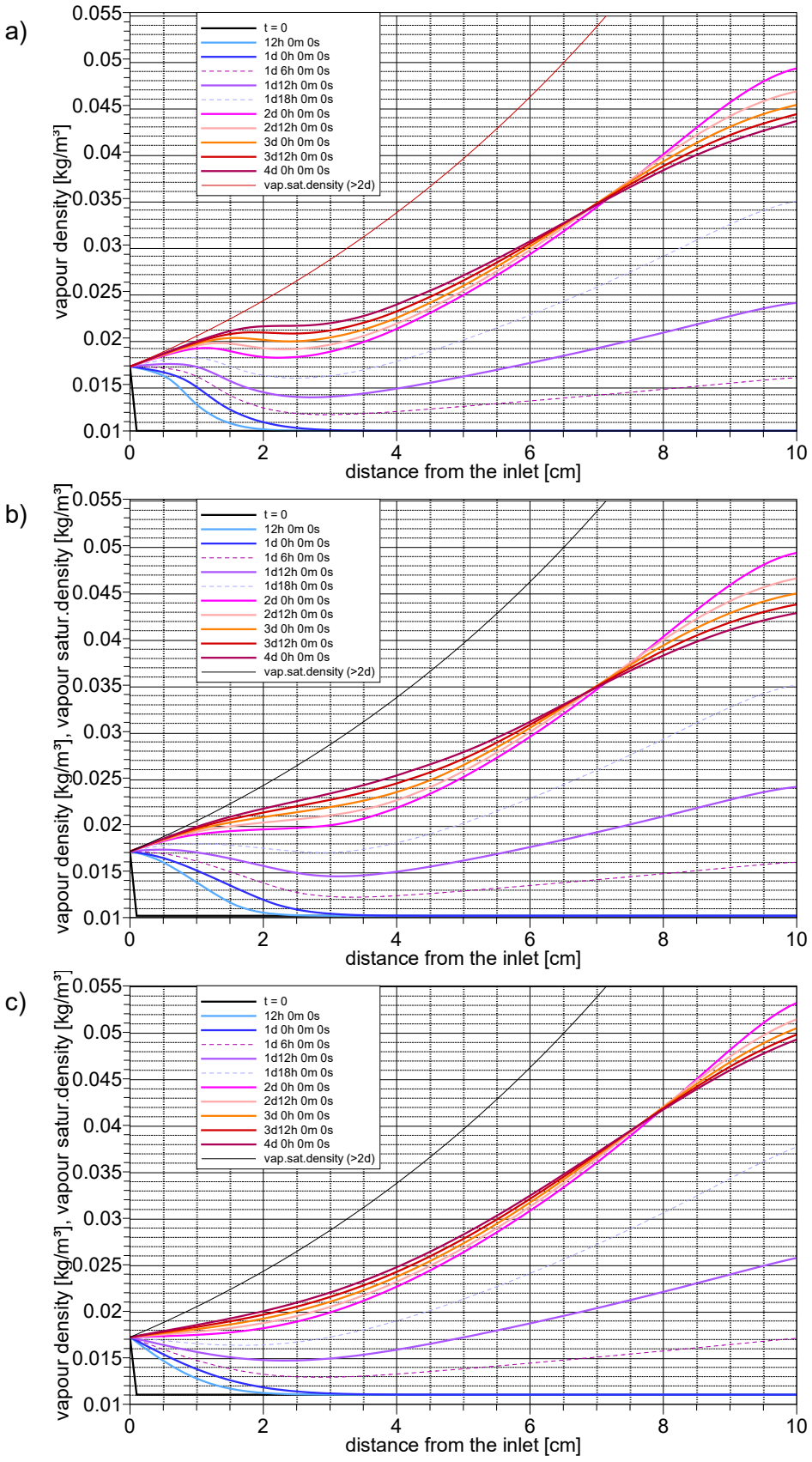

Fig. 8.29 Evolution of the vapour partial density in the three models;
a) MX-80, b) Calcigel, c) linear isotherm

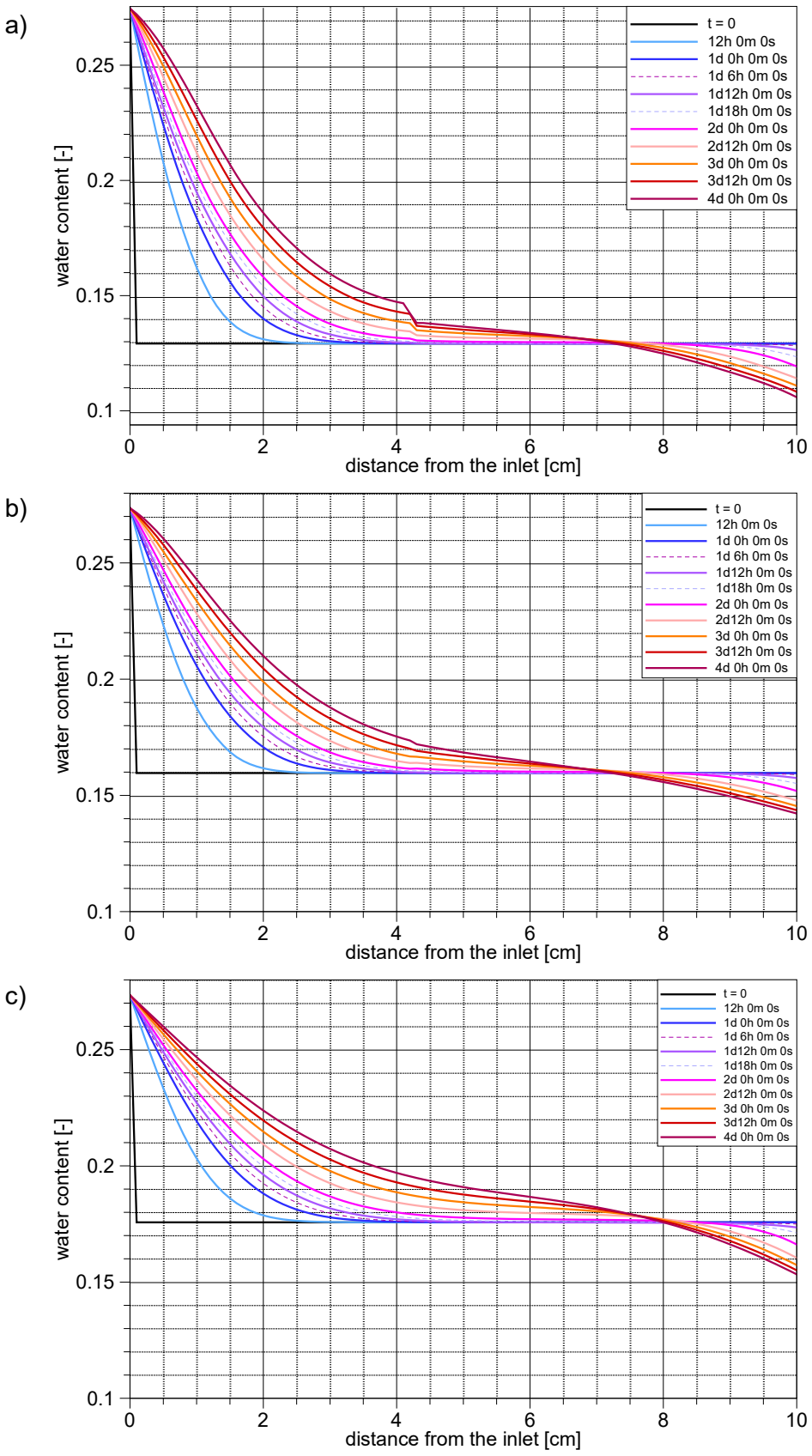

Fig. 8.30 Evolution of the water content in the three models;
a) MX-80, b) Calcigel, c) linear isotherm

9 Summary, conclusions and recommendations

9.1 Summary and conclusions

Many designs of geological repositories for radioactive waste include bentonite in form of compacted blocks or in form of pellets as a vital part of the geotechnical barrier. While on principle, the initially air-dry bentonite cannot prevent a contact of groundwater with the waste canisters, it forms eventually an extremely effective impediment against water flow.

Despite the fact that the preceding transient phase of water uptake is rather short in comparison to the envisaged lifetime of a bentonite buffer, the water uptake dynamics during this phase have increasingly attracted interest for quite different reasons. On the process level, for instance, the time-dependent environmental conditions in the bentonite have apparently considerable influence on biological activities in the available pore space. On the integrated level, the time until reaching full saturation meaning the desired specs for long-term safety considerations can obviously be another critical information.

Depending on the area of application of the bentonite in a repository, the transient phase of water uptake may take years or decades, thus excluding a direct comprehensive performance assessment of the buffer by laboratory or field experiments. Predictions of the water uptake behaviour are therefore based on numerical models. Under these circumstances, reliability of these models is of utmost importance. However, the behaviour of bentonite during re-saturation is very complex and may be controlled by hydraulic, mechanical and thermal processes. Focus of the work presented here relates to the hydraulic aspect of re-saturation.

While isothermal re-saturation can often be described by adsorption of water in the interlamellar space of clay particles, non-isothermal conditions in particular may also lead to local drying which is a desorption process on a microscopic level. These processes are characterized by isotherms (or the equivalent retention curves) that relate the relative humidity in the pore space of the bentonite to the water content. The isotherms form a vital constitutive equation for a mathematical model of bentonite re-saturation and therefore need to reflect the true relationship to a sufficient degree. Four fields of topics addressing different aspects of isotherms are therefore covered by this report in order to improve the knowledge about this constitutive relation.

In simple materials, the equilibrium between the relative humidity in the pore atmosphere and the related water content is a single curve. For clayey materials, however, this relationship is more complex as the equilibrium follows a different path for drying than for wetting. The wetting path starting at complete dryness is called here “adsorption isotherm”, the drying path beginning at full saturation “desorption isotherm”. Detailed investigation of the hysteresis of the isotherms for MX-80 and Calcigel defines the first topic in this report.

For a realistic assessment of the actual state of the bentonite it must be considered, though, that the bentonite undergoes alternating conditions with respect to wetting and drying between mining, production and emplacement in a repository. A multitude of changes between wetting or drying conditions has to be assumed to occur during the period before emplacement in a repository. It has furthermore to be assumed that these changes occur when the bentonite is only partly saturated. In these cases, the equilibrium between relative humidity and water content must therefore follow scanlines that connect adsorption and desorption isotherms. The scanlines diverging from an adsorption isotherm after a change from wetting to drying are called here “desorption scanlines” and the scanlines diverging from the desorption isotherm are called “adsorption scanlines”. Presently, there exists no systematic data on scanlines for bentonite. Second topic in this report is thus determination of the scanlines for MX-80 and Calcigel bentonite.

The name “isotherm” implies that the equilibrium data for relative humidity and water content refer to a specific temperature. It has been shown already, though, that MX-80 loses small quantities of hydrated water due to heating /GAI 05/. Furthermore, this effect changes the shape of the isotherms with temperature. This phenomenon is of utmost importance for the thermally induced moisture re-distribution in the bentonite buffer around heated waste canisters. The small water loss is difficult to measure and thus forms the third topic of this report.

While the first three topics concern bentonite under free-swelling conditions, the fourth topic refers to confined conditions. Microstructural changes of the clay after repeated wetting and drying under confined conditions have been reported in the literature /SEI 14/. As these conditions can occur in the vicinity of emplaced canisters for heat-producing radioactive waste, it is of interest to investigate the conditions under which these changes have relevant consequences.

The results and conclusions, summarized in the following, are structured according to these four topics.

9.1.1 Topic 1: Hysteresis of the isotherms

A device called Vapour Sorption Analyzer (VSA) has been used for most of the measurements in this project. As the VSA was new to the GRS laboratory, its accuracy was tested first by repeated measurement campaigns aiming at the hysteretic isotherms of MX-80 bentonite. The data from the control tests matched the first data excellently. The measurements performed with the VSA compare favourably with the highly resolved isotherms determined by /KAH 86/.

Due to the technical limits of the VSA, measurements were restricted to a range between 5 % and 95 % relative humidity. Since neither complete dryness nor full saturation could be reached, the starting points of the isotherms are subject to a certain error. A comparison to other detailed measurements of the adsorption isotherm with respect to the dry end of the isotherm reveals, though, that this error is quite marginal as the water content is rather low in this region anyway (e.g. (KAH 86/). The error at the wet end of the isotherm is not critically either, since the water content at 95 % relative humidity under free swelling conditions marks the maximum uptake by bentonite with a dry density of close to 1500 kg/m³ /KRÖ 11/. For MX-80 bentonite this refers to the minimum degree of compaction that is relevant for use in a nuclear waste repository (e.g. /LUT 17/). Wetting to a higher degree is therefore nor relevant for the intended use of the data.

The resulting shapes of adsorption and desorption isotherms are rather complex as they include several inflection points. The change to a strongly exponential increase of the water content in the range beyond 95 % relative humidity as observed in the literature[18] is indicated. The difference stemming from the mode of hydration – adsorption or desorption – is substantial. The maximum difference between adsorption and desorption isotherm amounts to a water content about 5 % in the range between 55 % and 60 % relative humidity.

The difference between adsorption and desorption isotherm for Calcigel is much less and amounts only to about 2 % between 60 % and 70 % relative humidity. Another

[18] cp. /KRÖ 11/.

striking difference between the isotherms of MX-80 and Calcigel is the shape of the curves. For Calcigel, they are much more smoothly curved than those of MX-80.

Analytical formulations were derived for the adsorption and desorption isotherms for MX-80 and Calcigel. Using Kelvin's law to convert relative humidity to suction allowed for plotting also the equivalent retention curves.

The difference between adsorption and desorption path for MX-80 results at 10 % water content in a suction of 66 MPa on the adsorption path in comparison to 113 MPa on the desorption path. For Calcigel at 10 % water content the analogous suction values are 188 MPa and 216 MPa. These differences should have a considerable impact on re-saturation simulations.

9.1.2 Topic 2: Scanlines

Generally valid results

Scanlines form two families of functions, adsorption and desorption scanlines. It is assumed here, that scanlines of one type – adsorption or desorption scanlines – are unique and that scanlines of the same type do not intersect each other. Each scanline can then be defined by the point where the scanline branches off the adsorption or desorption isotherm, respectively. This point is called here the "starting point of a scanline" and can be characterized by the relative humidity r_{h0} at that point.

As for the endpoints, the derived data for the scanlines were most surprising in that the endpoints appeared to be independent of the starting point. They were always found at the extreme ends of the isotherms: the endpoints for adsorption scanlines at full saturation and the endpoints for desorption scanlines at complete dryness. A scanline can therefore uniquely be defined by the parameter r_{h0} as the hydration path, adsorption or desorption, is defined by the type of isotherm (desorption or adsorption isotherm) from which the scanline branches off.

This observation has consequences for the view on isotherms as outstanding constitutive curves. In fact, isotherms can rather be interpreted as particular and extreme cases of the scanlines. The adsorption scanline with the starting point$r_{h0} = 0$, for instance, is conceptually identical with the adsorption isotherm. For usage in a simulation code it thus

appears to be advantageously if the mathematical formulations for the scanlines include the isotherms as a special case.

Concerning consistency with the data on hysteresis, it has to be noted that the measurements of the scanlines have been done in campaigns where several scanlines were measured in one sweep. Wetting and drying paths connecting the endpoint of one scanline with the starting point of the next one followed therefore, at least partly, the adsorption and the desorption isotherm, respectively. This provided additional data for the isotherms.

The additional data matched the adsorption isotherm for MX-80 and the desorption isotherm for Calcigel nicely. However, data from the latest campaigns for the desorption isotherm for MX-80 and the adsorption isotherm for Calcigel deviate somewhat from the earlier ones, even if they still confirm the complexity of the shape of the isotherms. Looking at the internal consistency of the newer data let the deviations appear to be less reliable than the older data.

Ignoring some of the newer data on the isotherms meant, however, that the scanlines measured in the latest measurement campaigns are not always fully compatible with data from older ones. The general approach followed for finding analytical formulations for the scanlines is therefore, when in doubt, to put emphasis rather on the general characteristics than on perfect matching of the data points.

In general, the adsorption scanlines for MX-80 as well as those for Calcigel appear to be quite closely bundled above a relative humidity of about 70 to 75 %. The same observation holds even more true for the desorption scanlines of both bentonites below about 20 % relative humidity. In case of insufficient resolution of the scanlines in the r_h-w-plane, this bundling can easily be mistaken for an early touching the opposite isotherm instead of converging towardsthe endpoint of this isotherm. Note that bundling is more pronounced in the desorption scanlines for Calcigel than those for MX-80.

Results concerning specifically MX-80

The isotherms for MX-80 bentonite are already quite complex. This applies even more so to the family of adsorption scanlines which is reflected in the complexity of the mathematical formulation.The match of the analytical functions to the measured scanline data is not perfect but satisfying, considering that the measured data points are affected by a

little uncertainty. The deviations, however, amount to less than 1 % water content. Even more difficult was, surprisingly, deriving the formulation for the desorption scanlines. Analytical formulation and measurements appear to agree reasonably well, though.

Results concerning specifically Calcigel

The comparatively simple shape of the isotherms for Calcigel helps to find less demanding formulations for the scanlines than those for MX-80. As the isotherms and scanlines for Calcigel let already expect, the retention curves are similarly unspectacular. Noteworthy here is again the smoothness with which the scanlines approach the opposite isotherm. The narrow bandwidth of the hysteresis loop for Calcigel made it therefore difficult to differentiate between the individual scanlines.

9.1.3 Topic 3: Temperature-dependence of the isotherms

9.1.3.1 Measurements up to 90 °C in an oven

The idea of checking on water losses of the bentonite due to heating with samples in a desiccator had initially appeared to be conceptually straightforward. Humidity was supposed to be controlled by a salt solution at the bottom of a desiccator and the temperature was to be varied by placing the desiccators in an oven at three different temperature levels. The temperature could be kept constant to a sufficient degree.

Using ten desiccators with different salt solutions, the temperature-dependent water loss was to be scanned at 10 different relative humidities. The samples were dried at 105 °C for 24 hours to ensure that all data referred to the adsorption isotherm. In order to optimise the accuracy of determining the water content by weighing, a high sample mass was aimed at. Based on a pre-test, it was chosen to lie in the range 100 g.

However, during the tests, several procedural difficulties became evident. Besides the usual problems of long-term tests such as power failures and malfunctioning sensors, there were several unforeseen effects somewhat compromising the results:

(1) The time for reaching equilibrium of relative humidity and water content was proportional to the level of humidity, particularly during the first phase at 30 °C and amounted to up to several months. From the fact, that it took also quite some time for the relative

humidity to reach the target value, it can be concluded that the desiccators did not provide as much vapour as the bentonite samples were able to take up. Apparently, optimising the sample mass should have taken this effect into account which would have led to less sample mass.

(2) The influence of temperature on the salt solubility has been strongly underestimated. To be sure to have reached maximum dissolution of the respective salt, an insolvable rest of salt was left in the solution. In some cases, this rest simply disappeared after increasing the temperature in the oven, leading to a temporary decrease of relative humidity in the affected desiccator until salt was replenished.

(3) In some cases, the desiccators ran dry and water had to be replenished.

(4) The test turned out to be sensitive to disturbances of the desiccators such as weighing or replenishing water.

In the end, the results were not entirely satisfying. The data uncertainty related to the test methodology was inherently too high. While it was possible to confirm the adsorption isotherm from /KAH 86/ quite nicely, the goal of this test – determination of the influence of temperature on the adsorption isotherm – has been missed.

9.1.3.2 Measurements up to 55 °C with the VSA

Finding a successful strategy

An alternative to the eventually unsatisfying measurements in the desiccators was found in the Vapour Sorption Analyzer (VSA). This device proved to be able to measure a complete hysteresis cycle in a matter of weeks instead of months or years. A certain limitation was, though, that the VSA can handle only temperatures up to 60 °C.

Following the concept for the tests with the desiccators, the first idea was to measure complete isotherms and scanlines at different temperatures. While the required testing times were accelerated considerably, it still meant that the related measurement campaigns would take some time. Due to several technical difficulties with the VSA, the tests had to be interrupted time and again. It was therefore not possible to perform these tests in one go. As a consequence, not all tests were done under exactly the same conditions

and with the same samples. The resulting data uncertainties prevented a meaningful evaluation.

An alternative strategy was tried and found to be more successful. Instead of running the whole hysteresis cycle up and down at one temperature, the change of water content was measured for specific relative humidities at three different temperature levels, namely at 25, 40 and 55 °C. Having become aware of the related high accuracy requirements, a more stringent accuracy criterion for the equilibrium between relative humidity and weight of the sample was applied. The stepped-up accuracy criterion could not prevent some scatter in the data but averaging related data provided a clear trend.

The results show that there is no significant difference between data from cooling and data from heating. A hysteresis with respect to temperature can thus not be substantiated in the investigated temperature range.

One peculiarity in the data has been found, though. The averages for the first heating phase seem to be slightly different by a few tenths of a percent in water content from the subsequent averages. This is a feature that can be observed for all other relative humidities and both types of bentonite except for MX-80 bentonite at 55 °C. There is no good explanation, neither for the phenomenon in general nor for the exception in particular.

For the final evaluation, all equilibrium data for the same temperature level were averaged irrespective of determination from a heating or from a cooling phase. For the reasons discussed above, those from the first heating phase were not taken into account, though.

Results for MX-80

The data for the water loss of MX-80 due to a temperature increase of 30 °C appear to be consistent with the data from /GAI 05/ as they show the maximum at approximately the same relative humidity and indicate a trend towards zero mass loss for a completely dry and a fully vapour-saturated atmosphere.

Despite scarceness of data and scatter, the test results were evaluated at r_h=70 % with respect to a possible non-linearity between water loss and temperature increase. The

average for the losses induced by temperature increases of 15 °C is approximately the same, thus indicating a linear relationship in the temperature range investigated.

Presuming further that the linear relationship between temperature increase and water loss can be extended up to 100 °C, allows for a quantification of consistency of the present results with the data from /GAI 05/. The “thermal water loss” expressed in terms of decrease of water content per degree Celsius has been calculated for both data sets. For the present tests, it amounts to about 0.015 $\%_{\text{water content}}$/°C and thereby differs from the data from /GAI 05/ only by a factor of less than 2.

The loss of water content $\Delta w(r_h, T)$ due to heating as a function of relative humidity is analytically quite well described by two quadratic parabolas[19].Their maximum value as well as its position on the r_h-axis could be varied in order to find the best fit with the data as determined at T_{max}.

Following the notion of a linear relationship between temperature increase and water loss (see above), the approach suggested here consists basically of the curve $\Delta w_{max}(r_h, T_{max})$ at maximum temperature T_{max} that is reduced linearly with T down to a reference temperature T_{ref} where the loss $\Delta w(r_h, T_{ref})$ is zero everywhere. This approach fits the data for 55 °C very well and the data for 40 °C at least reasonably well.

Results for Calcigel

The data points for Calcigel appear to follow a somewhat different trend than those for MX-80 as they indicate a more or less constant water loss with heating over a large range of relative humidities. However, the assumption of no temperature-dependence of the water content for completely dry and fully vapour-saturated air is assumed to apply to Calcigel as well.

Tentatively fitting the bi-quadratic approach for MX-80 to the data for Calcigel did not result in a fully satisfying fit. Neither arranging the peak at 30 % relative humidity nor at 60 % was successful. Instead, the two parabolas were separated by a horizontal straight line in such a way that the maximum loss in water content is not associated with one

[19] an approach that is implemented ad hoc in code VIPER /KRÖ 11/

specific relative humidity but with a rather large range of humidities. While the resulting analytical function looks a bit strange, it appears to fit the data best.

9.1.4 Topic 4: Microstructural changes under confined conditions

Tests with confined samples of MX-80 compacted bentonite have been shown to undergo structural changes on the microscopic level during a full wetting that appear to change the water uptake characteristics, namely the isotherms/retention curves. The idea of the tests under topic 4 was therefore to find a critical dry density above which the effect of microstructural changes might become relevant for the behavior of a bentonite buffer in a nuclear waste repository. Later it was learned, though, that safety considerations with a view to the range of permissible swelling pressures of the buffer affect the requirements for the dry density (e.g. /LUT 17/). Based on this information, a dry density of 1600 kg/m³ was considered to represent at the upper end of a possible range of dry densities.

In order to detect changes in the isotherms, a sample with a dry density of 1600 kg/m³ was envisaged to be wetted, dried and wetted again. Differences in the adsorption path would then indicate possible microstructural changes in the bentonite. Small cells for the compacted bentonite samples had to be constructed in order to use them in the VSA. This purpose required that they had not only to be small and tough but also very light in order not to overstrain the sensitive scale of the VSA. The initial construction with titanium was dropped, though, because difficulties in the manufacturing process were anticipated. It was replaced then by utilizing 3D-printing technology using tough plastics.

While producing test cells by means of a 3D-printing had obvious advantages over a conventionally manufactured cell, several unexpected difficulties arose with this method. The initial construction using threads for connecting the cell parts had to be dropped because printing working threads obviously requires quite some insight. Also not anticipated was the fact that mechanical properties of printed materials depend on the curing time, the time required to harden the printed plastics permanently. Appropriate tests were therefore performed to optimize the curing time.

Side-tracked by the totally missing hints in the literature about water uptake by plastic materials, the biggest problem came only delayed into awareness. A simple wetting and drying test with a prototype cell in the VSA showed clearly that the cell weight follows the ambient humidity. Water uptake is thereby not „instantaneous“ but requires some time.

Furthermore, the weight was observed to fall below ist initial value while drying which suggests that the amount of adsorbed water in the sample is related to the humidity of the surrounding atmosphere. The total weight change of prototype cell, while not complete in this test, indicates a water uptake of about 3 % by weight. By comparison, water uptake of MX-80 amount to a value of about 19 % by weight.

A test with transparent test cubes with a side length of 1 cm in a potassium permanganate solution showed, that water taken up by the printer resin is not stuck in an outer zone but penetrates the whole printed body for all practical purposes.

Next were tests concerning the water uptake dynamics. Weight change and expansion were checked with test cubes again with a side length of 1 cm. In order to get an impression of the effect and possibly finding a particularly suitable material, a collection of cubes was compiled which were produced by 4 different printing principles using 7 printing materials including 3 postprocessing variants on one material. Depending on availability, batches of 2, 3, or 4 cubes were arranged to provide control measurements.

The intention had been to cover the wetting as well as a subsequent drying phase with appropriate time steps, but the corona pandemic compromised that plan. Detailed data thus exist only for the first few days. Measurements were averaged over the number of cubes in a batch. The resulting mean of the curves for each batch appeared to be rather meaningful. As expected, no material is entirely water tight. Water uptake between 0.4 % and 14.1 % by weight were observed within the first 3 days.

The length measurements were unfortunately not as informative. Length readings with the calliper were obviously interfered with by printing artefacts such as the remains of support material, leading to rather high uncertainties. Linear expansion lay between 0.06 % and 5.20 % in the first three days.

In general, the characteristics of a diffusive process of water uptake that were indicated in the literature for plastics in general (see above), were confirmed for the printed materials, as shown by reference to the weight gain rates. This requires careful planning of hydraulic tests with printed parts but can certainly not outweigh the new possibilities that are coming with this new technology.

The pre-tests have shown that in a system of plastic test cell and bentonite sample, the effect of water uptake by the printed material cannot be neglected. Not totally unlike

bentonite, plastics in general respond to contact with water with swelling and weight increase, doing so with diffusion-like dynamics. Measuring the weight changes during wetting and drying in a cell thus needs to be complemented by a second measurement, a correction step, of the cell only in order to subtract out the effect of water uptake by the cell.

Adding to the delays by the unplanned for series of pre-tests and the additional impediment by the Corona pandemic was the also unexpected long time for just one measurement campaign that was induced by the test cell. Determination of one data point took up to 10 times longer than uptake by unconfined bentonite powder. Time restrictions prevented therefore unfortunately the completion of the experiment, in particular the complimentary test that would have been the basis for weight correction.

9.1.5 Influence on modelling

The new analytical functions concerning isotherms, scanlines and the water loss due to heating that have been derived from the measurements have been implemented in code VIPER. The impact of the new features on simulations has been illustrated by simple generic and easily comparable one-dimensional numerical models. Modelling results are presented by the transient distributions of the vapour partial density, the relative humidity and the water content. These three quantities represent the primary variable in the numerical model (vapour saturation density), the only measurable transient quantity during a water uptake tests (relative humidity) and the actual quantity of interest, the water content.

Isothermal wetting

Results from three model set-ups with different adsorption isotherms have been compared where wetting started at the same relative humidity. Because of the different isotherms, the initial water content differed from model to model, though.

For vapour partial density and relative humidity, the initial and the final values are the same for all three models, so that the biggest differences can be observed somewhere during the transient phase. The relevant sections of the three isotherms used here show quite different shapes and these appear to be reflected in the calculated curves. The differences between the curves at a specific time were moderate. The results affirm,

though, that deriving the water content from relative humidity data requires good knowledge about the applicable isotherm/scanline.

Because of the different initial values, the water content curves could be compared only qualitatively. The uptake dynamics assessed by means of penetration depths, appeared to be very similar in all three models.

Isothermal drying

The second test case was that of drying of a rather saturated bentonite towards a boundary that was open to the atmosphere, based on the same three different materials as in the wetting case. The calculated curves for the relative humidity lie much closer together than in the wetting case which can probably be ascribed to the fact that the initial values are less widely spread. Also, the difference between initial and boundary values is less pronounced.

The three curves for the water content after one day show basically the same penetration depth into the bentonite and at 10 days they just have met the opposite (closed) boundary. As in the wetting case, the results might have been quite similar, had the initial and the boundary water content been the same.

“Arbitrary” initial conditions

Having applied different initial conditions with a fixed water content but varying relative humidity, the relative humidity curves show a large initial spreading. While they are qualitatively similar during the simulation, the differences remain to be substantial until advanced times where they appear to converge at last.

Surprisingly, very little effect of the varying initial conditions has been observed with respect to the calculated water content distributions. The maximum difference amounts to little more than 1 % water content. From the perspective of predicting the water uptake dynamics in a compacted bentonite, the model considered here appears to be quite insensitive to the initial relative humidity. It should be kept in mind, though, that this observation cannot be generalized, yet, but requires further substantiating investigations.

The results affirm furthermore that the interpretation of the relative humidity with a view to water content requires knowledge about the applicable isotherm/scanline. This can only be determined by a known starting point in the relative humidity-water content plane.

Changing boundary conditions between wetting and drying

With the fourth and last isothermal model, the ability of code VIPER to switch from an adsorption to a desorption scanline during a simulation was to be tested and demonstrated. Since such a switch can only occur at a change from wetting to drying or vice versa, it was forced on the model by changing the boundary conditions from high relative humidity to low humidity in the midst of a simulation. The first half of the model run was thereby quite similar to the wetting case. But the adjoining drying phase was different to the drying case presented earlier in that it started with a non-uniform distribution of secondary variables and in that the switch to the desorption scanlines occurred not at once for all nodes but successively. Furthermore, different desorption scanlines were changed to at different locations because the switch occurred at different degrees of saturation

The results for the drying phase were therefore more different among the three models than in the previous cases. This observation seems to suggest that considering a system of isotherms and scanlines in a re-saturation model becomes increasingly relevant with increasing complexity of the model.

Moisture re-distribution due to heating

Proceeding to non-isothermal models increases the physical complexity of the model considerably due to several temperature-dependent secondary variables. Prescribing the same temperature evolution in all models introduces these complexities in the same way in all three models, though. The differences in the results for the three models with different constitutive equations are therefore not as pronounced as had intuitively been expected.

Starting with a simple wetting scenario but increasing the temperature linearly over the model in space and time resulted in rather moderate differences with respect to vapour partial density, relative humidity, and water content. As in the previous case, the differences are noticeable but not to the point where they appear to be alarming. To a certain extent, the observation from the previous case seems to hold, though, that the

differences between the model results increase with the model complexity. It may therefore be significant that all the numerical models considered here are extremely simple in terms of geometry. Differences in using the three constitutive relations may therefore become more relevant if more complex model geometries, boundary or initial conditions are taken into account in possible future comparisons.

9.2 Recommendations

9.2.1 General remark

Since wetting or drying of a bentonite follows different isotherms and scanlines, respectively, there is no unique relation between relative humidity and water content. The initial state of a bentonite with respect to these two quantities thus depends on the sequence and duration of the ambient conditions to which the bentonite has been exposed. Before bentonite is hydraulically tested in the laboratory or in the field or is someday deployed as buffer material in a final repository for radioactive waste, it has been subject to an uncontrolled history of drying and wetting between mining and usage. It is therefore equally advisable for experimentalists as well as for modelers to be keenly aware of this fact and to prepare for controlled initial conditions in this respect wherever possible.

9.2.2 Experimental work

Practical work

While it is not possible to follow the wetting and drying history of a bentonite sample from mining to deployment for the ultimate usage conclusively, it may be possible under certain circumstances to create well-defined hydration conditions in the laboratory. An easy and straightforward way to assure such a state is to have the bentonite undergoing the drying procedure at 105 °C for 24 hours that has already become popular in the bentonite testing community. Defining the resulting state as one of complete dryness allows for the assumption that subsequent wetting follows the adsorption isotherm. Unfortunately, this is no option for large-scale experiments for obvious reasons.

After such a drying, it is equally important to avoid drying conditions for the bentonite samples during the preparatory work as well as during the test itself. Otherwise, the state of the bentonite would switch from adsorption along the adsorption isotherm to a

desorption scanline. If this goes unnoticed, it can compromise knowledge of the true initial state of the bentonite as well as the choice of the appropriate adsorption isotherm/scanline. If noticed, it may be more straightforward to start the preparation process all over again and to repeat the drying procedure instead of finding means for correction.

Quite some issues concern hydraulic experiments taking advantage of the rather new possibilities of 3D-printing. The main difficulty stems from the fact that plastics including printed resins generally take up water. At laboratory temperatures, the materials respond to contact with liquid water with water vapour in the same way and to a comparable degree.

The degree to which this happens depends on the material, though. It has also to be noted that this effect applies also to at least a selection of tracers which means that plastics can act as sinks in a tracer transport test. Contact time of 3D-prints with water should therefore be minimised if dimensional accuracy is of importance in order to avoid losses to the printed material. Further testing of printed materials appears to be advisable as dimensional accuracy might also depend on other conditions during printing such as temperature, layer thickness and printer firmware as well as conditions after printing like light or general aging.

Theoretical considerations

The extensive work on isotherm hysteresis and scanlines presented here has been addressed at free swelling bentonites in order to get an impression on the material behaviour and a feeling for measurement requirements. For practical purposes, such data are required for confined conditions of pre-compacted bentonite, though. So far, the modification of an adsorption isotherm by the approach of /DUE 07/ had been sufficient for this purpose. However, it is highly advisable to investigate theoretically as well as experimentally if this approach holds also for scanlines and the desorption retention curve.

9.2.3 Modelling

For the numerical simulation of bentonite re-saturation, most often only the retention curve for adsorption is used, implying that the relation between relative humidity and water content is indeed unique. It thus requires some creativity from the modeller if the initial state of the bentonite lies actually somewhere above the retention curve. But this

has probably gone unnoticed as a subsequent wetting follows an adsorption scanline that has a very similar characteristic shape to the actual adsorption retention curve. On the other hand, it may also lead to the conclusion that the retention curve (singular) depends on the initial water content (e.g. /DUE 04/). The present results call for revisiting the basis for this conclusion.

Another observation is based on work of an experienced international group of modellers in the framework of the Task Force on EBS by SKB (e.g. /GEN 19/).Well-defined tasks on bentonite re-saturation were tackled by numerical simulations in whichmostly a capillary pressure approach after van Genuchten /VGN 80/ was used to describe a unique retention curve. The related parameters, however, showed quite some scatter and more than once, the van Genuchten-approach was modified to fit the experimental results /KRÖ 16/. Calibrating a singular retention curve without being aware of the uncertainties about the initial state of the bentonite might have caused this scatter. If still possible, this would also be worth to be checked.

Application of the system of isotherms and scanlines to the problems set up here, proves to be of rather little to moderate influence on the modeling results. This could be if the hydraulics in general are quite robust with respect to the constitutive equations. From experience it is known, however, that the classical THM-models tend to be very sensitive to deviations in the retention curve (e.g. /GEN 18/[20]). Which of the two explanations hold true could be found out by implementing the new set of retention curves in a THM-model and for instance re-running the models described in this report.

While it has been possible to model different set-ups with the new features in code VIPER, the coding has proved to be less than satisfactory with a view to accuracy. In particular, the tabular method applied for calculating the water content in a confined bentonite as a function of relative humidity r_h and the starting point of a scanline $r_{h\,0}$ needs to be improved in order to increase robustness of the numerical scheme. Also, the excessively complex formulations for adsorption and desorption scanlines should be revised as it is rather easily conceivable that simpler formulation can be found.

The tests of the numerical model as realized in code VIPER could only be performed as one-dimensional models. This might have been a serious limitation for the sensitivity

[20] Verbatim: “Retention curves are very sensitive animals.“

tests reported here. Advancing the possibilities of this code to two- and three-dimensional geometries thus appears to be advisable.

Final note: The retention curves for Calcigel are quite smooth, thereby suggesting that of the approach of van Genuchten might be a good approximation in this case. A systematic comparison of the retention curves derived here and the van Genuchten approach used in classic THM-models might be quite revealing.

References

/CAS 92/ J. M. Cases , I. Berend , G. Besson , M.: Mechanism of adsorption and desorption of water vapor by homoionic montmorillonite. 1. The sodium-exchanged Form. Langmuir, 1992, 8, 2730-2739, American Chemical Society, 1992.

/DRU05/ Drummy, L.F., Koerner, H., Farmer, K., Tan, A., Farmer, B.L., Vaia, R.A.: High-Resolution Electron Microscopy of Montmorillonite and Montmorillonite/Epoxy Nanocomposites. J. Phys. Chem. B 2005, 109, 11868–17878, 2005.

/DUE 04/ Dueck, A.: Hydro-mechanical properties of a water unsaturated sodium bentonite - Laboratory study and theoretical interpretation. Doctoral thesis, Department of Building and Environmental Technology, Lund University, Division of Soil Mechanics and Foundation Engineering, 2004.

/DUE 07/ Dueck, A. and Börgesson, L.: Model suggested for an important part of the hydro-mechanical behavior of a water unsaturated bentonite. Engineering Geology 92, pp. 160-169, 2007.

/GAI 05/ Gailhanou, H.: Détermination expérimentale des proprieties thermodynamiques et étude des nanostructures de minéraux argileux. PhD Thesis, University Aix-Marseille III, 2005.

/GEN 18/ Gens, A.: Comment during the Meeting of the Task Force on EBS, Helsinki, 2018.

/GEN 19/ Gens, A.: Task Force on Engineered Barrier System (EBS), Task 1 Laboratory tests. Technical Report TR-14-24, Svensk Kärnbränslehantering AB, Solna, 2019.

/KAH 86/ Kahr, G., Kraehenbuehl, F., Müller-Vonmoos, M., Stoeckli, H. F.: Wasseraufnahme und Wasserbewegung in hochverdichtetem Bentonit. Nagra Technical Report NTB 86-14, 1986.

/KRI 11/ Kristensson, O.: Report on the modeling with initially available data. PEBS deliverable (D3.3-2), Svensk Kärnbränslehantering AB and Clay Technology, 2011.

/KRN 06/ Karnland, O., Olsson, S., Nilsson, U.: Mineralogy and sealing properties of various bentonites and smectite-rich clay materials. Technical Report TR-06-30, Svensk Kärnbränslehantering AB, 2006.

/KRÖ 08/ Kröhn, K.-P.: Simulating water uptake of compacted bentonite under non-isothermal conditions, decoupled from the mechanics and without feedback of hydraulics to heat transport. Proceedings of the Workshop on “Long-term performance of smectitic clays embedding canisters with highly radioactive waste” held in Lund, 2007, Applied Clay Science, Vol. 47, pp. 28-35, 2010; Online: http://dx.doi.org/10.1016/j.clay.2008.06.004, 2008; printed version: 2010.

/KRÖ 11/ Kröhn, K.-P.: Code VIPER - Theory and Current Status. Status report, FKZ 02 E 10548 (BMWi), Gesellschaft für Anlagen- und Reaktorsicherheit (GRS) mbH, GRS-269, Köln, 2011.

/KRÖ 19/ Kröhn, K.-P.: Re-saturation of compacted bentonite under repository-relevant flow conditions. FKZ 02 E 11102 (BMWi). Geomechanics for Energy and the Environment, Elsevier, 2019.
DOI:10.1016/j.gete.2018.09.003

/KRÖ 20/ Kröhn, K.-P. and Kröhn, M.: Producing fractures with a 3D-printer for flow experiments – The price to pay for the easy way out. Poster at the session HS8.2.3/ HS8.2 at thevirtual conference EGU 2020, 2020.

/KRV 20/ Kunststoffrohrverband e.V: WIPO Wissensportal. https://www.krv.de/artikel/feuchtigkeits-und-wasseraufnahme, Stand 2020.

/LUT 17/ Luterkort, D., Johannesson, L.-E., Eriksson, P.: Buffer design and installation method – Installation report. Technical Report TR-17-06, Svensk Kärnbränslehantering AB, Stockholm, 2006.

/MOO 52/ Mooney, R. W., A., G. Keenan und L. A. Wood: Adsorption of Water Vapour by Montmorillonite; I: Heat of Desorption and Application of BET Theory. Journal of the American Chemical Society, Nol. 74, No. 6, 1952.

/PMS 19/ Polymer Service GmbH Merseburg: Lexikon der Kunststoffprüfung, https://wiki.polymerservice-merseburg.de/index.php/Wasseraufnahme, Stand 2019.

/PUS06/ Pusch R. and Yong, R., 2006. Microstructure of Smectite Clays and Engineering Performance. Taylor & Francis, London and New York.

/SEI 14/ Seiphoori, A., Ferrari, A. and Laloui, L.: Water retention behaviour and microstructural evolution of MX-80. Géotechnique 64, No. 9, 721–734 [http://dx.doi.org/10.1680/geot.14.P.017], 2014.

/STO 98/ Stoeckhert, K., Woebcken, W. (eds.): Kunststoff-Lexikon. Carl Hanser Verlag, München, 1998. (cited in /PMS 19/)

/SUZ 17/ Suzuki, A., Watanabe, N., Li, K., Horne, R.N.: Fracture network created by 3D-printerand its validation using CT images. Water Resources Research, 53, pp. 6330-6339, 2017. Doi: 10.1002/2017WR021032

/VSA 20/ Website of the distributor of the Vapour Sorption Analyzer: https://www.metergroup.com/food/products/vsa/

/WAD04/ Wadsö, L., Svennberg, K., Dueck, A.: An experimentally simple method for measuring sorption isotherms. Drying technology, vol. 22, no10, pp. 2427-2440, Taylor & Francis , 2004.

Table of figures

List of tables

A Appendix: Pre-test for measurements with desiccators

The pre-test for measurements up to 90 °C was intended to determine a) the accuracy of the methodology as such and b) the time to reach equilibrium depending on the mass of the samples. For this purpose, two test batches were prepared, one sample of 300 g and three samples each of 100 g of MX-80 bentonite powder, by heating them at 105 °C for 24 hours. The three 100 g-samples were placed in desiccator 1 over a saturated NaCl-solution providing a relative humidity of 75 %. The 300 g-sample was put to the same conditions in desiccator 2.

Since the test started with dried samples, equilibrium was reached under water adsorbing conditions in the bentonite. The desiccators were equipped with humidity sensors providing continuous data on the relative humidity in the desiccators. To determine the water content, the samples were quickly taken out of the desiccator, weighed, and replaced.

After about 105 days, the samples in desiccator 1 appeared to be in equilibrium while it was not entirely clear if that applied to the big sample as well (cp. Fig. A.1). After this weighing campaign, however, the NaCl-solution was exchanged for a saturated LiCl-solution providing subsequently an atmosphere of 12 % relative humidity (cp. Tab. 1.1).

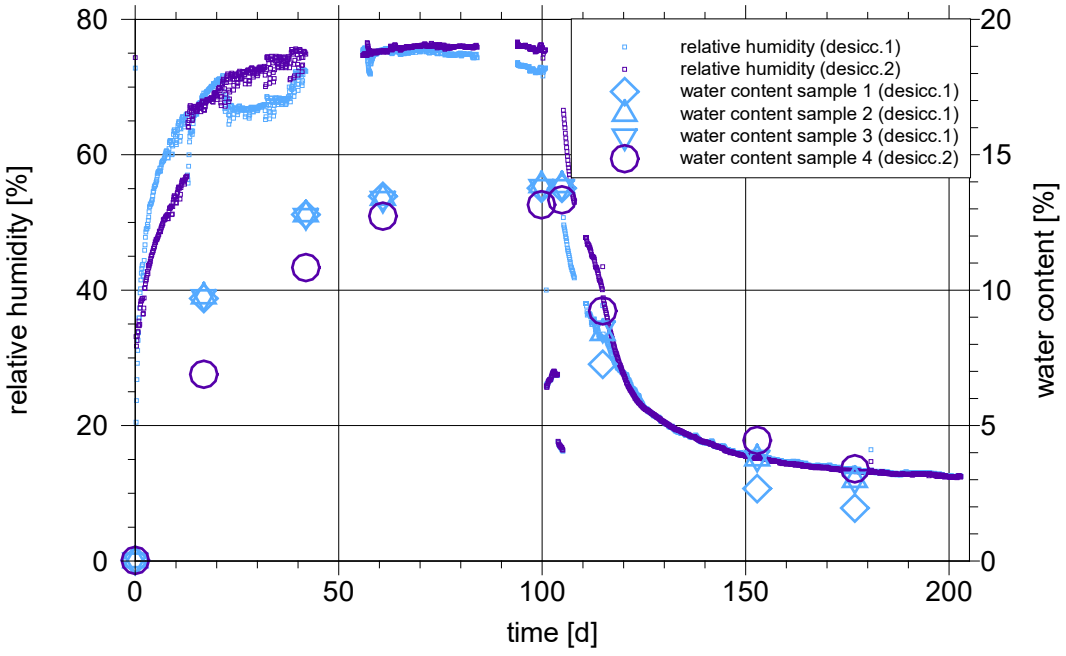

Fig. A.1 relative humidity and water content during the pre-test

This exchange of the salt solution marked the change to desorbing conditions. The test was terminated after 205 days without clearly reaching equilibrium as the questions to the test could be answered already.

The three water content values from desiccator 1 matched each other very well. The data were thus reproducible and suggested to be a reference for the data from the big sample.

Under adsorbing conditions, the equilibrium in water content lags behind the equilibrium in humidity. This observation suggests that water adsorption in the bentonite was initially quicker than evaporation of water from the salt solution. Only when the water content was already comparatively close the end value and further uptake had slowed down sufficiently, the humidity in the desiccator stabilised. Under adsorbing conditions, the relative humidity is apparently no good indicator for the water content in the samples.

The time required for reaching equilibrium was remarkably long and is apparently proportional to the sample mass. Use of 100 g-samples rather than 300 g-samples thus were advisable. This applied even more so as smaller samples allow for a larger number of samples in the desiccator, thus achieving a better grip on the equilibrium data.

The time lag between relative humidity and water content under desorbing conditions (after 105 days) is not as pronounced as under adsorbing conditions. In order to determine to which extent the relative humidity actually relates to the water content, the test would have required to be run until equilibrium, though.

The data suggests that the desorption phase would not have been quicker than the adsorption phase. This is a bit surprising as /DUE 07/ reported with respect to similar tests much faster desorption than adsorption.

B Appendix: Measurement results for free swelling bentonite

B.1 MX-80

B.1.1 Hysteresis

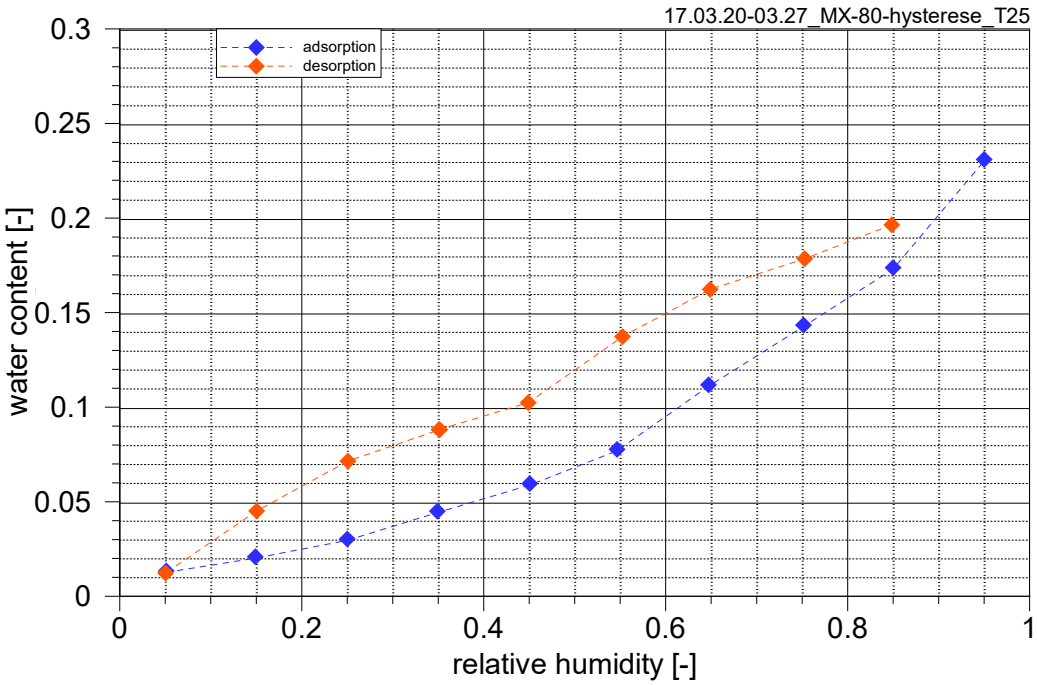

Fig. B.1 Hysteresis of the isotherm for MX-80 at 25 °C

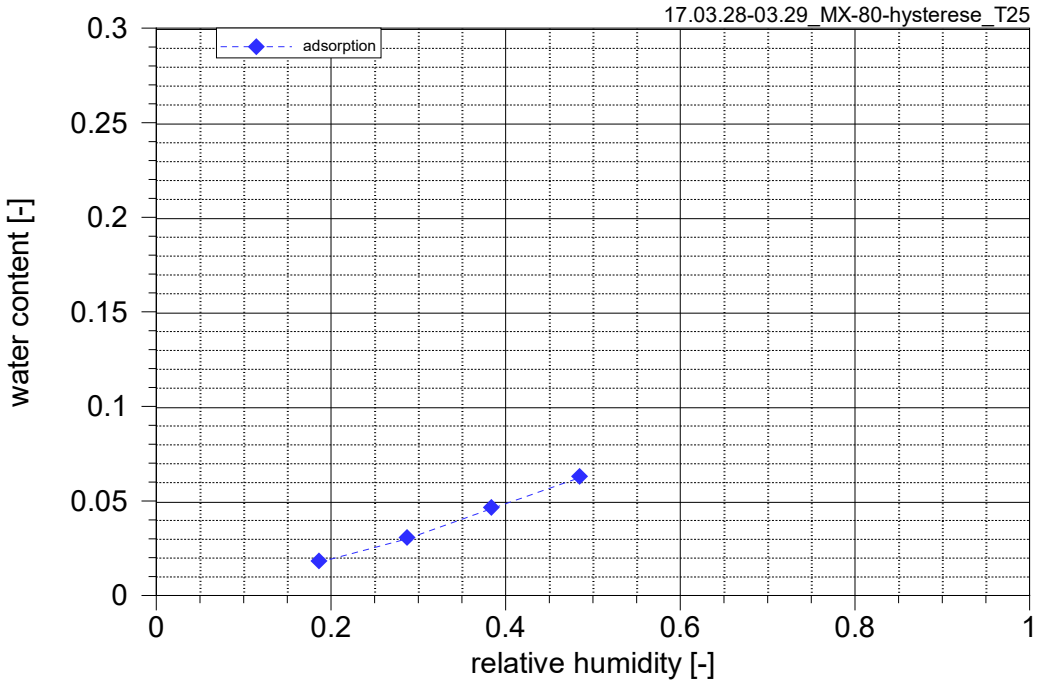

Fig. B.2 Part of the adsorption isotherm for MX-80 at 25 °C

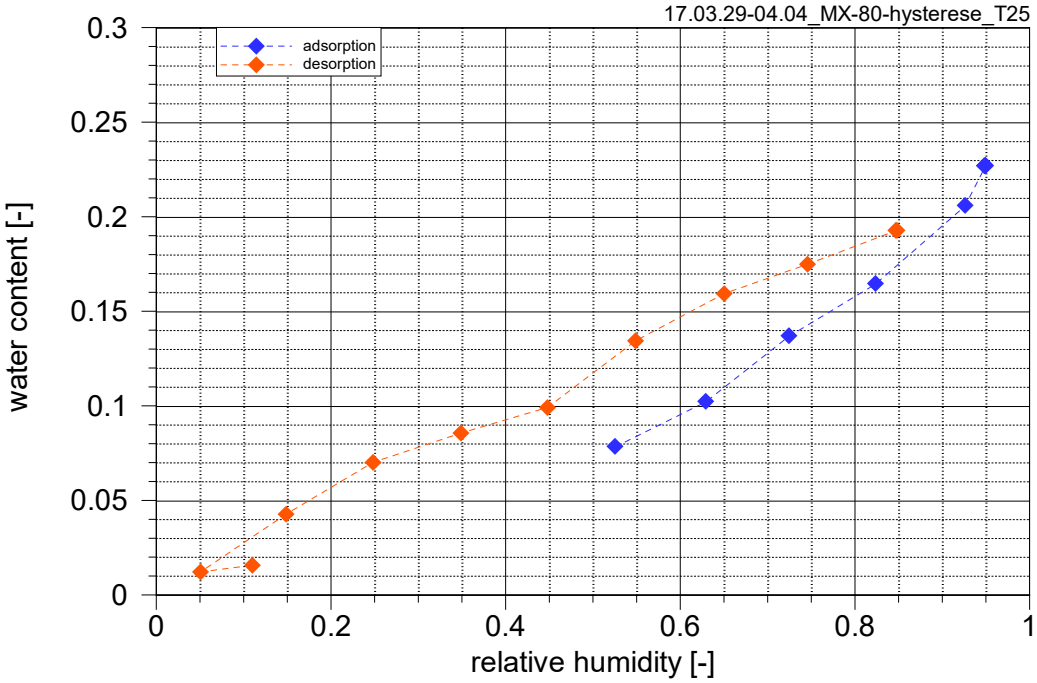

Fig. B.3 Desorption and part of the adsorption isotherm for MX-80 at 25 °C

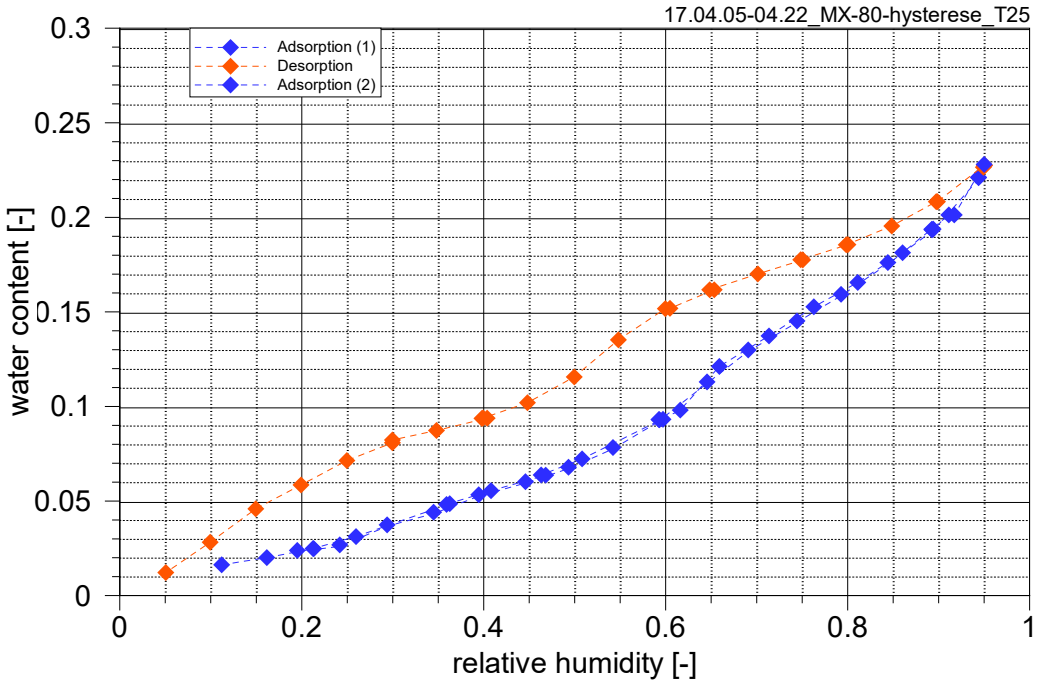

Fig. B.4 Hysteresis of the isotherm for MX-80 at 25 °C with accuracy check for the adsorption isotherm

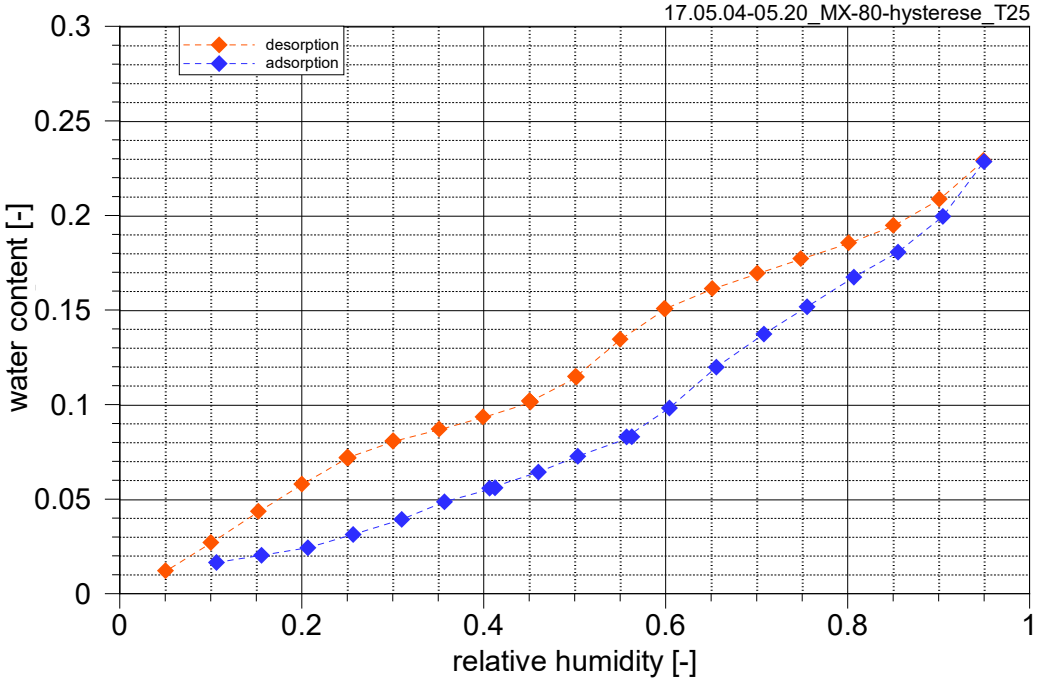

Fig. B.5 Hysteresis of the isotherm for MX-80 at 25 °C; different measurements

B.1.2 Adsorption scanlines

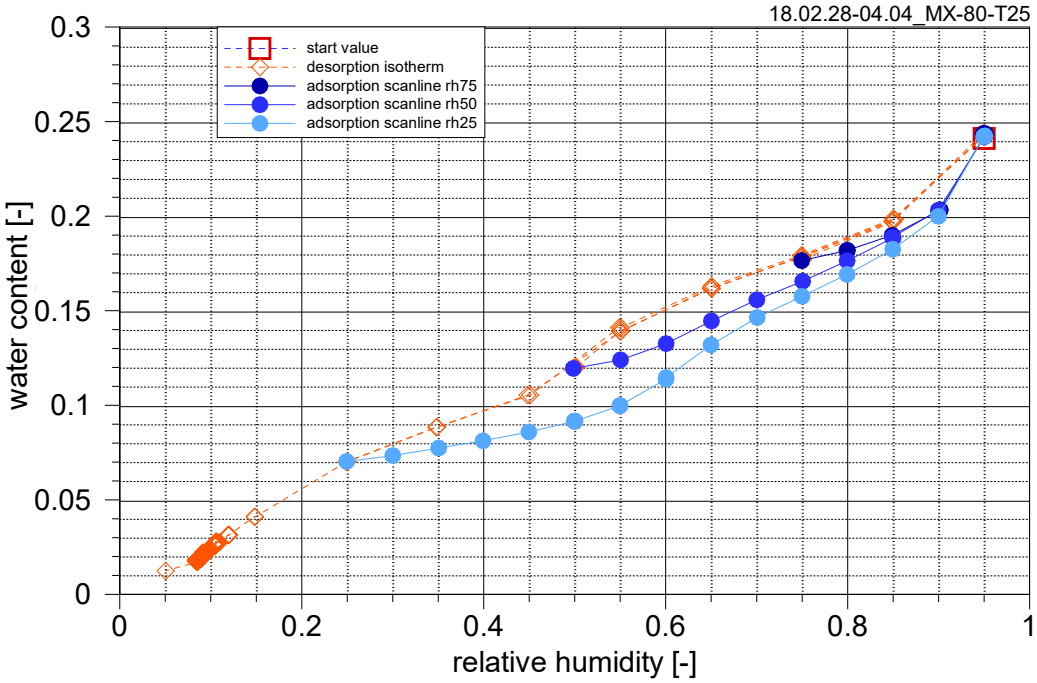

Fig. B.6 Adsorption scanlines for MX-80 at 25 °C; starting at 75, 50, and 25 % relative humidity

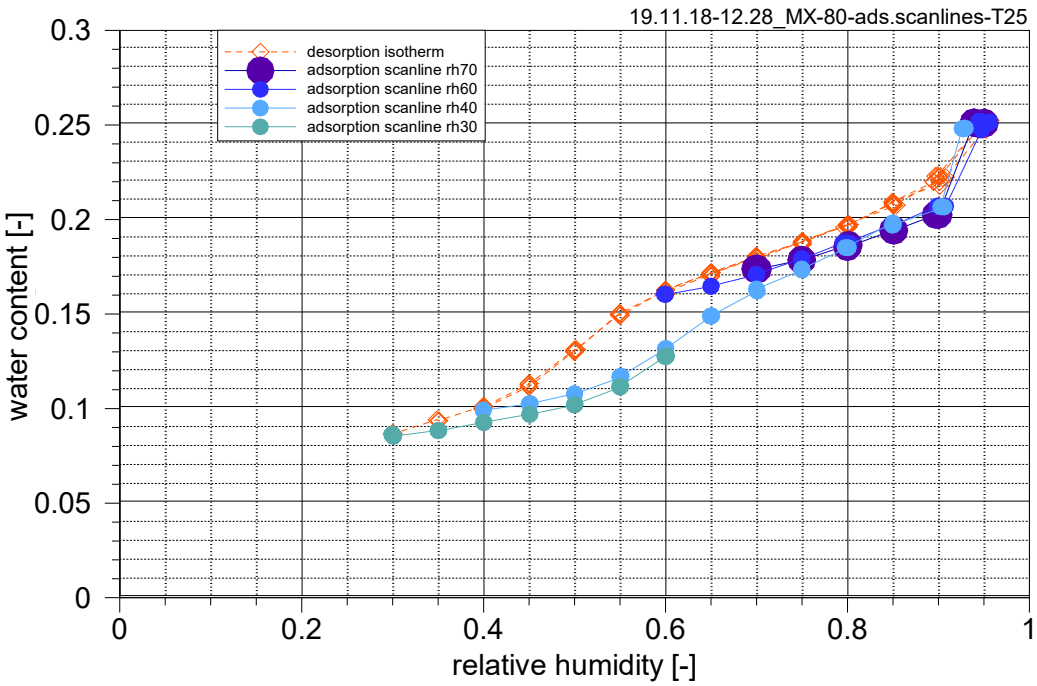

Fig. B.7 Adsorption scanlines for MX-80 at 25 °C; starting at 70, 60, 40, and 30 % relative humidity

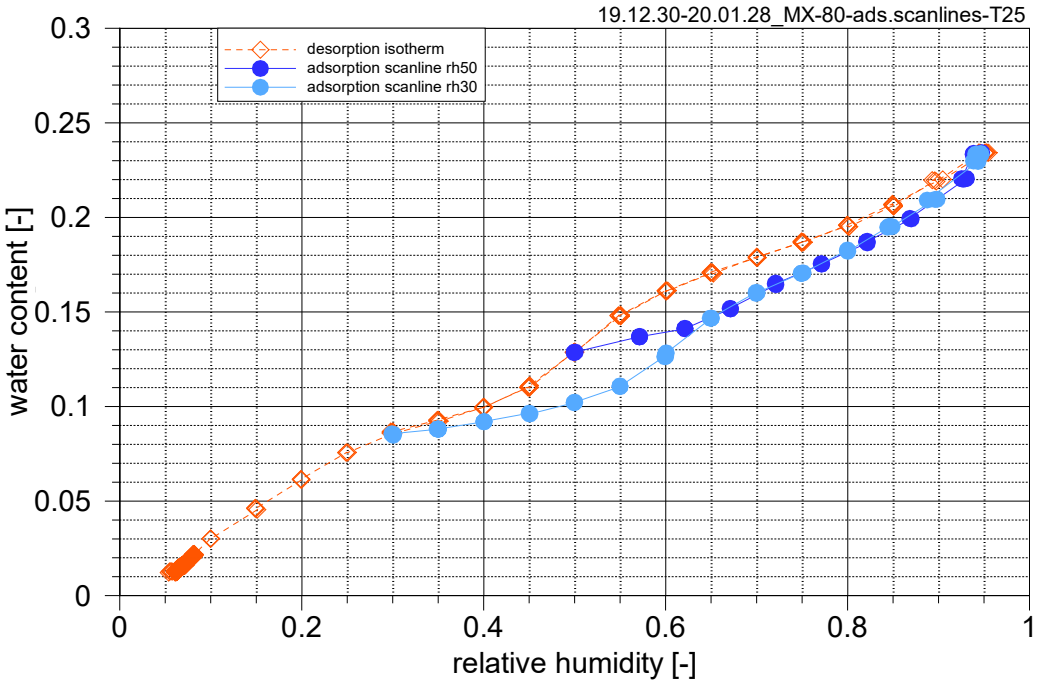

Fig. B.8 Adsorption scanlines for MX-80 at 25 °C; starting at 50 and 30 % relative humidity

B.1.3 Desorption scanlines

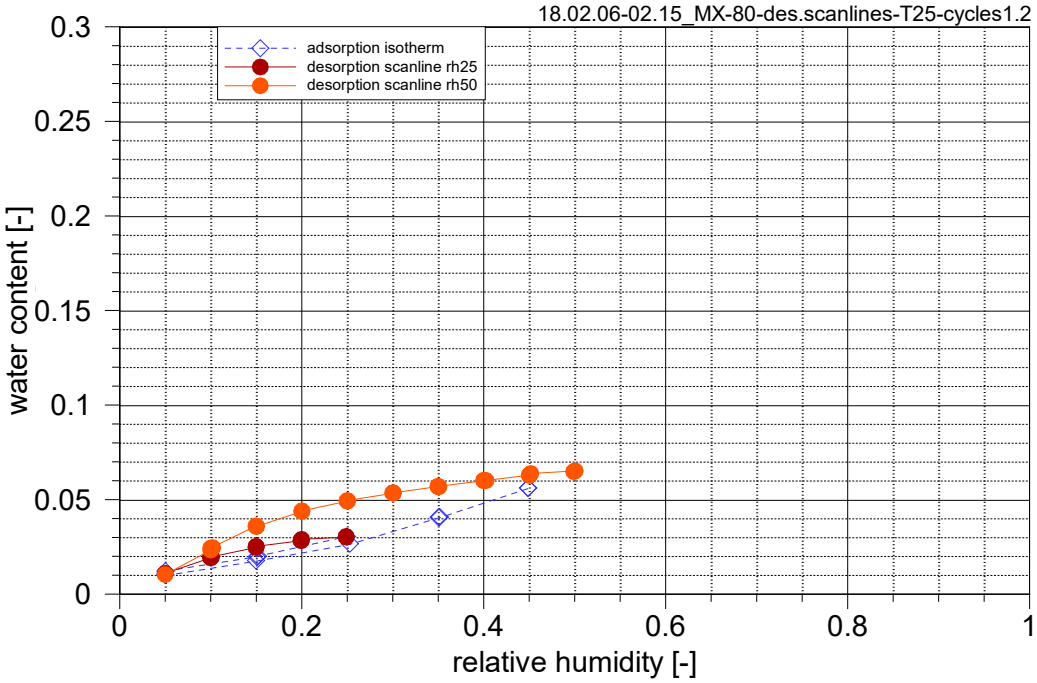

Fig. B.9 Desorption scanlines for MX-80 at 25 °C; starting at 25 and 50 % relative humidity

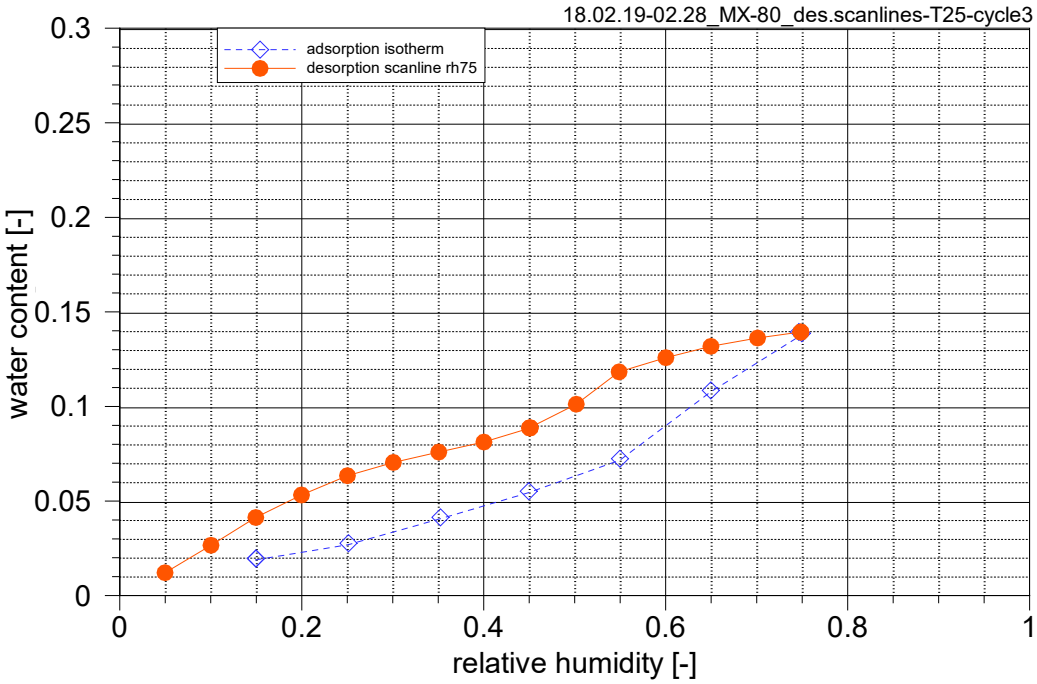

Fig. B.10 Desorption scanline for MX-80 at 25 °C; starting at 75 % relative humidity

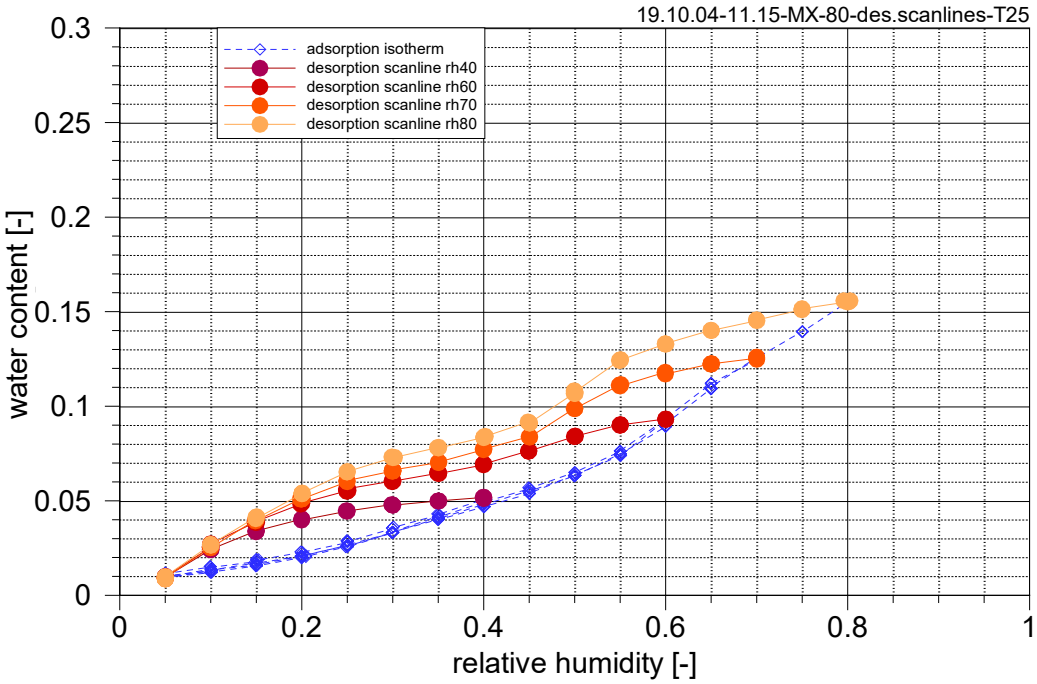

Fig. B.11 Desorption scanline for MX-80 at 25 °C; starting at 40, 60, 70, and 80 % relative humidity

B.1.4 Temperature dependence

B.1.4.1 Hysteresis and scanlines at increased temperature

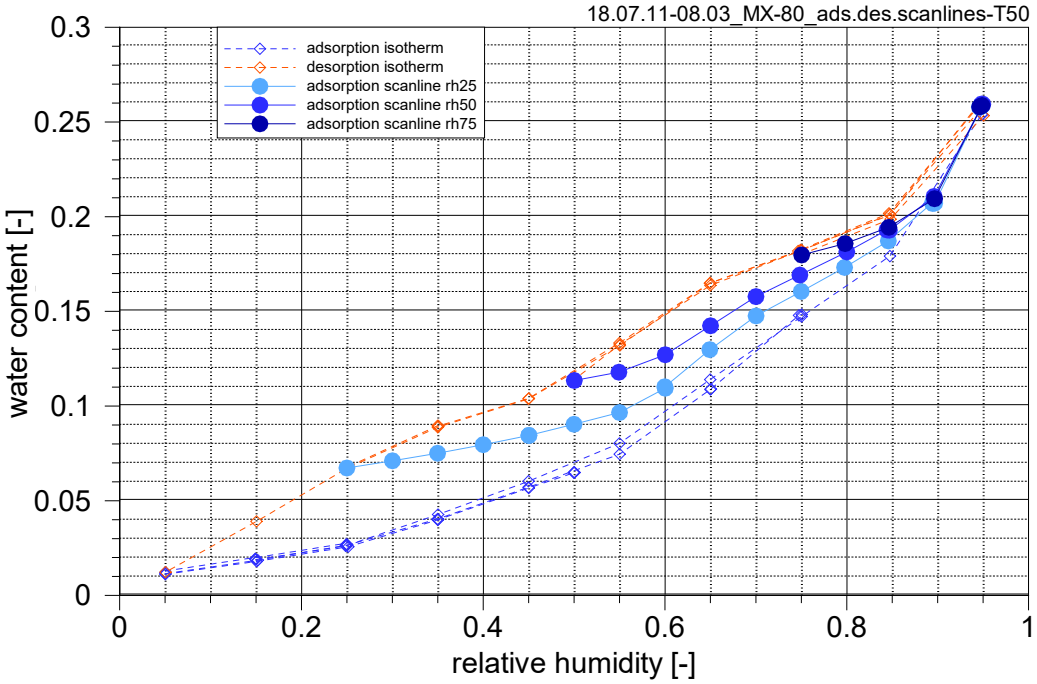

Fig. B.12 Adsorption scanlines for MX-80 at 50 °C; starting at 75, 50, and 25 % relative humidity

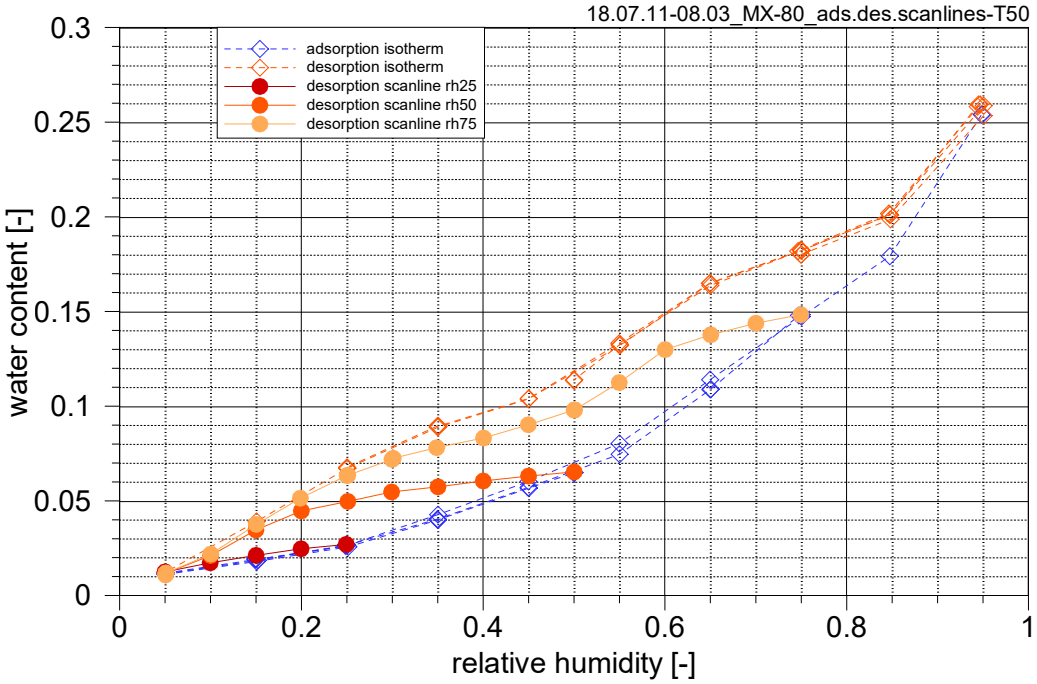

Fig. B.13 Desorption scanlines for MX-80 at 50 °C; starting at 75, 50, and 25 % relative humidity

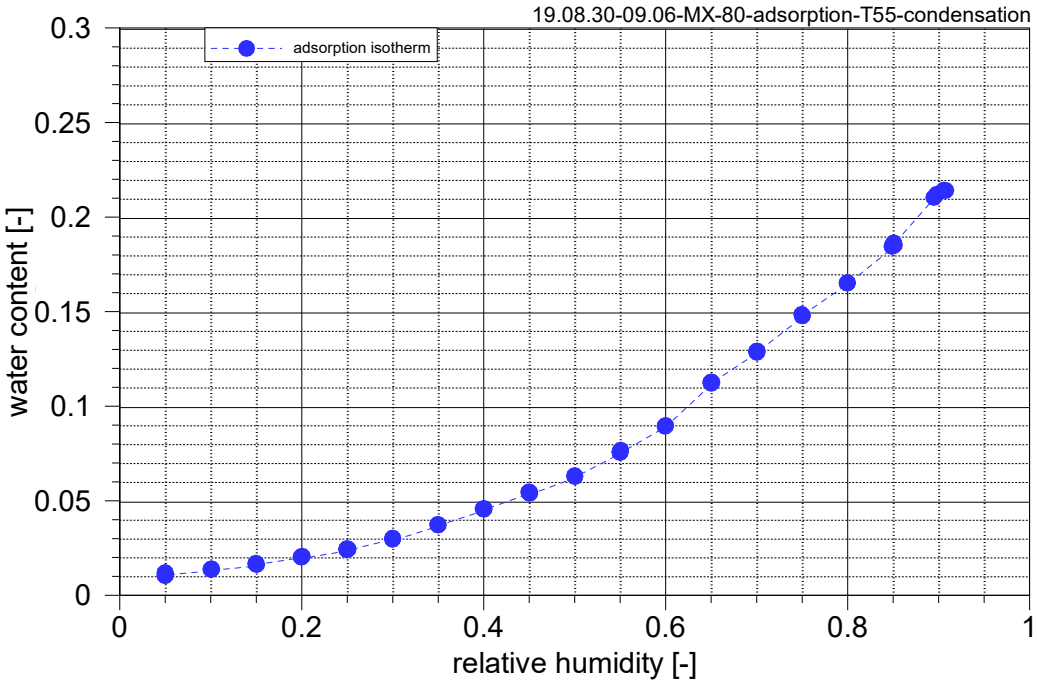

Fig. B.14 Adsorption isotherm for MX-80 at 55 °C

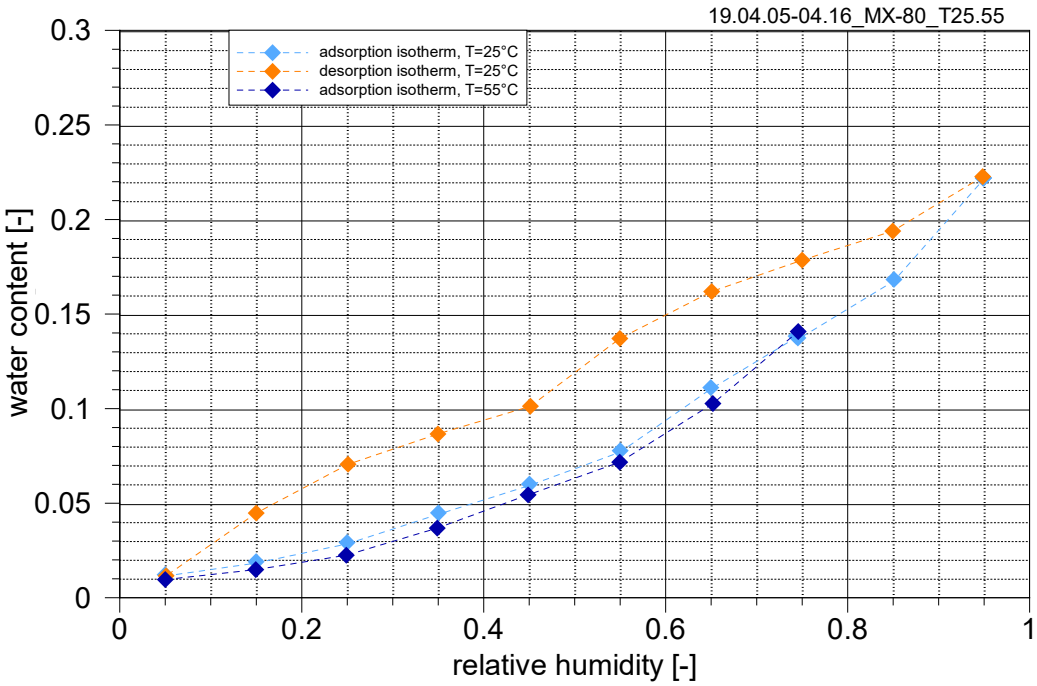

Fig. B.15 Adsorption isotherms for MX-80 at 25 and 55 °C; desorption at 15 °C

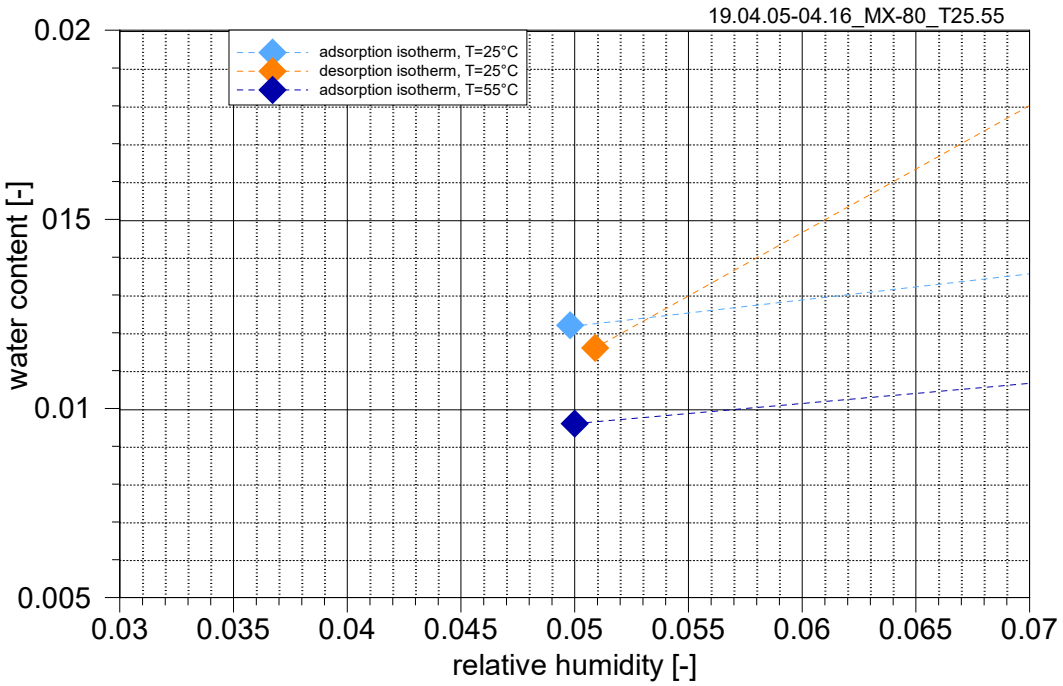

Fig. B.16 Adsorption isotherms for MX-80 at 25 and 55 °C (close-up from Fig. B.15)

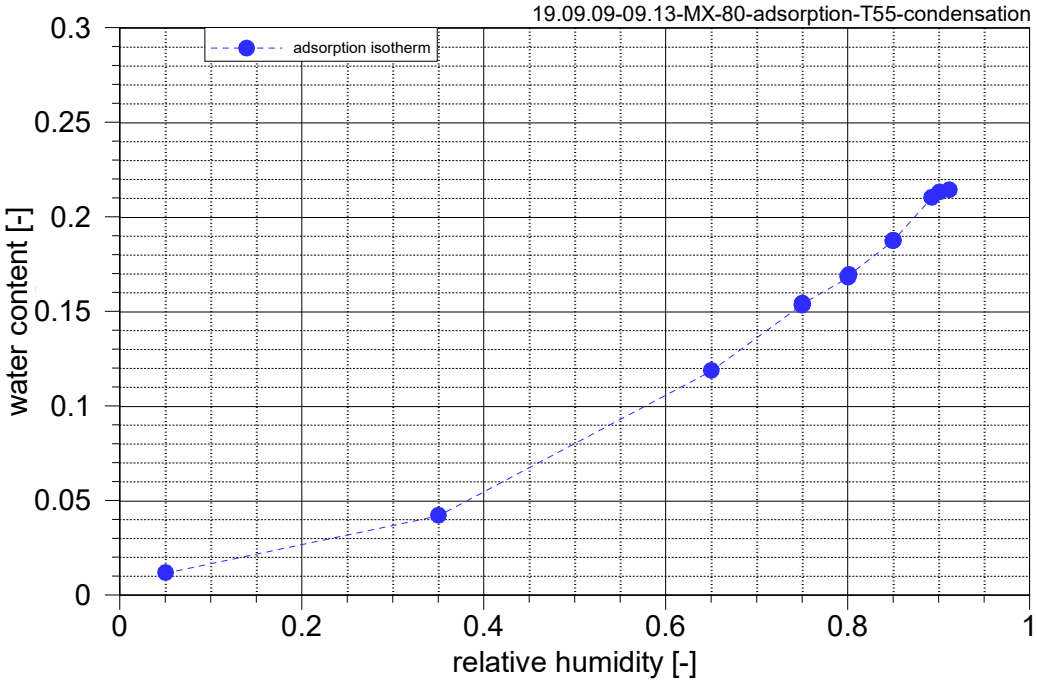

Fig. B.17 Adsorption isotherm for MX-80 at 55 °C, second measurement

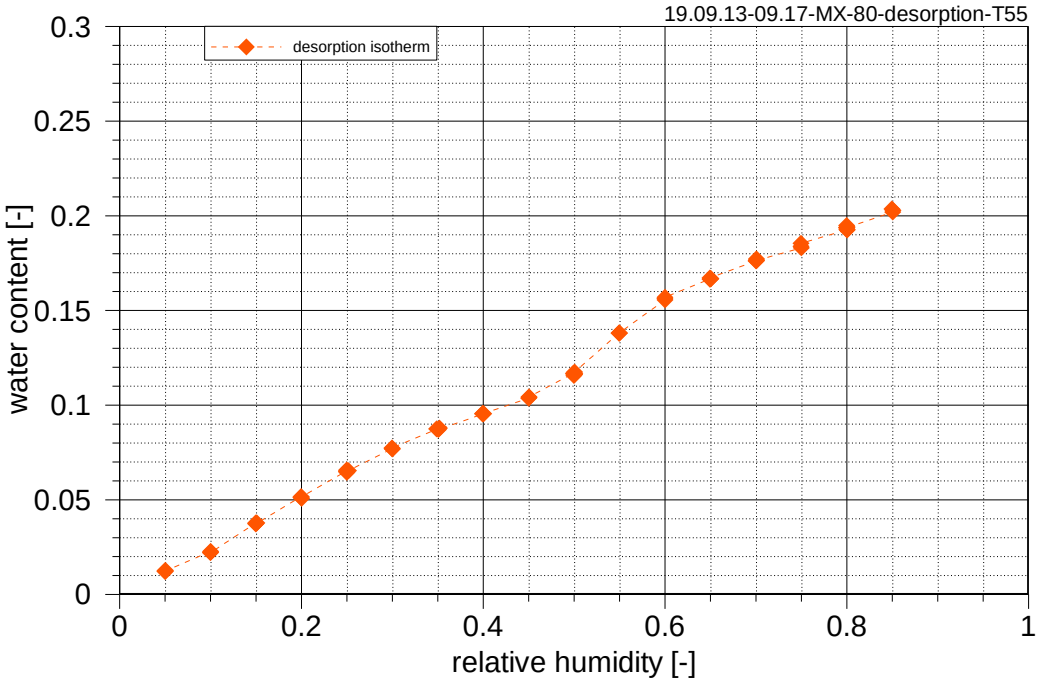

Fig. B.18 Desorption isotherm for MX-80 at 55 °C

B.1.4.2 Weight at varying temperature

B.1.4.2.1 Test conditions

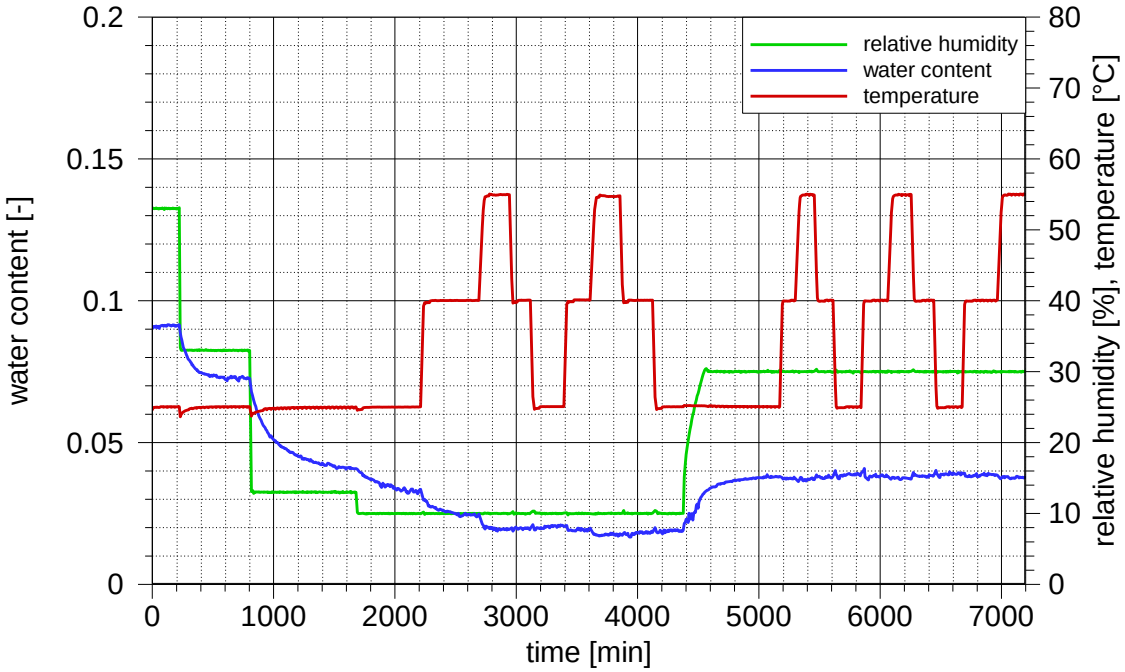

Fig. B.19 Test conditions for the campaign with 10 and 30 % relative humidity

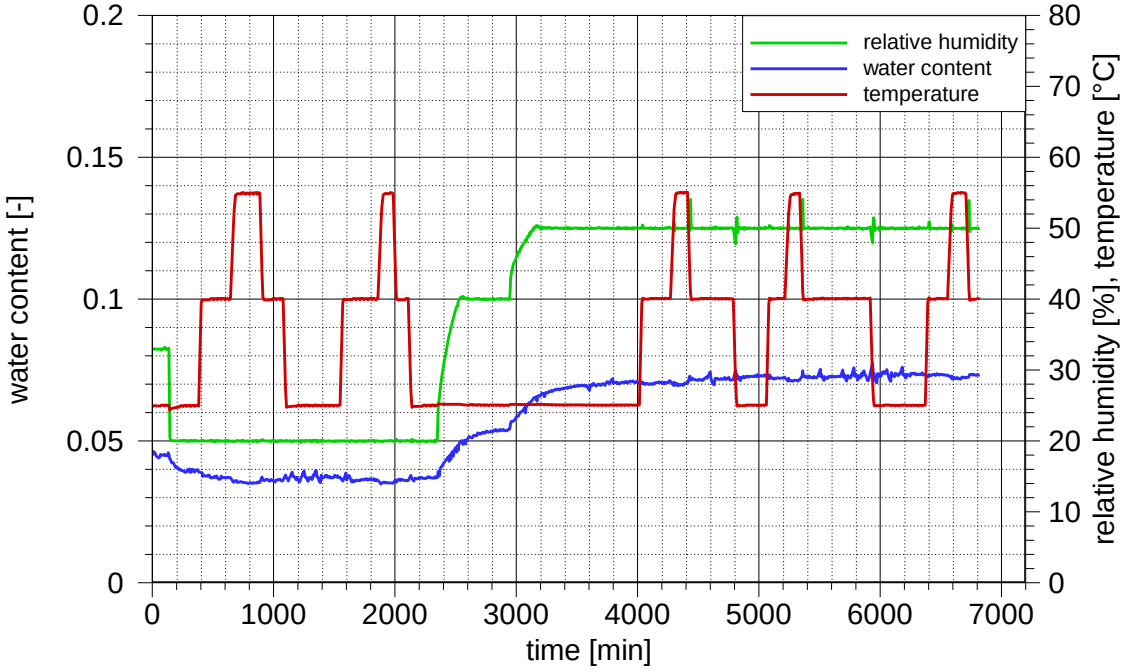

Fig. B.20 Test conditions for the campaign with 20 and 50 % relative humidity

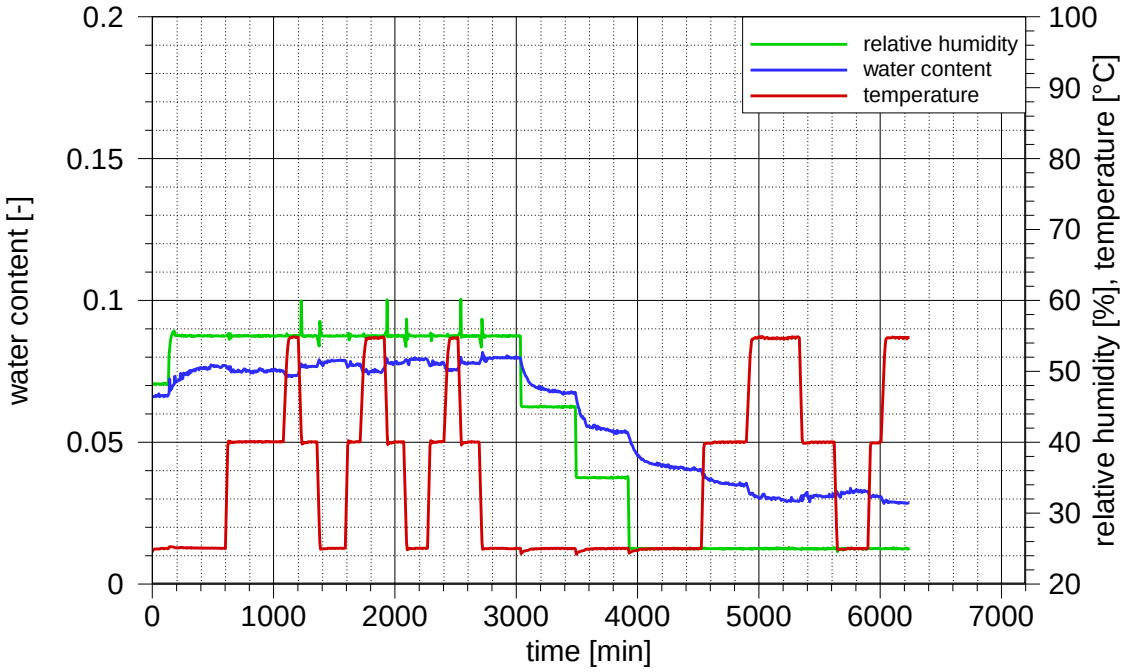

Fig. B.21 Test conditions for the campaign with 55 and 25 % relative humidity

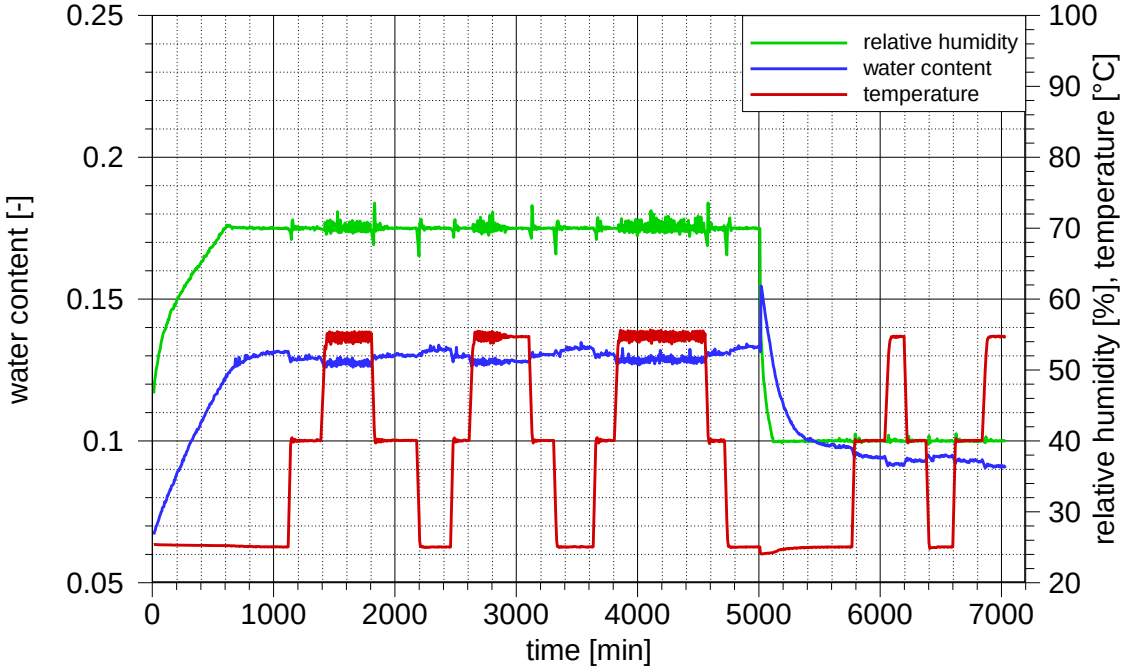

Fig. B.22 Test conditions for the campaign with 70 and 40 % relative humidity

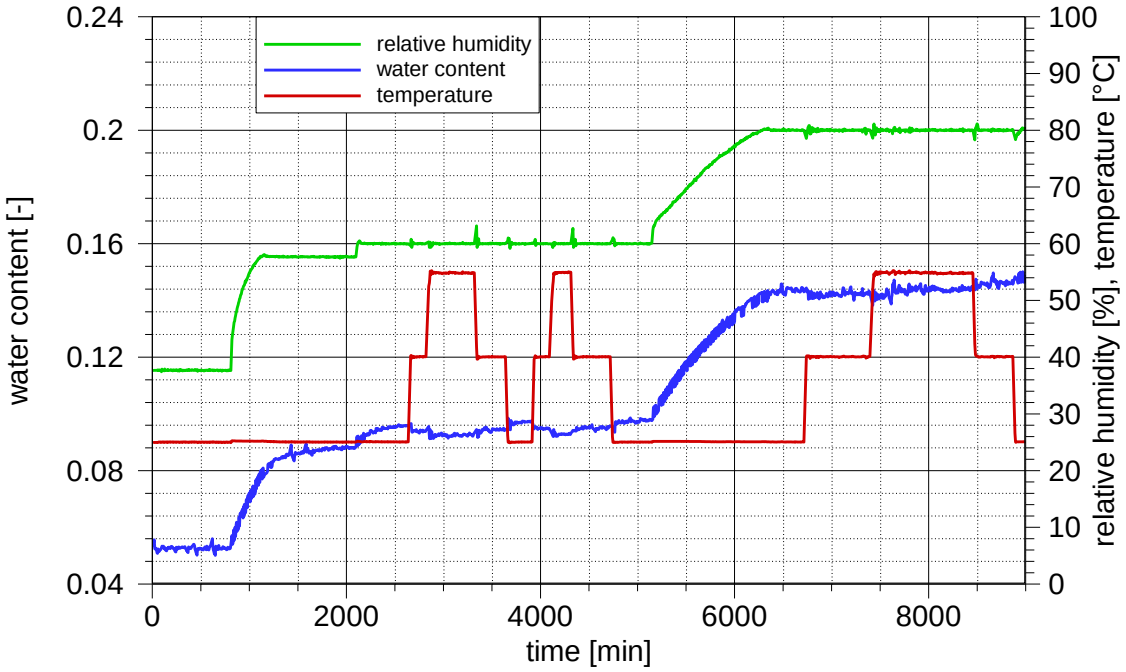

Fig. B.23 Test conditions for the campaign with 60 and 80 % relative humidity

B. 1.4.2.2 Test results

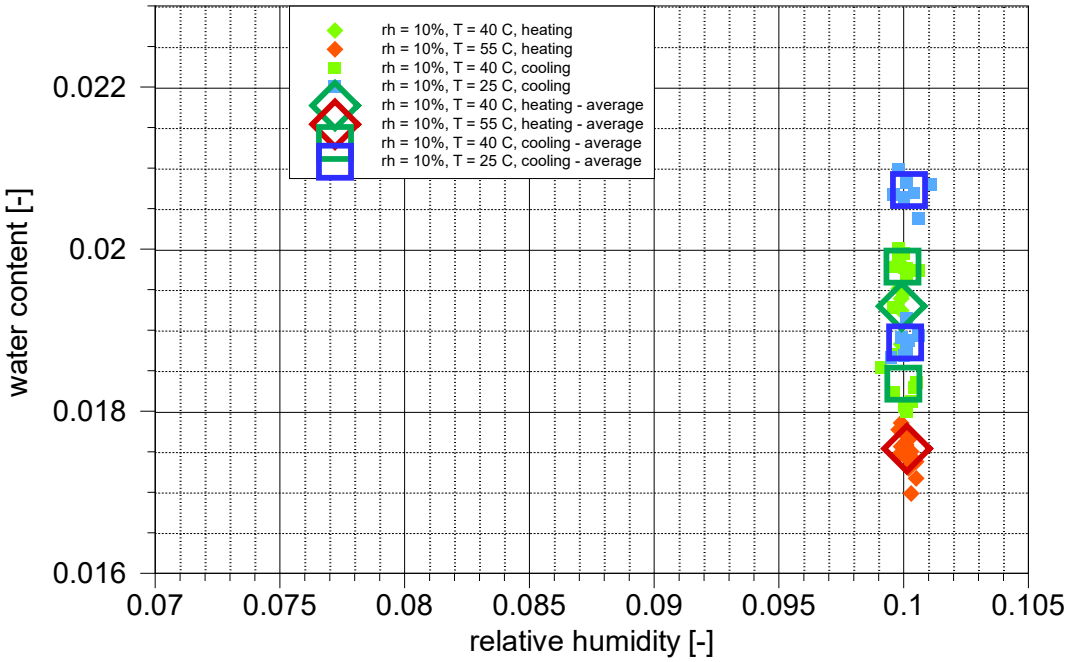

Fig. B.24 Heating and cooling of MX-80 at a relative humidity of 10 %

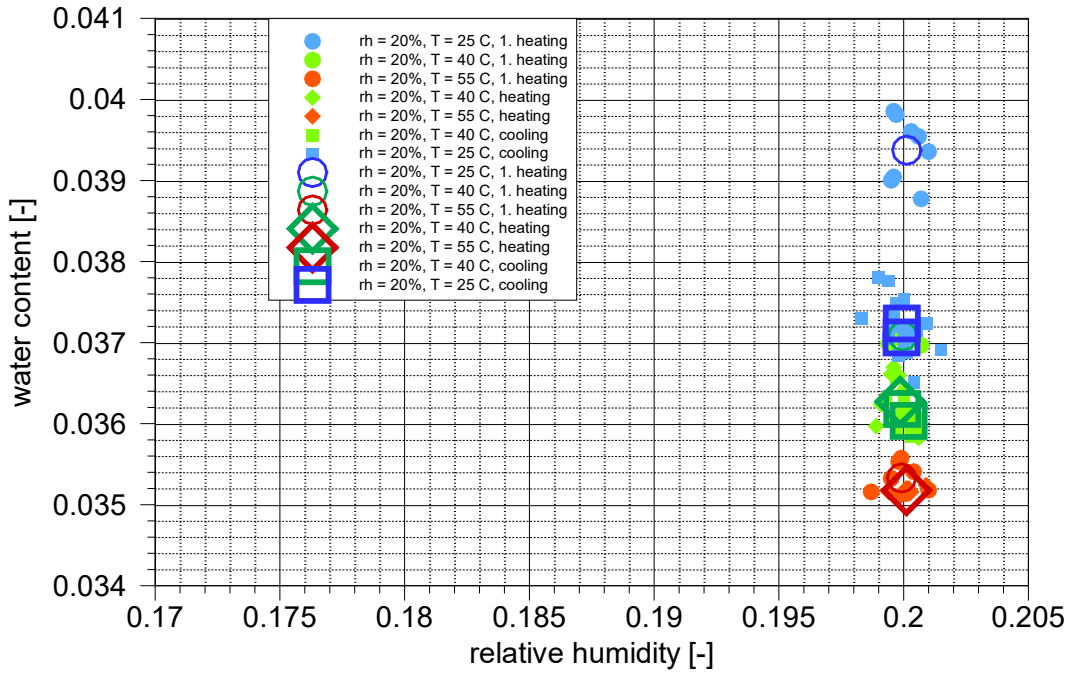

Fig. B.25 Heating and cooling of MX-80 at a relative humidity of 20 %

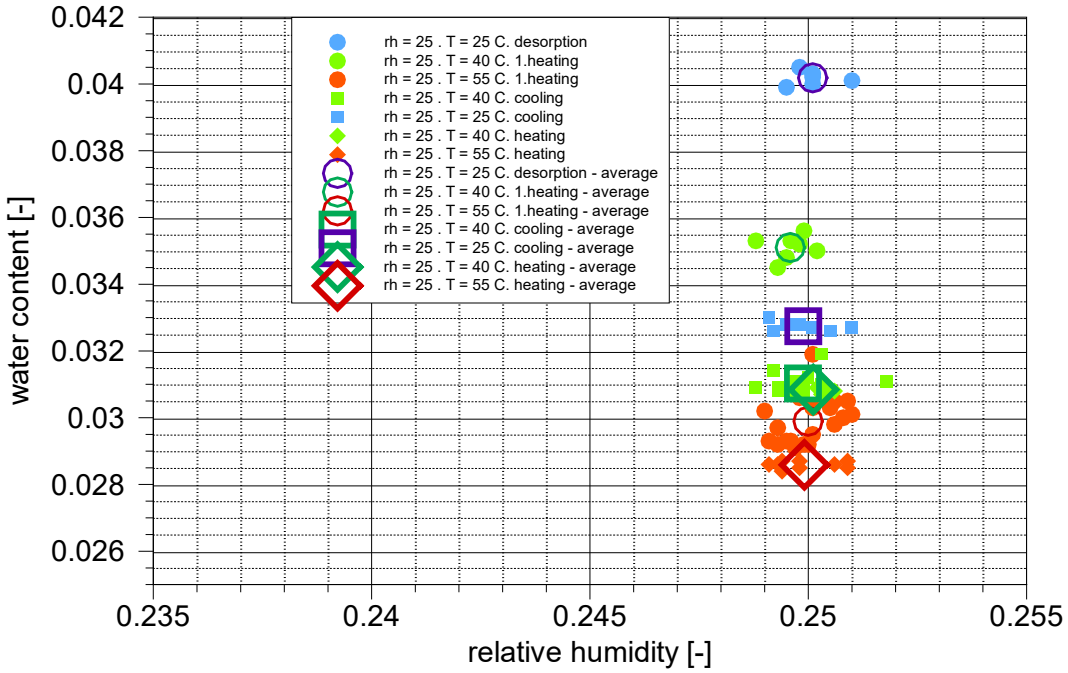

Fig. B.26 Heating and cooling of MX-80 at a relative humidity of 25 %

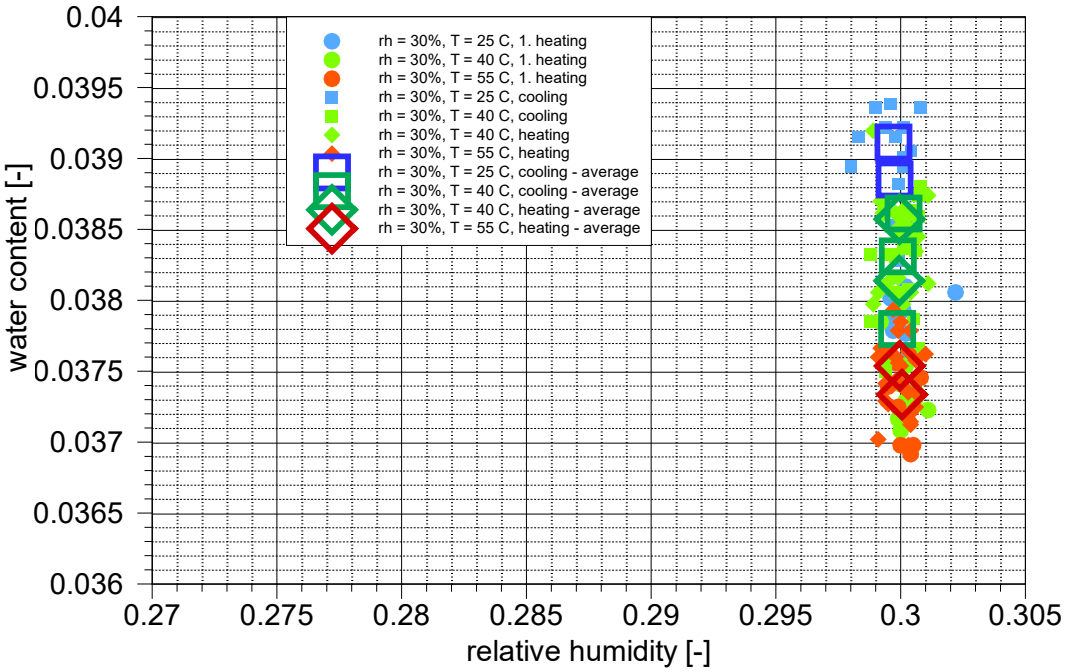

Fig. B.27 Heating and cooling of MX-80 at a relative humidity of 30 %

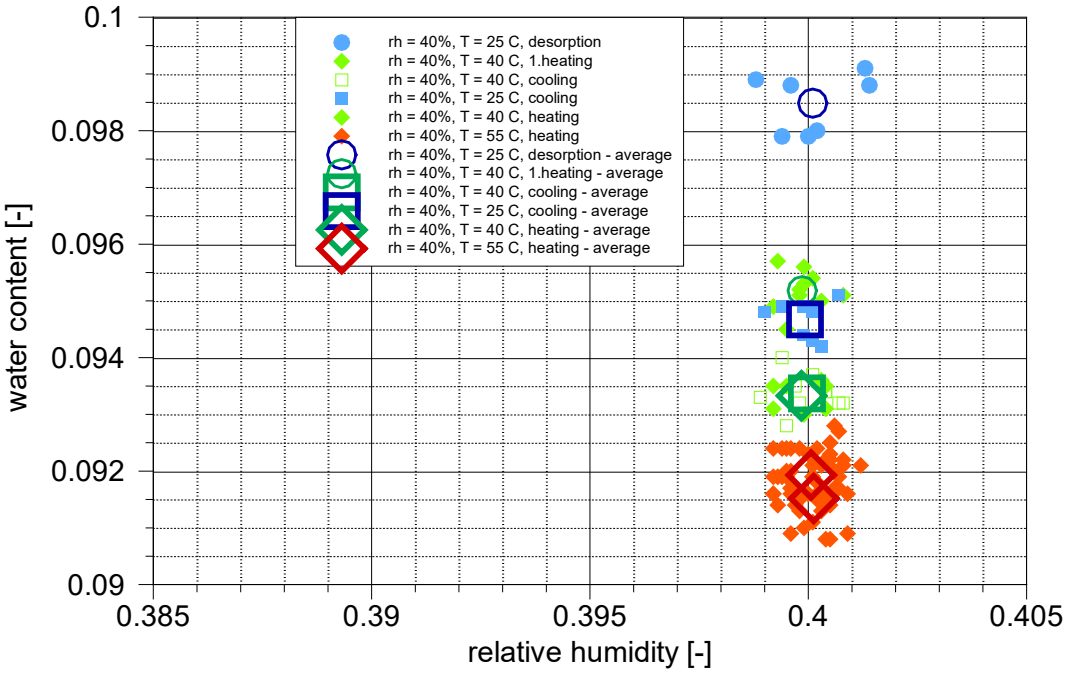

Fig. B.28 Heating and cooling of MX-80 at a relative humidity of 40 %

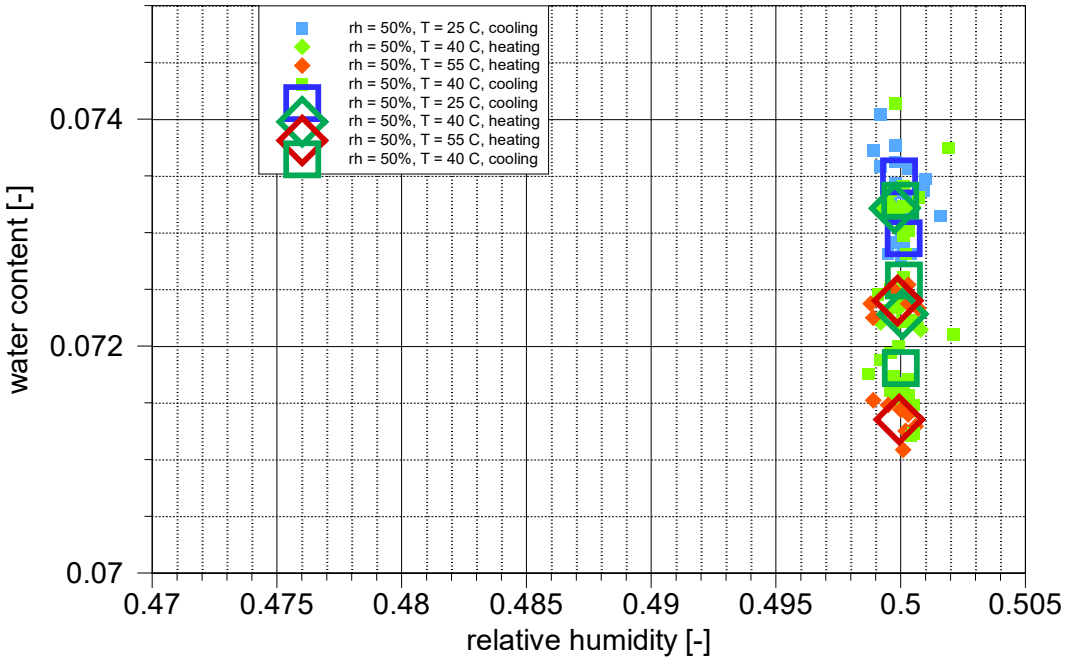

Fig. B.29 Heating and cooling of MX-80 at a relative humidity of 50 %

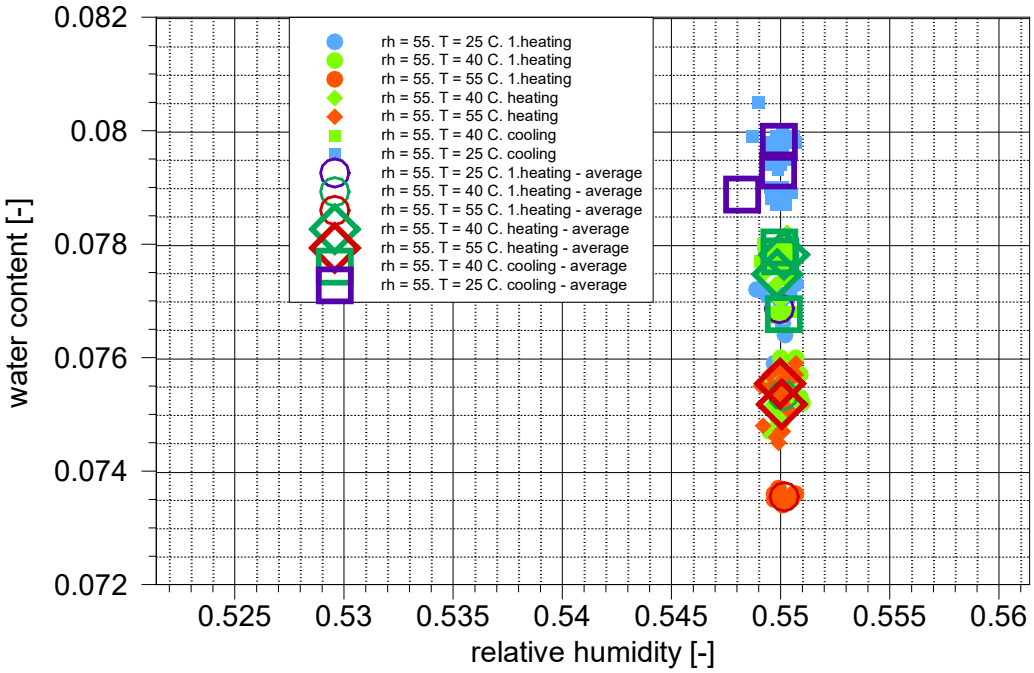

Fig. B.30 Heating and cooling of MX-80 at a relative humidity of 55 %

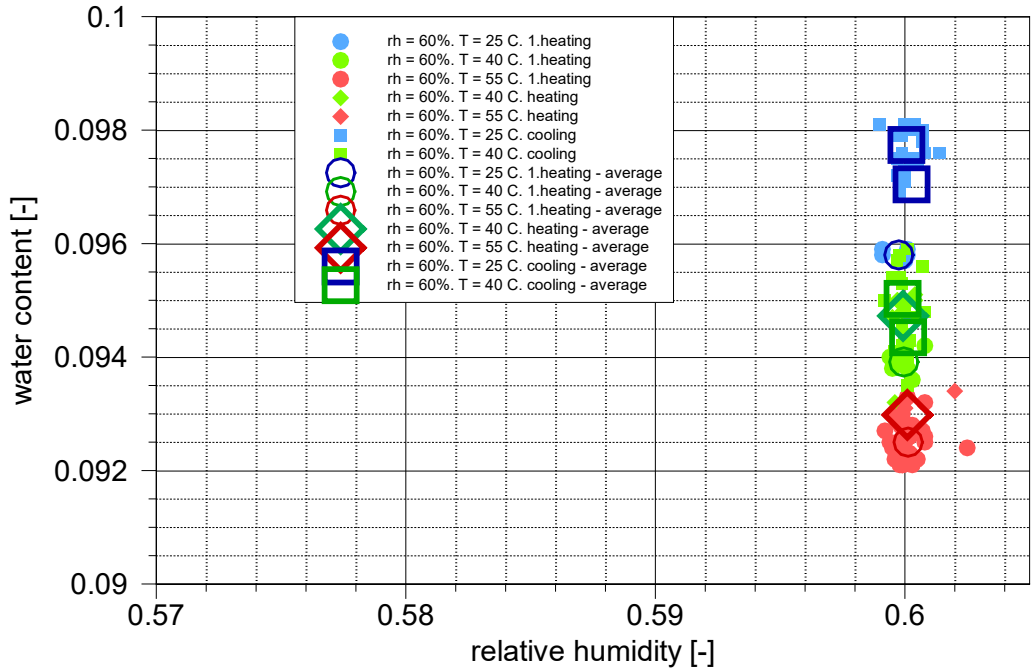

Fig. B.31 Heating and cooling of MX-80 at a relative humidity of 60 %

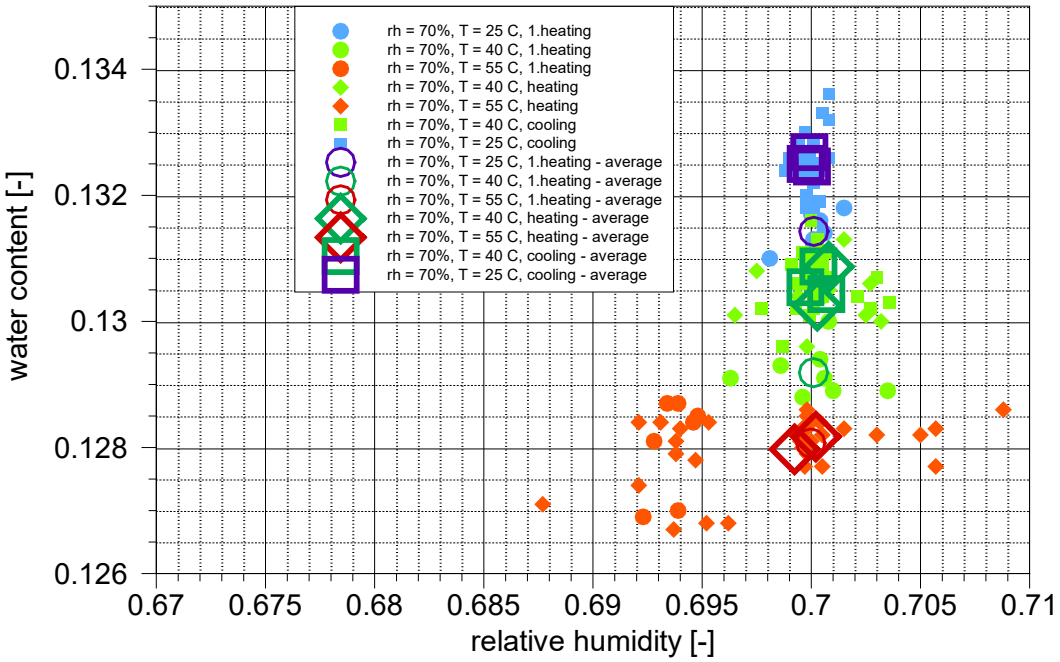

Fig. B.32 Heating and cooling of MX-80 at a relative humidity of 70 %

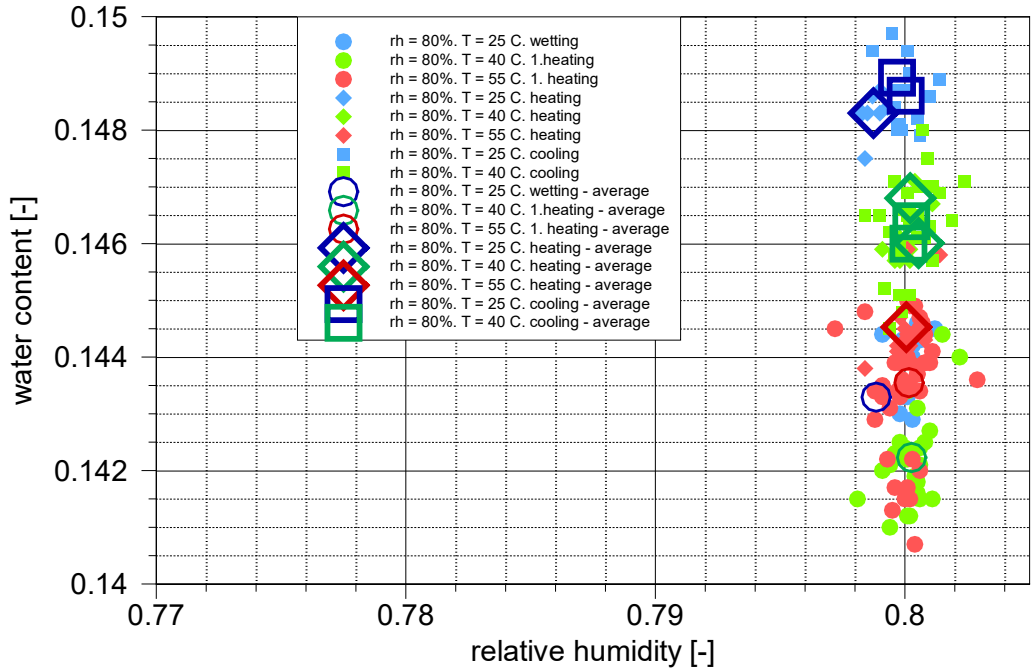

Fig. B.33 Heating and cooling of MX-80 at a relative humidity of 80 %

B.2 Calcigel

B.2.1 Hysteresis

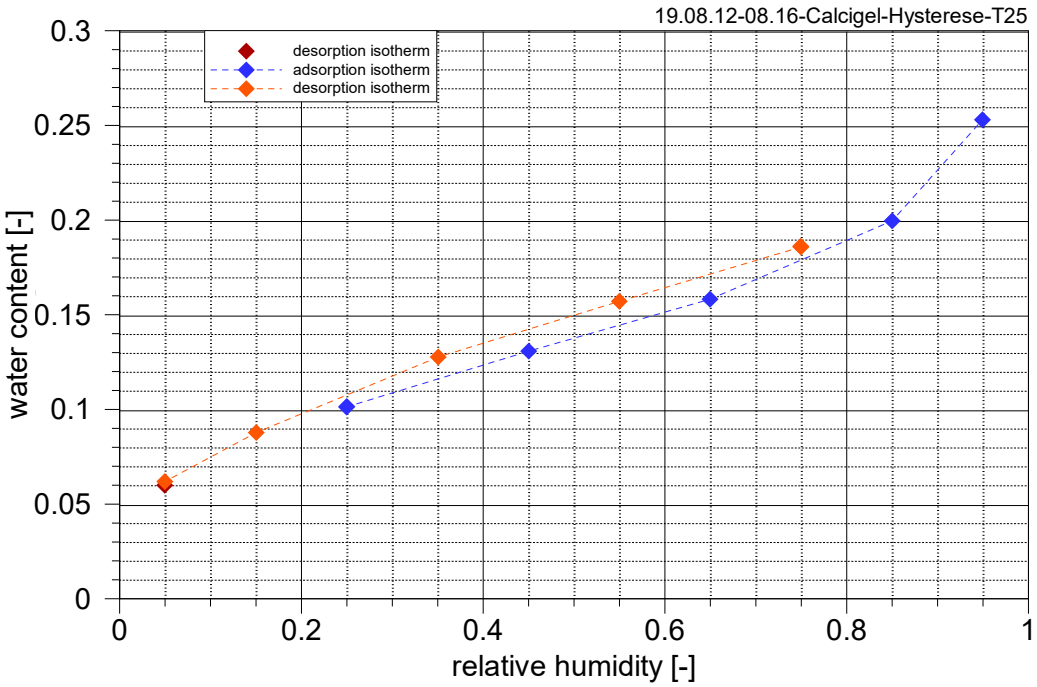

Fig. B.34 Hysteresis of the isotherm for Calcigel at 25 °C

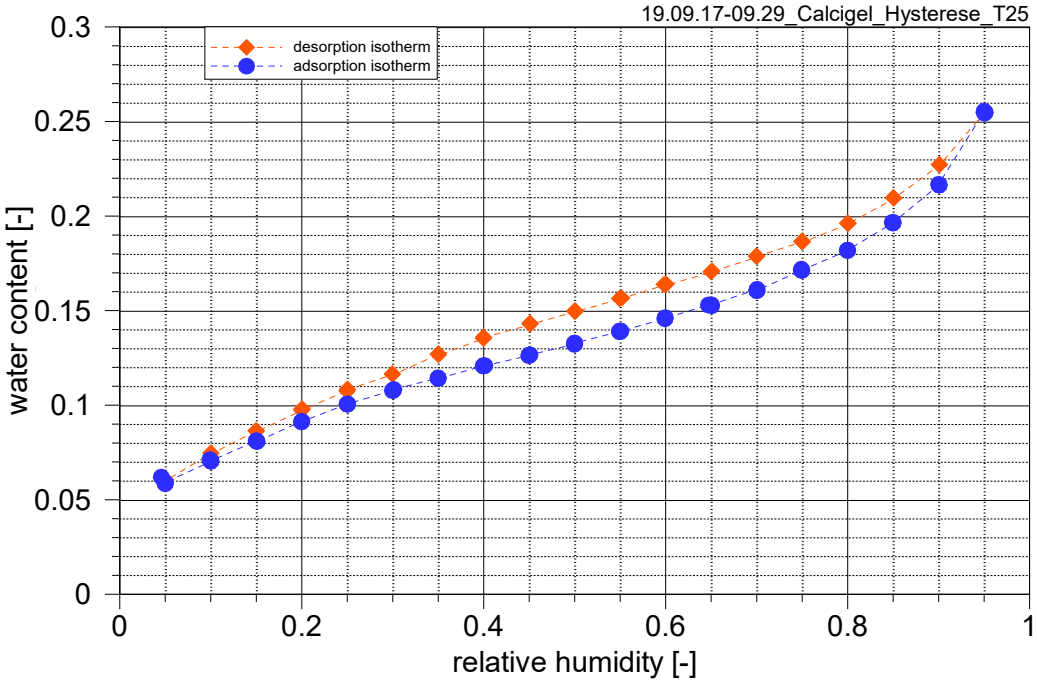

Fig. B.35 Hysteresis of the isotherm for Calcigel at 25 °C, higher resolution

B.2.2 Adsorption scanlines

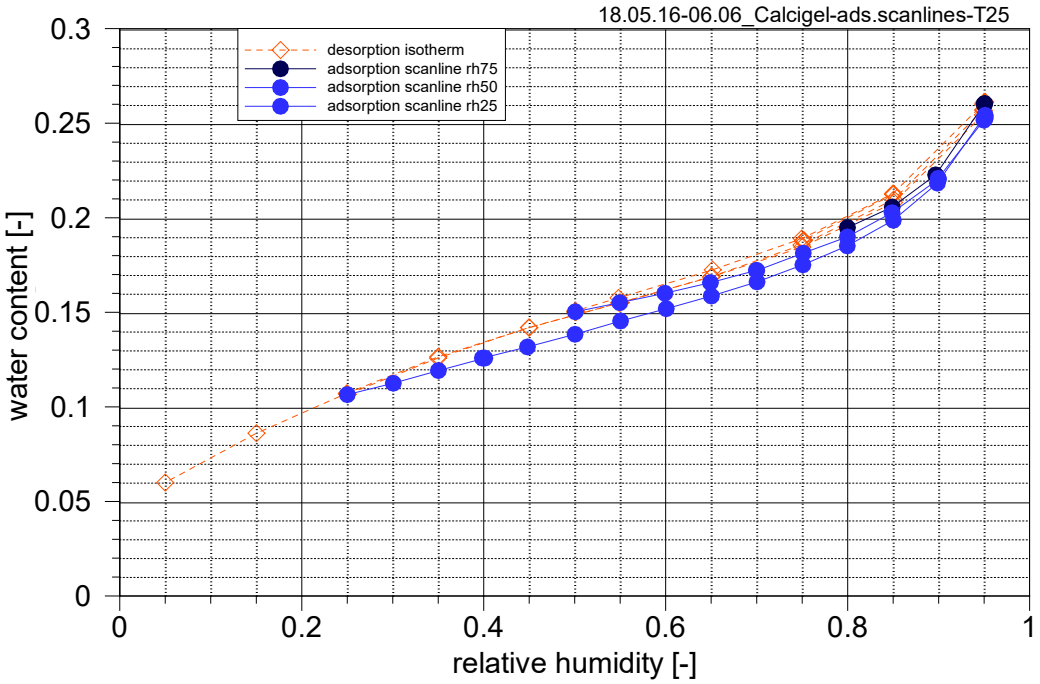

Fig. B.36 Adsorption scanlines for Calcigel at 25 °C starting at 75, 50, and 30 % relative humidity

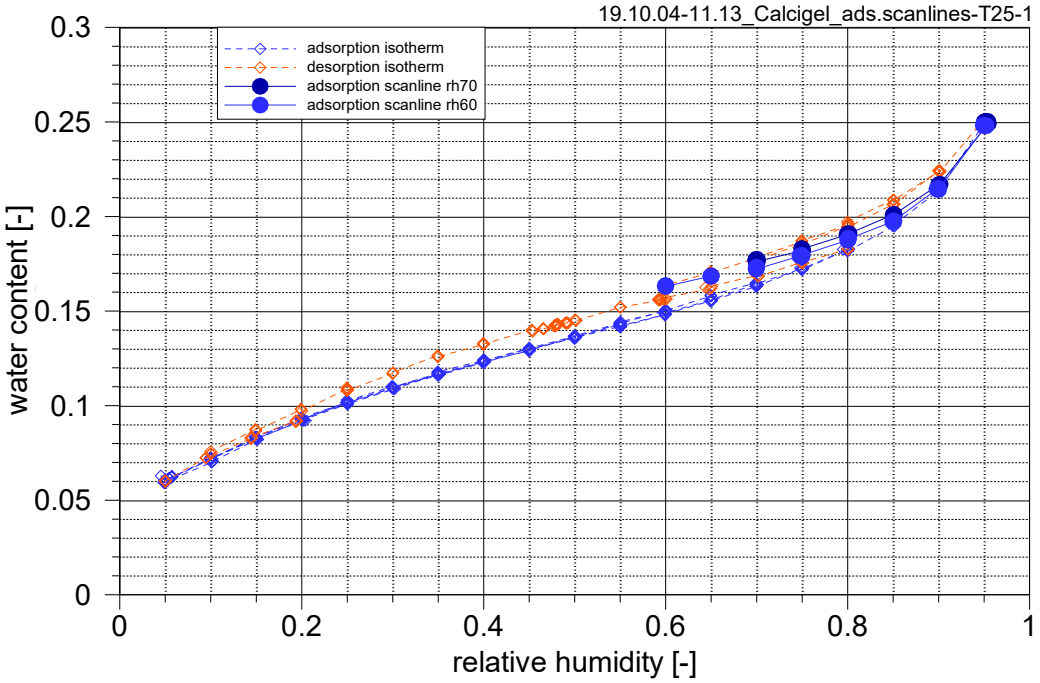

Fig. B.37 Adsorption scanlines for Calcigel at 25 °C starting at 70 and 60 % relative humidity

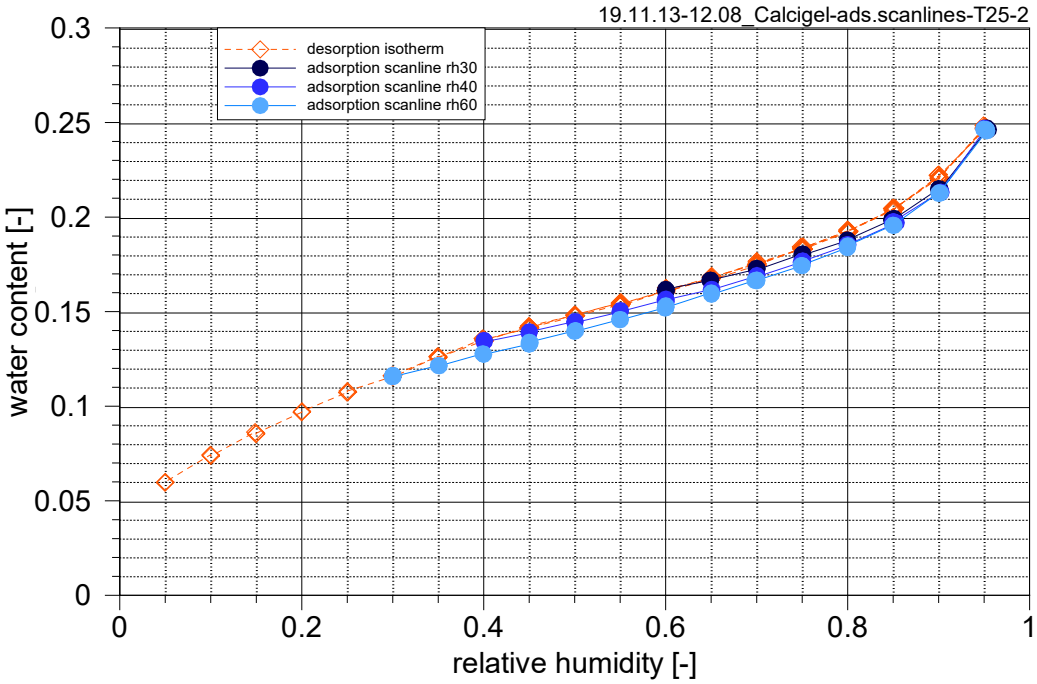

Fig. B.38 Adsorption scanlines for Calcigel at 25 °C starting at 60, 40 and 30 % relative humidity

B.2.3 Desorption scanlines

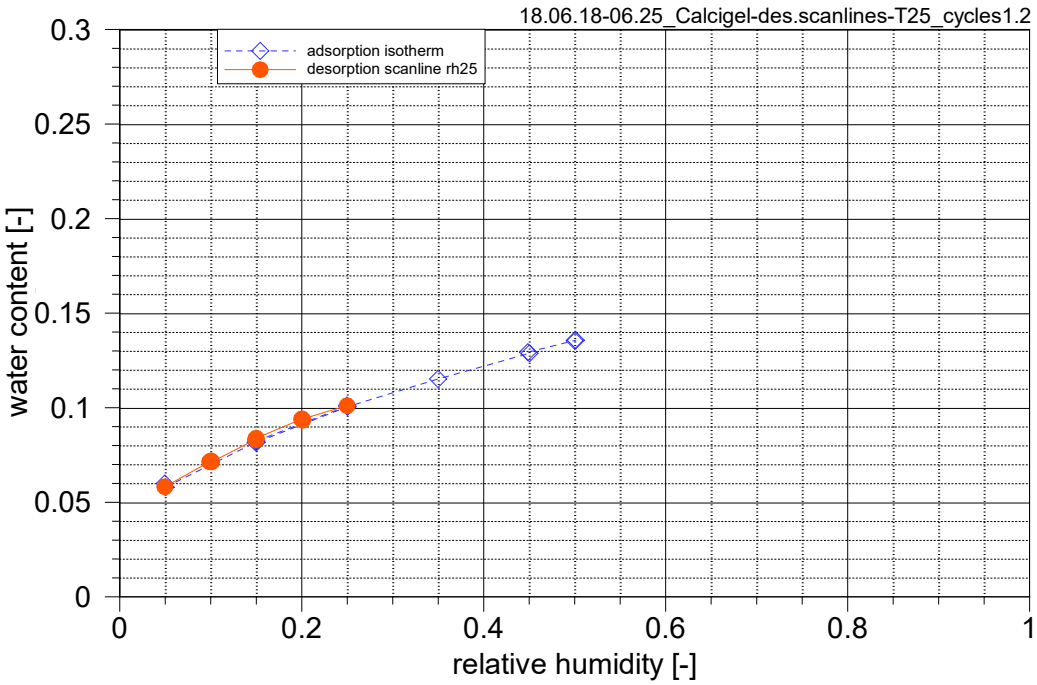

Fig. B.39 Desorption scanline for Calcigel at 25 °C starting at 25 % relative humidity

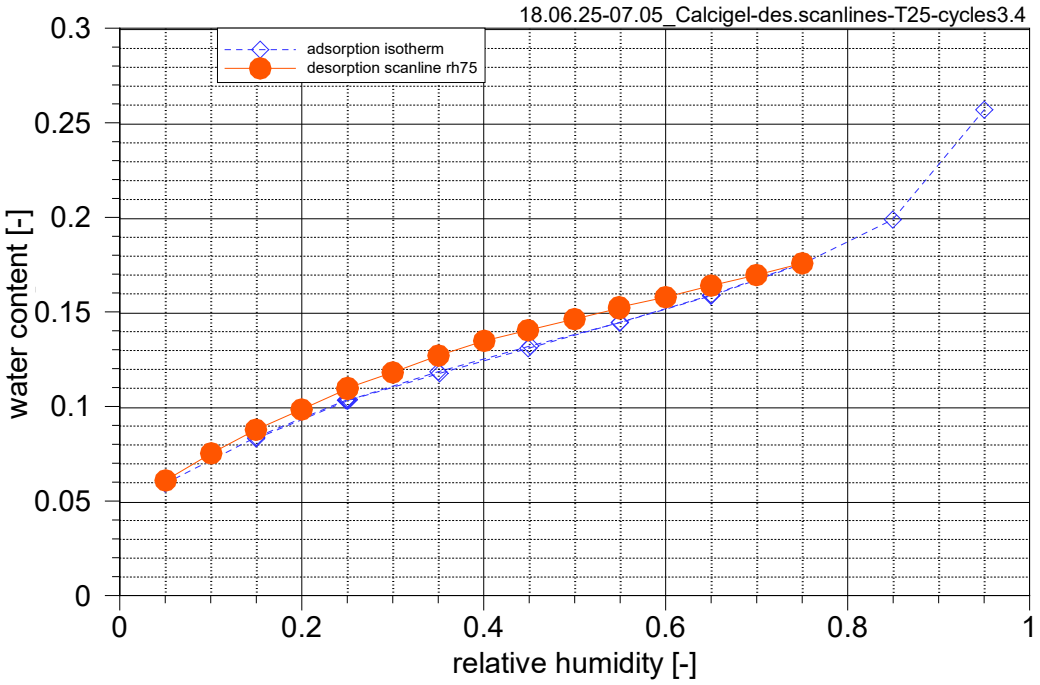

Fig. B.40 Desorption scanlines for Calcigel at 25 °C starting at 75 % relative humidity

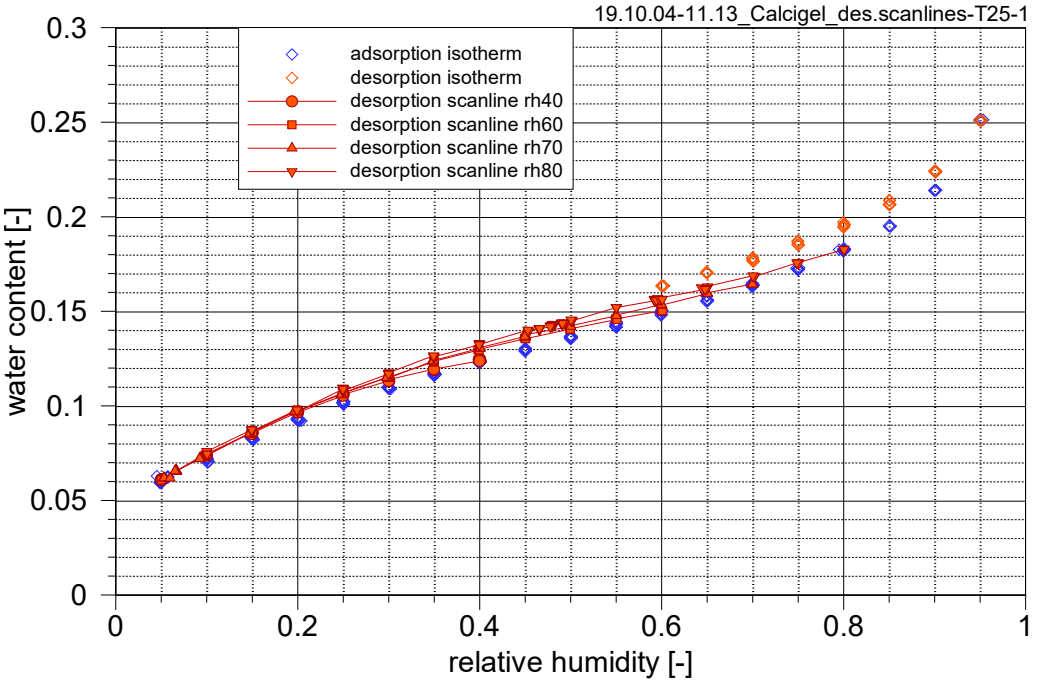

Fig. B.41 Desorption scanlines for Calcigel at 25 °C starting at 40, 60, 70, and 80 % relative humidity

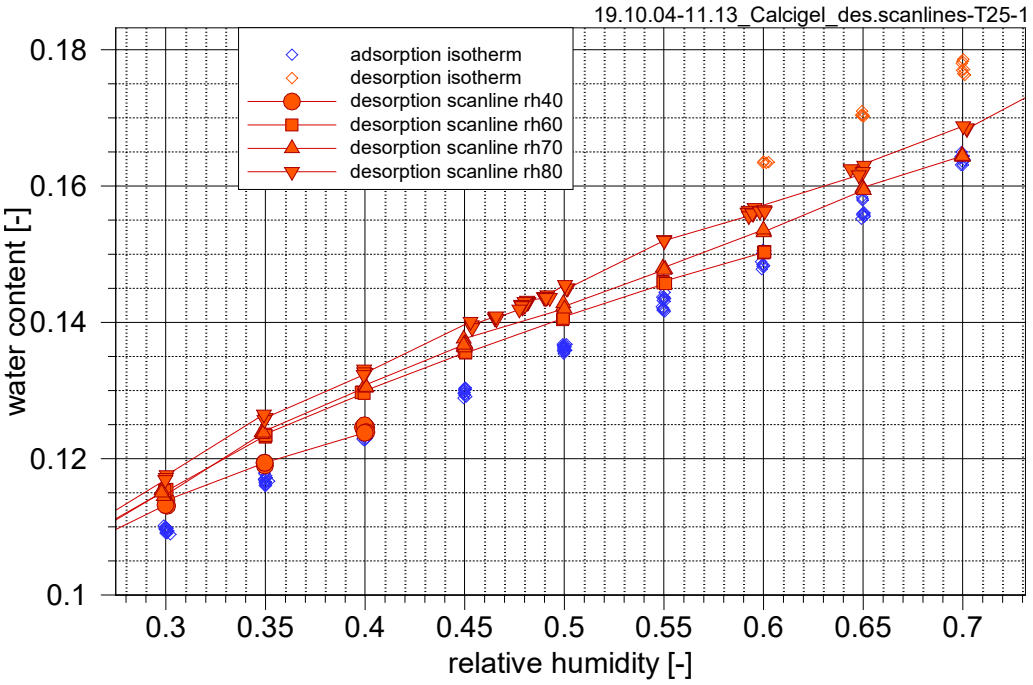

Fig. B.42 Desorption scanlines for Calcigel at 25 °C, close-up of Fig. B.35.

B.2.4 Temperature dependence

B.2.4.1 Hysteresis and scanlines at increased temperature

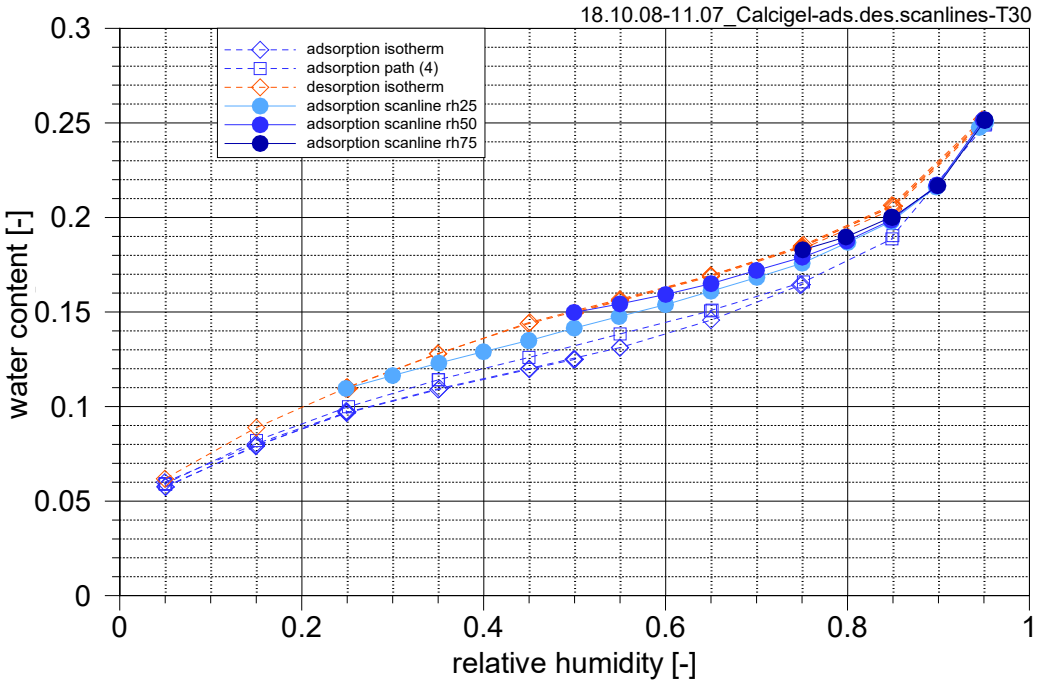

Fig. B.43 Adsorption scanlines for Calcigel at 30 °C starting at 25, 50, and 75 % relative humidity

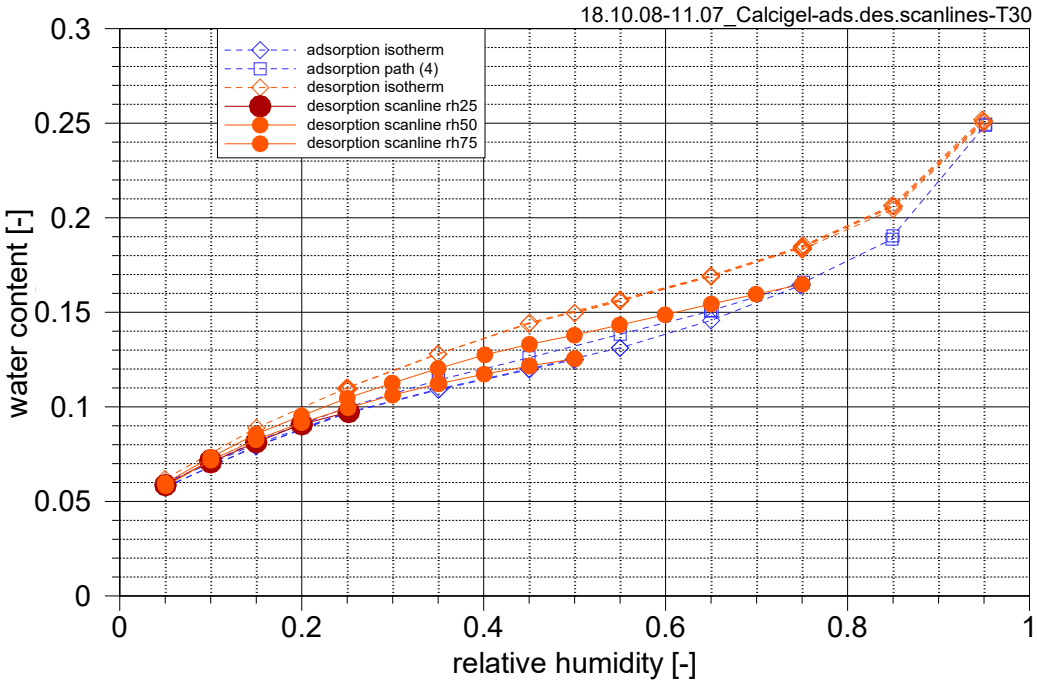

Fig. B.44 Desorption scanlines for Calcigel at 30 °C starting at 25, 50, and 75 % relative humidity

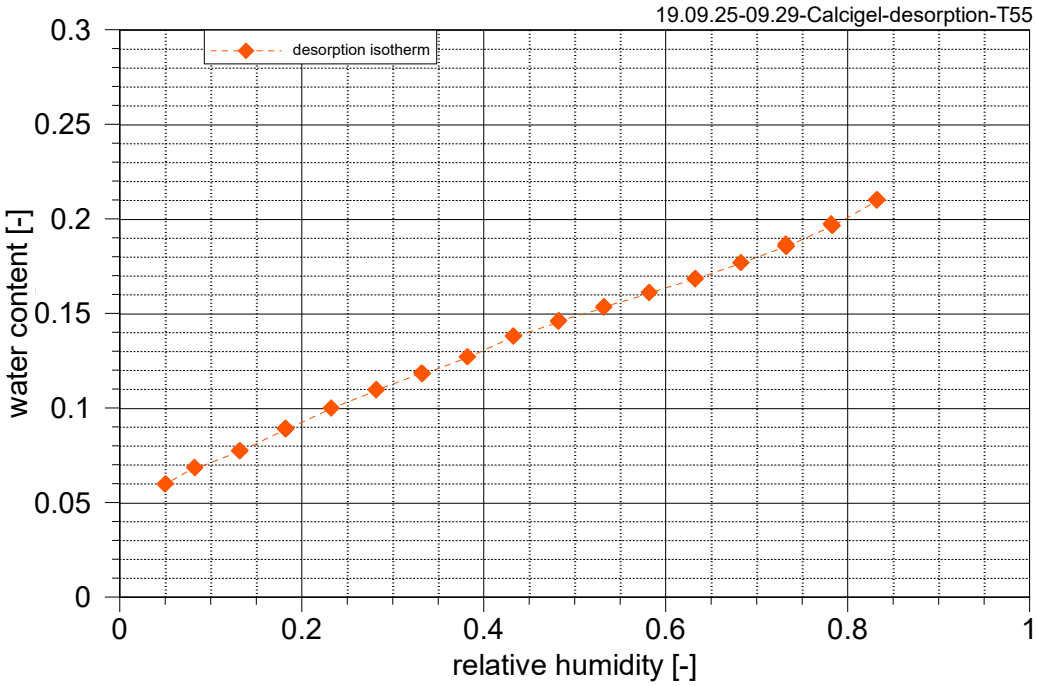

Fig. B.45 Desorption isotherm for Calcigel at 55 °C

B.2.4.2 Weight at varying temperature

B.2.4.2.1 Test conditions

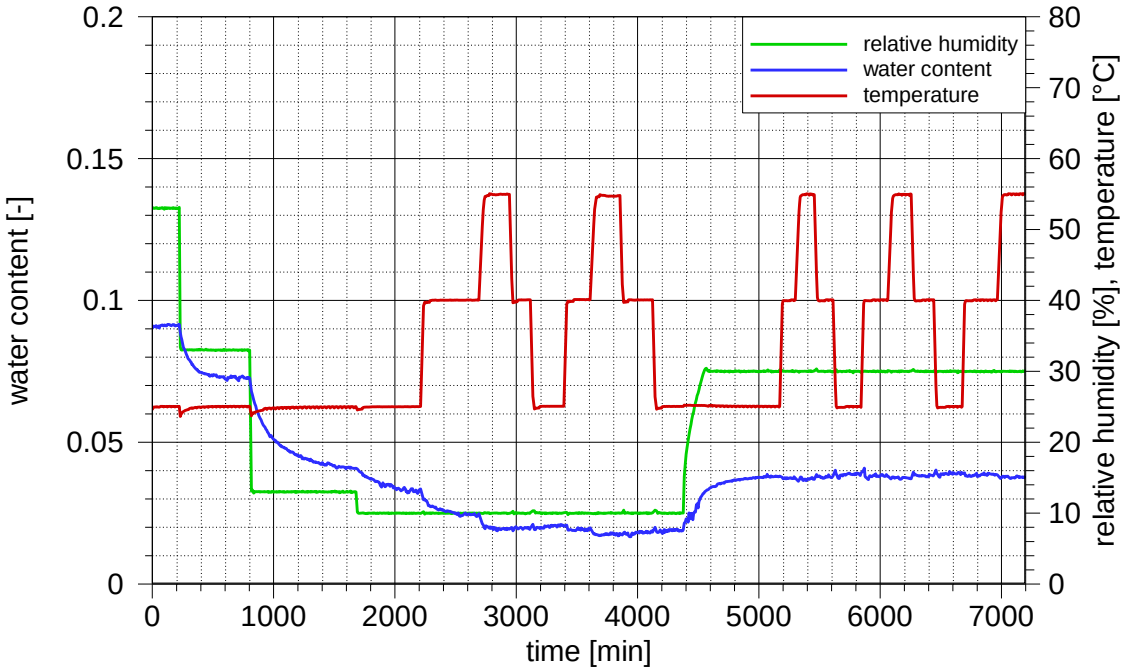

Fig. B.46 Test conditions for the campaign with 10 and 30 % relative humidity

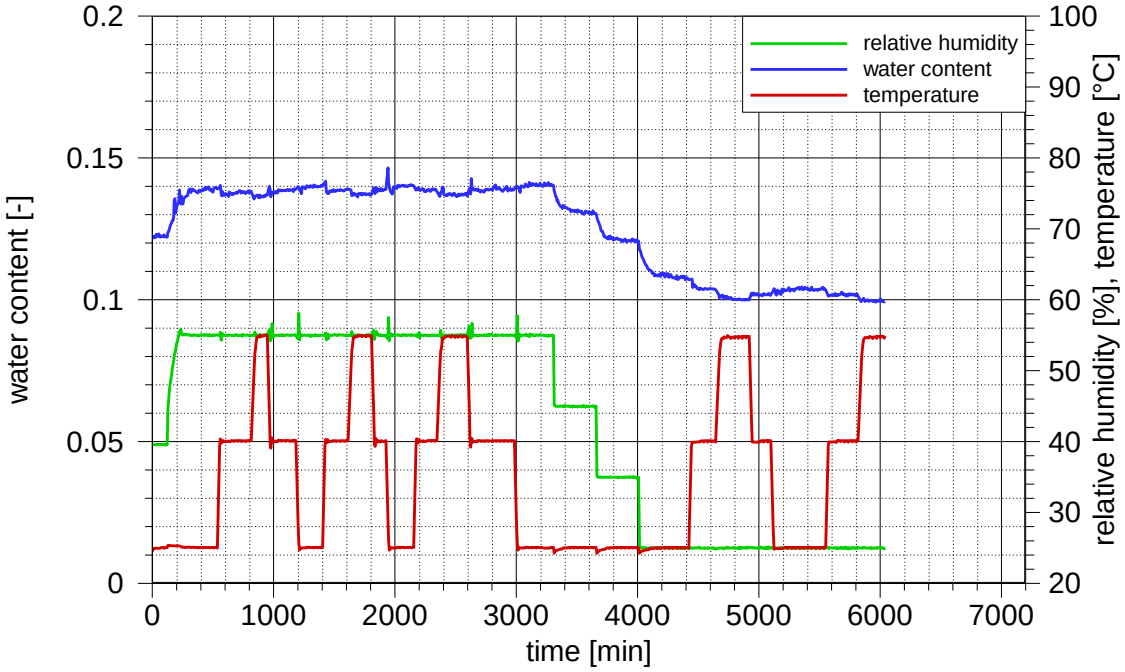

Fig. B.47 Test conditions for the campaign with 55 and 25 % relative humidity

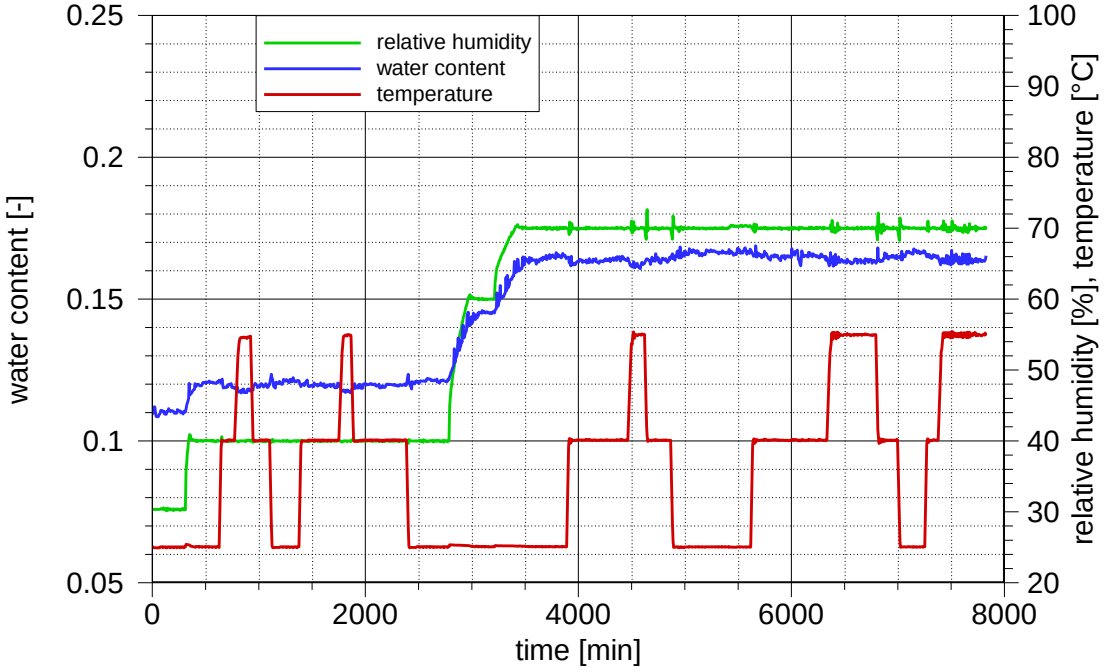

Fig. B.48 Test conditions for the campaign with 40 and 70 % relative humidity

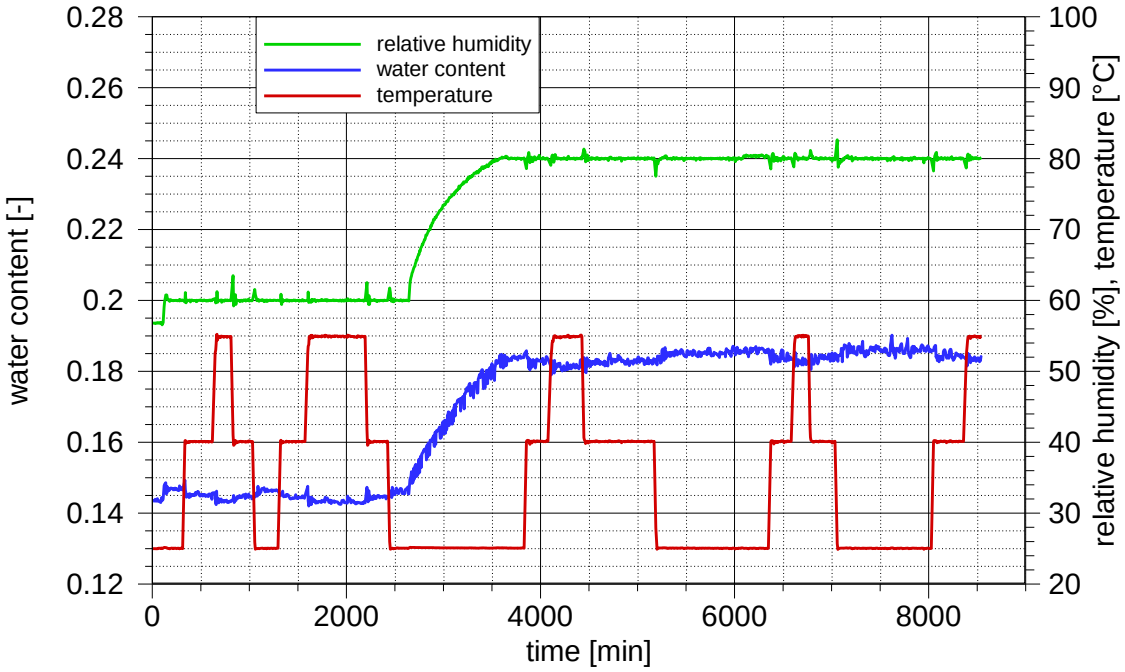

Fig. B.49 Test conditions for the campaign with 60 and 80 % relative humidity

B.2.4.2.2 Test results

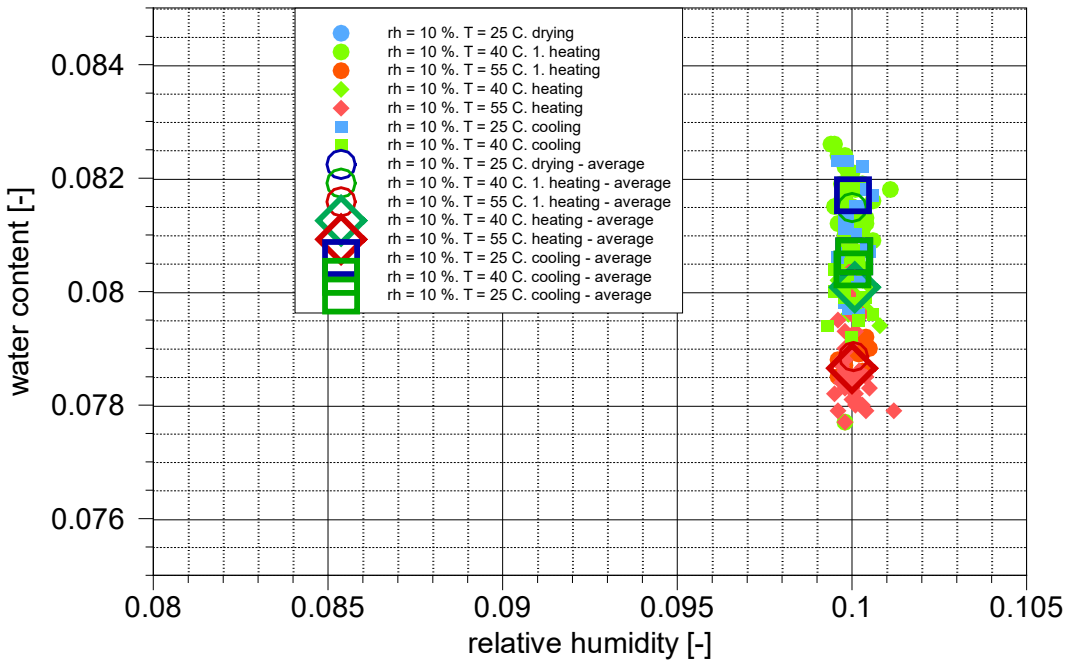

Fig. B.50 Heating and cooling of Calcigel at a relative humidity of 10 %

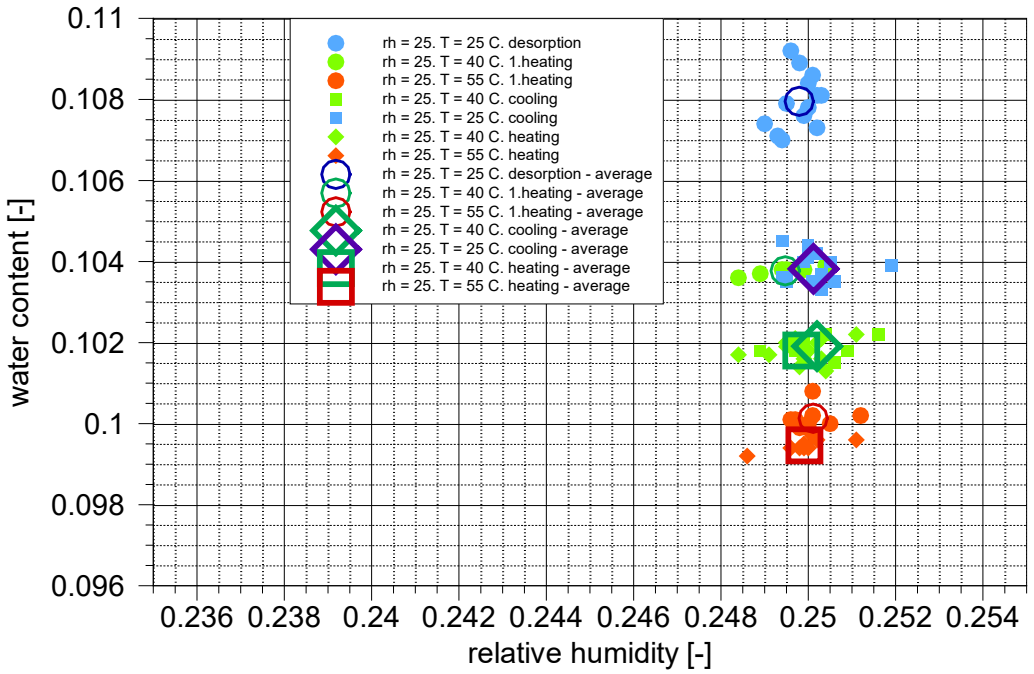

Fig. B.51 Heating and cooling of Calcigel at a relative humidity of 25 %

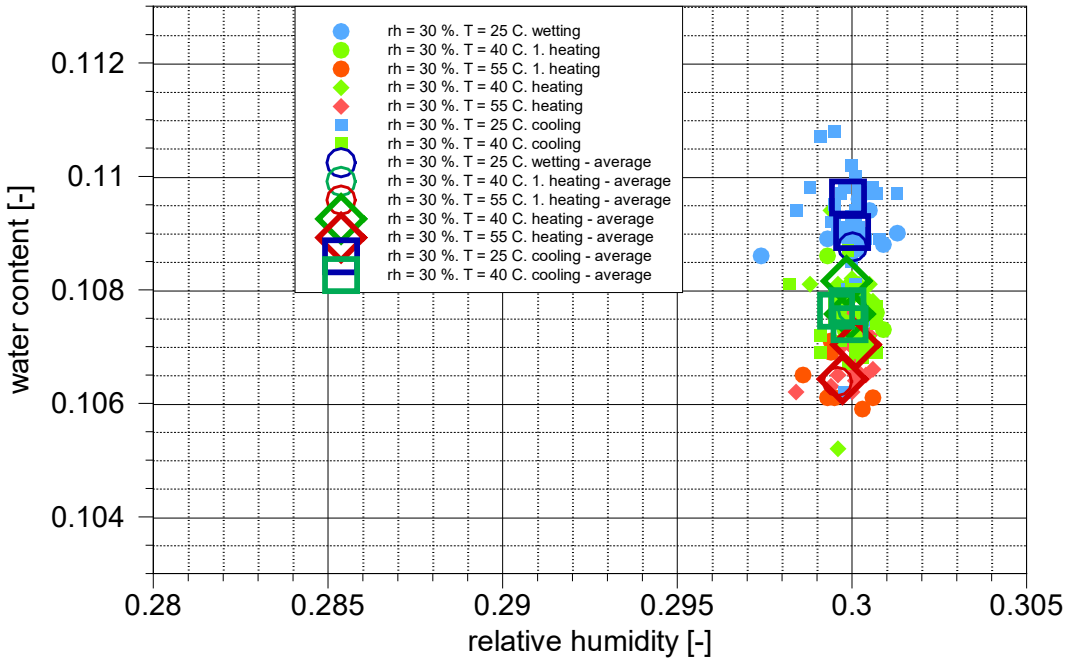

Fig. B.52 Heating and cooling of Calcigel at a relative humidity of 30 %

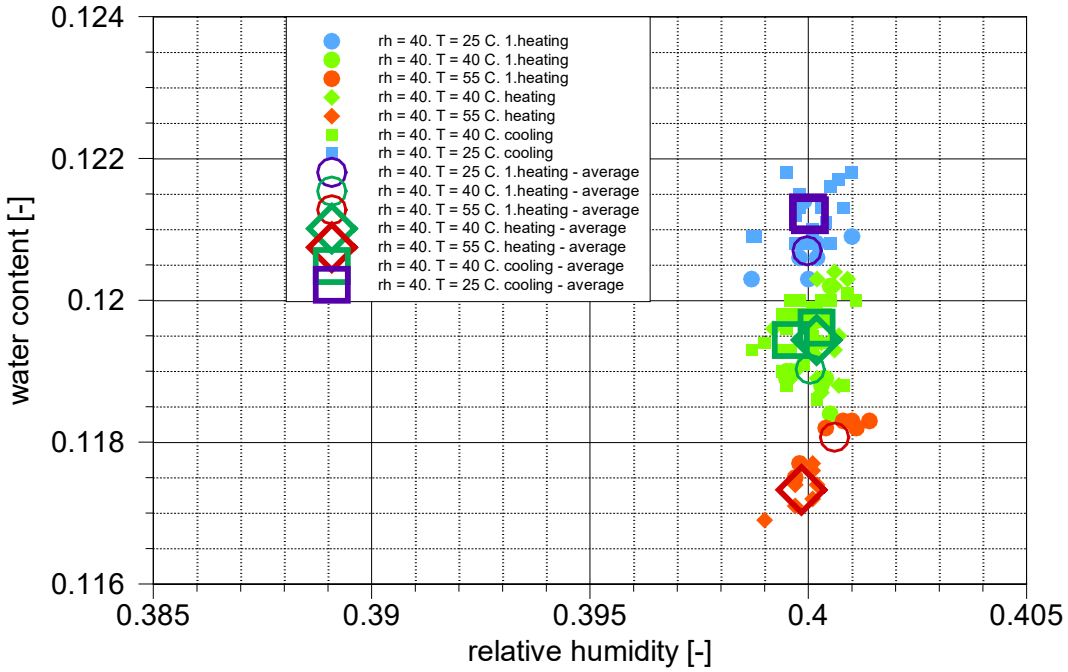

Fig. B.53 Heating and cooling of Calcigel at a relative humidity of 40 %

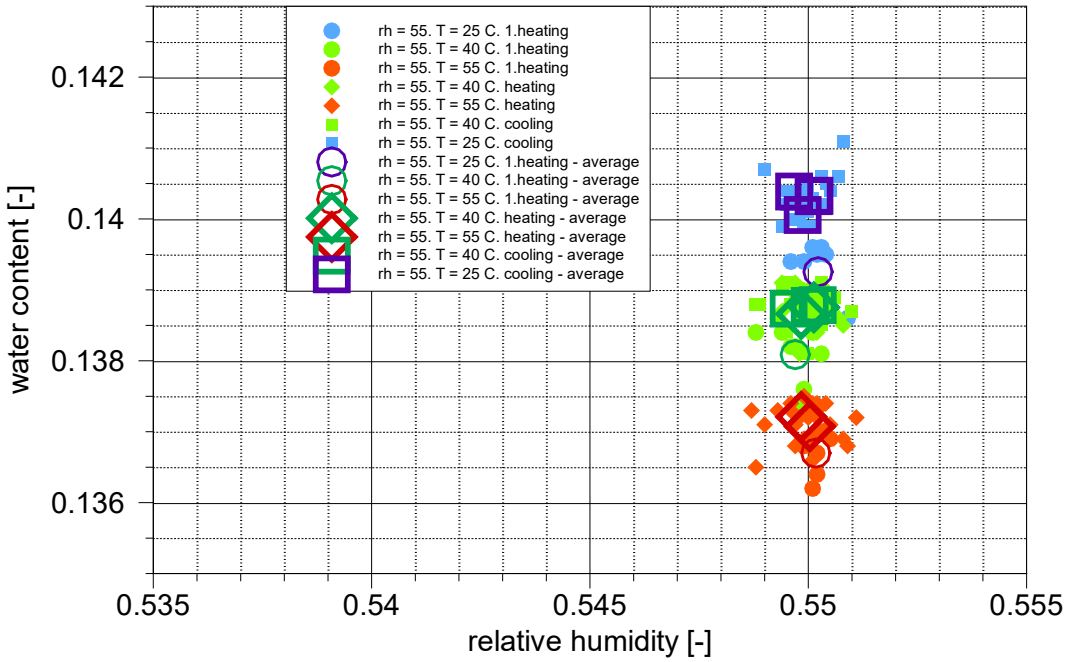

Fig. B.54 Heating and cooling of Calcigel at a relative humidity of 55 %

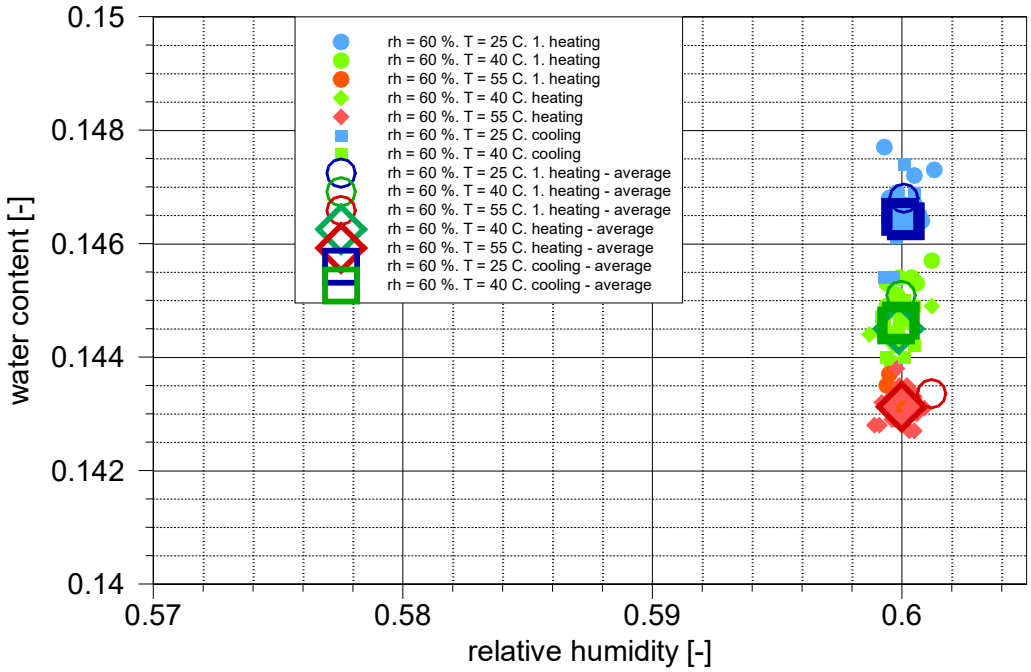

Fig. B.55 Heating and cooling of Calcigel at a relative humidity of 60 %

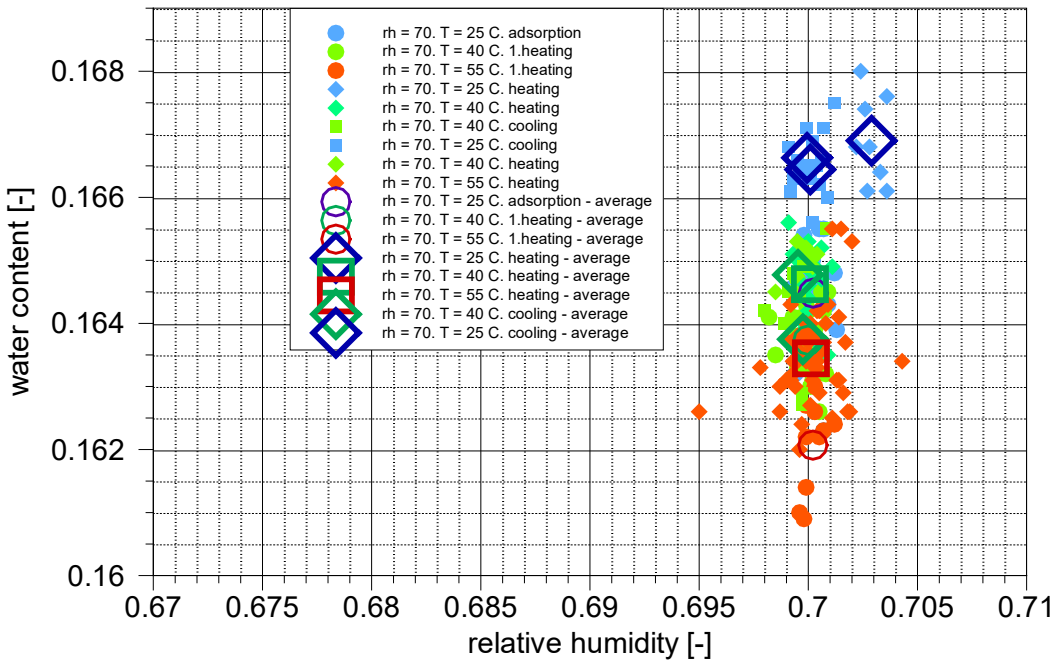

Fig. B.56 Heating and cooling of Calcigel at a relative humidity of 70 %

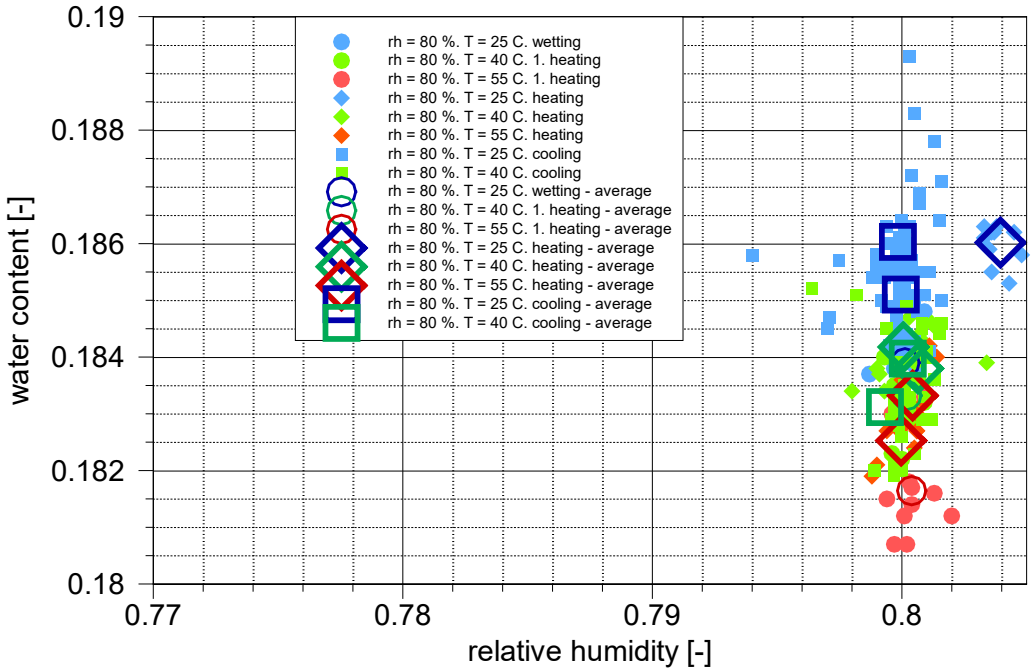

Fig. B.57 Heating and cooling of Calcigel at a relative humidity of 80 %

C Appendix: Descriptions of numerical models

C.1 Reference data set

The numerical models described in this report aim at evaluating clearly the influence of different features in the constitutive relation between relative humidity and water content on the dynamics of bentonite re-saturation. The models are set up to vary in as few aspects as possible. For this purpose, they are devised as variants of a reference model with the necessary minimum of deviations.

A complete and numbered set of data characterising the reference model, including the input data for code VIPER, is listed in Tab. C.1. In section C.2, the variants are simply characterised by their deviations from the reference data set.

Tab. C.1 General characteristic data for the numerical models run with code VIPER

	Model domain	
1	Type of model	constant cross-section
2	Model length	10 cm
3	Cross-sectional area	1 m²
	Discretisation	
4	Number of elements	100
5	Element length	1 mm
6	Time step (subject to time step control)	1 s
	Physicalquantities	
7	Density of clay grains	2780 kg/m³
8	Density of water	1000 kg/m³
9	Tortuosity of the pore space	0.65
10	**Constitutive relation between water content and relative humidity**	Analytical equations for MX-80, Calcigel and a linear isotherm
	Interlayercharacteristics	
11	Initial porosity	15 %(MX-80) / 22.5 % (Calcigel)
12	Tortuosity	0.4
13	Diffusion coefficient 1[21,22]	$1 \cdot 10^{-9}$ m²/s
14	Diffusion coefficient 2	$2 \cdot 10^{-9}$ m²/s
15	Diffusion coefficient 3	$2 \cdot 10^{-9}$ m²/s
16	Threshold between layer 1 and 2	17 % water content
17	Threshold between layer 2 and 3	18 % water content
	Dry bentonite	
18	Dry density	1500 kg/m³
19	Porosity	46 %
	Saturated bentonite	
20	Residual porosity	5 %
21	Water content	27.4 %
22	Degree of saturation	89.1 %
23	Total water content[23]	30.7 %
	Initial conditions	
24	Density	1650 kg/m³
25	Porosity	31 % (MX-80) / 23.5 % (Calcigel)
26	Water content	10 % (MX-80) / 15 % (Calcigel)
27	Relative humidity	60 %
28	Degree of saturation	32.6 % (MX-80)/ 48.9 % (Calcigel)
29	Constant temperature	20 °C
30	Saturation vapour density	0.0173 kg/m³
	Hydraulic boundary conditions	
31	Left hand side (x/r=0)	Max. water content from t=0 on
32	Right handside	no-flow
	Temperature boundary conditions	(not applicable; isothermal model)
	Output	
33	Breakthrough curves	none
34	Distributions	at t = 1, 10, 100 days

[21] The number represents the number of cation layers.

[22] For the lack of better knowledge, the diffusion data for MX-80 are applied to Calcigel as well

[23] including the residual porosity

C.2 Variations

In the following, the model data used in this report are described in the order of appearance. The descriptions relate to the reference model that is fully characterised in Tab. C.1. Thus, only the differences to the reference model are listed here.

Subsection 8.2: Isothermal wetting

- Parameters were set according to Tab. C.1 (reference model)

Subsection 8.3: Isothermal drying

- Parameters according to Tab. C.1 except for
  - Initial relative humidity: 80 %
  - Initial water content[24]: 18 % (MX-80), 19 % (Calcigel)

Subsection 8.4: "Arbitrary" initial conditions

- Parameters for MX-80 according to Tab. C.1 except for
  - Initial relative humidity: 45 % (one model)

- Parameters for Calcigel according to Tab. C.1 except for
  - Initial relative humidity: 51, 55 % (two models)

Subsection 8.5: Changing boundary conditions between wetting and drying

- Parameters according to Tab. C.1 except for
  - Initial relative humidity: 60 %
  - Initial water content[25]: 13 % (MX-80), 16 % (Calcigel)
  - Left boundary condition:
    - day 0 to day 50 85 % relative humidity
    - day 50 linear decrease with time
    - day 51 to day 100 10 % relative humidity

[24] leading to an increase of interlayer porosity, degree of saturation, and initial bentonite density and a decrease of pore space porosity

[25] leading to an increase of interlayer porosity, degree of saturation, and initial bentonite density and a decrease of pore space porosity

Subsection 8.6: Moisture re-distribution due to heating

- Parameters according to Tab. C.1 except for
  - Temperature evolution
    - Initial temperature (20 °C) fixed at the inflow boundary
    - Linear increase at the closed boundary from 20 °C to 50 °C between 24 h < t < 48 h
    - Linear temperature increase over the model domain, if applicable

Gesellschaft für Anlagen- und Reaktorsicherheit (GRS) gGmbH

Schwertnergasse 1
50667 Köln
Telefon +49 221 2068-0
Telefax +49 221 2068-888

Forschungszentrum
Boltzmannstraße 14
85748 Garching b. München
Telefon +49 89 32004-0
Telefax +49 89 32004-300

Kurfürstendamm 200
10719 Berlin
Telefon +49 30 88589-0
Telefax +49 30 88589-111

Theodor-Heuss-Straße 4
38122 Braunschweig
Telefon +49 531 8012-0
Telefax +49 531 8012-200

www.grs.de

ISBN 978-3-949088-01-8